Université d'Ottawa · University of Ottawa

Université d'Ottawa · University of Ottawa

FACULTÉ DE ÉTUDES SUPÉRIEURES ET POSTDOCTORALES

FACULTY OF GRADUATE AND POSTDOCTORAL STUDIES

Jennifer SNELGROVE

AUTEUR DE LA THÈSE - AUTHOR OF THESIS

Ph.D. (Chemistry)

GRADE - DEGREE

Department of Chemistry

FACULTÉ, ÉCOLE, DÉPARTEMENT - FACULTY, SCHOOL, DEPARTMENT

TITRE DE LA THÈSE - TITLE OF THE THESIS

Aryloxide Complexes of Early and Late Transition Metals : Applications in Olefin Metathesis

D. Fogg

DIRECTEUR DE LA THÈSE - THESIS SUPERVISOR

P. Sundararajan

CO-DIRECTEUR DE LA THÈSE - THESIS CO-SUPERVISOR

EXAMINATEURS DE LA THÈSE - THESIS EXAMINERS

H. Alper

S. Barry

S. Gambarotta

D. Stephan

J.-M. De Koninck, Ph.D

LE DOYEN DE LA FACULTÉ DES ÉTUDES SUPÉRIEURES ET POSTDOCTORALES

DEAN OF THE FACULTY OF GRADUATE AND POSTDOCTORAL STUDIES

Aryloxide Complexes of Early and Late Transition Metals: Applications in Olefin Metathesis

By

JENNIFER L. SNELGROVE

Thesis submitted to the
School of Graduate Studies and Research
University of Ottawa
in partial fulfillment of the requirements for the degree of

Doctor of Philosophy

Ottawa-Carleton Chemistry Institute
The University of Ottawa
Ottawa, Ontario
September 2003

Your file Votre référence
ISBN: 0-494-01762-7
Our file Notre référence
ISBN: 0-494-01762-7

ABSTRACT

Treatment of ruthenium chloride complexes $RuCl_2(PPh_3)_3$ **1a** or $RuHCl(PPh_3)_3$ **1b** with monodentate aryloxides in non-alcohol solvents affords π-bound aryloxide derivatives with the general formula $Ru(\eta^5\text{-ArO})(o\text{-}C_6H_4PPh_2)(PPh_3)_2$ **9** or $RuX(\eta^5\text{-ArO})(PPh_3)_2$ (X = H (**3a**) or Cl (**11b**)). In the presence of alcohols, hydridocarbonyl complexes with the general formula $RuXY(CO)(PPh_3)_3$ (X = H, Y = H **2a**; X = H, Y = Cl **2b**) are generated by hydride abstraction and decarbonylation of formaldehyde. Treatment of **1a** with one equivalent of aryloxide in the presence of isopropanol liberates the phenol and acetone, affording clean **1b** in quantitative yields. Treatment of **3a** with ethereal HCl gives $[RuH(\eta^6\text{-ArOH})(PPh_3)_2]Cl$ **12a**.

Arresting σ→π isomerization was attempted using a P,O-chelate ligand ((±)-2-(diphenylphosphino)-2'-hydroxy-1,1'-binaphthyl (binop; **29**). The entropy gain was not favourable enough to prevent isomerization. The binop ligand in the product, $RuCl_2(binop)(PPh_3)$ **31**, is σ-bound via the phosphorus donor, and π-bound via the 'phenoxide' ring, as indicated by detailed spectroscopic and MALDI-mass spectrometric analysis.

Reaction of $RuHCl(PPh_3)_3$ **1b** with 3-chloro-3-methyl-1-butyne effects transformation into the alkylidene complex $RuCl_2(=CHCH=CMe_2)(PPh_3)_2$ **34**. $RuHCl(PPh_3)_3$ **1b** is commercially available or obtained via quantitative reaction of $RuCl_2(PPh_3)_3$ **1a** with alkali aryloxides, as described above. Phosphine exchange between **34** and PCy_3 is rapid at room temperature, affording $RuCl_2(=CHCH=CMe_2)(PCy_3)_2$ **37**. Complex **34** is stable indefinitely in the solid state at room temperature under N_2, but dimerizes slowly in solution to give $RuCl(PPh_3)_2(\mu\text{-}Cl)_3Ru(=CHCH=CMe_2)(PPh_3)_2$ **36**. A side-product arising from use of excess 3-chloro-3-methyl-1-butyne in the synthesis of **34** was identified as a Ru(IV) carbyne complex $RuCl_3(\equiv CCH=CMe_2)(PPh_3)_2$ **35**.

t,t-Benzaldehyde azine **40** is formed as a byproduct in the synthesis of phenyldiazomethane **39**. Azine **40** coordinates to ruthenium at room temperature, generating $Ru_2Cl_4(dppb)_2$(*t,t*-benzaldehyde azine) **52**. At 50 °C, a novel N-N activation reaction yields $Ru_2Cl_4(dppb)_2$(NCPh) **43** and $Ru_2Cl_4(dppb)_2$(HN=CHPh) **44** in a 1:1 ratio. The structure of **43** was confirmed by X-ray analysis.

A systematic investigation into ROMP of 2,3-dicarboalkoxynorbornadienes **53-55** and 2,3-diphenylamidonorbornadiene **56** via molybdenum biphenolate catalysts **49** showed that polymer tacticity was dependent on biphenolate and monomer substituents. Thermal analysis of the polymers by DSC, TGA and IR experiments showed that polymers prepared from 2,3-dicarboalkoxynorbornadiene monomers underwent C=C degradation even at 80 °C. In contrast, the bulky amide polymer was stable up to 275 °C. All of the polymers decompose above 300 °C. Investigations of the tertiary structure of the polymers indicated no helicity in solution: though high crystallinity in the solid state could result from helicity, the extreme mechanical sensitivity of the samples precluded confirmation by wide-angle X-ray diffraction.

TABLE OF CONTENTS

ABSTRACT.....ii

TABLE OF CONTENTS.....iv

TABLE OF COMPOUND NUMBERS.....xv

LIST OF TABLES.....xvii

LIST OF SCHEMES.....xviii

LIST OF FIGURES.....xx

LIST OF ABBREVIATIONS.....xxii

CONTRIBUTIONS TO RESEARCH.....xxiv

ACKNOWLEDGEMENTS.....xxv

CHAPTER 1.....1

1.1. Olefin Metathesis.....1

1.2. Ring-Opening Metathesis Polymerization.....2

1.3. Molybdenum Olefin Metathesis Catalyst Evolution.....3

1.4. Ruthenium Olefin Metathesis Catalysts.....4

1.5. Selectivity and Tacticity Determination.....7

1.6. Materials Applications.....9

1.7. Scope of Thesis Work.....10

1.8. References.....11

CHAPTER 2.....15

2.1. Materials.....15

2.1.1. Solvents....15

2.1.2. Gases....15

2.1.3. Phosphines....16

2.1.4. Other Materials....16

2.2. Instrumentation....17

2.3. Ruthenium Precursors....18

2.3.1. $RuCl_2(PPh_3)_3$ **1a**....19

2.3.2. $RuCl_2(CO)_2(PPh_3)_2$ **14**....19

2.3.3. $RuCl_2(dppb)(PPh_3)$ 19

2.3.4. $[RuCl(dppb)]_2(\mu\text{-}Cl)_2(\mu\text{-}H_2O)$ **41**....20

2.3.5. $Ru_2Cl_4(dcypb)_2(N_2)$....20

2.4. Aryloxide Salts....21

2.4.1. $C_6H_5O^-K^+$....21

2.4.2. $p\text{-}Bu^tC_6H_4O^-K^+$....21

2.5. Reaction of Ruthenium Precursor 1a with Aryloxides....21

2.5.1. Reaction of $RuCl_2(PPh_3)_3$ with 1 equiv $p\text{-}^tBuC_6H_4O^-K^+$....21

2.5.2. Reaction of $RuCl_2(PPh_3)_3$ with 2 equiv $p\text{-}^tBuC_6H_4O^-K^+$....22

2.5.3. Labelling Studies....22

2.5.4. $RuHCl(PPh_3)_3$ **1b**....23

2.5.5. $Ru(\eta^5\text{-}^tBu\text{-}C_6H_4O)(o\text{-}C_6H_4PPh_2)(PPh_3)\cdot HOAr$ **9a•HOAr**....23

2.5.6. $Ru(\eta^5\text{-}C_6H_5O)(o\text{-}C_6H_4PPh_2)(PPh_3)\cdot HOPh$ **9b•HOPh**....24

2.6. Reaction of **1b** with Aryloxides....24

2.6.1. $RuH(\eta^5\text{-}^tBu\text{-}C_6H_4O)(PPh_3)_2$ **3a**....24

2.6.2. $RuCl(\eta^5\text{-}C_6H_5O)(PPh_3)_2$ **11b**. 25

2.6.3. $[RuH(\eta^5\text{-}^t\text{Bu-}C_6H_4O)(PPh_3)_2]Cl$ **12a**.....26

2.7. Miscellaneous Reactions Yielding $RuH_2(CO)(PPh_3)_3$ **2a** and $RuHCl(CO)(PPh_3)_3$ **2b**.....26

2.7.1. $RuHCl(CO)(PPh_3)_3$ **2b** from $RuHCl(PPh_3)_3$ **1b**.....26

2.7.2. $RuH_2(CO)(PPh_3)_3$ **2a** from .$RuHCl(CO)(PPh_3)_3$ **2b**.....27

2.8. Reaction of $RuCl_2(CO)_2(PPh_3)_2$ **14** with Aryloxides.....27

2.8.1. $RuCl(\sigma\text{-}^t\text{BuC}_6H_4O)(CO)_2(PPh_3)_2$ **15**.....27

2.8.2. $2K[Ru(\sigma\text{-}^t\text{BuC}_6H_4O)_3(CO)_2(PPh_3)]_2$ **17**.....28

2.9. Binop Ligand Preparation.....29

2.9.1. 2,2'-Bis((trifluoromethanesulfonyl)oxy)-1,1'-binaphthyl[17] **26**....29

2.9.2. 2-(Diphenylphosphinyl)-2'-((trifluoromethanesulfonyl)oxy)-1-1'-binaphthyl[17] **27**.....29

2.9.3. 2-(Diphenylphosphinyl)-2'-hydroxybinaphthyl[17] **28**.....30

2.9.4. General Procedure for the Reduction to 2-(Diphenylphosphino)-2'-lithium-1,1'-binapthyl **29** (Binop) 30

2.9.4.1.From 2-(Diphenylphosphinyl)-2'-((trifluoromethanesulfonyl)oxy)-1-1'-binaphthyl **27** in Toluene.....31

2.9.4.2.From 2-(Diphenylphosphinyl)-2'-hydroxybinaphthyl **28** in Toluene.....31

2.9.4.3.From 2-(Diphenylphosphinyl)-2'-hydroxybinaphthyl **28** in Chlorobenzene.....31

2.9.5. 2-(Diphenylphosphino)-2'-sodium-1, 1'-binaptholate **30**.....31

2.9.6. $RuCl(binop)(PPh_3)$ **31**.....32

2.10. Preparation of a New Ruthenium Alkylidene.....33

2.10.1. $RuCl_2(=CHCH=CMe_2)(PPh_3)_3$ **34**.....33

2.10.2. One-Pot Synthesis of $RuCl_2(=CHCH=CMe_2)(PCy_3)_2$ **37**.....34

2.11. Synthesis of Phenyldiazomethane **39** and *t,t*-Benzaldeyde Azine **40**.....35

2.11.1. Benzaldehyde Tosylhydrazone **38**.....35

2.11.2. Phenyldiazomethane **39**.....35

2.11.3. *t,t*-Benzaldehyde Azine **40**.....36

2.12. Reaction of $[RuCl(dppb)]_2(\mu\text{-}Cl)_2(\mu\text{-}H_2O)$ **41** with *t,t*-Benzaldehyde azine **40** 36

2.12.1. $Ru_2Cl_4(dppb)_2$(*t,t*-benzaldehyde azine) **42** 36

2.12.2. $Ru_2Cl_4(dppb)_2(N{\equiv}CPh)$ **43** and $Ru_2Cl_4(dppb)_2(NH{=}CHPh)$ **44**...37

2.12.3. Hydrolysis of $Ru_2Cl_4(dppb)_2(NH{=}CHPh)$ **44** with Liberation of Benzaldehyde.....38

2.13. 2,3-Dicarboxylic Acid Norbornadiene.....38

2.14. Preparation of diphenylamine and menthol salts for transesterification.....38

2.14.1. Lithium Diphenylamide.....38

2.14.2. Potassium Menthoxide.....39

2.15. Vilsmeier Reagent.....39

2.16. Norbornadiene based ROMP monomer preparation.....39

2.16.1. 2,3-Dicarbomethoxynorbornadiene **53**.....39

2.16.2. 2,3-Dicarbo^{t}butoxynorbornadiene **54**.....40

2.16.3. 2,3-Dicarbomenthoxynorbornadiene **55**.....40

2.16.4. 2,3-Diphenylamidenorbornadiene **56**.....42

2.17. Benzyl Potassium.....42

2.18. Biphenolate Ligand Preparation.....43

2.18.1. 3,3',5,5'-tetra-*tert*-butyl-biphenyl-2,2'-diol **51a** and Dipotassium 3,3',5,5'-tetra-*tert*- butylbiphenolate **52a**.....43

2.18.2. Dipotassium 5,5',6,6'-tetramethyl-3,3'-di-*tert*-butylbiphenolate **52b**.....43

2.18.3. Dipotassium (R)-(+)-5,5',6,6'-tetramethyl-3,3'-di-*tert*-butylbiphenolate (R)-(+)-**52b**.....43

2.18.4. 3,3',5,5'-tetra-*tert*-butyl-6,6'-dimethylbiphenyl-2,2'-diol **51c** and Dipotassium 3,3',5,5'-tetra-*tert*-butyl-6,6'-dimethylbiphenolate **52c**.....44

2.19. Neophyl Grignard Preparation for Molybdenum Precursor Synthesis.....44

2.20. Molybdenum Precursors.....45

2.20.1. $MoCl_2(NAr)_2(DME)$ 45

2.20.2. $Mo(CH_2Me_2Ph)_2(NAr)_2$.....45

2.20.3. $Mo(CHCMe_2Ph)(NAr)(OSO_2CF_3)_2(DME)$ **50**.....46

2.21. Molybdenum Biphenolate Catalysts **49a-d**.....47

2.21.1. General Procedure.....47

2.21.2. $Mo(=CHCMe_2Ph)$(NAr)(3,3',5,5'-tetra-*tert*-butyl-1,1'-biphenyl-2,2'-diolate) **49a**.....47

2.21.3. $Mo(=CHCMe_2Ph)$(NAr)(5,5',6,6'-tetramethyl-3,3'-di-*tert*-butyl-1,1'-biphenyl-2,2'-diolate) **49b**.....48

2.21.4. (R)-(+)-$Mo(=CHCMe_2Ph)$(NAr)(5,5',6,6'-tetramethyl-3,3'-di-*tert*-butyl-1,1'-biphenyl-2,2'-diolate) (R)-(+)-**49b**.....48

2.21.5. $Mo(=\overline{CH}CMe_2Ph)$(NAr)(3,3',5,5'-tetra-*tert*-butyl-6,6'-dimethyl-1,1'-biphenyl-2,2'-diolate) **49c**.....49

2.21.6. $Mo(=CHCMe_2Ph)(NAr)(O^tBu)_2$ **49d**.....49

2.22. General Procedure for the ROMP of 2,3-Dicarboalkoxy/diamidonorbornadienes (**53-56**) using Molybdenum Alkylidene Initiators **49**. 50

2.22.1. Polymer of 2,3-Dicarbomethoxynorbornadiene **53**.....50

2.22.2. Polymer of 2,3-Dicarbo'butoxynorbornadiene **54**.....51

2.22.3. Polymer of 2,3-Dicarbomenthoxynorbornadiene **55**.....51

2.22.4. Polymer of 2,3-Diphenylamidenorbornadiene **56**.....52

2.22.5. General Procedure for Preparation of Copolymers of MTD and **53**.....52

2.23. References.....53

CHAPTER 3.....55

3.1. Introduction.....55

3.2. Reaction of $RuCl_2(PPh_3)_3$ **1a** with Aryloxidein the Presence of Alcohols.....56

3.2.1. Reaction of **1a** with Two Equivalents of Aryloxide.....56

3.2.2. Reaction of **1a** with 1 Equivalent of Aryloxide.....60

3.2.3. Molecular Structures of $RuH_2(CO)(PPh_3)_3$ **2a** and $RuHCl(CO)(PPh_3)$ **2b**.....62

3.3. Isomerization vs. Decarbonylation for Reaction of $RuHCl(PPh_3)_3$ with KOAr.....64

3.4. A Clean, High-Yield Route to $RuHCl(PPh_3)_3$ **1b** via Reaction with Isopropanol...64

3.5. Reaction of $RuCl_2(PPh_3)_3$ with Aryloxide in the Absence of Alcohol.....65

3.5.1. Formation of *ortho*-Metallated Complexes **9a** and **9b**.....65

3.5.2. Molecular Structures of **9a**•$(HOAr)_2$ and **9b**•(HOPh).....68

3.6. Effect of Aryloxide Substitution on Product Formation.....70

3.6.1. Molecular Structures of $RuCl(\eta^5\text{-}C_6H_5O)(PPh_3)_2$ **11b** and $[RuH(\eta^6\text{-}C_6H_4{}^tBuOH)(PPh_3)_2]Cl$ **12a**.....72

3.7. Reaction of Aryloxide with a Coordinatively Saturated Ruthenium Complex.....75

3.7.1. Crystal Structure Analysis of $2K[Ru_2(CO)_4(OAr)_6(PPh_3)_2]$ **17**.....77

3.8. Conclusions.....79

3.9. References.....80

CHAPTER 4.....82

4.1. Introduction.....82

4.2. Preparation of (±)-2-(Diphenylphosphino)-2'-Hydroxy-1,1'-Binaphthyl (binop; **29**).....83

4.3. Transformation of binop to its Alkali Metal Salts.....84

4.4. Reaction of $RuCl_2(PPh_3)_3$ **1a** with Na-binop **30**.....85

4.4.1. Molecular Composition of **31**.....86

4.4.2. Proposed Structure for $RuCl(binop)(PPh_3)$ **31**.....89

4.4.3. ^{31}P Coupling Anomalies in NMR Data for **31**.....97

4.5. Diastereomeric Bias within **31**.....99

4.6. Conclusions.....102

4.7. References.....103

CHAPTER 5.....105

5.1. Introduction.....105

5.2. Preparation of a Versatile Precursor to New Ruthenium Alkylidene Complexes..107

5.2.1 Formation of Byproducts.....107

5.2.2 Use of **44** as a Precursor.....109

5.3. Azine Poisoning Studies.....110

5.3.1 Formation of an Azine Adduct of Ruthenium.....111

5.3.2. Azine Activation Products.....114

5.3.3. Mechanism of Formation of **43** and **44**.....116

5.3.4. Hydrolysis of Imine Complex **44**.....117

5.3.5. Molecular Structure of $Ru_2Cl_4(dppb)_2(NCPh)$ **43**.....118

5.4. Conclusions.....121

5.5. References.....122

CHAPTER 6.....125

6.1. Introduction.....125

6.2. Preparation of Biphenolate ROMP Catalysts.....129

6.3. Synthesis of Norbornadiene Monomers.....131

6.4. ROMP of Norbornadiene Monomers with Molybdenum Biphenolate Catalysts...132

6.4.1. Cis/Trans Selectivity and Tacticity Determination.....136

6.5. Solution Analysis of Polymer Tertiary Structure 139

6.6. TGA and DSC Results for Polymers of **53-56**. 140

6.6.1. Polymer Crystallinity: X-Ray Powder and Thin Film Diffraction Analyses.....144

6.6.2. Infrared Analysis.....148

6.7. Conclusions.....149

6.8. References.....151

CHAPTER 7.....153

APPENDICES.....157

Appendix A. Crystallographic Information for $RuH_2(CO)(PPh_3)_3 \cdot CH_2Cl_2$ (**2a**).....158

Table A.1. Crystal data and structure refinement for $RuH_2(CO)(PPh_3)_3 \cdot CH_2Cl_2$ (**2a**).....158

Table A.2. Bond lengths [Å] and angles [°] for $RuH_2(CO)(PPh_3)_3 \cdot CH_2Cl_2$ (**2a**).....159

Appendix B. Crystallographic Information for $RuHCl(CO)(PPh_3)_3$ (**2b**).....163

Table B.1. Crystal data and structure refinement for $RuHCl(CO)(PPh_3)_3$ (**2b**).....163

Table B.2. Bond lengths [Å] and angles [°] for $RuHCl(CO)(PPh_3)_3$ (**2b**).....145

Appendix C. Crystallographic Information for Ru(η^5-ArO)(o-$C_6H_4PPh_2$)(PPh_3)•(2ArOH)($CHCl_3$) (**9a**).....166

Table C.1. Crystal data and structure refinement for Ru(η^5-ArO)(o-$C_6H_4PPh_2$)(PPh_3)•(2ArOH)($CHCl_3$) (**9a**).....166

Table C.2. Bond lengths [Å] and angles [°] for Ru(η^5-ArO)(o-$C_6H_4PPh_2$)(PPh_3)•(2ArOH)($CHCl_3$) (**9a**).....173

Appendix D. Crystallographic Information for Ru(η^5-PhO)(o-$C_6H_4PPh_2$)(PPh_3)•(2PhOH) (**9b**).....173

Table D.1. Crystal data and structure refinement for Ru(η^5-PhO)(o-$C_6H_4PPh_2$)(PPh_3)•(2PhOH) (**9b**).....173

Table D.2. Bond lengths [Å] and angles [°] for Ru(η^5-PhO)(o-$C_6H_4PPh_2$)(PPh_3)•(2PhOH) (**9b**).....174

Appendix E. Crystallographic Information for $RuCl(\eta^5$-PhO)$(PPh_3)_2$•CH_2Cl_2 (**11b**).....179

Table E.1. Crystal data and structure refinement $RuCl(\eta^5$-PhO)$(PPh_3)_2$•CH_2Cl_2 (**11b**).....179

Table E.2. Bond lengths [Å] and angles [°] for $RuCl(\eta^5$-PhO)$(PPh_3)_2$•CH_2Cl_2 (**11b**).....180

Appendix F. Crystallographic Information for $[RuH(\eta^6$-ArOH)$(PPh_3)_2]$Cl•ArOH (**12a**).....185

Table F.1. Crystal data and structure refinement for $[RuH(\eta^6$-ArOH)$(PPh_3)_2]$Cl•ArOH (**12a**).....185

Table F.2. Bond lengths [Å] and angles [°] for $[RuH(\eta^6$-ArOH)$(PPh_3)_2]$Cl•ArOH (**12a**).....186

Appendix G. Crystallographic Information for $2K[Ru(OAr)_3(CO)_2(PPh_3)]_2$ (**17**).....191

Table G.1. Crystal data and structure refinement for $2K[Ru(OAr)_3(CO)_2(PPh_3)]_2$ (**17**).....191

Table G.2. Bond lengths [Å] and angles [°] for $2K[Ru(OAr)_3(CO)_2(PPh_3)]_2$ (**17**).....192

Appendix H. Crystallographic Information for $Ru_2Cl_4(dppb)_2(N{\equiv}CPh)$ (**43**).....205

Table H.1. Crystal data and structure refinement for $Ru_2Cl_4(dppb)_2(N{\equiv}CPh)$ (**43**).....205

Table H.2. Bond lengths [Å] and angles [°] for $Ru_2Cl_4(dppb)_2(N{\equiv}CPh)$ (**43**).....206

Appendix I NMR Spectroscopic Data for $RuCl(binop)(PPh_3)$ **31**.....212

Figure I.1. $^{31}P\{^1H\}$ NMR Spectrum for **31** ($CDCl_3$).....212

Figure I.2. Expansion of Upfield Region of the ^1H NMR of **31** at a) 300K and b) 324K.....212

Figure I.3. $^{13}C\{^1H\}$ NMR Spectrum of **31** ($CDCl_3$).....213

Figure I.4. $^{13}C\{^1H\}$ DEPT 135 Spectrum of **31** ($CDCl_3$).....231

Figure I.5. ^1H-^1H COSY NMR Spectrum of **31**.....214

Figure I.6. ^1H-^{13}C HMQC NMR Spectrum of **31**.....215

Figure I.7. ^1H-^1H TOCSY NMR Spectrum of **31**.....216

Figure I.8. ^1H-^{13}C HMBC NMR Spectrum of **31**.....217

Figure I.9. ^1H-^{31}P HMQC NMR Spectrum of **31** (optimized for 10 Hz coupling)...218

Figure I.10. ^1H-^{31}P HMQC NMR Spectrum of **31** (optimized for 5 Hz coupling).....219

Appendix J Ivin and Rooney ROMP Mechanism.....220

Appendix K $^{13}C\{^1H\}$ NMR Spectra for Polymers of a) **53** b) **54** c) **55** and d) **56**.....221

Appendix L Thermal Analysis of Polymers of **53-56**.....223

Figure L.1. Representative DSC Thermograms of Polymers of a) **53** b) **54** c) **55** and d) **56**.....223

Figure L.2. Relative Mass Loss (TGA) for Polymers of a) **53** b) **54** c) **55** and d) **56**.....225

Figure L.3. Relative IR Absorption vs. Time for Polymers of a) **53** b) **54** c) **55** and d) **56**.....226

TABLE OF COMPOUND NUMBERS

	Compound
1	
1a	$RuCl_2(PPh_3)_3$
1b	$RuHCl(PPh_3)_3$
2	
2a	$RuH_2(CO)(PPh_3)_3$
2b	$RuHCl(CO)(PPh_3)_3$
3	
3a	$RuH(\eta^5\text{-}C_6H_5{}^tBuO)(PPh_3)_2 \bullet MeOH$
3b	$RuH(\eta^5\text{-}C_6H_5O)(PPh_3)_2$
9	$Ru(\eta^5\text{-}ArO)(o\text{-}C_6H_4PPh_2)(PPh_3)$
9a	$Ru(\eta^5\text{-}C_6H_5{}^tBuO)(o\text{-}C_6H_4PPh_2)(PPh_3) \bullet ArOH$
9b	$Ru(\eta^5\text{-}C_6H_5O)(o\text{-}C_6H_4PPh_2)(PPh_3) \bullet PhOH$
11b	$RuCl(\eta^5\text{-}C_6H_5O)(PPh_3)_2$
12a	$[RuH(\eta^6\text{-}C_6H_5O)(PPh_3)_2]Cl$
14	$RuCl_2(CO)_2(PPh_3)_2$
15	$RuCl(OAr)(CO)_2(PPh_3)_2$
17	$[K_2][Ru_2(CO)_4(OAr)_6(PPh_3)_2]$
26	2,2'-Bis((trifluoromethanesulfonyl)oxy)-1,1'-binaphthyl
27	2-(Diphenylphosphinyl)-2'-((trifluoromethanesulfonyl)oxy)-1-1'-binaphthyl
28	2-(Diphenylphosphinyl)-2'-hydroxybinaphthyl
29	(±)-2-(Diphenylphosphino)-2'-hydroxy-1,1'-binaphthyl (binop)
30	2-(Diphenylphosphino)-2'-sodium-1, 1'-binaptholate
31	$RuCl(binop)(PPh_3)$
34	$RuCl_2(=CHCH=CMe_2)(PPh_3)_2$
35	$RuCl_3(\equiv CHCMe_2)(PPh_3)_2$
36	$RuCl(PPh_3)_2(\mu\text{-}Cl)_3Ru(PPh_3)_2(=CHCH=CMe_2)$
37	$RuCl_2(=CHCH=CMe_2)(PCy_3)_2$
38	-Benzaldehyde tosylhydrazone
39	Phenyldiazomethane ($PhCHN_2$)
40	*t,t*-Benzaldehyde azine
41	$Ru_2Cl_4(H_2O)(dppb)_2$
41a	$Ru_2Cl_4(dppb)_2$
41b	$Ru_2Cl_4(N_2)(dppb)_2$
42	$Ru_2Cl_4(dppb)_2$(*t,t*-benzaldehyde azine)
43	$Ru_2Cl_4(dppb)_2(NCPh)$
44	$Ru_2Cl_4(dppb)_2(HN=CHPh)$
49	Molybdenum BiPhen initiators
49a	Mo(=$CHCMe_2Ph$)(NAr)(3,3',5,5'-tetra-*tert*-butyl-1,1'-biphenyl-2,2'-diolate)
49b	Mo(=$CHCMe_2Ph$)(NAr)(5,5',6,6'-tetramethyl-3,3'-di-*tert*-butyl-1,1'-biphenyl-2,2'-diolate)

49c	Mo(=CHCMe$_2$Ph)(NAr)(3,3',5,5'-tetra-*tert*-butyl-6,6'-dimethyl-1,1'-biphenyl-2,2'-diolate)
49d	Mo(=CHCMe$_2$Ph)(NAr)(O^{t}Bu)$_2$
50	Mo(CHCMe$_2$Ph)(NAr)(OSO$_2$CF$_3$)$_2$(DME)
51	Biphenol Ligands
51a	3,3',5,5'-tetra-*tert*-butyl-biphenyl-2,2'-diol
51c	3,3',5,5'-tetra-*tert*-butyl-6,6'-dimethylbiphenyl-2,2'-diol
52	Dipotassium Biphenolate Ligands
52a	Dipotassium 3,3',5,5'-tetra-*tert*- butylbiphenolate
52b	Dipotassium 5,5',6,6'-tetramethyl-3,3'-di-*tert*-butylbiphenolate
52c	Dipotassium 3,3',5,5'-tetra-*tert*-butyl-6,6'-dimethylbiphenolate
53	2,3-Dicarbomethoxynorbornadiene
54	2,3-Dicarbo^{t}butoxynorbornadiene
55	2,3-Dicarbomenthoxynorbornadiene
56	2,3-Diphenylamidonorbornadiene
57	**53**/MTD block copolymer
57a	4:1
57b	1:1
57c	1:4

LIST OF TABLES

Table 3.1. NMR Spectroscopic Data for **2a**, **2b**, **1b** and **3**..... 58

Table 3.2. Selected Bond Distances (Å) and Angles (°) for **2a** and **2b**. 63

Table 3.3. Selected Bond Lengths (Å) and Angles (°) for **9a** and **9b**.....69

Table 3.4. Selected Bond Distances (Å) and Angles (°) for **11b** and **12a**. 73

Table 3.5. Least-squares deviation from plane for **9a**, **9b**, **11b** and **12a** 74

Table 3.6. Summary of ^{31}P (121 MHz) NMR data for CO complexes **14-17**..... 76

Table 3.7. Selected Bond Lengths (Å) and Angles (°) for **17**. 77

Table 4.1. $^{13}C\{^1H\}$ and ^1H NMR Assignments for **31**..... 90

Table 4.2. Anticipated and Observed ^{13}C-^1H Correlations for **31** via HMBC experiments. 94

Table 5.1. $^{31}P\{^1H\}$ NMR data (C_6D_6) for **42** under Ar, **43** and **44** under N_2..... 115

Table 5.2. Selected Bond Lengths (Å) and Angles (°) for **43** and **45**. 119

Table 6.1. Summary of Literature Microstructure Data for Highly Tactic ROMP Polymers. 129

Table 6.2. Solution Properties of Polymers **53-56** Prepared using Catalyst **49** in THF. 135

Table 6.3. Polymer Tacticity and cis Content from $^{13}C\{^1H\}$ NMR Analysis. 138

Table 6.4. Summary of Thermal Transitions from TGA and DSC Data. 141

Table 6.5. Percent Crystallinity for Polymers **53** and **54** Before and After Annealing. 145

Table 6.6. Powder and Film X-Ray Diffraction *d* Spacings for Polymers **53** and **57**. 147

LIST OF SCHEMES

Scheme 1.1. A simplified representation of the olefin metathesis reaction 1

Scheme 1.2. Metathesis pathways: ADMET, CM, ROM, RCM and ROMP..... 1

Scheme 1.3. ROMP f norbornene and ozonlysis of the resultant polymer. 2

Scheme 1.4. Chauvin mechanism for ROMP.....4

Scheme 1.5. Deactivation pathway of $RuCl_2L_2(=CHR)$ complexes. 6

Scheme 3.1. Anticipated transmetallation reaction of $RuCl_2(PPh_3)_3$ with aryloxide.....57

Scheme 3.2. Products formed in reaction of **1a** + 2 KOAr (Ar = *p*-$C_6H_4{}^tBu$).....57

Scheme 3.3. Methanolysis vs. isomerization: generation of **2a** and **3a**. 59

Scheme 3.4. Product mixture formed in reaction of **1a** + 1 KOAr (Ar = *p*-$C_6H_4{}^tBu$). 60

Scheme 3.5. Proposed mechanism for formation of **2b**. 62

Scheme 3.6. Reaction of **1b** with one equivalent of aryloxide to form **3a** and **2a**..... 64

Scheme 3.7. Formation of *o*-metallated complex **9**. 65

Scheme 3.8. Proposed mechanism for formation of **9**. 67

Scheme 3.9. Formation of $RuCl(\eta^5\text{-}OPh)(PPh_3)_3$ **11b**. 71

Scheme 3.10.Formation of **12a** by reaction of **3a** with $HCl{\bullet}Et_2O$. 71

Scheme 3.11.Anticipated products from reaction of **14** with KOAr. 75

Scheme 3.12.Proposed reaction cascade leading to **17**..... 76

Scheme 3.13.Reaction of $RuH(\sigma\text{-}C_6H_4Me)(PMe_3)_4$ with CO. 78

Scheme 4.1. Path A: Literature route to **29**. Path B: Optimized route to **29**. 84

Scheme 4.2. Proposed reaction of $RuCl_2(PPh_3)_3$ **1a** with Na-Binop **30** 86

Scheme 4.3. Possible $\sigma \rightarrow \pi$ isomerization of the second-generation Hoveyda catalyst **20**.....103

Scheme 5.1. Preparation of the first well-characterized ruthenium-alkylidene complex **32**..... 105

Scheme 5.2. Reaction of $RuH(H_2)Cl(PCy_3)_2$ propargyl chlorides..... 106

Scheme 5.3. Reaction of **1b** with 3-chloro-3-methyl-1-butyne. 107

Scheme 5.4. Synthesis of vinylcarbyne **35**. 108

Scheme 5.5. Dimerization of **34** to **36** in solution..... 109

Scheme 5.6. One-pot synthesis of **37** from **1b**..... 109

Scheme 5.7. Preparation of phenyldiazomethane **39** or *t,t*-benzaldehyde azine **40**..... 110

Scheme 5.8. Preparation of $Ru_2Cl_4(dppb)_2$ **41a** in solution..... 111

Scheme 5.9. Coordination of azine to **41a**..... 113

Scheme 5.10.Thermolysis of **42** to yield **43** and **44**. 114

Scheme 5.11.Proposed mechanism for overall reaction of azine **40** with $Ru_2Cl_4(dppb)_2$ **41a**. .. 116

Scheme 5.12 Proposed mechanism for hydrolysis of **44** by residual H_2O.....118

Scheme 6.1. Synthesis of Mo ROMP catalysts used..... 130

Scheme 6.2. Preparation of 2,3-dicarbomethoxynorbornadiene **53** and transesterification generating **54** and **55**. 131

Scheme 6.3. In situ preparation of diacid chloride en route to **55**. 132

Scheme 6.4. Preparation of diphenylamido monomer **56**. 132

Scheme 6.5. Syn- and anti-rotamers of molybdenum imido complexes..... 133

Scheme 6.6. Monomer docking orientations leading to (a) trans; (b) cis double bonds..... 136

Scheme 7.2. Stabilization of the Ru-O σ-bond by a trans CO ligand. 135

LIST OF FIGURES

Figure 1.1. Olefin Metathesis Catalysts based on Molybdenum and Ruthenium..... 4

Figure 1.2. Monomer attack on the accessible CNO face of a molybdenum catalyst.....4

Figure 1.3. Stereocentres generated from ROMP of 2,3-disubstituted norbornadienes 7

Figure 1.4. Four regular ROMP polymer structures: a) cis, isotactic b) cis, syndiotactic c) trans, isotactic d) trans, syndiotactic. 9

Figure 3.1. $^{31}P\{^{1}H\}$ NMR spectrum for reaction of **1a** with 1 equiv KOAr.....61

Figure 3.2. Molecular structures of $RuHX(CO)(PPh_3)_3$.....63

Figure 3.3. $^{31}P\{^{1}H\}$ NMR spectrum of $Ru(\eta^5\text{-}ArO)(o\text{-}C_6H_4PPh_2)(PPh_3)$ **9a**..... 66

Figure 3.4. ^{1}H NMR spectrum of $Ru(\eta^5\text{-}ArO)(o\text{-}C_6H_4PPh_2)(PPh_3)$ **9a**..... 66

Figure 3.5. Molecular structures of **9a**•$(ArOH)_2(CHCl_3)$ and **9b**•PhOH..... 70

Figure 3.6. Molecular structures of $RuCl(\eta^5\text{-}C_6H_5O)(PPh_3)_2$ **11b** and $[RuH(\eta^6\text{-}C_6H_4{}^tBuOH)(PPh_3)_2]Cl$ **12a**..... 74

Figure 3.7. Displacement of Ru from the centroid of the arene ring **11b**. 74

Figure 3.8. Molecular structure of $[K_x][Ru_2(CO)_4(OAr)_6(PPh_3)_2]$ **17**.. 78

Figure 4.1. The "Hoveyda" catalyst **20** contains a chelating carbene-aryloxide ligand..... 82

Figure 4.2. Reported, examples of η^2-P,O 83

Figure 4.3. Heterobifunctional binap and "binop" ligands..... 83

Figure 4.4. a) η^6:η^1-bound Ru complexes of 2-(diphenylphosphino)-1,1'-binaphthyl and b) CpRu(binap)... 86

Figure 4.5. MALDI-MS for **31** (anthracene). 87

Figure 4.6. MALDI-MS spectrum for **31** (dithranol).....88

Figure 4.7. NMR peak assignments of carbon and hydrogen atoms for naphthol-based nuclei in **31**.....90

Figure 4.8. ^{1}H NMR spectrum for **31**..... 91

Figure 4.9. Naphthol portion of the binop ligand 93

Figure 4.10. ^{1}H-^{13}C HMBC NMR spectrum for **31** ($CDCl_3$). 94

Figure 4.11. ^{1}H-^{1}H COSY NMR spectrum for **31**. 96

Figure 4.12. Top-view of the predicted orientation of **31**. 98

Figure 4.13. Stereoisomers of RuCl(binop)(PPh_3) **31**.....99

Figure 4.14. Literature example of a binaphthyl tethered ligand Ru complex.....101

Figure 5.1. $^{31}P\{^{1}H\}$ NMR spectrum of a) starting material **41a**; b) **42**.....112

Figure 5.2. $^{31}P\{^{1}H\}$ NMR spectrum of a) starting material (**41a**); b) **41** + 5 equiv azine, RT 24 h (**42**); c) 50 °C, 140 h **43** (∧) and **44** (*)). 114

Figure 5.2. Molecular structure of $Ru_2Cl_4(dppb)_2(NCPh)$ **43**..... 120

Figure 6.1. Literature examples of helical polymers..... 125

Figure 6.2. ROMP polymers for which a helical structure has been proposed. 126

Figure 6.3. ROMP catalysts used: biphenolates **49a-c** and alkoxide **49d**..... 128

Figure 6.4. Steric repulsion between bulky substituents in a norbornadiene polymer.....128

Figure 6.5. Biphenol ligands used.....130

Figure 6.6. Numbering system for polynorbornenes 137

Figure 6.7. Proposed structure of amylose, showing deformed helical regions.....140

Figure 6.8. Powder diffraction trace of polymer **57a**..... 145

Figure 6.9. Wide angle X-ray film diffraction of polymer **57a**. 146

Figure 6.10 Representative plot of IR band area vs. time for polymer **53**.....148

LIST OF ABBREVIATIONS

$^{13}\{^{1}H, ^{31}P]$	proton and phosphorous decoupled carbon-13 (NMR)
$^{13}C\{^{1}H\}$	proton-decoupled carbon-13 (NMR)
$^{31}P\{^{1}H\}$	proton-decoupled phosphorus-31 (NMR)
Å	angstrom
ABq	AB quartet
ADMET	Acyclic Diene METathesis
ARCM	Asymmetric Ring-Closing Metathesis
ArO	aryloxide ligand
binap	rac 2,2'-bis(diphenylphosphino)-1,1'-binaphthyl
binop	2-(diphenylphosphino)-2'-hydroxy'1,1'binaphthyl
br	broad
CD	circular dichroism
CM	Cross Metathesis
COD	cyclooctadiene
COSY	Correlated Spectroscopy
Cp*	pentamethylcyclopentadienyl, η^5-$C_5(CH_3)_5$
CSD	Cambridge Structural Database
d	doublet; NMR
dcypb	1,4-bis(dicyclohexylphosphino)butane
dd	doublet of doublets; NMR
DEPT	Distortionless Enhancement by Polarization Transfer
DME	dimethoxyethane
DMSO	dimethylsulfoxide
dppb	diphenylphosphinobutane
DSC	differential scanning calorimetry
EtOAc	ethyl acetate
FPT	freeze-pump-thaw
GPC	Gel Permeation Chromatography
HMBC	Heteronuclear Multiple Bond Coherence

HMQC	Heternuclear Multiple Quantum Coherence
Hz	Hertz, cycles per second
INADEQUATE	Incredible Natural Abundance DoublE QUAntum Transfer Experiment
^{i}PrOH	isopropyl alcohol
IR	infrared spectroscopy
J	coupling constant, in Hz
L	ligand
LAH	lithium aluminum hydride ($LiAlH_4$)
M	central metal atom in a complex
m	meta
m	multiplet; NMR
MeOH	methanol
MTD	methylter….
NBDF6	2,3-bis(trifluoromethyl)norbornadiene
n-BuLi	*n*-butyllithium
Neopentyl	=CH-*t*-Bu
Neophyl	$=CMe_2Ph$
NMR	Nuclear Magnetic Resonance
o	ortho
ORD	Optical Rotatory Dispersion
ORTEP	Oak Ridge Thermal Ellipsoid Projection
p	para
PCy_3	tricyclohexylphosphine
PDI	PolyDispersity Index
PhO	phenoxide ligand
PP	ditertiary phopshine
PPh_3	triphenylphosphine
RCM	Ring-Closing Metathesis
ROM	Ring-Opening Metathesis
ROMP	Ring Opening Metathesis Polymerization

RT	room temperature
s	singlet; NMR
t	triplet; NMR
T_c	crystallization temperature
T_d	thermal degradation temperature
tert-, ^{t}	tertiary
T_g	glass transition temperature
TGA	Thermal Gravimetric Analysis
THF	tetrahydrofuran
tlc	thin-layer chromatography
T_m	melting temperature
TOCSY	TOtal Correlation SpectroscopY
Triflate	$-SO_2CF_3$
XRD	X-Ray Diffraction
δ	chemical shift (in ppm)
η	descriptor for hapticity
μ	descriptor for bridging
υ	frequency (in cm^{-1})

CONTRIBUTIONS TO RESEARCH

J. L. Snelgrove, J. C. Conrad, G. P. A. Yap, D. E. Fogg*, "The Kinetic Instability of σ-Bound Aryloxide in Coordinatively Unsaturated or Labile Complexes of Ruthenium", *Inorg. Chim. Acta* (special issue in honour of Dick Schrock: invited contribution), **2003**, *345*, 268.

D. E. Fogg*, D. Amoroso, S. D. Drouin, J. L. Snelgrove, J. C. Conrad, F. Zamanian, "Ligand Manipulation and Design for Ruthenium Metathesis and Tandem Metathesis-Hydrogenation Catalysis" *J. Mol. Catal. A* (special issue on olefin metathesis: invited contribution), **2002**, *190*, 177.

D. Amoroso, J. L. Snelgrove, J. C. Conrad, G. P. A. Yapp, D. E. Fogg*, " Versatile, Efficient Routes to Metathesis Catalysts Based on Phenoxide as a Hydride Equivalent", *Advanced Synthesis & Catalysis* (special issue on olefin metathesis: invited contribution), **2002**, *344*, 757.

ACKNOWLEDGEMENTS

My last task with regards to this thesis is to thank those people who have helped and supported me along the way. To my supervisor, Prof. Deryn Fogg. I thank you whole-heartedly for your enthusiasm for chemistry and its details and for impromptu, stress relieving 'lab champagne' Fridays. I would like to thank my co-supervisor Prof. Sundararajan and his Carleton lab group for welcoming me into your lab.

To my Ottawa U. lab-mates past and present who have maintained my sanity and sense of humour, Jay, Yuwen, Nicola, Amir, Pawel, Maeve, Yuwen, Ureshini, Heather and Emily, to you I owe the most sincere thanks. I would especially like to thank Dino and Sam who started this journey with me so long ago, but remain my friends despite having relinquished their position as 'Fogg denizen.'

Thank you to Matt Heuft, for all of the organic chats and squash games, Glenn Facey, for your NMR expertise and Dan Lafleur and Robert Nadon who made T.A.ing something to look forward to. I also need to thank my friends out side of the university (the 'Trent gang') including Karin, LeeAnne, Dan, Chewy, Leanne, Fiona, Brock and Monica and their cohorts Jon, Tim, Darlene, Kathy, Raymond and Allen. You have watched over and supported me my entire university career. Thank you so much for being apart of my life. A greater group of friends I could not ask for.

And finally I want to thank my Mom, Dad, brothers Philip and Derek, sister Charlotte, brother-in-law George and nephew Zachary. Although I know you don't always understand what it is I'm doing, whether it be in the lab or in life, your continued love and support is something I do not take for granted. Thank you for everything.

CHAPTER 1

Introduction

1.1. Olefin Metathesis

Over the past decade, advances in catalyst design have transformed olefin metathesis into a powerful synthetic tool in organic[1-3] and materials[4] chemistry. Olefin metathesis refers to an interchange reaction of alkylidene groups between alkenes (Scheme 1.1).[1]

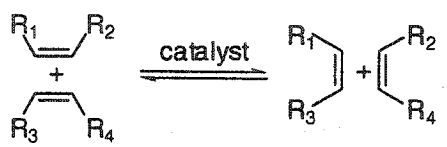

Scheme 1.1. A simplified representation of the olefin metathesis reaction.[1]

Metathesis is formally grouped into several subtypes, including acyclic diene metathesis (ADMET), cross metathesis (CM) and ring-closing metathesis (RCM) of acyclic olefins, and ring-opening metathesis (ROM) or ring-opening metathesis polymerization (ROMP) of cyclic olefins (Scheme 1.2).[1,5]

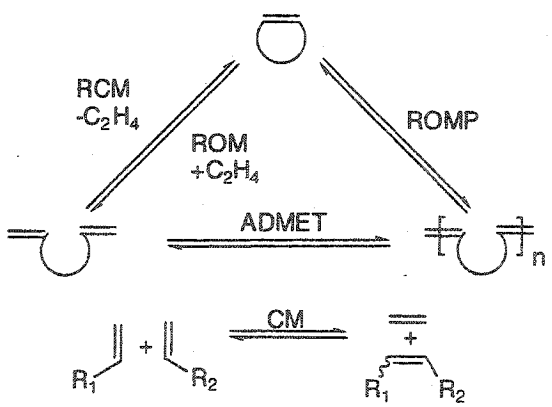

Scheme 1.2. Metathesis pathways: ADMET, CM, ROM, RCM and ROMP.[1]

Two dominant lines of experimental progress have emerged for RCM and ROMP, centred around the molybdenum and ruthenium catalysts pioneered by Schrock[6-8] and Grubbs,[9,10] respectively. A key feature of the Schrock systems is the presence of imido and aryloxide or alkoxide ligands that enable steric and electronic tuning of the active site.[2] Chiral biphenolate and binaphtholate derivatives, in particular, have led to impressive advances in asymmetric ring-closing metathesis (ARCM)[11-14] and ROMP.[15-18] The latter has not yet been fully exploited for the development of new materials with potentially interesting functions, including polymers for tissue engineering applications[19-21] and helical polymers. The latter possibility is discussed in more detail below.

1.2. Ring-Opening Metathesis Polymerization

Olefin metathesis was born of investigation into Ziegler[22] addition polymerization. Attempts to polymerize norbornene[23] and other cyclic olefins[24] in 1950 using the Ziegler catalyst $TiCl_4$/EtMgBr resulted in a novel polymer. Subsequent ozonolysis of the norbornene polymer revealed that the number of double bonds were preserved (Scheme 1.3).[25]

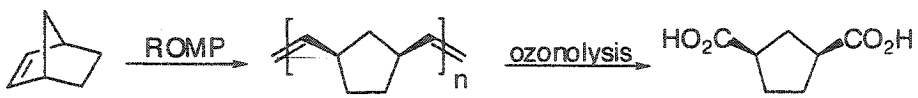

Scheme 1.3. ROMP of norbornene and ozonolysis of the resultant polymer.

The generally accepted mechanism of ROMP was proposed in 1970 by Chauvin (Scheme 1.4).[26] The Chauvin mechanism posits, as the first step, attack of a metal carbene on the olefinic double bond, forming a metallacyclobutane intermediate. A new alkylidene is generated by ring-opening of the metallacyclobutane, which can then react

with another equivalent of monomer. This process continues until all of the olefin has been consumed. Where the cycloolefin is highly strained, the reaction is essentially irreversible. This new polymerization reaction was termed ring-opening metathesis polymerization (ROMP).[27]

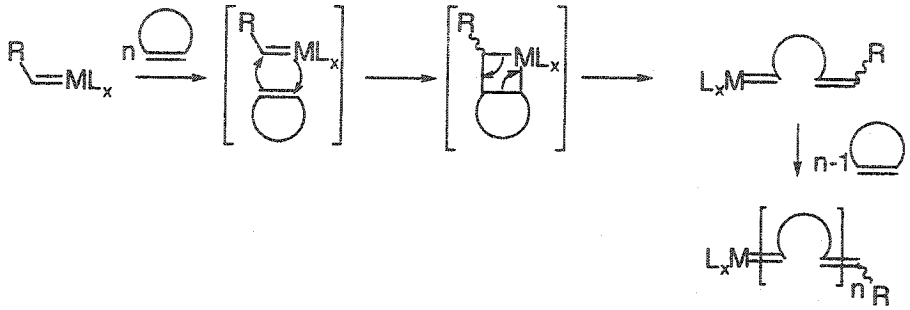

Scheme 1.4. Chauvin mechanism for ROMP (L_x denotes a generalized ligand coordination sphere).

Support for the metallacyclobutane mechanism came with the discovery of metal alkylidene complexes[28] active for olefin metathesis, and from the fact that ROMP produces high molecular weight polymers at low yields[29] while for a step-growth polymerization, high molecular weight polymers should only be possible at high yields. In addition, characterization of intermediates, including metallacyclobutanes[8,30,31] support the Chauvin mechanism.

1.3. Molybdenum Olefin Metathesis Catalyst Evolution

Enormous research effort has focused on the synthesis of novel olefin metathesis catalysts. The first well-defined catalysts for olefin metathesis were designed by Schrock.[27,32,33] Rigorous consideration of mechanistic and design principles led to early transition metal catalysts that exhibit high activity and remarkable selectivity. These catalysts exploit the stability of Group 6 metal-heteroatom bonds (W-X[27,34] and Mo-

X[32,33]), incorporating bulky imido and alkoxide ligands (Figure 1.1a). The imido ligand increases the selectivity of alkylidene complexes because it is oriented in such a way that one isopropyl group partially blocks one face of the M=C bond and forces the monomer to add repeatedly to the same face[33] (Figure 1.2).

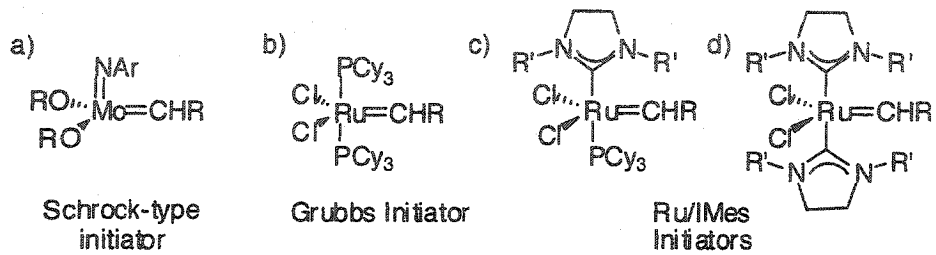

Figure 1.1. Olefin metathesis catalysts based on molybdenum and ruthenium.

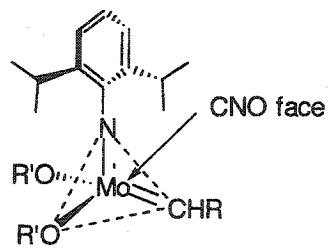

Figure 1.2. Monomer attack on the accessible CNO face of a molybdenum catalyst.

Further steric definition of the metal centre was achieved by the addition of bulky alkoxide ligands. The use of alkoxides in place of chloride ligands prevents deactivation through bimolecular coupling reactions: it also enables judicious incorporation of steric bulky into the ligand set.[32,33] Incorporation of chelating, enantiopure binaphtholate or biphenolate groups enabled stereoselective ROMP.[16,17]

1.4. Ruthenium Olefin Metathesis Catalysts

Despite their high selectivity, the Group 6 catalysts are limited by the oxophilicity of the metal centre, which necessitates rigorously dry, anaerobic reaction conditions. The

discovery by Grubbs that ruthenium alkylidene complexes are highly active for all types of olefin metathesis reactions[9,10,35-37] has expanded uptake of this reaction, particularly in synthetic organic chemistry. Late-metal alkylidene complexes,[1,3,5,38-40] are attractive for their greater robustness, increased tolerance for functional groups, and less stringent requirements for reagent / atmosphere purity.[41-49] Such catalysts are limited, however, in terms of tolerance toward basic functional groups such as nitriles and amines.[3] Substrates containing 'soft' sulfur or phosphine functionalities often react smoothly with the "hard" Mo(VI) catalysts, but can poison the Ru alkylidene system.[50]

The first ruthenium complex known as a metathesis initiator was $RuCl_3 \cdot xH_2O$.[44,51,52] Metathesis induction periods were long, however, and only a small amount of the ruthenium became catalytically active.[53] The yields of polymers were quite poor, and the polymerizations were not living. High trans polymers were generally produced; the first sign of some level of cis / trans selectivity using Ru catalysts was noted on addition of small amounts of chelating diolefins (norbornadienes or endo-dicyclopentadiene) to $RuCl_3$, which led to high-cis polymers.[54]

The synthesis of well-defined ruthenium olefin metathesis catalysts has been a focus of much research effort[55-61] since Grubbs' pioneering development of catalysts of the type $RuCl_2(=CHPh)(PCy_3)_2$ (Figure 1.1b).[9,10] More recently, incorporation of N-heterocyclic carbenes in place of one phosphine ligand has significantly increased the activity of these catalysts (Figure 1.1 c, d).[62,63] The majority of ruthenium alkylidene catalysts have a common structural motif: two chloride anionic ligands and two neutral, two-electron donor ligands.[1]

Recently, our group reported an important deactivation pathway for alkylidene catalysts of the type $RuCl_2(=CHR)L_2$.[64,65] Deactivation occurs via extrusion of the alkylidene ligand and formation of face-bridged dimers of the general structure $RuClL_2(\mu\text{-}Cl)_3Ru(=CHR)L_2$ (Scheme 1.5). The stability of the $Ru_2(\mu\text{-}Cl)_3$ structural motif results in very low metathesis activity.

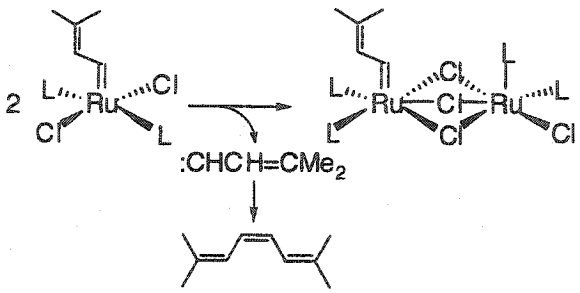

Scheme 1.5. Deactivation pathway of $RuCl_2L_2(=CHR)$ complexes.

Replacement of the chloride ligands with alternative anionic donors is attractive as a means of both arresting deactivation via dimerization pathways, and increasing selectivity via increased structural definition of the active site. The latter goal, which would ultimately enable stereoselective metathesis via ruthenium alkylidenes, is an ongoing challenge. Asymmetric metathesis via chiral Ru catalysts has been little investigated, and indeed only two such catalysts have so far been reported.[62] These were applied to asymmetric ring-closing metathesis (ARCM), but resulted in low enantioselectivites. Slow initiation is likely to limit the utility of these systems for construction of ROMP polymers with well-defined molecular weights and microstructures.

1.5. Selectivity and Tacticity Determination

ROMP of symmetrically disubstituted norbornene or norbornadiene based monomers can give rise to stereochemically well-defined materials. In turn, the stereoregularity of a polymer determines its bulk properties and its commercial applications.[66] More than fifty years ago, Natta described the relationship between tacticity and the polymer physical properties for materials obtained by polymerization of α-olefins. The original microstructures were determined by solid-state X-ray crystallography,[67-69] but with the advent of high-field NMR techniques, microstructures can now be established in solution.[66,70-72] The tacticity of ROMP polymers was first explored by Ivin and Rooney using ^{13}C NMR methods.[73-75]

ROMP polymers are microstructurally more complex than addition polymers, as the double bond stereochemistry must be considered in addition to tacticity.[76] Ring-opening of a cyclic olefin generates a cyclopentylenevinylene repeat unit. The series of configurations of the tertiary carbon atoms on the five-membered rings (Figure 1.3) define the tacticity of the polymer. Thus, -RS-RS-RS- represents an isotactic sequence,[77] while –RS-SR-RS- represents a syndiotactic sequence.[69]

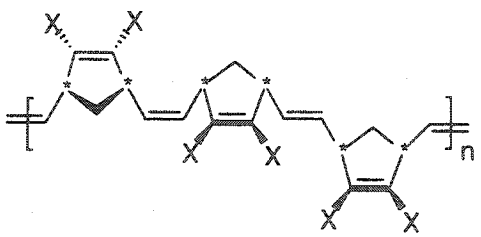

Figure 1.3. Stereocentres generated from ROMP of 2,3-disubstituted norbornadienes (stereocenter denoted with *).

Comparison of the microstructures of ROMP polymers generated from classical Ziegler-type catalysts and those generated from well-defined transition metal alkylidenes show the dependence of selectivity on catalyst structure. Systems of the type $Mo(NAr)(OR')_2(=CHR)$ (R = $-CMe_2Ph$, R' = binaphtholate, biphenolate, Ar = 2,6-diisopropylphenyl[15-18]) give cis, isotactic and trans, syndiotactic polymers. In contrast, initiators such as $ReCl_5$,[73] $W(mesitylene)(CO)_3/EtAlCl_2$,[78] and $OsCl_3/PhC{\equiv}CH$[79] give cis, syndiotactic and trans, isotactic polymers. A direct, elegant ^1H NMR method developed by Schrock and coworkers[16] corroborates this seemingly contradictive finding.

The development and application of NMR spectroscopy for the determination of tacticity was first accomplished using optically active monomers and was based on the degree of splitting of the main resonances. This is particularly useful if both tactic and atactic forms of the polymer are available for comparison. Analysis of the tacticity of disubstituted norbornene-type polymers requires the analysis of at least two consecutive repeat units, or dyads (Figure 1.4). *Meso* (*m*) dyads are related by a symmetry element that bisects the C=C bond between two cyclopentylene rings.[66] This can be a mirror plane (cis linkages, Fig 1.4a), or an inversion centre (trans linkages, Fig 1.4c): in either case the dyad is isotactic. In *racemic* (*r*) dyads, a C_2 axis relates both the cis (Fig 1.4b) and trans (Fig 1.4d) linkages, which are thus syndiotactic.[66]

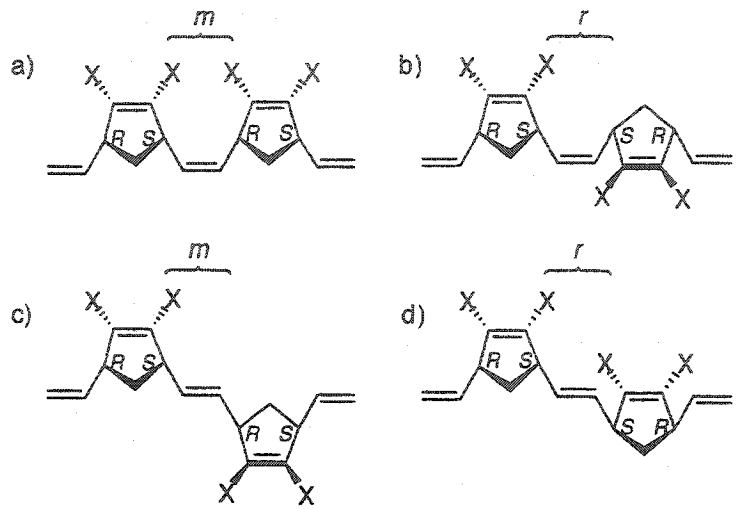

Figure 1.4. Four regular ROMP polymer structures: a) cis, isotactic b) cis, syndiotactic c) trans, isotactic d) trans, syndiotactic.[17]

Most literature reports use NMR analysis, particularly ^{13}C NMR, for microstructure analysis. Key information relates to variations in the ratio of cis and trans double bonds. Because the fine structure arising from tacticity may be concealed by that due to the cis / trans double bonds, the tacticity in ROMP polymers is less easily determined than that for addition polymers. A further complication in the tacticity determination is that there is no direct relationship between the double bond stereochemistry and the dyad tacticity (cis or trans lines in spectra may have varying *m* and *r* components).

1.6. Materials Applications

ROMP polymers with a highly stereoregular microstructure may have interesting tertiary structures. Highly selective molybdenum ROMP catalysts[7,15-18,80,81] may open the door to helical ROMP polymers. Few synthetic polymers possess a helical structure that remains stable in solution.[82-88] Those that do are constrained by bulky side groups, which

restrict rotation around the single bonds in the polymer backbone. However, helical parameters such as pitch and radius cannot be varied. In ROMP polymers, helicity could potentially enable tunable helix parameters[89] of potential interest as molecular wire or a molecule capable of encapsulation.

1.7. Scope of Thesis Work

This thesis work is directed at expanding the ligand sets accessible to ruthenium catalysts (ultimately directed at development of stereoselective ruthenium metathesis catalysts), as well as exploration of existing, highly stereoselective molybdenum catalysts for construction of topologically-defined polymers.

Chapter 3 describes fundamental investigations of the behaviour of ruthenium-phosphine complexes with aryloxide ligands. These studies are directed at gaining insight into the stability of the Ru-OAr bond. Reactions of coordinatively saturated and unsaturated ruthenium precursors with monodentate aryloxide ligands are explored, in protic and non-protic solvents. Chapter 4 focuses on the possibility of stabilizing the Ru-O bond via incorporation of a chelating heterobifunctional P,O-ligand. The synthesis of a versatile Ru-alkylidene "starting material" with labile phosphine ligands is described in Chapter 5. The potential for catalyst deactivation by coordination of azine (a byproduct in the preparation of phenyldiazomethane, the ultimate source of benzylidene ligand) is also discussed. Chapter 6 describes ROMP of 2,3-disubstituted norbornadienes by three molybdenum biphenolate initiators, presenting a systematic investigation into the differing selectivities of these catalysts for ROMP of four difference monomers. The

thermal stability and tertiary structure of the polymer is also explored. Finally, general conclusions and recommendations for future work are provided in Chapter 7.

1.8. References

(1) Fürstner, A. *Angew. Chem. Int. Ed.* **2000**, *39*, 3012.
(2) Schrock, R. R. *Tetrahedron* **1999**, *55*, 8141.
(3) Trnka, T. M.; Grubbs, R. H. *Acc. Chem. Res.* **2001**, *34*, 18.
(4) Buchmeiser, M. R. *Chem. Rev.* **2000**, *100*, 1565.
(5) Frenzel, U.; Nuyken, O. *J. Polym. Sci. Part A: Polym. Chem.* **2002**, *40*, 2895.
(6) Schrock, R. R.; Murzdek, J. S.; Bazan, G. C.; Robbins, J.; DiMare, M.; O'Reagan, M. *J. Am. Chem. Soc.* **1990**, *112*, 3875.
(7) Bazan, G. C.; Khosravi, E.; R., S. R.; Feast, W. J.; Gibson, V. C.; O'Regan, M. B.; Thomas, J. D.; Davis, W. M. *J. Am. Chem. Soc.* **1990**, *112*, 8378.
(8) Bazan, G. C.; Oskam, J. H.; Cho, H. N.; Park, L. Y.; Schrock, R. R. *J. Am. Chem. Soc.* **1991**, *112*, 6899.
(9) Schwab, P.; France, M. B.; Ziller, J. W.; Grubbs, R. H. *Angew. Chem. Int. Ed.* **1995**, *34*, 2039.
(10) Schwab, P.; Grubbs, R. H.; Ziller, J. W. *J. Am. Chem. Soc.* **1996**, *118*, 100.
(11) La, D. S.; Alexander, J. B.; Cefalo, D. R.; Graf, D. D.; Hoveyda, A. H.; Schrock, R. R. *J. Am. Chem. Soc.* **1998**, *120*, 9720.
(12) Alexander, J. B.; La, D. S.; Cefalo, D. R.; Hoveyda, A. H.; Schrock, R. R. *J. Am. Chem. Soc.* **1998**, *120*, 4041.
(13) Weatherhead, G. S.; Ford, J. G.; Alexanian, E. J.; Schrock, R. R.; Hoveyda, A. H. *J. Am. Chem. Soc.* **2000**, *122*, 1828.
(14) Zhu, S. S.; Cefalo, D. R.; La, D. S.; Jamieson, J. Y.; Davis, W. M.; Hoveyda, A. H.; Schrock, R. R. *J. Am. Chem. Soc.* **1999**, *121*, 8251.
(15) Totland, K. M.; Boyd, T. J.; Lavoie, G. G.; Davis, W. M.; Schrock, R. R. *Macromolecules* **1996**, *29*, 6614.
(16) O'Dell, R.; McConville, D. H.; Hofmeister, G. E.; Schrock, R. R. *J. Am. Chem. Soc.* **1994**, *116*, 3414.
(17) McConville, D. H.; Wolf, J. R.; Schrock, R. R. *J. Am. Chem. Soc.* **1993**, *115*, 4413.
(18) Alexander, J. B.; Schrock, R. R.; Davis, W. M.; Hultzsch, K. C.; Hoveyda, A. H.; Houser, J. H. *Organometallics* **2000**, *19*, 3700.
(19) Walsh, E. B. S., Matthew J.; Grinstaff, Mark W In *Abstracts of Papers - American Chemical Society 220th*, 2000, pp POLY-319.
(20) Maynard, H. D.; Grubbs, R. H. *Polymer Preprints (American Chemical Society, Division of Polymer Chemistry)* **1998**, *39*, 523.
(21) Maynard, H. D.; Grubbs, R. H. In *Book of Abstracts 216th ACS National Meeting*: Boston, 1998.
(22) Fink, G.; Mülhaupt, R.; Brintzinger, H. H., Eds. *Ziegler Catalysts*; Springer: Berlin, 1995.
(23) Anderson, A. W.; Merckling, N. G.: U. S. Patent No. 2,72,1189, 1955.

(24) Eleuterio, H. S.: U.S. Patent No. 3,074,918, 1963.
(25) Truett, W. L.; Johnson, D. R.; Robinson, I. M.; Montague, B. A. *J. Am. Chem. Soc.* **1960**, *82*, 2337.
(26) Hérisson, J.-L.; Chauvin, Y. *Makromol. Chem.* **1970**, *141*, 161.
(27) Schrock, R. R. *Acc. Chem. Res.* **1990**, *23*, 158.
(28) Schrock, R. R. *Acc. Chem. Res.* **1979**, *12*, 98.
(29) Dolgoplosk, B. A.; Makovetsky, K. L.; Golenko, T. G.; Korshak, Y. V.; Tinyakova, E. I. *Eur. Polym. J.* **1974**, *10*, 901.
(30) Howard, T. R.; Lee, J. B.; Grubbs, R. H. *J. Am. Chem. Soc.* **1980**, *102*, 6876.
(31) Kress, J.; Osborn, J. A.; Greene, R. M. E.; Ivin, K. J.; Rooney, J. J. *J. Am. Chem. Soc.* **1987**, *109*, 899.
(32) Schrock, R. R. *Topics in Organometallic Chem.* **1998**, *1*, 1.
(33) Schrock, R. R. In *Metathesis Polymerization and Olefins and Polymerization of Alkynes*; Imamoglu, Y., Ed.; Kluwer Academic Publishers: Netherlands, 1998; Vol. 23, p 1991.
(34) O'Donoghue, M. B.; Schrock, R. R.; LaPointe, A. M.; Davis, W. M. *Organometallics* **1996**, *15*, 1334.
(35) Wu, Z.; Nguyen, S. T.; Grubbs, R. H.; Ziller, J. W. *J. Am. Chem. Soc.* **1995**, *117*, 5503.
(36) Nguyen, S. T.; Johnson, L. K.; Grubbs, R. H.; Ziller, J. W. *J. Am. Chem. Soc.* **1992**, *114*, 3974.
(37) Nguyen, S. T.; Grubbs, R. H.; Ziller, J. W. *J. Am. Chem. Soc.* **1993**, *114*, 9858.
(38) Ivin, K. J. *J. Mol. Catal.* **1998**, *133*, 1.
(39) Grubbs, R. H.; Chang, S. *Tetrahedron* **1998**, *54*, 4413.
(40) Schuster, M.; Blechert, S. *Angew. Chem. Int. Ed.* **1997**, *36*, 2026.
(41) Novak, B. M.; Grubbs, R. H. *J. Am. Chem. Soc.* **1988**, *110*, 7542.
(42) Fu, G. C.; Nguyen, S. T.; Grubbs, R. G. *J. Am. Chem. Soc.* **1993**, *115*, 9856.
(43) Hillmyer, M. A.; Lepetit, C.; McGrath, D. V.; Novak, B. M.; Grubbs, R. H. *Macromolecules* **1992**, *25*, 3345.
(44) Feast, W. J.; Harrison, D. B. *J. Mol. Catal.* **1991**, *65*, 63.
(45) Mohr, B.; Lynn, D. M.; Grubbs, R. H. *Organometallics* **1996**, *15*, 4317.
(46) Lynn, D. M.; Mohr, B.; Grubbs, R. H. *J. Am. Chem. Soc.* **1998**, *120*, 1627.
(47) Lynn, D. M.; Mohr, B.; Grubbs, R. H.; Henlig, L. M.; Day, M. W. *J. Am. Chem. Soc.* **2000**, *122*, 6601.
(48) Kirkland, T. A.; Lynn, D. M.; Grubbs, R. H. *J. Org. Chem.* **1998**, *63*, 9904.
(49) France, M. B.; Paciello, R. A.; Grubbs, R. H. *Macromolecules* **1993**, *26*, 4739.
(50) Armstrong, S. K.; Christie, B. A. *Tetrahedron Lett.* **1996**, *37*, 9373.
(51) Novak, B. M.; Grubbs, R. H. *J. Am. Chem. Soc.* **1988**, *110*, 960.
(52) Lu, S. Y.; Quayle, P.; Heatley, F.; Booth, C.; Yeates, S. G.; Padget, J. C. *Macromolecules* **1992**, *25*, 2692.
(53) Novak, B. M.; Grubbs, R. H. *J. Am.Chem. Soc.* **1988**, *110*, 7542.
(54) Gillan, E. M. D.; Hamilton, J. G.; Mackey, O. N. D.; Rooney, J. J. *J. Mol. Catal.* **1988**, *46*, 359.
(55) Demonceau, A.; Noels, A. F.; Saive, E.; Hubert, A. J. *J. Mol. Catal.* **1992**, *76*, 123.
(56) Hafner, A.; Mühlebach, A.; van der Schaaf, P. A. *Angew. Chem. Int. Ed.* **1997**, *36*, 2121.

(57) Stumpf, A. W.; Saive, E.; Demonceau, A.; Noels, A. F. *J. Chem. Soc., Chem. Commun.* **1995**, 1127.
(58) Stüer, W.; Wolf, J.; Werner, H.; Schwab, P.; Schulz, M. *Angew. Chem. Int. Ed.* **1998**, *37*, 3421.
(59) Fürstner, A.; Ackermann, L. *J. Chem. Soc., Chem. Commun.* **1999**, 95.
(60) Fürstner, A.; Picquet, M.; Bruneau, C.; Dixneuf, P. H. *J. Chem. Soc., Chem. Commun.* **1998**, 1315.
(61) Picquet, M.; Touchard, D.; Bruneau, C.; Dixneuf, P. H. *New. J. Chem.* **1999**, *23*, 141.
(62) Scholl, M.; Ding, S.; Lee, C. W.; Grubbs, R. H. *Org. Lett.* **1999**, *1*, 953.
(63) Weskamp, T.; Koh, F. J.; Hieringer, W.; Gleich, D.; Herrmann, W. A. *Angew, Chem. Int. Ed.* **1999**, *38*, 2416.
(64) Amoroso, D.; Snelgrove, J. L.; Conrad, J.; Drouin, S. D.; Yap, G. P. A.; Fogg, D. E. *Adv. Synth. Catal.* **2002**, *344*, 757.
(65) Amoroso, D.; Yap, G. P. A.; Fogg, D. E. *Organometallics* **2002**, *21*, 3335.
(66) Hamilton, J. G. *Polymer* **1998**, *39*, 1669.
(67) Natta, G.; Corradini, P. *Makromol. Chem.* **1955**, *16*, 77.
(68) Natta, G.; Corradini, P.; Bassi, I. W. *Makromol. Chem.* **1956**, *21*, 240.
(69) Natta, G.; Corradini, P. *J. Polym. Sci.* **1956**, *20*, 251.
(70) Hamilton, J. G.; Ivin, K. J.; Rooney, J. J. *J. Mol. Catal.* **1985**, *28*, 255.
(71) Ivin, K. J.; Kenwright, A. M.; Hofmeister, G. E.; McConville, D. H.; Schrock, R. R.; Amir-Ebrahimi, V.; Carvill, A. G.; Hamilton, J. G. *Macromol. Chem. Phys.* **1998**, *199*, 547.
(72) Amir-Ebrahimi, V.; Corry, D. A. K.; Hamilton, J. G.; Rooney, J. J. *J. Mol. Catal. A* **1998**, *133*, 115.
(73) Ho, H. T.; Ivin, K. J.; Rooney, J. J. *Makromol. Chem.* **1982**, *183*, 1629.
(74) Ivin, K. J.; Laverty, D. T.; Rooney, J. J. *Makromol. Chem.* **1977**, *178*.
(75) Ivin, K. J.; Lapienis, G.; Rooney, J. J. *Polymer* **1980**, *21*, 436.
(76) Ivin, K. J.; Rooney, J. J. *Olefin Metathesis and Metathesis Polymerization*; Academic Press Ltd.: Toronto, 1997.
(77) Natta, G. *J. Polym. Sci.* **1955**, *16*, 143.
(78) Devine, G. I.; Ivin, K. J.; Mohamed, M. A.; Rooney, J. J. *J. Chem. Soc., Chem. Commun.* **1982**, 1229.
(79) Amir-Ebrahimi, V.; Carvill, A. G.; Hamilton, J. G.; Rooney, J. J.; Tufy, C. *J. Mol. Catal.* **1997**, *115*, 85.
(80) Sunaga, T.; Ivin, K. J.; Hofmeister, G. E.; Oskam, J. H.; Schrock, R. R. *Macromolecules* **1994**, *27*, 4043.
(81) Schrock, R. R.; Lee, J. K.; O'Dell, R.; Oskam, J. H. *Macromolecules* **1995**, *28*, 5933.
(82) Deming, T. J.; Novak, B. M. *J. Am. Chem. Soc.* **1992**, *114*, 7926.
(83) Nolte, R. J. M.; van Beijnen, A. J. M.; Drenth, W. *J. Am. Chem. Soc.* **1974**, *96*, 6932.
(84) Nolte, R. J. M. *Chem. Soc. Rev.* **1994**, 11.
(85) van Beijnen, A. J. M.; Nolte, R. J. M.; Drenth, W.; Hezemans, A. M. F. *Tetrahedron* **1976**, *32*, 2017.
(86) Goodman, M.; Chem, S. C. *Macromolecules* **1970**, *3*, 398.

(87) Nieh, M. P.; Goodwin, A. A.; Stewart, J. R.; Novak, B. M.; Hoagland, D. A. *Macromolecules* **1998**, *31*, 3151.
(88) Nakano, T.; Mori, M.; Okamoto, Y. *Macromolecules* **1993**, *26*, 867.
(89) Mainville-Dale, R. M. E. *M.Sc. Thesis*; University of Ottawa: Ottawa, 2002.

CHAPTER 2

Experimental

2.1. Materials

2.1.1. Solvents

Reagent grade toluene, hexanes, diethyl ether and tetrahydrofuran (BDH) were dried and degassed using an Anhydrous Engineering solvent purification system. Other solvents were refluxed over and distilled from an appropriate drying agent under an atmosphere of N_2: benzene over sodium benzophenone ketyl; pentane over sodium; dichloromethane over calcium hydride, methanol and 2-propanol over Mg/I_2. All solvents (with the exception of methanol and 2-propanol) were stored over Linde 4Å molecular sieves under an atmosphere of N_2. Dimethoxyethane (DME, anhydrous grade) was purchased from Aldrich.

Deuterated solvents ($CDCl_3$, CD_2Cl_2, C_6D_6, CD_3OD, CH_3OD and D_2O) were obtained from Cambridge Isotope Laboratories Ltd. $CDCl_3$ was refluxed over and distilled from Drierite under an atmosphere of N_2. C_6D_6 was deoxygenated by consecutive freeze / pump / thaw cycles and stored over Linde 4Å molecular sieves. Ampoules of CD_2Cl_2 were used as received. CD_3OD and CH_3OD were distilled under an atmosphere of N_2. All deuterated solvents save D_2O were stored under N_2.

2.1.2. Gases

Carbon Monoxide (Praxair, 99.5%) was passed through an indicating column of Drierite.

2.1.3. Phosphines

All phosphines, other than those independently synthesized, were of reagent grade and used as received. Triphenylphosphine (PPh_3), 1,4-bis(diphenylphosphino)butane (dppb), and tricyclohexylphosphine ($HPCy_3$) were obtained from Strem Chemical Co. All phosphines (with the exception of dppb and PPh_3) were stored under an N_2 atmosphere.

2.1.4. Other Materials

Triethylene glycol, *p*-toluenesulfonehydrazide, *n*-butyllithium (2.5 M in hexanes), paraformaldehyde ($[CH_2O]_n$), potassium tri(*sec*-butyl)borohydride (1.0 M in Et_2O), 3-chloro-3-methyl-1-butyne, diphenylamine, 4-*tert*-butylphenol, phenol, dicyclopentadiene, dimethyl acetylenedicarboxylate, acetylenedicarboxylic acid, lithium *tert*-butoxide, 2,4-di-*tert*-butyl-phenol, 2,4-di-*tert*-butyl-5-methylphenol, $K_2Cr_2O_7$, diphenylphosphine oxide ($HP(O)Ph_2$) and (1R, 2S, 5R)-(-)-menthol were purchased from Aldrich and used as received. Benzaldehyde was distilled under N_2, 2,6-diisopropyl aniline was distilled from KOH under N_2, and neophyl chloride was stirred with concentrated HCl, separated, washed with H_2O, Na_2CO_3 and distilled from $CaCl_2$ under N_2. Potassium hydride (KH) was purchased as a suspension in oil from Aldrich and was washed with hexanes prior to use.

Hydrated $RuCl_3$ (38-43% Ru), thallium(I)ethoxide (TlOEt), palladium acetate ($PdOAc_2$), and racemic and (R)-(+)-5,5'6,6'-tetramethyl-3,3'-di-*tert*-butyl-1,1'-biphenyl-2,2'-diol were obtained from Strem Chemical Co. and used as received.

$RuH(\eta^5\text{-}OPh)(PPh_3)_2$ (**3b**) was prepared by Jay Conrad.[1] $RuCl_3(\equiv CHCMe_2)(PPh_3)_2$ (**35**) was prepared and characterized by Dino Amoroso.[2]

2.2. Instrumentation

Unless otherwise stated, all reactions were carried out at ambient temperatures (~ 22 °C) under an inert atmosphere using standard Schlenk or drybox techniques.

Infrared spectra were recorded on a Bomem MB100 IR spectrometer. Nuclear magnetic resonance (NMR) spectra were recorded on a Varian Gemini 200 (200 MHz for ^{1}H), a Varian XL-300 (121 MHz for ^{31}P, 75 MHz for ^{13}C), a Bruker Avance 300 (300 MHz for ^{1}H, 121 MHz for ^{31}P, 75 MHz for ^{13}C), or a Bruker AMX-500 (500 MHz for ^{1}H, 202 MHz for ^{31}P, 125 MHz for ^{13}C) FT-NMR spectrometer. For ^{1}H and ^{13}C NMR spectra, the residual proton and carbon signals of the deuterated solvent were used as internal standards. $^{31}P\{^{1}H\}$ NMR spectra were referenced against PPh_3 (δ -5.06, C_6D_6; -5.46, $CDCl_3$; -5.64, CD_2Cl_2); shifts are reported relative to 85% H_3PO_4. Downfield shifts are taken as positive for all nuclei. Variable temperature NMR spectra and 2D experiments (HMQC and HMBC) were carried out on the Bruker Avance 300 or the Bruker AMX-500 instrument. Proton and phosphorus decoupling experiments were carried out on a Bruker Avance 500 (500 MHz for ^{1}H, 202 MHz for ^{31}P, 125 MHz for ^{13}C) FT-NMR spectrometer with a triple resonance probe.

Elemental analyses were performed by V. Kuznetsov of this department, using a Perkin Elmer Series II CHNS/O instrument, or by Guelph Chemical Laboratories. Dr. Glenn P. A. Yap of the departmental crystallographic service carried out single crystal X-ray diffraction studies.

Gel Permeation Chromatography (GPC) data were obtained with CH_2Cl_2 as the eluant (flow rate 1.0 mL/min; samples 1-2 mg/mL) using a Wyatt DAWN light-scattering instrument equipped with an Optilab DSP refractometer, HPLC system with a Waters model 515 pump, Rheodyne model 7725i injector with a 200 μL injection loop, and Waters Styragel HR3 and HR4 columns in series.

Thermal analysis was performed using a TA instruments DuPont 910 differential scanning calorimeter at a heating rate of 10 °C/min. The DSC instrument was calibrated for temperature and energy with indium and tin reference samples. DSC traces were recorded with 5-10 mg of sample, in a nitrogen atmosphere.

Thermogravimetric (TG) analysis was conducted using a Seiko (SSC5200) instrument. During the evaluation of mass loss, the amount of char remaining at the end of the thermal program was measured. The measurements were taken over a temperature range of ambient to 450 °C, at a heating rate of 10 °C/min.

X-ray diffraction data were collected using a Philips automated powder diffractometer Model PW 1710. Nickel-filtered Cu Kα radiation (λ = 1.54Å) was used at 40 kV and 40 mA. The MDI Data Scan 3.2 software (Materials Data Inc., Livermore, CA)) was used for data collection. The results were analysed using MDI Jade 5 to determine crystallinity (X_c).

FTIR spectroscopic measurements were carried out at 80 °C using a Michelson M129 BOMEM Fourier Transform Infrared (FT-IR) spectrometer. All the data were collected using BOMEM GRAMS/386 software. FT-IR spectra of polymers of **53-56** were obtained in the form of transparent KBr pellets. A background spectrum was measured for each experiment using the identical sample holder.

2.3. Ruthenium Precursors

The following complexes were prepared by literature methods (unless otherwise indicated) for use as starting materials for the synthesis of various ruthenium complexes.

2.3.1. $RuCl_2(PPh_3)_3$ 1a

A solution of $RuCl_3 \cdot x\ H_2O$ (0.970 g, 3.87 mmol) in MeOH (100 mL) was refluxed under N_2 for 1 h, then allowed to cool. Solid PPh_3 (6.097 g, 23.2 mmol) was added under a strong flow of N_2, and the mixture refluxed for an additional 3 h. The resulting brown precipitate was filtered off, washed with MeOH (4 × 20 mL), then with warm hexanes (50 °C) (6 × 10 mL, or until the washings showed no trace of residual phosphine by tlc), and dried under vacuum. Yield 3.544 g (96%). ^1H and $^{31}P\{^1H\}$ NMR data match values previously reported.[3-5] $^{31}P\{^1H\}$ NMR ($CDCl_3$, 121 MHz): δ 42.1 (br s, 3P); resolves upon cooling to 183 K into the reported[6] AX_2 pattern: δ 75.6 (t, $^2J_{PP}$ = 30.6 Hz, 1P); 24.1 (d, $^2J_{PP}$ = 30.6 Hz, 2P). ^1H NMR ($CDCl_3$, 300 MHz): δ 7.45-6.92 (m, 45H, Ph).

2.3.2. $RuCl_2(CO)_2(PPh_3)_2$ 14

A solution of $RuCl_2(PPh_3)_3$ **1a** (656 mg, 0.684 mmol) in CH_2Cl_2 (60 mL) was stirred under CO until the solution turned yellow. The solvent was stripped off and the residue washed with hexanes. The product was then precipitated from CH_2Cl_2/hexanes and dried under vacuum. Yield 494 mg (96%; 8% cis, 92% trans). ^1H and $^{31}P\{^1H\}$ NMR data match values previously reported.[7] $^{31}P\{^1H\}$ NMR ($CDCl_3$, 121 MHz): δ 18.2 (s, 2P). ^1H NMR ($CDCl_3$, 300 MHz): δ 7.80 (m, 12H); 7.34 (m, 18H).

2.3.3. $RuCl_2(dppb)(PPh_3)$

A dark green solution of $RuCl_2(PPh_3)_3$ **1a** (1.07 g, 1.12 mmol) and dppb (0.478 g, 1.12 mmol) in CH_2Cl_2 (20 mL) was stirred at RT for 2 h, then filtered to remove any $Ru_2Cl_4(dppb)_3$ formed. (None of this CH_2Cl_2-insoluble green precipitate[8] is obtained if the ruthenium precursor

is free of residual PPh_3).[9] The solution was then concentrated to 5 mL and MeOH (10 mL) was added to precipitate the product. The mixture was stirred for 1 h, after which the green solid was filtered off, washed with MeOH (2 × 5 mL) and hexanes (3 × 15 mL), and dried under vacuum. Yield 0.87 g (90%). ^1H and $^{31}P\{^1H\}$ NMR data match values previously reported.[10,11]

2.3.4. $[RuCl(dppb)]_2(\mu\text{-}Cl)_2(\mu\text{-}H_2O)$ 41

To a solution of $RuCl_2(dppb)(PPh_3)$ (Section 2.3.3) (0.336 g, 0.39 mmol) in C_6H_6 (20 mL) was added degassed H_2O (5 mL). The mixture was refluxed under N_2 for 2.5 h, after which the orange product was precipitated by addition of hexanes (25 mL). Stirring was continued for 30 min, after which the product was filtered off, washed with MeOH (1 × 10 mL) and hexanes (8 × 10 mL), and dried under vacuum. Yield 0.219 g (93%). ^1H and $^{31}P\{^1H\}$ NMR data match values previously reported.[12] $^{31}P\{^1H\}$ NMR ($CDCl_3$, 121 MHz): δ 63.4 (d, $^2J_{PP}$ = 47 Hz, 2P); 54.2 (d, $^2J_{PP}$ = 47 Hz, 2P). ^1H NMR ($CDCl_3$, 300 MHz): δ 7.9-7.2 (m, 40H, Ph); 3.40 (br m, 2H, CH_2); 2.62-1.67 (br m, 10H, CH_2); 1.60 (s, 2H, free H_2O); 1.33 (br m, 4H, CH_2).

2.3.5. $Ru_2Cl_4(dcypb)_2(N_2)$[13]

A green solution of $RuCl_2(PPh_3)_3$ **1a** (0.40 g, 0.42 mmol) and dcypb (0.195 g, 0.425 mmol) in C_6H_6 (5 mL) was stirred under N_2. Within 30 minutes the solution had become orange and an orange precipitate was evident. After 19 h, hexanes (5 mL) was added to precipitate the remaining orange solid, which was filtered off, washed with hexanes (3 × 5 mL) and dried under a flow of N_2. Yield 0.26 g (97%). ^1H and $^{31}P\{^1H\}$ NMR data match values previously reported.[13] $^{31}P\{^1H\}$ ($CDCl_3$, 121 MHz): δ 57.5 (d, $^2J_{PP}$ = 39 Hz), 45.0 (d, $^2J_{PP}$ = 27 Hz), 44.6 (d, $^2J_{PP}$ = 39 Hz), 42.3 (d, $^2J_{PP}$ = 27 Hz). ^1H NMR ($CDCl_3$, 300 MHz): δ 3.1-0.7 (br, C*H*, CH_2).

2.4. Aryloxide Salts

2.4.1. Potassium Phenolate (KOPh)

To a solution of C_6H_5OH (530 mg, 5.63 mmol) in THF (10 mL) was slowly added (over the course of 30 min) solid KH (225 mg, 5.63 mmol). Vigorous evolution of hydrogen gas ensued. The solution was stirred for 30 min after addition of KH was complete, then reduced to dryness, leaving a white solid. The solid was washed with hexanes (3 × 2 mL) and dried under vacuum. Yield 615 mg (88 %). ^{1}H NMR (C_6D_6, 200 MHz): δ 7.85 (m, 2H, Ar), 6.26 (m, 3H, Ar).

2.4.2. Potassium 4-*tert*-butylphenolate (KOAr)

To a solution of 4-*tert*-butylphenol (3.862 g, 25.7 mmol) in THF (30 mL) was slowly added (over the course of 30 min) solid KH (1.031 g, 25.7 mmol). Vigorous evolution of hydrogen gas ensued. The pale yellow solution was stirred for 30 min after addition of KH was complete, and then reduced to dryness, leaving a white solid. The solid was washed with hexanes (3 × 5 mL) and dried under vacuum. Yield 4.614 g (95 %). ^{1}H NMR (C_6D_6, 200 MHz): δ 7.15 (br s, 2H, Ar), 6.63 (br s, 2H, Ar), 1.23 (s, 9H, CH_3).

2.5. Reaction of Ruthenium Precursor 1a with Aryloxides

2.5.1. Reaction of $RuCl_2(PPh_3)_3$ with 1 equiv KOAr

Addition of KOAr (3.9 mg, 0.021 mmol) in MeOH (400 μL) to a solution of $RuCl_2(PPh_3)_3$ **1a** (20 mg, 0.021 mmol) in CH_2Cl_2 (1.60 mL) gave a mixture of $RuCl_2(PPh_3)_3$ **1a**, $RuHCl(PPh_3)_3$ **1b**, $RuH_2(CO)(PPh_3)_3$ **2a**, $RuHCl(CO)(PPh_3)_3$ **2b** and $RuH(\eta^5\text{-ArO})(PPh_3)_2$ **3a** (ratio 1:5:3:25:3) after 24 h by $^{31}P\{^1H\}$ NMR analysis (see Chapter 3 for discussion).

2.5.2. Reaction of $RuCl_2(PPh_3)_3$ with 2 equiv KOAr

Addition of KOAr (7.9 mg, 0.042 mmol) in MeOH (400 μL) to a solution of $RuCl_2(PPh_3)_3$ **1a** (20 mg, 0.021 mmol) in CH_2Cl_2 (1.60 mL) effected complete conversion to $RuH_2(CO)(PPh_3)_3$ **2a**, and $RuH(\eta^5\text{-ArO})(PPh_3)_2$ **3a** (Section 2.6.1) (ratio ca. 3:1) within 15 min. Over 24 h in solution, a new singlet due to $[RuH(\eta^5\text{-ArO})(PPh_3)_2]Cl$ **12a** (Section 2.6.3) appeared (ca. 24% integrated intensity). Control experiments with isolated $RuH(\eta^5\text{-ArO})(PPh_3)_2$ **3a** indicated ca. 20% chlorination in neat CH_2Cl_2 over this period, proceeding to completion over 5 d at RT. ^1H NMR and IR for **2a** match values previously reported.[14,15] $^{31}P\{^1H\}$ NMR ($CDCl_3$, 121 MHz): δ 57.0 (d, $^2J_{PP}$ = 17.4 Hz, 2P), 45.2 (t, $^2J_{PP}$ = 17.4 Hz, 1P). ^1H NMR (CD_2Cl_2, 300 MHz) δ 7.6-6.7 (m, 45H, Ph), -6.8 (tdd, $^2J_{HP(A)}$ = 30 Hz, $^2J_{HP(B)}$ = 16 Hz, $^2J_{HH}$ = 6 Hz, 1H, Ru*H*), -8.8 (dtd, $^2J_{PH(B)}$ = 73 Hz, $^2J_{PH(A)}$ = 30 Hz, $^2J_{HH}$ = 6 Hz, 1H, Ru*H*). IR (Nujol, cm^{-1}): 1960, 1898 (m, $\nu_{Ru\text{-}H}$), 1940 (s, $\nu_{C\text{-}O}$).

2.5.3. Labelling Studies

(a) A solution of KOAr (10.0 mg, 0.0532 mmol) in CH_3OD (0.35 mL) was added to a solution of $RuCl_2(PPh_3)_3$ **1a** (25.5 mg, 0.0266 mmol) in CH_2Cl_2 (0.35 mL). After 24 h at RT, ^2H NMR showed incorporation of deuterium into the aryloxide as *4-tert*-butyl-C_6H_4OD; ^1H (C_6D_6) showed hydride peaks for $RuH_2(CO)(PPh_3)_3$ **2a**, and $RuH(\eta^5\text{-ArO})(PPh_3)_2$ **3a**. Some $RuHCl(CO)(PPh_3)_3$ **2b** was also evident. A control experiment carried out in the absence of **1a** showed no deuteration of KOAr. (b) The corresponding experiment with CD_3OD gave ArOD, $RuDCl(CO)(PPH_3)_3$, $RuD_2(CO)(PPh_3)_3$ and $RuD(\eta^5\text{-ArO})(PPh_3)_2$. Some deuteration of the aromatic rings was observed. No hydride peaks were evident by ^1H NMR.

2.5.4. $RuHCl(PPh_3)_3$ 1b

(a) Addition of a solution of KOAr (37.4 mg, 0.199 mmol) in methanol (6 mL) to $RuCl_2(PPh_3)_3$ **1a** (200 mg, 0.209 mmol) dissolved in CH_2Cl_2 (2 mL) caused an immediate colour change from brown to purple. After 8 h, the solution was reduced in volume (ca. 0.5 mL) and filtered to obtain purple **1b** as a mixture with **2a** (10%). (b) A solution of **1a** (1.007 g, 1.05 mmol) in C_6H_6 (40 mL) was treated with a solution of KOAr (0.198 g, 1.12 mmol) in 2-propanol (10 mL). The resulting solution was refluxed under N_2 for 8 h, resulting in formation of a purple suspension. The solvent was reduced in volume (ca. 2 mL), and hexanes (10 mL) added to ensure complete precipitation. Purple **1b** was filtered off, washed with hexanes (4 × 5 mL) and methanol (4 × 3 mL), and dried under vacuum. Yield 0.940 g (97%). ^1H and $^{31}P\{^1H\}$ NMR data agree with values reported.[6,14] $^{31}P\{^1H\}$ NMR (CH_2Cl_2, 121 MHz): δ 57 (br s); resolves upon cooling to 183 K into the reported[6] AX_2 pattern: δ 94.2 (t, $^2J_{PP}$ = 27 Hz, 1P), 38.4 (d, $^2J_{PP}$ = 27 Hz, 2P). ^1H NMR ($CDCl_3$, 300 MHz): δ 7.40-6.87 (m, 45H, Ph), -17.7 (q, $^2J_{HP}$ = 25.9 Hz, 1H). IR (Nujol, cm^{-1}): 1929 (m, ν_{Ru-H}).

2.5.5. $Ru(\eta^5\text{-}^t Bu\text{-}C_6H_4O)(o\text{-}C_6H_4PPh_2)(PPh_3)\cdot HOAr$ 9a·HOAr.

A suspension of $RuCl_2(PPh_3)_3$ **1a** (52 mg, 0.055 mmol) and KOAr (20.6 mg, 0.109 mmol) in toluene (2 mL) was stirred for 12 h, until no peaks for **1a** were evident by ^{31}P NMR analysis. The solution was filtered (Celite) to remove an insoluble orange precipitate, concentrated, and treated with cold hexanes to precipitate the bright yellow product, which was reprecipitated from Et_2O/hexanes. Yield 39 mg (66%). X-ray quality crystals, grown by slow concentration of a $CHCl_3$ solution of the filtrate, revealed the presence of two solvating phenol molecules and a molecule of chloroform in the unit cell. $^{31}P\{^1H\}$ NMR ($CDCl_3$, 121 MHz): δ

49.3 (d, $^2J_{PP}$ = 39 Hz, 1P), -27.5 (d, $^2J_{PP}$ = 39 Hz, 1P). ^{1}H NMR (CD_2Cl_2, 300 MHz): δ 9.2 (br s, 1H, ArO*H*), 8.04 (m, 1H, Ph), 7.5-6.7 (m, 32H, Ph), 4.60 (d, $^3J_{HH}$ = 4.6 Hz, 1H, η^5-ArO), 4.53 (d, $^3J_{HH}$ = 4.6 Hz, 1H, η^5-ArO), 4.32 (d, $^3J_{HH}$ = 4.6 Hz, 1H, η^5-ArO), 4.22 (d, $^3J_{HH}$ = 4.6 Hz, 1H, η^5-ArO), 1.34 (s, 9H, η^5-ArO), 1.01 (s, 9H, ArOH). IR (Nujol, cm^{-1}): 3100 (m, br, ν_{C-O}), 1539 (m, ν_{C-O}). Anal. Calcd for $C_{56}H_{56}O_2P_2Ru$: C, 72.79; H, 6.11. Found: C, 72.69; H, 6.05.

2.5.6. Ru(η^5-C_6H_5O)(*o*-$C_6H_4PPh_2$)(PPh_3)•HOPh 9b•HOPh.

Addition of KOPh (36 mg, 0.272 mmol) to $RuCl_2(PPh_3)_3$ **1a** (130.5 mg, 0.136 mmol) was carried out as for **9a**, using THF (5 mL) as solvent to overcome the low solubility of KOPh. Complex **9b** was obtained as a phenol solvate. Yield 60 mg (54%). Crystals were grown by slow diffusion of hexanes into a benzene solution. ^{31}P{^{1}H} NMR ($CDCl_3$, 121 MHz): δ 49.3 (d, $^2J_{PP}$ = 38 Hz, 1P), -27.6 (d, $^2J_{PP}$ = 38 Hz, 1P). ^{1}H NMR ($CDCl_3$, 300 MHz): δ 9.0 (s, 1H, PhO*H*), 8.04 (m, 1H, Ph), 7.63-6.55 (m, 34H, Ph), 5.06 (t, $^3J_{HH}$ = 5.5 Hz, 2H, *m*-η^5-C_6H_5O), 4.68 (t, $^3J_{HH}$ = 5.5 Hz, 1H, *p*-η^5- C_6H_5O), 4.37 (d, $^3J_{HH}$ = 5.5 Hz, 2H, *o*-η^5-5-C_6H_5O). IR (Nujol, cm^{-1}): 3100 (m, br, ν_{C-O}), 1530 (m, ν_{C-O}), 1275 (s, ν_{C-O}). Anal. Calcd for $C_{48}H_{40}O_2P_2Ru$: C, 71.01; H, 4.97. Found: C, 71.45; H, 4.97.

2.6. Reaction of 1b with Aryloxides

2.6.1. RuH(η^5-^{t}Bu-C_6H_4O)(PPh_3)$_2$ 3a

(a) Addition of solid KOAr (20.2 mg, 0.107 mmol) to a stirred purple solution of $RuHCl(PPh_3)_3$ **1b** (100 mg, 0.107 mmol) in CH_2Cl_2 (5 mL) caused a slow colour change to yellow as the salt dissolved. The solution was stirred for 2 h, then filtered (Celite), concentrated, and treated with cold hexanes to precipitate the bright yellow product. This was reprecipitated

from C_6H_6/hexanes and dried under vacuum. Yield 73 mg (88%). $^{31}P\{^1H\}$ NMR (C_6D_6 121 MHz) δ 59. 3 (br s); partially resolved at 180 K (CD_2Cl_2) δ (overlapping) 60.9 (d, $^2J_{PP}$) = 48 Hz), 58.6 (br s). ^1H NMR (C_6D_6, 300 MHz): δ 8.5-6.8 (m, 30H, Ph), 5.12 (d, $^3J_{HH}$ = 6.5 Hz, 2H, η^5-ArO), 3.85 (d, $^3J_{HH}$ = 6.5 Hz, 2H, η^5-ArO), 1.10 (s, 9H, ^{t}Bu of η^5-ArO), -11.6 (t, $^2J_{HP}$ = 35 Hz, 1H, Ru*H*). IR (Nujol, cm^{-1}): 1977 (m, ν_{Ru-H}); 1558 (m, $\nu_{C=O}$). Anal. Calcd for $C_{46}H_{44}OP_2Ru$: C, 71.21; H, 5.72. Found: C, 71.75; H, 6.29. (b) **3a**•MeOH. Use of methanol to predissolve the KOAr salt (1:1 MeOH-CH_2Cl_2) gave much more rapid reaction, with near-quantitative conversion within 10 min at RT. NMR parameters agreed with those for **3a**, with the addition of peaks for methanol. A small amount of **2a** (ratio 8:1) was also evident. c) **3a**•ArOH. The ArOH solvate was obtained by addition of one equivalent of phenol to the product in (a). NMR parameters agreed with those for **3a**, with the addition of peaks for ArOH.

2.6.2. RuCl(η^5-C_6H_5O)(PPh_3)$_2$ 11b.

(a) Addition of KOPh (29 mg, 0.22 mmol) to a stirred solution of $RuHCl(PPh_3)_3$ **1b** (200 mg, 0.21 mmol) in CH_2Cl_2 (4 mL) caused a colour change from deep purple to bright orange. The solution was stirred for 2 h, then filtered (Celite), concentrated, and treated with cold hexanes to precipitate an orange powder. This was filtered off, washed with hexanes (3 × 1 mL) then dried under vacuum. Yield 132 mg (83%). RuH(η^5-C_6H_5O)(PPh_3)$_2$ **3b** was not detected. $^{31}P\{^1H\}$ NMR ($CDCl_3$, 121 MHz) δ 29.1 (s). ^1H NMR ($CDCl_3$, 300 MHz): δ 7.44 (m, 12H, Ph), 7.26 (m, 6H, Ph), 7.13 (m, 12H, Ph), 5.34 (t, $^3J_{HH}$ = 6 Hz, 2H, *m*-η^5-C_6H_5O), 4.10 (t, $^3J_{HH}$ = 6 Hz, 2H, *p*-η^5-C_6H_5O), 3.77 (d, $^3J_{HH}$ = 6 Hz, 2H, *o*-η^5-C_6H_5O). IR (Nujol, cm^{-1}): 1589 (s, ν_{C-O}). Anal. Calcd for $C_{42}H_{35}ClOP_2Ru$: C, 65.16; H, 4.56. Found: C, 65.20; H, 4.75. (b) **11b**•HOPh. Addition of phenol (2 equiv) to a CD_2Cl_2/hexanes solution of **11b** formed as in (a) resulted in

slow crystallization to yield X-ray quality, red-orange crystals. A molecule of co-crystallized phenol was observed in the unit cell. NMR parameters were essentially identical to those in (a), with the addition of peaks for the phenol molecule.

2.6.3. [RuH(η^5-^{t}Bu-C_6H_4O)(PPh_3)$_2$]Cl 12a.

(a) Addition of ethereal HCl (1M, 1.0 mL, 1.0 mmol) to a solution of RuH(η^5-ArO)(PPh_3)$_2$•HOAr **3a**•HOAr (65 mg, 0.08 mmol) in CH_2Cl_2 (2 mL) caused a colour change from yellow to orange. The solution was stirred for 1 h, then stripped of solvent. Reprecipitation from CH_2Cl_2/hexanes gave pale orange **12a**. Yield 50 mg (74%). (b) A solution of **3a**•HOAr (10 mg) in $CDCl_3$ (1 mL) underwent gradual conversion to **12a** over 5 d at RT. Pale orange, X-ray quality crystals deposited from solution. $^{31}P\{^1H\}$ NMR (C_6D_6 121 MHz): δ 52.5 (s). ^1H NMR (C_6D_6, 300 MHz): δ 8.87 (br s, 1H, ArO*H*), 7.4-7.0 (m, 33H, Ph and ArO*H*), 6.93-6.82 (m, 2H, Ph), 5.63 (d, $^3J_{HH}$ = 6.4 Hz, 2H, η^6-ArO), 3.94 (d, $^3J_{HH}$ = 6.4 Hz, 2H, η^6-ArO), 1.25 (s, 9H, *t*Bu of η^6-ArO), 1.19 (s, 9H, ArOH), -10.8 (t, $^2J_{HP}$ = 36 Hz, Ru*H*). Anal. Calcd for $C_{56}H_{59}ClO_2P_2Ru$: C, 69.88; H, 6.18. Found: C, 70.27; H, 6.38.

2.7. Miscellaneous Reactions Yielding $RuH_2(CO)(PPh_3)_3$ 2a and $RuHCl(CO)(PPh_3)_3$ 2b.

2.7.1. $RuHCl(CO)(PPh_3)_3$ 2b from $RuHCl(PPh_3)_3$ 1b

A solution of $RuHCl(PPh_3)$ **1b** (225 mg, 0.242 mmol) in CH_2Cl_2 (10 mL) was stirred with solid paraformaldehyde (200 mg) for 2 d, after which unreacted paraformaldehyde was filtered off (Celite). The filtrate was reduced to dryness, redissolved in C_6H_6 and treated with hexanes to precipitate a light brown powder. Reprecipitation from CH_2Cl_2/hexanes gave pale beige **2b**. Yield 212 mg (92%). ^1H NMR and IR data agree with the values reported.[15] $^{31}P\{^1H\}$

NMR (CD_2Cl_2, 121 MHz): δ 41.9 (br s, 2P), 15.2 (br s, 1P). An A_2B pattern emerges at 253 K: δ 42.3 (d, $^2J_{PP}$ = 15.7 Hz, 2P), 14.6 (t, $^2J_{PP}$ = 15.7 Hz, 1P). ^{1}H NMR ($CDCl_3$, 300 MHz): δ 8.2-6.5 (m, 45H, PPh_3); -7.2 (dt, $^2J_{HP}$ = 23, 105 Hz, 1H, Ru*H*).

2.7.2. $RuH_2(CO)(PPh_3)_3$ 2a from $RuHCl(CO)(PPh_3)_3$ 2b

(a) To a solution of $RuHCl(CO)(PPh_3)_3$ **2b** (10 mg, 0.0104 mmol) in CH_2Cl_2 (0.75 mL) was added a solution of KOAr (2 mg, 0.0106 mmol) in MeOH (2 drops) and stirred overnight. Quantitative conversion to $RuH_2(CO)(PPh_3)_3$ **2a** was evident by $^{31}P\{^1H\}$ NMR analysis. (b) To a mixture of **2b** (188 mg, 0.197 mmol) suspended in C_6H_6 (10 mL) was added excess LAH (200 mg) and stirred for 2 h. The mixture was quenched by the slow addition of EtOH (2 mL) and then filtered (Celite). The filtrate was filtered again (Celite), concentrated, and treated with hexanes to precipitate the product as a white powder, which was washed with hexanes and dried under vacuum. Yield 103 mg (57%). ^{1}H NMR and IR data agree with the values reported for **2a**.[14,15] $^{31}P\{^1H\}$ NMR ($CDCl_3$, 121 MHz): δ 57.0 (d, $^2J_{PP}$ = 17.4 Hz, 2P), 44.7 (t, $^2J_{PP}$ = 17.4 Hz, 1P). ^{1}H NMR ($CDCl_3$, 300 MHz) δ 7.6-6.7 (m, 45H, Ph), -6.8 (tdd, $^2J_{HP(A)}$ = 30 Hz, $^2J_{HP(B)}$ = 16 Hz, $^2J_{HH}$ = 6 Hz, 1H, Ru*H*), -8.8 (dtd, $^2J_{PH(B)}$ = 73 Hz, $^2J_{PH(A)}$ = 30 Hz, $^2J_{HH}$ = 6 Hz, 1H, Ru*H*).

2.8. Reaction of $RuCl_2(CO)_2(PPh_3)_2$ 14 with Aryloxides

2.8.1. $RuCl(\sigma\text{-}^tBuC_6H_4O)(CO)_2(PPh_3)_2$ 15

A solution of KOAr (200 mg, 1.06 mmol) in THF (14 mL) was added slowly to a solution of $RuCl_2(CO)_2(PPh_3)_3$ **14** (400 mg, 0.532 mmol) in THF (60 mL). After 1 h, ^{31}P NMR analysis revealed starting **14**, $RuCl(\sigma\text{-}^tBuC_6H_4O)(CO)_2(PPh_3)_2$ **15**, and $[Ru(\sigma\text{-}^tBuC_6H_4O)_2(CO)_2(PPh_3)_2{\bullet}KO^tBuC_6H_4]_2$ **17** (Section 2.8.2), and an unidentified species (possibly

$Ru(\sigma\text{-}^tBuC_6H_4O)_2(CO)_2(PPh_3)_2$ **16**); singlet at 15.4 ppm in the ^{31}P NMR spectrum) (35:1:3). In an attempt to isolate the mono-aryloxide complex the solvent was reduced to dryness, and the residue redissolved in C_6H_6 and filtered (Celite). The filtrate was concentrated with cold pentane to precipitate a bright yellow powder, which was reprecipitated until only $RuCl(\sigma\text{-}^tBuC_6H_4O)(CO)_2(PPh_3)_2$ **15** was evident by ^{31}P NMR analysis. Yield 50 mg (11%). $^{31}P\{^1H\}$ NMR (C_6D_6, 121 MHz): δ 14.8 (s). ^1H NMR (C_6D_6, 300 MHz): δ 8.09 (m, 12H, Ph), 7.0 (m, 18H, Ph), 6.91 (d, 2H, σ-OAr, $^3J_{HH}$ = 8.7 Hz), 6.42 (d, 2H, σ-OAr, $^3J_{HH}$ = 8.7 Hz), 1.28 (s, 9H, ^{t}Bu). $^{13}C\{^1H\}$ NMR (C_6D_6, 75 MHz): δ 195.5 (t, $^2J_{CP}$ = 11 Hz, *C*O), 195.0 (t, $^2J_{CP}$ = 11 Hz, *C*O). IR (Nujol, cm^{-1}): 2043, 1977 (s, $\nu_{C\text{-}O}$), 1284, (m, $\nu_{C\text{-}O}$). Anal. Calcd for $C_{48}H_{43}ClO_3P_2Ru$: C, 66.55; H, 5.00. Found: C, 66.38; H, 5.18.

2.8.2. $K_2[Ru(\sigma\text{-}^tBuC_6H_4O)_3(CO)_2(PPh_3)]_2$ 17

A solution of $RuCl_2(CO)_2(PPh_3)_3$ **14** (100 mg, 0.133 mmol) and KOAr (75 mg, 0.399 mmol) in THF (18 mL) was stirred for 3 d, until a single product was evident by ^{31}P NMR analysis. The solvent was then reduced to dryness, and the residue redissolved in benzene and filtered (Celite). The filtrate was concentrated to a viscous oil and cold (-35 °C) hexanes added to precipitate the product as an orange powder. Yield 92 mg (77%). $^{31}P\{^1H\}$ NMR (C_6D_6, 121 MHz): δ 33.2 (s). ^1H NMR (C_6D_6, 300 MHz): δ 7.55 (m, 24H, σ-OAr), 7.05 (m, 30 H, Ph), 1.37 (s, 18H, -^{t}Bu), 1.30 s, 36H, -^{t}Bu). $^{13}C\{^1H\}$ NMR (C_6D_6, 75 MHz): δ 197.9 (d, $^2J_{CP}$ = 14 Hz, 2C, *C*O). IR (Nujol, cm^{-1}): 2038, 1967 (s, $\nu_{C\text{-}O}$). Anal. Calcd for $C_{100}H_{108}O_{10}P_2Ru_2$: C, 66.28; H, 6.01. Found: C, 65.89; H, 5.85.

2.9. Binop Ligand Preparation

2.9.1. 2,2'-Bis((trifluoromethanesulfonyl)oxy)-1,1'-binaphthyl[16] 26

To a solution of 1,1'-bi-2,2'-naphthol (2.5 g, 8.73 mmol) and pyridine (2.07 g, 26.2 mmol) in CH_2Cl_2 (20 mL) was added trifluoromethanesulfonic anhydride (5.91 g, 21.0 mmol) at 0 °C. The mixture was stirred for 17 h at RT, then washed with 10% HCl (3 × 50 ml), saturated $NaHCO_3$ (50 mL), and brine (50 mL), and finally dried ($MgSO_4$). Concentration and purification, by flash chromatography on silica gel (25% EtOAc/hexanes), afforded 2,2'-bis((trifluoromethanesulfonyl)oxy)-1,1'-binaphthyl **26** as a white solid. Yield 4.42 g (92%). ^1H NMR ($CDCl_3$, 300 MHz): δ 8.13 (d, $^3J_{HH}$ = 8.5 Hz, 2H); 8.01 (d, $^3J_{HH}$ = 8.5 Hz, 2H), 7.58 (m, 4H), 7.40 (t, $^3J_{HH}$ = 8.5 Hz, 2H), 7.24 (m, 2H).

2.9.2. 2-(Diphenylphosphinyl)-2'-((trifluoromethanesulfonyl)oxy)-1-1'-binaphthyl[16] 27

To a mixture of 2,2'-bis((trifluoromethanesulfonyl)oxy)-1,1'-binaphthyl **26** (1.0 g, 1.8 mmol), 1,4-bis(diphenylphosphino)butane (dppb, 39 mg, 0.091 mmol), diphenylphosphine oxide (734 mg, 3.63 mmol) and palladium diacetate (20 mg, 0.091 mmol) were added DMSO (10 mL) and NEt_3 (735 mg, 7.26 mmol). The mixture was heated at 100 °C for 19 h, then cooled to room temperature. Anhydrous Et_2O (100 mL) was added, and the solution washed with H_2O (3 × 50 mL), saturated $NaHCO_3$ (2 × 50 mL), and brine (50 mL), then dried ($MgSO_4$). Concentration and purification by flash chromatography on silica gel (20%, 50% EtOAc/hexanes), afforded 2-(diphenylphosphinyl)-2'-((trifluoromethanesulfonyl)oxy)-1-1'-binaphthyl **27** as a slightly beige foam. Yield 994 mg (91%). ^1H and $^{31}P\{^1H\}$ NMR data match values previously reported.[16] $^{31}P\{^1H\}$ NMR ($CDCl_3$, 121 MHz): δ 27.9 (s, 1P). ^1H NMR ($CDCl_3$, 300 MHz): δ 8.2-7.0 (m, 22H aromatic).

2.9.3. 2-(Diphenylphosphinyl)-2'-hydroxy-1-1'-binaphthyl[16] 28

To a solution of 2-(diphenylphosphinyl)-2'-((trifluoromethanesulfonyl)oxy)-1-1'-binaphthyl **27** (536 mg, 0.889 mmol) in THF (11 mL) was added a solution of LiOH (426 mg, 17.8 mmol) in distilled H_2O (4 mL) and stirred vigorously at room temperature for 21 h. The resulting two-phase solution was partitioned between Et_2O (32 mL) and 10% HCl (20 mL) and separated. The organic phase was washed with H_2O (2 × 25 mL), causing 2-(diphenylphosphinyl)-2'-hydroxybinaphthyl **28** to precipitate as a white solid. This was filtered off, and the organic phase separated and concentrated to afford a second crop. Yield 380 mg (91%). ^1H and $^{31}P\{^1H\}$ NMR data match values previously reported.[16] $^{31}P\{^1H\}$ NMR ($CDCl_3$, 300 MHz): δ 30.8 (s, 1P). ^1H NMR ($CDCl_3$, 300 MHz): δ), 9.04 (br s, 1H, -O*H*), 8.22-6.41 (m, 22H, aromatic).

2.9.4. General Procedure for Reduction to 2-(Diphenylphosphino)-2'-hydroxy-1,1'-binapthyl 29 (binop)

A solution of 2-(diphenylphosphinyl)-2'-((trifluoromethanesulfonyl)oxy)-1-1'-binaphthyl **27** or 2-(diphenylphosphinyl)-2'-hydroxy-1,1'-binaphthyl **28** and Et_3N (7 equiv) in the specified solvent (toluene or chlorobenzene) was treated with trichlorosilane (5 equiv). This solution was stirred at an elevated temperature for 16 h; after cooling, it was diluted with Et_2O and quenched with saturated $NaHCO_3$. The resulting salt (a white gel) was filtered through Celite, which was then washed with Et_2O (3 × 30 mL). The combined, two-phase filtrate was separated and the organic phase dried ($MgSO_4$). Concentration and purification by flash chromatography on silica gel (20% EtOAc/hexanes) afforded 2-(diphenylphosphino)-2'-hydroxy-1,1'-binapthyl **29**. ^1H and $^{31}P\{^1H\}$ NMR data match values previously reported.[16] $^{31}P\{^1H\}$ NMR (C_6D_6, 121 MHz): δ -13.39 (s). ^1H NMR (C_6D_6, 300 MHz): δ 8.22-6.42 (m, 22H, aromatic), 4.63 (br s, 1H, -O*H*).

2.9.2.1. From 2-(Diphenylphosphinyl)-2'-((trifluoromethanesulfonyl)oxy)-1-1'-binaphthyl 27 in Toluene [16]

Following the general procedure above, a solution of 2-(diphenylphosphinyl)-2'-((trifluoromethanesulfonyl)oxy)-1-1'-binaphthyl **27** (677.4 mg, 1.124 mmol) and base (796 mg, 7.87 mmol) in toluene (20 mL) was treated with trichlorosilane (761 mg, 5.62 mmol) and stirred at 100 °C for 16 h. Yield 409 mg (80%).

2.9.4.2. From 2-(Diphenylphosphinyl)-2'-hydroxy-1-1'-binaphthyl 28 in Toluene[16]

Following the general procedure above, a solution of 2-(diphenylphosphinyl)-2'-hydroxy-1,1'-binaphthyl **28** (150 mg, 0.319 mmol) and base (232 mg, 2.30 mmol) in toluene (8 mL) was treated with trichlorosilane (216 mg, 1.59 mmol) and stirred at 100 °C for 16 h. Yield 65 mg (45%).

2.9.4.3. From 2-(Diphenylphosphinyl)-2'-hydroxy-1,1'-binaphthyl 28 in Chlorobenzene

Following the general procedure above, a solution of 2-(diphenylphosphinyl)-2'-hydroxy-1,1'-binaphthyl **28** (150 mg, 0.319 mmol) and base (232 mg, 2.30 mmol) in chlorobenzene (26 mL) was treated with trichlorosilane (216 mg, 1.59 mmol) and stirred at 120 °C for 16 h. Yield 106 mg (73%).

2.9.5. 2-(Diphenylphosphino)-2'-sodium-1, 1'-binaptholate 30

To a solution of 2-(diphenylphosphino)-2'-hydroxy-1,1'-binapthyl **29** (93.0 mg, 0.205 mmol) in CH_2Cl_2 (5 mL) was added solid Na_2CO_2 (732 mg, 6.91 mmol). The solution was stirred at RT for 24 h, after which the mixture was filtered through Celite to remove excess Na_2CO_3. The solvent was removed under vacuum to give 2-(diphenylphosphino)-2'-sodium-1, 1'-

binaptholate **30** as a white solid. Yield 87 mg (89%). $^{31}P\{^{1}H\}$ NMR (C_6D_6, 121 MHz): δ -13.36 (s).

2.9.6. RuCl(binop)(PPh_3) 31

(a) To a solution of $RuCl_2(PPh_3)_3$ **1a** (106.0 mg, 0.111 mmol) in CH_2Cl_2 (4 mL) was added a solution of 2-(diphenylphosphino)-2'-sodium-1,1'-binaptholate **30** (52.7 mg, 0.111 mmol) in CH_2Cl_2 (3 mL). The solution was stirred for 24 h until only two doublets (**31**) were observed by $^{31}P\{^{1}H\}$ NMR analysis. The solvent was removed, the residue redissolved in C_6H_6 and filtered (Celite). The dark orange filtrate was concentrated (ca. 1 mL) and pentane added to precipitate the product as an orange powder. An impurity was typically evident at *ca.* 52 ppm in the $^{31}P\{^{1}H\}$ NMR spectrum, for reactions carried out on preparative scale. No sign of this species was observed in NMR-scale experiments. This unknown species was removed by redissolving the crude powder in CH_2Cl_2 (0.5 mL), and purifying by column chromatography on silica gel (100% EtOAc). After this treatment, the unknown species had decomposed to a deep green band at the top of the column. Purified RuCl(binop)(PPh_3) **31** was then precipitated from C_6H_6/pentane, filtered, washed with pentane and dried under vacuum. Yield 86.1 mg (91%).

(b) To a solution of $RuCl_2(PPh_3)_3$ **1a** (158 mg, 0.165 mmol) in CH_2Cl_2 (5 mL) was added a solution of 2-(diphenylphosphino)-2'-hydroxy-1,1'-binapthyl **29** (75.0 mg, 0.165 mmol) in CH_2Cl_2 (6 mL). Solid Na_2CO_3 (350 mg, 3.30 mmol) was added, and the mixture was stirred for 24 h until only RuCl(binop)(PPh_3) **31** and two equivalents of free PPh_3 were evident by $^{31}P\{^{1}H\}$ NMR analysis. The mixture was filtered through Celite to remove excess Na_2CO_3. The solvent was stripped off, and the residue redissolved in C_6H_6 and filtered (Celite). The dark orange filtrate was concentrated (ca. 1 mL) and pentane added to precipitate the product as an orange

powder. Purification by column chromatography was carried out if necessary. Yield 126.5 mg (90%). $^{31}P\{^{1}H\}$ NMR ($CDCl_3$, 121 MHz): δ 49.42 (d, $^{2}J_{PP}$ = 58 Hz, 1P), 46.89 (d, $^{2}J_{PP}$ = 58 Hz, 1P). ^{1}H NMR (300 K, $CDCl_3$, 500 MHz): δ 7.98-7.52 (m, 7H), 7.51 (d, $^{3}J_{HH}$ = 8 Hz, 1H, *H5*), 7.49-7.37 (m, 3H), 7.36 (t, $^{3}J_{HH}$ = 8 Hz, 1H, *H6*), 7.35- 6.74 (m, 19H), 6.34 (m, 3H, *H7* + 2H), 6.01 (dd, $^{3}J_{HH}$ = 7.5 Hz, $^{3}J_{HP}$ = 3 Hz, 1H, *H4*), 5.93 (d, $^{3}J_{HH}$ = 8 Hz, 1H, *H8*), 4.49 (dd, $^{3}J_{HH}$ = 7.5 Hz, $^{3}J_{HP}$ = 3 Hz, 1H, *H3*). ^{1}H NMR (324 K, $CDCl_3$, 500 MHz): δ 8.05-7.52 (m, 7H), 7.51 (d, $^{3}J_{HH}$ = 8 Hz, 1H, *H5*), 7.49-7.37 (m, 3H), 7.36 (t, $^{3}J_{HH}$ = 8 Hz, 1H, *H6*), 7.35- 6.74 (m, 19H), 6.43 (m, 2H), 6.37 (t, $^{3}J_{HH}$ = 8 Hz, 1H, *H7*), 5.96 (m, 2H, *H4+H8*), 4.57 (dd, $^{3}J_{HH}$ = 8 Hz, $^{3}J_{HP}$ = 4.0 Hz, 1H, *H3*). $^{1}H\{^{31}P\}$ NMR (300 K, $CDCl_3$, 500 MHz): δ 7.98-6.73 (m, 31H), 6.36 (m, 3H, *H7* + 2H), 6.00 (d, $^{3}J_{HH}$ = 7 Hz, 1H, *H4*), 5.93 (d, $^{3}J_{HH}$ = 8 Hz, 1H, *H8*), 4.50 (d, $^{3}J_{HH}$ = 7 Hz, 1H, *H3*). $^{1}H\{^{31}P\}$ NMR (324 K, $CDCl_3$, 500 MHz): δ 8.05-6.73 (m, 31H), 6.43 (m, 2H), 6.37 (t, $^{3}J_{HH}$ = 8 Hz, 1H, *H7*), 5.96 (m, 2H, *H4* + *H8*), 4.57 (d, $^{3}J_{HH}$ = 7 Hz, 1H, *H3*). Selected ^{13}C peaks. $^{13}C\{^{1}H\}$ NMR ($CDCl_3$, 125 MHz): δ 155.8 (s, *C2*), 133.8 (d, $^{2}J_{CP}$ = 10.0 Hz), 133.7 (s), 133.0 (d, $^{2}J_{CP}$ = 11.3 Hz), 131.1 (s, *C6* + *C7*), 128.9 (s, *C8*), 128.5 (s, *C5*), 112.6 (s, *C9*), 103.5 (s, *C10*), 97.3 (d, $^{2}J_{CP}$ = 10.0 Hz, *C3*), 94.7 (d, $^{2}J_{CP}$ = 8.9 Hz, *C4*), 83.0 (s, *C1*). $^{13}C\{^{1}H, ^{31}P\}$ NMR ($CDCl_3$, 125 MHz): δ 155.8 (*C2*), 133.9, 133.8, 132.97, 131.1 (*C6* + *C7*), 128.9 (*C8*), 128.5 (*C5*), 112.6 (*C9*), 103.5 (*C10*), 97.4 (*C3*), 94.7 (*C4*), 83.0 (*C1*). IR (Nujol, cm^{-1}): 1585 (m, ν_{C-O}). MALDI-MS (anthracene): M-Cl = 817, M = 852. Anal. Calcd for ($RuCl(binop)PPh_3$•hexanes) $C_{56}H_{51}ClOP_2Ru$: C, 71.67; H, 5.48. Found: C, 71.45; H, 5.25.

2.10. Preparation of a New Ruthenium Alkylidene

2.10.1. $RuCl_2(=CHCH=CMe_2)(PPh_3)_3$ 34

To a purple solution of $RuHCl(PPh_3)_3$ **1b** (1.11 g, 1.2 mmol) in CH_2Cl_2 (10 mL) was

added freshly distilled 3-chloro-3-methyl-1-butyne (148 μL, 1.32 mmol), causing an immediate colour change from deep purple to brown. The solution was stirred for 30 min, then concentrated (ca. 1 mL). Addition of hexanes (10 mL) precipitated a brown solid, which was filtered off, washed with cold (-35 °C) hexanes (5 × 3 mL) and dried under vacuum. Yield 0.803 g (88%). A minor co-product (<5% of total integrated ^{31}P NMR intensity) was identified as carbyne complex **35**.[2] Reprecipitation from CH_2Cl_2/hexanes gave **34**, contaminated, however, with trace **35**. Yield 0.762 g (83%). $^{31}P\{1H\}$ NMR ($CDCl_3$, 121 MHz): δ 30.0 (s). ^{1}H NMR ($CDCl_3$, 300 MHz): δ 18.20 (q, 1H, $^{3}J_{HH} = {}^{3}J_{HP}$ = 9.4 Hz, Ru=CH), 6.85-7.65 (m, 31H, Ar + CHCH), 1.23 (s, 3H, CH_3), 0.96 (s, 3H. CH_3). $^{13}C\{1H\}$ NMR (CD_2Cl_2, 75 MHz): δ 291.4 (t, $^{2}J_{CP}$ = 5.7 Hz, Ru=C), 132.1 (t, $^{2}J_{CP}$ = 20 Hz, Ph), 130.4 (s, Ph), 128.5 (t, $^{2}J_{CP}$ = 4.7 Hz, Ph), 27.3 (s, CH_3), 20.9 (s, CH_3). IR (Nujol, cm^{-1}): 1568 (m, $\nu_{C=C}$). Anal. Calcd for $C_{41}H_{38}Cl_2P_2Ru$: C, 64.40; H, 5.01%. Found: C, 63.85; H, 5.36%; the discrepancy arises from the presence of trace **35**.

2.10.2. One-Pot Synthesis of $RuCl_2(=CHCH=CMe_2)(PCy_3)_2$ 37

To a solution of $RuHCl(PPh_3)_3$ **1b** (100 mg, 0.108 mmol) in CH_2Cl_2 (5 mL) was added 3-chloro-3-methyl-1-butyne (12.2 μL, 0.108 mmol) at RT. After 30 min, solid PCy_3 (60.6 mg, 0.216 mmol) was added, causing a colour change from brown to purple. After 10 min, the solvent was removed under vacuum, and the residue redissolved in benzene and filtered (Celite) to remove small amounts of a black precipitate. The filtrate was concentrated and cold MeOH (-35 °C) (4 mL) added to precipitate the product as a purple solid, which was filtered off and washed with cold MeOH (3 × 2 mL). The solid was reprecipitated from C_6H_6/MeOH and dried under vacuum. Yield 76 mg (88%). ^{1}H and $^{31}P\{^{1}H\}$ NMR data match values previously reported.[17] ^{31}P NMR (C_6D_6, 121 MHz): δ 36.3 (s, 2P). ^{1}H NMR (C_6D_6, 300 MHz): δ 19.8 (d,

$^3J_{HH}$ = 11.8 Hz, 1H, RuC*H*), 8.45 (d, $^3J_{HH}$ = 11.8 Hz, 1H, RuCHC*H*), 3.0-1.0 (m, 72H, P*Cy*$_3$ + Me).

2.11. Synthesis of Phenyldiazomethane 39 and *t,t*-Benzaldeyde Azine 40

2.11.1. Benzaldehyde Tosylhydrazone 38[18]

In air, solid *p*-toluenesulfonehydrazide (9.2 g, 49 mmol) was suspended in methanol (20 mL). The resulting slurry was stirred as benzaldehyde (5 mL, 49 mmol) was added. Upon addition of the aldehyde, the *p*-toluenesulfonehydrazide quickly dissolved, and within 5 min the tosylhydrazone product began to crystallize. The white product was filtered, washed with cold methanol (0 °C), and dried under vacuum. Yield 8.199 g (61%). ^{1}H NMR data agree with the values reported.[18] ^{1}H NMR ($CDCl_3$, 200 MHz): δ 7.9-7.2 (m, 10H, Ar), 2.39 (s, 3H, C*H*$_3$). Melting point: 125.2-126.4 °C (lit: 124-125 °C).[18]

2.11.2. Phenyldiazomethane 39[18]

To a solution of sodium (0.336 g, 14.6 mmol) in triethylene glycol (30 mL) at 65 °C was added solid benzaldehyde tosylhydrazone **38** (2.0 g, 7.3 mmol). The solution was stirred for 5 min, after which cold distilled water (20 mL) was added. Addition of hexanes (15 mL) resulted in a two-phase solution that was separated. The organic phase was dried ($MgSO_4$) and concentrated to yield a thick, red oil of $PhCHN_2$, which was stored under N_2 at -35 °C Yield 0.26 g (30%). ^{1}H NMR data agree with the values reported.[18] ^{1}H NMR (C_6D_6, 200 MHz): δ 7.0-6.9 (m, 2H, Ar), 6.8-6.7 (m, 1H, Ar), 6.55-6.45 (m, 2H, Ar), 4.05 (s, 1H, C*H*N_2).

2.11.3. *t,t*-Benzaldehyde Azine 40

To a solution of sodium (0.420 g, 18.3 mmol) in triethylene glycol (23 mL) at 65 °C was added solid benzaldehyde tosylhydrazone **38** (0.25 g, 9.1 mmol). The solution was stirred for 24 h. Addition of cold (0 °C) distilled water (20 mL) afforded a yellow precipitate, which was isolated by filtration and recrystallized from hot methanol. Yield 0.30 g (31%). ^{1}H NMR data agree with the values reported.[19] ^{1}H NMR ($CDCl_3$, 200 MHz): δ 8.65 (s, -C*H*N, 2H), 7.80-7.85 (m, Ar, 2H), 7.30-7.35 (m, Ar, 3H).

2.12. Reaction of [RuCl(dppb)]$_2$(μ-Cl)$_2$(μ-H$_2$O) 41 with *t,t*-Benzaldehyde azine 40

2.12.1. Ru$_2$Cl$_4$(dppb)$_2$(*t,t*-benzaldehyde azine) 42

(a) *In Situ:* A solution of [RuCl(dppb)]$_2$(μ-Cl)$_2$(μ-H$_2$O) **41** (17 mg, 0.014 mmol) and *t,t*-benzaldehyde azine **40** (2.9 mg, 0.014 mmol) in $CDCl_3$ (0.75 mL) was freeze-thaw degassed (× 3), thawed under Ar and monitored by ^{31}P{^{1}H} NMR spectroscopy. After 4 d, conversion to Ru$_2$Cl$_4$(dppb)$_2$(*t,t*-benzaldehyde azine) **42** was nearly complete (ca. 6% residual Ru$_2$Cl$_4$(dppb)$_2$ **41a**). (b) 5 Equiv *t,t*-Benzaldehyde Azine: A solution of [RuCl(dppb)]$_2$(μ-Cl)$_2$(μ-H$_2$O) **41** (10 mg, 0.0082 mmol) and *t,t*-benzaldehyde azine **40** (9 mg, 0.041 mmol) in $CDCl_3$ (0.75 mL) was freeze-thaw degassed (× 3) and thawed under Ar. After 24 h, conversion to Ru$_2$Cl$_4$(dppb)$_2$(*t,t*-benzaldehyde azine) **42** was nearly complete (3% residual Ru$_2$Cl$_4$(dppb)$_2$ **41a**). (c) Product Isolation: To a solution of [RuCl(dppb)]$_2$(μ-Cl)$_2$(μ-H$_2$O) **41** (77 mg, 0.063 mmol) in CH_2Cl_2 (1.5 mL) was added solid *t,t*-benzaldehyde azine **40** (130 mg, 0.62 mmol) and stirred under N_2 until only Ru$_2$Cl$_4$(dppb)$_2$(*t,t*-benzaldehyde azine) **42** was evident by ^{31}P{^{1}H} NMR analysis (24 h). The solution was concentrated to *ca.* 0.5 mL and hexanes were added to precipitate the product as an orange powder. This was stirred with hexanes to remove excess *t,t*-benzaldehyde azine **40**,

filtered and dried under vacuum. Yield 0.055 g (62 %). $^{31}P\{^{1}H\}$ NMR ($CDCl_3$, 202 MHz): δ 53.8 (d, $^{2}J_{PP}$ = 43 Hz, 2P), 52.8 (d, $^{2}J_{PP}$ = 43 Hz, 1P), 48.0 (d, $^{2}J_{PP}$ = 37 Hz, 1P). $^{31}P\{^{1}H\}$ NMR (256 K, $CDCl_3$, 202 MHz): δ 54.6 (d, $^{2}J_{PP}$ = 43 Hz, 1P), 54.2 (d, $^{2}J_{PP}$ = 37 Hz, 1P), 52.6 (d, $^{2}J_{PP}$ = 43 Hz, 1P), 49.0 (br s, 1P). $^{31}P\{^{1}H\}$ NMR (CD_2Cl_2, 121 MHz): δ 54.0 (d, $^{2}J_{PP}$ = 37 Hz, 1P), 53.8 (d, $^{2}J_{PP}$ = 43 Hz, 1P), 53.1 (d, $^{2}J_{PP}$ = 43 Hz, 1P), 48.6 (d, $^{2}J_{PP}$ = 37 Hz, 1P). ^{1}H NMR ($CDCl_3$, 500 MHz): δ 7.9-6.35 (m, 50H, Ph), 6.0 (br s, 2H), 3.82 (br s, 1H), 3.0-0.7 (m, 15H, dppb). Anal. Calcd for $C_{70}H_{68}Cl_4N_2P_4Ru_2$: C, 59.83; H, 4.88; N, 1.99. Found: C, 59.56; H, 4.78; N, 1.79.

2.12.2. $Ru_2Cl_4(dppb)_2(N{\equiv}CPh)$ 43 and $Ru_2Cl_4(dppb)_2(NH{=}CHPh)$ 44

(a) The solution made in 2.12.1a was heated to 50 °C after 4 d at room temperature. After 67 h $Ru_2Cl_4(dppb)_2$(*t,t*-benzaldehyde azine) **42** (53%) was evident by $^{31}P\{^{1}H\}$ NMR analysis, accompanied by $Ru_2Cl_4(dppb)_2(N{\equiv}CPh)$ (30%) **43** and $Ru_2Cl_4(dppb)_2(NH{=}CHPh)$ **44** (17%) After 140 h, only **43** and **44** remained (ratio 1:1). Slow evaporation of the solvent yielded X-ray quality orange crystals of **43**. (b) A solution of $Ru_2Cl_4(dppb)_2$(*t,t*-benzaldehyde azine) **42** (20 mg, 0.014 mmol) in $CDCl_3$ (1 mL) was freeze-thaw degassed (× 6), thawed under Ar and heated to 50 °C for 2 d wherein only **43** and **44** were evident by $^{31}P\{^{1}H\}$ NMR analysis (ratio 1:1).

IR (thin film; 1:1 mixture of **43** and **44**, cm^{-1}): 3200 (br, ν_{NH}); 2236 (w, $\nu_{C{\equiv}N}$); 1571 (m, $\nu_{C=N}$).

43: $^{31}P\{^{1}H\}$ NMR ($CDCl_3$, 121 MHz): δ 53.2 (d, $^{2}J_{PP}$ = 44 Hz, 1P), 52.4 (d, $^{2}J_{PP}$ = 44 Hz, 1P), 51.0 (d, $^{2}J_{PP}$ = 36 Hz, 1P), 45.3 (d, $^{2}J_{PP}$ = 36 Hz, 1P). This matches the $^{31}P\{^{1}H\}$ NMR spectrum reported for $Ru_2Cl_4(dppb)_2(N{\equiv}CPh)$.[9]

44: $^{31}P\{^{1}H\}$ NMR ($CDCl_3$, 121 MHz): δ 53.0 (d, $^{2}J_{PP}$ = 37 Hz, 1P), 52.9 (d, $^{2}J_{PP}$ = 43 Hz, 1P), 50.3 (d, $^{2}J_{PP}$ = 37 Hz, 1P), 47.2 (d, $^{2}J_{PP}$ = 43 Hz, 1P). Selected ^{1}H NMR ($CDCl_3$, 500 MHz): δ

9.37 (d, $^3J_{HH}$ = 21 Hz, 1H, *HN*=CHPh), 8.18 (d, *J* = 21 Hz, 1H, HN=C*H*Ph). ^{15}N-^{1}H HSQC ($CDCl_3$, 500 MHz, optimized for 50 Hz): δ 434.2 (br s, HN=CHPh).

2.12.3. Hydrolysis of $Ru_2Cl_4(dppb)_2(NH{=}CHPh)$ 44 with Liberation of Benzaldehyde

To an NMR solution of **43** and **44** in C_6D_6 (ca. 1 mL) was added one drop of freeze-thaw degassed H_2O via syringe. The mixture was left for 1 h with occasional mixing. ^{31}P analysis showed evidence of a new complex (thought to be $Ru_2Cl_4(dppb)_2(NH_3)$with remaining **43** and **44** (See discussion Chapter 5; Section 5.3.4). Selected ^{1}H NMR peaks for benzaldehyde (C_6D_6, 500 MHz): δ 10.32 (s). ^{13}C{^{1}H} NMR (C_6D_6, 125 MHz): δ 192.3 (s).

2.13. 2,3-Dicarboxylic Acid Norbornadiene[21]

To a solution of freshly cracked cyclopentadiene (0.6 g, 721 μL, 9.07 mmol) in Et_2O (3 mL) was added solid acetylenedicarboxylic acid (1.0 g, 8.77 mmol). The solution was stirred overnight at RT, over which time the product precipitated. The white precipitate was filtered off, washed with hexanes and dried under vacuum. Yield 1.5 g (92%). ^{1}H NMR ($CDCl_3$, 200 MHz): δ 11.45 (br s, 2H, CO_2H), 6.81 (s, 2H, C*H*=C*H*), 4.25 (s, 2H, C*H*CH$_2$C*H*), 2.31 (m, 2H, CHC*H*$_2$CH). ^{13}C{^{1}H} ($CDCl_3$, 75 MHz): δ 167.1, 157.9, 142.2, 73.2, 54.3.

2.14. Preparation of Diphenylamine and Menthol Salts for Transesterification

2.14.1. Lithium Diphenylamide

To a solution of diphenyl amine (6.0 g, 35.5 mmol) in C_6H_6 (175 mL) was added *n*-butyllithium (2.5 M, 14.9 mL, 37.2 mmol) by syringe under N_2. A white precipitate formed immediately. The mixture was stirred for 1 h, after which the product filtered off, washed with

hexanes (3 × 10 mL) and dried under vacuum. Yield 6.10 g (98%).

2.14.2. Potassium Menthoxide

Solid KH (258 mg, 6.43 mmol) was added slowly to a solution of (1R, 2S, 5R)-(-)-menthol (1.0 g, 6.4 mmol) in THF (10 mL). A white precipitate was formed instantaneously. The mixture was stirred for 2 h as the precipitate slowly redissolved. The solvent was stripped off leaving the product as a white solid. Yield 1.12 g (90%).

2.15. Vilsmeier Reagent[20]

To a solution of DMF (4.72 g, 64.6 mmol) in CH_2Cl_2 (50 mL) at 0 °C was added oxalyl chloride (2M in CH_2Cl_2, 34.0 mL, 67.8 mmol) by syringe. The Vilsmeier reagent precipitated immediately from solution. The mixture was stirred for 1 h at 0 °C, the white precipitate filtered off under N_2 and washed with CH_2Cl_2 to remove excess oxalyl choride. Yield 7.72 g (93%).

2.16. Norbornadiene based ROMP monomer preparation

2.16.1. 2,3-Dicarbomethoxynorbornadiene 53[21]

To a solution of dimethyl acetylenedicarboxylate (17.84 g, 125.6 mmol) in CH_2Cl_2 (100 mL) at 0 °C was added freshly cracked cyclopentadiene (9.97 g, 151 mmol, 12.0 mL) in 1 mL portions. The solution was stirred overnight at room temperature and the solvent stripped off to yield a clear, colourless oil, which was distilled under vacuum (bp = 81-83°C at 0.05 mtorr) (lit.[22] bp 134-135 °C at 10-11 mtorr). Yield 22.9 g, (88%). ^{1}H NMR data match values previously reported.[21] ^{1}H NMR ($CDCl_3$, 300 MHz): δ 6.81 (t, $^3J_{HH}$ = 2 Hz, 2H, *H*C=C*H*), 3.84 (t, $^3J_{HH}$ = 2 Hz, 2H, C*H*CH_2C*H*), 3.75 (s, 6H, CO_2CH_3), 2.20 (dd, $^3J_{HH}$ = 7 Hz, 1H, CHCH_2CH), 2.06 (dd,

$^3J_{HH}$ = 7 Hz, 1H, CHCH_2CH).

2.16.2. 2,3-Dicarbo-*tert*-butoxynorbornadiene 54

(a) To a solution of di-*tert*-butyl acetylenedicarboxylate (2.0 g, 8.8 mmol) in CH_2Cl_2 (20 mL) at 0 °C was added freshly cracked cyclopentadiene (0.701 g, 10.6 mmol, 845 µL) in one portion. The solution was stirred overnight at room temperature, after which the solvent was stripped off to leave a slightly yellow, solid residue. This was dissolved in a minimum of hot hexanes, and the product was precipitated as a white solid by cooling to –5 °C. The solid was isolated by filtration and washed with cold hexanes (0 °C). Yield 1.44 g (56%). (b) To a solution of lithium *tert*-butoxide (810 mg, 10.1 mmol) in THF (8 mL) was added a solution of 2,3-dicarbomethoxynorbornadiene **53** (1.0 g, 4,8 mmol) in THF (2 mL). White methoxide precipitated within 5 min. The mixture was stirred for 2 h and filtered (Celite). The filtrate was stripped of solvent and the residue redissolved in Et_2O (20 mL). This solution was washed with H_2O (2 × 10 mL) and the organic phase was dried ($MgSO_4$), filtered (Celite) and stripped of solvent to yield a white solid, which was recrystallized from hot hexanes. Yield 1.37 g, (98%). mp 86.5-86.9 °C. ^{1}H NMR data agree with values reported.[23] ^{1}H NMR ($CDCl_3$, 300 MHz): δ 6.86 (t, $^3J_{HH}$ = 2 Hz, 2H, *H*C=C*H*), 3.82 (t, $^3J_{HH}$ = 2 Hz, 2H, C*H*CH$_2$C*H*), 2.21 (dd, $^3J_{HH}$ = 7.4 Hz, 1H, CHCH_2CH); 2.02 (dd, $^3J_{HH}$ = 7.4 Hz, 1H, CHCH_2CH), 1.49 (s, 18H, C(CH_3)$_3$). ^{13}C{^{1}H} NMR ($CDCl_3$, 300 MHz): δ 165.2, 152.7, 142.9, 81.1, 72.1, 54.5, 28.3.

2.16.3. 2,3-Dicarbomenthoxynorbornadiene 55

(a) This compound was prepared by a modified literature procedure.[20] The diacid chloride of 2,3-dicarboxylic acid norbornadiene (Section 2.13) was prepared in situ (not isolated

as in the literature procedure) by addition of Vilsmeier reagent (Section 2.15) to 2,3-dicarboxylic acid norbornadiene as follows. To a cold (-35 °C) mixture of Vilsmeier reagent (329 mg, 2.57 mmol) in THF (8 mL) and MeCN (8 mL) was added a mixture of 2,3-dicarboxylic acid norbornadiene (232 mg, 1.29 mmol) and pyridine (203 mg, 2.57 mmol, 208 μL) in THF (8 mL). The mixture was stirred under N_2 at -30 °C for 1 h, -20 °C for 30 min. and the solvent stripped off. The residue was dissolved in dry THF (20 mL), potassium menthoxide (500 mg, 2.57 mmol) added and stirred overnight at RT under N_2. The mixture was filtered (Celite) to remove liberated KCl and the filtrate concentrated and purified by silica gel column chromatography (2% EtOAc in hexanes). The slightly beige solid was recrystallized from hot MeOH to give 2,3-dicarbomenthoxynorbornadiene **55** as a white solid. Yield 318 mg (54%). (b) To a solution of potassium menthoxide (Section 2.14.2) (9.3 g, 48.0 mmol) in THF (25 mL) was added a solution of 2,3-dicarbomethoxynorbornadiene **53** (5.0 g, 24.0 mmol) in THF (130 mL). The mixture was stirred overnight under N_2. The solvent was then stripped off and the residue dissolved in Et_2O (50 mL). This solution was washed with H_2O (2 × 25 mL), dried ($MgSO_4$), filtered (Celite), and stripped of solvent. The product was purified by silica gel column chromatography (2% EtOAc in hexanes) to give a beige solid, which was recrystallized from hot MeOH and pumped on under vacuum to remove all residual MeOH. Yield: 7.70 g, (70%). ^{1}H NMR data match values previously reported.[24] ^{1}H NMR ($CDCl_3$, 300 MHz): δ 6.89 (m, 2H, *H*C=C*H*), 4.76 (dt, $^3J_{HH}$ = 4, 11 Hz, 2H, CO_2CH), 3.86 (t, $^3J_{HH}$ = 2 Hz, 2H,=CHC*H*), 2.27 (m, 4H), 2.05 (m, 1H, =CHCHCH_2), 1.76 (dt, 1H, =CHCHCH_2), 1.48 (m, 6H), 1.15 (m, 6H), 0.90-0.80 (d, 12H, C*H*), 0.76 (s, 3H, Me), 0.74 (s, 3H, Me).

2.16.4. 2,3-Diphenylamidonorbornadiene 56

To a solution of 2,3-dicarbomethoxynorbornadiene **53** (2.5 g, 12.0 mmol) in THF (25 mL) was added a solution of lithium diphenylamide (Section 2.14.1) (4.42 g, 25.2 mmol) in THF (50 mL) under N_2. The mixture was stirred overnight, after which Et_2O (30 mL) and H_2O (30 mL) were added to the solution and the layers separated. The aqueous phase was washed with Et_2O (2 × 20 mL), and the combined organic layers were dried ($MgSO_4$) and filtered (Celite). The solvent was stripped off and the residue purified by silica gel chromatography (20% EtOAc in hexanes). The off-white solid was recrystallized under N_2 with hot toluene/hexanes and dried under vacuum. Yield: 5.19 g (90%). ^{1}H NMR ($CDCl_3$, 300 MHz): 7.61-6.95 (m, 20H, Ph), 5.98 (s, 2H, C*H*=C*H*), 3.23 (s, 2H, CH_2), 1.69-1.61 (m, 2H, C*H*CH_2C*H*). ^{13}C{^{1}H} NMR ($CDCl_3$, 75 MHz): δ 166.9, 153.7, 142.5, 140.4, 129.1, 127.5, 126.7, 72.0, 53.6. IR (Nujol, cm^{-1}): 1643 (s, ν_{C-O}). MS (EI) M^+ = 482. Anal. Calcd for $C_{27}H_{26}N_2O_2$: C, 82.11; H, 5.44; N, 5.83. Found: C, 82.15; H, 5.23; N, 5.95.

2.17. Benzyl Potassium[25]

To dry toluene (100 mL) was added a solution of *n*-BuLi in hexanes (2.67 M, 38.5 mmol, 14.4 mL) and solid potassium *tert*-butoxide (4.3 g, 38 mmol). The resulting dark red mixture was stirred overnight under N_2. The red precipitate was filtered off and washed with toluene (2 × 30 mL) and hexanes (3 × 30 mL) and dried under vacuum. Yield 4.84 g (97%).

2.18. Biphenolate Ligand Preparation

2.18.1. 3,3',5,5'-Tetra-*tert*-butyl-biphenyl-2,2'-diol 51a and Dipotassium 3,3',5,5'-tetra-*tert*-butylbiphenolate 52a

To a solution of 2,4-di-*tert*-butyl phenol (10.0 g, 48.5 mmol) in glacial acetic acid (46 mL) at 55 °C was added (dropwise, over 30 min) a solution of $K_2Cr_2O_7$ (4.54 g, 18.8 mmol) dissolved in aqueous H_2SO_4 (48 mL H_2O, 9 mL conc H_2SO_4). The orange solution turned green and a yellow precipitate was evident. This precipitate was filtered off and purified by silica gel chromatography (hexanes). Yield 7.56 g (76%). mp = 238.6-239.8°C (lit.[26] mp 239-240°C). ^1H NMR ($CDCl_3$, 300 MHz): δ 7.35 (s, 2H), 7.10 (s, 2H), 1.47 (s, 9H), 1.30 (s, 9H). $^{13}C\{^1H\}$ NMR ($CDCl_3$, 75 MHz): δ 149.8, 143.0, 136.2, 125.3, 124.8, 122.3, 35.2, 34.5, 31.7, 29.7. The dipotassium salt of 3,3',5,5'-tetra-*tert*-butyl-biphenyl-2,2'-diol **51a** was prepared as described in the literature.[27] A red solution of benzyl potassium (Section 2.17) (1.08 g, 8.31 mmol) in THF (5 mL) was added dropwise to a solution of 3,3',5,5'-tetra-*tert*-butyl-biphenyl-2,2'-diol **51a** (1.706 g, 4.155 mmol) in THF (10 mL). Deprotonation was complete when a light orange colour persisted. The solvent was stripped off, leaving the product as an off-white solid, which was used without purification.

2.18.2. Dipotassium 5,5',6,6'-tetramethyl-3,3'-di-*tert*-butylbiphenolate 52b

The dipotassium salt of commercially available 3,3'-di-*tert*-butyl-5,5'6,6'-tetramethylbiphenyl-2,2'-diol **51b** was prepared by the method[27] described in Section 2.18.1.

2.18.3. Dipotassium (R)-(+)-5,5',6,6'-tetramethyl-3,3'-di-*tert*-butylbiphenolate (R)-(+)-52b

The dipotassium salt of commercially available (R)-(+)-5,5',6,6'-tetramethyl-3,3'-di-*tert*-

butylbiphenyl-2,2'-diol (R)-(+)-**51b** was prepared by the method[27] described in Section 2.18.1.

2.18.4. 3,3',5,5'-Tetra-*tert*-butyl-6,6'-dimethylbiphenyl-2,2'-diol 51c and Dipotassium 3,3',5,5'-tetra-*tert*-butyl-6,6'-dimethylbiphenolate 52c

To a solution of 2,4-di-*tert*-butyl-5-methyl phenol (5.0 g, 22.7 mmol) in glacial acetic acid (23 mL) at 55 °C was added a solution of $K_2Cr_2O_7$ (2.27 g, 7.72 mmol) dissolved in aqueous H_2SO_4 (24 mL H_2O, 4.5 mL conc H_2SO_4) dropwise over 30 min. The orange solution turned green and a precipitate was evident. This precipitate was filtered off and two compounds were isolated by silica gel chromatography (2% EtOAc in hexanes). The first compound was white 3,3',5,5'-tetra-*tert*-butyl-6,6'-dimethylbiphenyl-2,2'-diol **51c**. Yield 1.107 g (22%). The second compound (yellow 2-methyl-5-*t*-butylquinone) was also isolated. Yield 1.61 g (40%). **51c**: ^{1}H NMR data match values previously reported.[28] ^{1}H NMR ($CDCl_3$, 300 MHz): δ 7.36 (s, 2H, aromatic), 4.79 (s, 2H, O*H*), 1.99 (s, 6H, CH_3), 1.40 (s, 18H, C(CH_3)$_3$), 1.38 (s, 18H, C(CH_3)$_3$). The dipotassium salt of 3,3',5,5'-tetra-*tert*-butyl-6,6'-dimethylbiphenyl-2,2'-diol **51c** was prepared by the method[27] described in Section 2.18.1.

2.19. Neophyl Grignard Preparation for Molybdenum Precursor Synthesis

A mixture of dry magnesium turnings (6.1 g, 251 mmol) and two crystals of I_2 in Et_2O (100 mL) was placed in a 3-necked flask which was fitted with a dropping funnel containing the neophyl chloride (31.47 g, 30.0 mL, 186 mmol) layered with Et_2O (10 mL). After a condenser was fitted, the neophyl chloride was added slowly under N_2 until the mixture became warm and started to reflux gently. The remaining neophyl chloride was then added slowly over 45 min, maintaining reflux temperatures. The mixture was heated overnight and the Grignard solution

cannulated into a Kontes flask and stored under N_2. A known volume of solution was titrated against methanol using 1,10-phenanthroline as the indicator (endpoint purple to yellow). Found titer 1.15 M.

2.20. Molybdenum Precursors

2.20.1. $MoCl_2(NAr)_2(DME)$

To a suspension of $(NH_4)_2Mo_2O_7$ (3.0 g, 8.82 mmol) in anhydrous dimethoxyethane (DME) (45 mL) was slowly added solutions of Et_3N (7.14 g, 70.6 mmol, 9.84 mL) in DME (3 mL), trimethylsilyl chloride (16.30 g, 150.0 mmol, 19.04 mL) in DME (6 mL) and 2,6-diisopropyl aniline (6.26 g, 35.3 mmol, 6.66 mL) in DME (3 mL). The brick-red solution was stirred for 18 h under N_2 and then heated for 6 h at 65 °C. The mixture was filtered (Celite) and rinsed with DME to remove all of the compound from the Celite. The filtrate was stripped of solvent and the red solid dried under vacuum. Yield 10.7 g (100%). ^{1}H NMR data match values previously reported.[29] ^{1}H NMR (C_6D_6, 300 MHz): δ 7.01 (d, 4H, H_m), 6.90 (t, 2H, H_p), 4.31 (sept, 4H, C*H*Me$_2$), 3.45 (s, 6H, DME), 3.19 (s, 4H, DME), 1.26 (d, 24H, CH(C*H*$_3$)$_2$.

2.20.2. $Mo(CH_2Me_2Ph)_2(NAr)_2$

A solution of $MoCl_2(NAr)_2(DME)$ (Section 2.20.1) (10.0 g, 16.5 mmol) in Et_2O (200 mL) was cooled to -35 °C, and a solution of neophyl Grignard (Section 2.19) (1.15 M, 32.9 mmol, 38.0 mL) was added dropwise by pipette. The orange mixture was stirred at RT for 4 h, filtered (Celite), washed with Et_2O and the filtrate concentrated until a precipitate appeared. The bright orange precipitate was filtered off and the filtrate was concentrated again to yield a second crop of product. Yield 7.09 g (60%). ^{1}H NMR data match values previously reported.[29] ^{1}H NMR

(C_6D_6, 300 MHz): δ 7.46 (d, 4H, aromatic), 7.25 (t, 4H, aromatic), 7.10 (t, 2H, aromatic), 7.01-6.91 (m, 6H, aromatic), 3.66 (sept, 4H, C*H*Me_2), 1.72 (s, 4H, CH_2CMe_2Ph), 1.50 (s, 12H, $CH_2C(CH_3)_2Ph$), 1.10 (d, 24H, $CH(CH_3)_2$. ^{13}C {^1H} NMR (C_6D_6, 75 MHz): δ 153.4, 143.2, 129.6, 127.1, 126.5, 125.8, 123.1, 79.4, 40.3, 32.9, 28.7, 24.3.

2.20.3. Mo(CHCMe_2Ph)(NAr)(OSO_2CF_3)$_2$(DME) 50

A chilled solution of triflic acid (5.0 g, 33.3 mmol) in anhydrous dimethoxyethane (DME) (150 mL) was added dropwise to a solution of Mo(CH_2Me_2Ph)$_2$(NAr)$_2$ (Section 2.20.2) (7.9 g, 11.1 mmol) at -35 °C. The mixture was allowed to warm to RT and stirred for 16 h. During this time the colour changed from orange to dark yellow. The solvent was stripped off to yield a yellow residue, which was extracted with chilled toluene (3 × 40 mL, or until washings colourless) and filtered (Celite). The filtrate was concentrated and cooled (-35 °C) to precipitate the product as a yellow powder, which was filtered off. Three crops were collected and the combined product was recrystallized from Et_2O at -35 °C to give a yellow powder. Yield 6.85 g (78%). ^1H NMR data match values previously reported.[29] ^1H NMR (C_6D_6, 300 MHz): δ 14.51 (s, 1H, C*H*CMe_2Ph), 7.58 (d, 2H, aromatic), 7.19 (t, 2H, aromatic), 6.70-6.88 (m, 4H, aromatic), 3.85 (sept, 2H, C*H*Me_2), 3.75 (s, 3H, OCH_3), 3.19 (m, 2H, OCH_2), 2.85-2.80 (m, 5H, OCH_3, OCH_2), 1.90 (s, 6H, $CHC(CH_3)_2Ph$), 1.35 (d, 6H, $CH(CH_3)_2$), 1.20 (d, 6H, $CH(CH_3)_2$). ^{13}C {^1H} NMR (C_6D_6, 750 MHz): δ 328.7, 152.1, 151.8, 148.6, 131.3, 129.1, 127.8, 124.5, 73.3, 70.1, 66.8, 62.3, 59.4, 31.0, 28.3, 26.7, 23.2.

2.21. Preparation of Molybdenum Biphenolate Catalysts 49a-c and *Tert*-butoxide catalyst 49d

2.21.1. General Procedure

To a solution of $Mo(CHCMe_2Ph)(NAr)(OSO_2CF_3)_2(DME)$ **50** (1.0 g, 1.3 mmol) in THF (20 mL) was added solid alkoxide (2 equiv) or biphenolate **52** (1 equiv). The mixture was stirred for 2 h at RT. The yellow solution turned dark red for biphenolate catalysts **49a-c** or orange for the alkoxide catalyst **49d**. The solvent was stripped off, the residue redissolved in pentane and filtered (Celite) to remove the triflate salts. The pentane was stripped off and the residue redissolved in toluene, filtered (Celite) and stripped off to remove any coordinated THF. The product was either recrystallized from Et_2O at -35 °C (**49a,b**) or pentane at –35 °C (**49d**), or was used as a dry friable foam (**49c**). Attempted recrystallization of **49c** from Et_2O or pentane at –35 °C were unsuccessful.

2.21.2. Mo(=CHCMe$_2$Ph)(NAr)(3,3',5,5'-tetra-*tert*-butyl-1,1'-biphenyl-2,2'-diolate) 49a [30]

To a solution of $Mo(CHCMe_2Ph)(NAr)(OSO_2CF_3)_2(DME)$ **50** (500 mg, 0.632 mmol) in THF (10 mL) was added solid dipotassium 3,3',5,5'-tetra-^{t}Bu-biphenolate **52a** (307 mg, 0.632 mmol). Workup as above gave a yellow solid. Yield: 431 mg (84%). ^{1}H NMR data match values found in the literature without coordinated THF.[30] ^{1}H NMR (C_6D_6, 300 MHz): δ 11.88 (s, 1H, *syn* Mo=C*H*), 7.82-6.93 (m, 12H, aryl), 3.81 (sept, 2H, C*H*Me$_2$), 1.98 (s, 3H, Me), 1.81 (s, 3H, Me), 1.62 (s, 9H, ^{t}Bu), 1.58 (s, 9H, ^{t}Bu), 1.38 (s, 9H, ^{t}Bu), 1.33 (s, 9H, ^{t}Bu), 1.18 (d, 6H, CH(CH_3), 0.83 (d, 6H, CH(CH_3)).

2.21.3. Mo(=CHCMe$_2$Ph)(NAr)(5,5',6,6'-tetramethyl-3,3'-di-*tert*-butyl-1,1'-biphenyl-2,2'-diolate) 49b

To a solution of Mo(CHCMe$_2$Ph)(NAr)(OSO$_2$CF$_3$)$_2$(DME) **50** (1.74 g, 2.20 mmol) in THF (25 mL) was added solid dipotassium 5,5',6,6'-tetramethyl-3,3'-di-*tert*-butylbiphenolate **52b** (948 mg, 2.20 mmol). Workup as above gave a red powder. Yield: 1.46 g (88%). ^{1}H and ^{13}C{^{1}H} NMR data match values found in the literature.[30] ^{1}H NMR (C$_6$D$_6$, 300 MHz): anti δ 12.76 (s, 1H, =C*H*), syn 10.99 (s, 1H, =C*H*), 7.44 (m, 3H, Biphen and *o*-Ph), 7.15 (m, 3H, Biphen and *m*-Ph), 7.05 (m, 1H, *p*-Ph), 6.93 (s, 3H, Ar), 3.71 (sept, $^3J_{HH}$ = 7 Hz, 2H, C*H*Me$_2$), 2.15 (s, 3H, Biphen), 2.05 (s, 3H, Biphen), 1.85 (s, 3H, Biphen), 1.75 (s, 3H, Biphen), 1.65 (s, 3H, C(C*H*$_3$)(MePh)), 1.60 (s, 9H, ^{t}Bu), 1.55 (s, 9H, ^{t}Bu), 1.15 (d, $^3J_{HH}$ = 7 Hz, 6H, CH(C*H*$_3$)(Me)), 1.13 (s, 3H, C(C*H*$_3$)(MePh)), 0.91 (d, $^3J_{HH}$ = 7 Hz, 6H, CH(C*H*$_3$)(Me)). ^{13}C{^{1}H} NMR (C$_6$D$_6$, 75 MHz): δ 277.3 (d, J_{CH} = 123 Hz, *C*HR), 154.8, 154.5, 154.3, 151.2, 147.5, 140.7, 138.3, 137.6, 136.7, 132.2, 131.9, 130.8, 130.6, 130.5, 129.9, 129.2, 128.5, 127.4, 126.8, 124.4, 54.7 (*C*Me$_2$Ph), 36.4, 35.3 (*C*Me$_3$), 33.2, 32.8 (C(*C*H$_3$)(MePh), 31.4, 30.6 (C(*C*H$_3$)$_3$), 28.8 (*C*HMe$_2$), 25.4 (CH(*C*H$_3$)$_2$), 20.8, 20.7, 17.1, 16.5.

2.21.4. (R)-(+)-Mo(=CHCMe$_2$Ph)(NAr)(5,5',6,6'-tetramethyl-3,3'-di-*tert*-butyl-1,1'-biphenyl-2,2'-diolate) (R)-(+)-49b

To a solution of Mo(CHCMe$_2$Ph)(NAr)(OSO$_2$CF$_3$)$_2$(DME) **50** (224 mg, 0.283 mmol) in THF (8 mL) was added solid dipotassium (R)-(+)-5,5',6,6'-tetramethyl-3,3'-di-^{t}Bu-biphenolate (R)-(+)-**52b** (122 mg, 0.283 mmol). Workup as above gave a red powder. Yield: 194.8 mg (82%). ^{1}H and ^{13}C{^{1}H} NMR data match values found in the literature.[30] ^{1}H NMR (C$_6$D$_6$, 300 MHz): *anti* δ 12.76 (s, 1H, =C*H*), *syn* 10.99 (s, 1H, =C*H*), 7.44 (m, 3H, Biphen and *o*-Ph), 7.15 (m, 3H, Biphen and *m*-Ph), 7.05 (m, 1H, *p*-Ph), 6.93 (s, 3H, Ar), 3.71 (sept, $^3J_{HH}$ = 7 Hz, 2H, C*H*Me$_2$),

2.15 (s, 3H, Biphen), 2.05 (s, 3H, Biphen), 1.85 (s, 3H, Biphen), 1.75 (s, 3H, Biphen), 1.65 (s, 3H, C(CH_3)(MePh)), 1.60 (s, 9H, ^{t}Bu), 1.55 (s, 9H, ^{t}Bu), 1.15 (d, $^3J_{HH}$ = 7 Hz, 6H, CH(CH_3)(Me)), 1.13 (s, 3H, C(CH_3)(MePh)), 0.91 (d, $^3J_{HH}$ = 7 Hz, 6H, CH(CH_3)(Me)). $^{13}C\{^1H\}$ NMR (C_6D_6, 75 MHz): δ 277.2 (d, J_{CH} = 123 Hz, *C*HR), 154.8, 154.5, 154.3, 151.4, 147.7, 140.3, 138.7, 137.4, 136.2, 132.1, 131.3, 130.8, 130.6, 130.5, 130.5, 129.7, 128.5, 127.6, 126.2, 124.8, 54.4 (*C*Me$_2$Ph), 36.7, 35.3 (*C*Me$_3$), 33.2, 32.7 (C(*C*H$_3$)(MePh), 31.1, 30.4 (C(*C*H$_3$)$_3$), 29.5 (*C*HMe$_2$), 25.3 (CH(*C*H$_3$)$_2$), 20.8, 20.7, 17.4, 16.5.

2.21.5. Mo(=CHCMe$_2$Ph)(NAr)(3,3',5,5'-tetra-*tert*-butyl-6,6'-dimethyl-1,1'-biphenyl-2,2'-diolate) 49c

To a solution of Mo(CHCMe$_2$Ph)(NAr)(OSO$_2$CF$_3$)$_2$(DME) **50** (500 mg, 0.632 mmol) in THF (10 mL) was added solid dipotassium 3,3',5,5'-tetra-^{t}Bu-6,6'-dimethylbiphenolate **52c** (488 mg, 0.948 mmol). Workup as described above gave a red friable foam. Yield: 506 mg (96%). ^{1}H NMR data matches that found in the literature.[28] ^{1}H NMR (C_6D_6, 300 MHz): δ 11.18 (s, 1H, C*H*CMe$_2$Ph), 8.00 (s, 1H, biphen Ar), 7.83 (s, 1H, biphen Ar), 7.59 (d, $^3J_{HH}$ = 8 Hz, 2H, imido Ar), 7.35 (s, 5H, neophyl Ar), 7.20 (t, $^3J_{HH}$ = 8 Hz, imido Ar), 4.06 (sept, $^3J_{HH}$ = 7 Hz, 2H, C*H*Me$_2$), 2.36 (s, 3H, biphen Me), 2.17 (s, 3H, biphen Me), 2.01 (s, 3H, neophyl Me), 1.81 (s, 9H, C(CH_3)$_3$), 1.41 (s, 3H, neophyl Me), 1.37 (d, $^3J_{HH}$ = 7 Hz, CH(CH_3)$_2$), 1.11 (d, $^3J_{HH}$ = 7 Hz, 6H, CH(CH_3)$_2$).

2.21.6. Mo(=CHCMe$_2$Ph)(NAr)(O-*tert*-Bu)$_2$ 49d

To a solution of Mo(CHCMe$_2$Ph)(NAr)(OSO$_2$CF$_3$)$_2$(DME) **50** (1.0 g, 1.3 mmol) in THF (20 mL) was added solid LiO-*tert*-Bu (203 mg, 2.53 mmol). Workup as above gave orange crystals. Yield: 536 mg (77%). ^{1}H NMR data matches that found in the literature.[29] ^{1}H NMR

(C_6D_6, 300 MHz): δ11.30 (s, 1H, C*H*CMe$_2$Ph), 7.43 (d, 2H, aromatic), 7.2-7.0 (m, 6H, aromatic), 3.98 (sept, 2H, C*H*Me$_2$), 1.73 (s, 3H, CHC(C*H*$_3$)$_2$Ph), 1.35 (s, 3H, CHC(C*H*$_3$)$_2$Ph), 1.31 (s, 18H, OC(C*H*$_3$)$_3$).

2.22. General Procedure for ROMP of 2,3-Dicarboalkoxy/diamidonorbornadienes (53-56) using Molybdenum Alkylidene Initiators 49.

To a rapidly stirring solution of molybdenum biphenolate/alkoxide initiator **49** in THF or CH_2Cl_2 (filtered through alumina) (7 mL) was rapidly added a solution of monomer (1 mL) in THF or CH_2Cl_2 (by pipette in one portion). The solution was stirred at RT until no residual monomer was evident by ^{1}H NMR analysis. The reaction was then quenched by addition of benzaldehyde (3 drops). If the polymer precipitated, CH_2Cl_2 (5 mL, filtered through alumina) was added to generate a solution which was stirred for 2 h. The solution was then concentrated to ca.1 mL and added dropwise to rapidly stirring MeOH, from which the polymer precipitated. The polymer was isolated by centrifugation or filtration as appropriate, washed with MeOH and dried under vacuum. Yields for polymers of 2,3-dicarbomethoxynorbornadiene **53**, 2,3-dicarbomenthoxynorbornadiene **55**, and 2,3-diphenylamidenorbornadiene **56** were >90%. Yields of polymers of 2,3-dicarbo^{t}butoxynorbornadiene **54** were ca. 85% owing to increased solubility in MeOH. Polymerization reactions were run in triplicate.

2.22.1. Polymer of 2,3-Dicarbomethoxynorbornadiene 53

^{1}H and ^{13}C{^{1}H} NMR data match values previously reported.[27] ^{1}H NMR ($CDCl_3$, 300 MHz): δ 5.48 (br s, 2H, *H*C=C*H*), 3.75 (br s, 6H, Me), 3.56 (br s, 2H, C*H*), 2.48 (m, 1H, C*H*$_2$), 1.49 (m, 1H, C*H*$_2$). ^{13}C{^{1}H} NMR ($CDCl_3$, 125 MHz) for polymer prepared with Mo(=CHCMe$_2$Ph)(NAr)(O^{t}Bu)$_2$ **49d**: δ 165.4 (*C*O), 142.2 (C$_3$), 132.4 (C$_1$ *trans*), 131.6 (C$_1$ *cis*),

52.1 (Me), 49.2 (m, C_2 *trans*), 44.3 (C_2 *cis*), 39.3 (C_4, *mm*), 39.2 (C_4, *mr/rm*), 39.0 (C_4, *rr*). Yield: 99%.

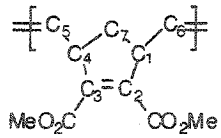

2.22.2. Polymer of 2,3-Dicarbo-*tert*-butoxynorbornadiene 54

^{1}H and ^{13}C{^{1}H} NMR data match values previously reported.[23] ^{1}H NMR ($CDCl_3$, 300 MHz): δ 5.48 (br s, 2H, *H*C=C*H*), 3.81 (br s, 2H, C*H*), 3.47 (br s, 1H, CH_2), 2.48 (br s, 1H, CH_2), 1.43 (s, 18 H, C(CH_3)). ^{13}C{^{1}H} NMR ($CDCl_3$, 125 MHz) for polymer prepared with Mo(=CHCMe$_2$Ph)(NAr)(O^{t}Bu)$_2$ **49d**: δ 164.2 (*C*O), 142.2 (C_3), 132.4 (C_1 *trans*), 131.6 (C_1 *cis*), 81.7 (-*C*(Me)$_3$), 49.0 (C_2 *trans*), 44.6 (C_2 *cis*), 39.7 (C_4, *mm*), 38.4 (C_4, *mr/rm*), 37.8 (C_4, *rr*),28.1 (Me). Yield: 86%

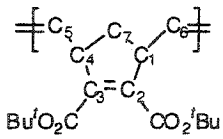

2.22.3. Polymer of 2,3-Dicarbomenthoxynorbornadiene 55

^{1}H and ^{13}C{^{1}H} NMR data match values previously reported.[24] ^{1}H NMR ($CDCl_3$, 300 MHz): δ 5.54 (m, 1H, *H*C=C*H*), 5.45 (m, 1H, *H*C=C*H*), 4.70 (br s, 2H, C*H*), 4.01 (br s, 1H, CH_2), 3.79 (br s, 1H, CH_2), 2.27 (br s, 1H, menthyl), 2.24 (br s, 2H, menthyl), 1.92 (br s, 2H, menthyl), 1.67 (br s, 4H, menthyl), 1.45 (br s, 5H, menthyl), 1.27 (br s, 3H, menthyl), 0.83 (br s, 14H, menthyl), 0.71 (br s, 7H, menthyl). ^{13}C{^{1}H} NMR ($CDCl_3$, 75 MHz) for polymer prepared with Mo(=CHCMe$_2$Ph)(NAr)(5,5',6,6'-tetramethyl-3,3'-di-*tert*-butyl-1,1'-biphenyl-2,2'-diolate) **49b**: δ 165.0 (*C*O), 164.1 (*C*O), 143.8 (C_3), 140.8 (C_3), 132.59 (C_1), 131.5 (C_1), 75.7 (CO_2*C*H),

75.3 (CO_2CH), 47.1 (C_2), 47.0, 45.6 (C_2), 44.8, 41.1, 39.7 (C_4), 34.7, 31.9, 25.9, 23.5, 22.55 (Me), 22.53 (Me), 21.42 (Me), 21.39 (Me), 16.6 (Me), 16.3 (Me) (all other resonances overlapping). Yield: 95%.

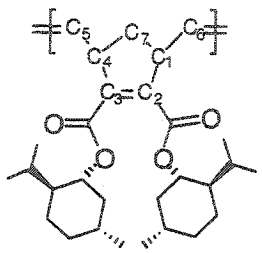

2.22.4. Polymer of 2,3-Diphenylamidenorbornadiene 56

For the polymer prepared with Mo(=CHCMe$_2$Ph)(NAr)(3,3',5,5'-tetra-*tert*-butyl-1,1'-biphenyl-2,2'-diolate) **49a**: In the ^{1}H NMR spectrum all the peaks are very broad in $CDCl_3$ at 50 °C with a rolling baseline. $^{13}C\{^1H\}$ NMR (1,3-dichlorobenzene, 100°C, 75 MHz): δ 166.1 (*C*O), 144.2, 131.9, 49.2 (C_2 trans), 44.8 (C_2 cis), 39.9 (C_4 *mm*), 39.6 (C_4, *mr/rm*), 39.0 (C_4, *rr*) (all other resonances overlap with solvent). Yield: 91%.

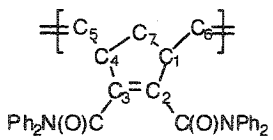

2.22.5. General Procedure for Preparation of Copolymers of MTD and 53

To a rapidly stirring solution of Mo(=CHCMe$_2$Ph)(NAr)(3,3',5,5'-tetra-*tert*-butyl-1,1'-biphenyl-2,2'-diolate) **49a** in THF (7 mL) was added a solution of MTD in THF (1 mL). After 1 h, a solution of 2,3-dicarbomethoxynorbornadiene **53** in THF (1 mL) was added quickly in one portion. The solution became opaque within 5 min. The mixture was stirred for 2 h and quenched with benzaldehyde (3 drops). CH_2Cl_2 (5 mL, filtered through alumina) was added to solubilize the polymer and stirred for 1 h. The solution was concentrated (*ca.* 1 mL) and added dropwise to

rapidly stirring MeOH to precipitate the polymer as a powder, which was isolated by centrifugation. All ^{1}H NMR resonances were very broad. ^{13}C{^{1}H} NMR resonances for the repeat unit derived from **53** are sharp and well defined, while those derived from MTD are very broad. ^{1}H ($CDCl_3$, 300 MHz): δ 5.40 (br s), 3.91 (br s), 3.72 (s), 2.93 (br s), 2.49-1.05 (m), 0.86 (br s), 0.38 (br s). ^{13}C {^{1}H} ($CDCl_3$, 125 MHz): δ 165.2 (**53**, *C*O), 142.2 (**53**, C_3), 131.9 (MTD), 131.4 (**53**, C_1, cis), 54.6 (MTD), 53.5 (MTD), 52.0 (**53**, Me), 46.3 (MTD), 45.4 (MTD), 44.3 (**53**, C_2, cis), 43.6 (MTD), 43.3 (MTD), 42.2 (MTD), 41.6 (MTD), 41.3 (MTD), 39.8 (MTD), 39.7 (MTD), 38.7 (**53**, C_4, *mm*), 36.4 (MTD), 36.2 (MTD), 34.1 (MTD), 34.0 (MTD), 32.5 (MTD), 29.6 (MTD), 21.8 (MTD), 17.5 (MTD), 17.3 (MTD). All other resonances are overlapping.

2.23. References

(1) Snelgrove, J. S.; Conrad, J. C.; Yap, G. P. A.; Fogg, D. E. *Inorg. Chim. Acta* **2003**, *345*, 268.
(2) Amoroso, D.; Snelgrove, J. L.; Conrad, J.; Drouin, S. D.; Yap, G. P. A.; Fogg, D. E. *Adv. Synth. Catal.* **2002**, *344*, 757.
(3) Adams, R. D.; Chodosh, D. F. *Inorg. Chem.* **1978**, *17*, 41.
(4) Hallman, P. S.; Stephenson, T. A.; Wilkinson, G. *Inorg. Synth.* **1970**, *12*, 237.
(5) Hoffman, P. R.; Caulton, K. G. *J. Am. Chem. Soc.* **1975**, *97*, 237.
(6) Hoffman, P. R.; Caulton, K. G. *J. Am. Chem. Soc.* **1975**, *97*, 4221.
(7) Armit, P. W.; Sime, W. J.; Stephenson, T. A. *J. Chem. Soc., Dalton* **1976**, *20*, 2121.
(8) Bressan, M.; Rigo, P. *Inorg. Chem.* **1975**, *14*, 2286.
(9) Fogg, D. E. *Ph.D. Thesis*; The Univerisity of British Columbia: Vancouver, 1994.
(10) Jung, C. W.; Garrou, P. E.; Hoffman, P. R.; Caulton, K. G. *Inorg. Chem.* **1984**, *23*, 726.
(11) Joshi, A. M.; Thorburn, I. S.; Rettig, S. J.; James, B. R. *Inorg. Chim. Acta* **1992**, *198-200*, 283.
(12) MacFarlane, K. S.; Thorburn, I. S.; Cyr, P. W.; Chau, D. E. K.-Y.; Rettig, S. J.; James, B. R. *Inorg. Chim. Acta* **1998**, *270*, 130.
(13) Amoroso, D.; Yap, G. P. A.; Fogg, D. E. *Can. J. Chem.* **2001**, *79*, 958.
(14) Hallman, P. S.; McGarvey, B. R.; Wilkinson, G. *J. Chem. Soc. A* **1968**, 3143.
(15) Levison, J. J.; Robinson, S. D. *J. Chem. Soc. A* **1970**, 2947.
(16) Uozumi, Y.; Tanahashi, A.; Lee, S.-Y. H., T. *J. Org. Chem.* **1993**, *58*, 1945.
(17) Wilhelm, T. E.; Belderrain, T. R.; Brown, S. N.; Grubbs, R. H. *Organometallics* **1997**, *16*, 3867.
(18) Creary, X. In *Organic Syntheses*; Wiley & Sons: Toronto, 1990; Vol. VII, p 438.

(19) Pouchert, J. J.; Behnke, J. In *Aldrich Library of NMR Data*; Aldrich Chemical Co.: Milwaukee, WI, 1993; Vol. 3, p 546(A).
(20) Fujisawa, T.; Sato, T. *Org. Synth.* **1988**, *66*, 121.
(21) Tabor, D. C.; White, F. H.; Collier, L. W.; Evans, S. A. *J. Org. Chem.* **1983**, *48*, 1638.
(22) Diels, O.; Alder, K. *Justus Leibigs Ann. Chem.* **1931**, *490*, 236.
(23) Schrock, R. R.; Lee, J. K.; O'Dell, R.; Oskam, J. H. *Macromolecules* **1995**, *28*, 5933.
(24) O'Dell, R.; McConville, D. H.; Hofmeister, G. E.; Schrock, R. R. *J. Am. Chem. Soc.* **1994**, *116*, 3414.
(25) Schlosser, R. R.; Hartmann, J. *Angew. Chem. Int. Ed.* **1973**, *12*, 508.
(26) Albert, H. E. *J. Am. Chem. Soc.* **1954**, *76*, 4983.
(27) McConville, D. H.; Wolf, J. R.; Schrock, R. R. *J. Am. Chem. Soc.* **1993**, *115*, 4413.
(28) Totland, K. M.; Boyd, T. J.; Lavoie, G. G.; Davis, W. M.; Schrock, R. R. *Macromolecules* **1996**, *29*, 6614.
(29) Schrock, R. R.; Murzdek, J. S.; Bazan, G. C.; Robbins, J.; DiMare, M.; O'Reagan, M. *J. Am. Chem. Soc.* **1990**, *112*, 3875.
(30) Alexander, J. B.; Schrock, R. R.; Davis, W. M.; Hultzsch, K. C.; Hoveyda, A. H.; Houser, J. H. *Organometallics* **2000**, *19*, 3700.

CHAPTER 3

The Kinetic Instability of the Ruthenium-Aryloxide Bond

3.1. Introduction

A recent resurgence in interest in aryloxide complexes of the late transition metals stems from the potential of the aryloxide group in catalysis, both as substrate (in, e.g., nucleophilic phenol functionalization[1] or carbonylation[2,3]) and as a sterically versatile pseudohalide ligand.[4-7] Within late transition metal complexes, the aryloxide ligand can bind either through the aryl ring or the oxygen group. Examples of both σ- and π-aryloxide derivatives are now known for groups 6 through 10.[8] σ-Bound aryloxide complexes are known for Pd,[3,7,9] Ni,[7] Rh[10] and Ru,[11-13] and π-bound complexes for Cr,[14] Fe,[15] Ir[1,16,17] and Ru.[18-23] While empirical trends associate π-bound aryloxide with PPh_3, COD, Cp*, and C_2H_4 ligands, and σ-bound aryloxide with CO and PMe_3, this pattern of behaviour is not invariable, and in some cases the σ- and π-derivatives are obtained by markedly similar routes.[11,19]

Whether or not Ru-phenoxide complexes can be isolated depends on the stability of the ruthenium-oxygen bond. Early metals form metal-heteroatom complexes more readily than late metal systems because they are more electropositive.[24] While the hard-soft formalism predicts low bond energies for late metal-heteroatom bonds,[25] experimentally measured bond strengths contradict this. These trends indicate that Ru-OAr bond energies, for example, are stronger than Ru-carbon bonds, in the order $L_4(H)Ru\text{-}H > L_4(H)Ru\text{-}OAr > L_4(H)Ru\text{-}NHPh > L_4(H)Ru\text{-}CH_2Ph$.[13]

The strength of the metal-heteroatom bond is affected by p_π/d_π interactions between the heteroatom lone pairs and electrons in metal d orbitals.[26] A strong case has been made that the filled p-orbitals of the heteroatom can stabilize an M-X complex where an empty d-orbital is present, but can *destabilize* complexes in which the d-orbital is filled. Flled / filled repulsion results in a higher M-X bond energy, and increases the reactivity of the heteroatom lone pair, which may be both nucleophilic and basic.

In the hope of disentangling the factors that determine the preference for π- vs. σ-coordination of aryloxide, we undertook a systematic investigation of the reactions of chlororuthenium phosphine complexes with simple aryloxide ligands. *p-tert*-Butylphenoxide ("OAr"), in which the *tert*-butyl group affords a valuable handle for ^{1}H NMR analysis, was employed as the aryloxide ligand of choice. Selected reactions were repeated with phenoxide: in general, reaction pathways were unperturbed, although one significant exception is described in Section 3.6.

3.2. Reaction of $RuCl_2(PPh_3)_3$ 1a with Aryloxide in the Presence of Alcohols

3.2.1. Reaction of 1a with Two Equivalents of Aryloxide

Stoichiometric control in transmetallation of $RuCl_2(PPh_3)_3$ **1a** with potassium or lithium aryloxide (Scheme 3.1) is hampered by the very different solubilities of the reagents. Of the common solvents, only THF permits dissolution of both aryloxide salt and the Ru precursor. However, reactions in THF yielded an intractable orange product, characterization of which was prevented by its complete insolubility in all solvents. The synthesis was therefore undertaken in a mixed organic-alcohol solvent system, in which methanol was used to predissolve the aryloxide salt. While protic solvents can lead to unexpected reaction pathways in organometallic

chemistry, the robustness of **1a** to methanolysis was inferred from its near-quantitative *synthesis* in refluxing methanol.[27] (At higher temperatures (150 °C), $Ru_2Cl_4(PPh_3)_4$ can be formed, along with methyl formate, hydrogen and dimethoxymethane as byproducts.[28])

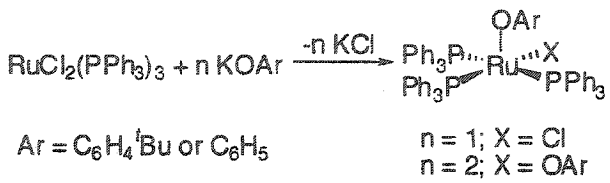

Scheme 3.1. Anticipated transmetallation reaction of $RuCl_2(PPh_3)_3$ with aryloxide.

Reaction of **1a** with one equivalent of KOAr in 1:4 MeOH-CH_2Cl_2 gave a mixture of products, in which observation of residual **1a** pointed toward disproportionation. Reactions with two equivalents of aryloxide were therefore explored. In 1:4 MeOH-CH_2Cl_2, the sole products are $RuH_2(CO)(PPh_3)_3$ **2a** and $RuH(\eta^5\text{-}OAr)(PPh_3)$ **3a**, formed in less than 15 minutes, in a ratio of 3:1 (Scheme 3.2). Complex **3a** was isolated (as the MeOH solvate) by extraction with methanol.

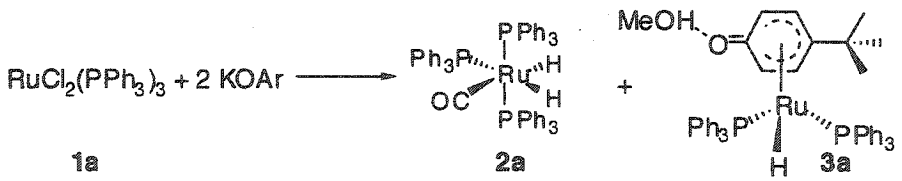

Scheme 3.2. Products formed in reaction of **1a** + 2 KOAr (Ar = *p*-$C_6H_4{}^tBu$).

Complex **2a** was identified as the known dihydride $RuH_2(CO)(PPh_3)_3$ on the basis of its characteristic[29] NMR data (Table 3.1). An A_2B pattern appears in the $^{31}P\{^1H\}$ NMR spectrum, while two hydride multiplets appear in the high field region of the ^1H NMR spectrum, with chemical shifts and coupling constants identical to values reported. IR data also agree with literature values;[30] ν(Ru-H) bands appear at 1960 and 1898 cm^{-1}, and the ν(CO) stretching band at 1940 cm^{-1}. Complex **3a** exhibits a broad singlet at 59 ppm in the $^{31}P\{^1H\}$ NMR spectrum,

which resolves at 180 K into a doublet and a broad singlet, the latter of which is assumed to conceal a second doublet. (This observation implies slowing of the rotation of the aryloxy ring to give two distinct conformers, one containing equivalent, and the other inequivalent phosphines.) The upfield location of four aromatic protons (doublets at 5.05 and 3.89 ppm; C_6D_6) indicates π-coordination of the aryloxide ligand. These signals correlate (HMQC) with two upfield aromatic signals in the $^{13}C\{^1H\}$ NMR spectrum (86.2 and 89.3 ppm, respectively). The $^{13}C\{^1H\}$ NMR spectrum also exhibits a downfield quaternary signal (DEPT) at 161.6 ppm, intermediate between values expected for a ketone carbonyl (~180 ppm) and a phenolic carbon (~140 ppm). This suggests some double bond character in the C-O bond. IR analysis of **3a** reveals a weak ν(Ru-H) stretch at 1977 cm^{-1}, and a ν(C=O) band of medium intensity at 1558 cm^{-1}. Independent synthesis of **3a** from the hydridochloro analogue of **1a**, $RuHCl(PPh_3)_3$ **1b**, is described in Section 3.3.

Table 3.1. NMR Spectroscopic Data for **2a**, **2b**, **1b** and **3**.

Compound	δ_P (ppm)	$^2J_{PP}$ (Hz)	δ_H (ppm)	$^2J_{PP}$ (Hz)
2a[a] (298 K)	57.0 (d, 2P), 44.7 (t, 1P)	17.4	-6.8 (tdd), -8.8 (dtd)	30, 16, 73, 30, 6
2b[b] (253 K)	42.3 (d, 2P), 14.6 (t, 1P)	15.7	–7.3 (dt)	105, 23
1b[a] (183 K)	94.2 (t, 1P) 38.4 (d, 2P)	27.0	-17.7 (q)	26
3[c]	59.3 (br s)	-	-11.6	35

Spectra obtained in [a] $CDCl_3$; [b] CD_2Cl_2 or [c] C_6D_6 solvent.

A proposed mechanism for the competing isomerization and decarbonylation pathways is illustrated in Scheme 3.3. Initial replacement of both chloride ligands, followed by methanolysis, would afford bis-methoxide **5**. Ensuing β-elimination would give $RuH_2(PPh_3)_3$ **6**, which could then decarbonylate formaldehyde to form $RuH_2(CO)(PPh_3)_3$ **2a**. Ample precedents

exist for both β-elimination of formaldehyde from Ru-methoxide complexes, and decarbonylation of the liberated formaldehyde;[31,32] in addition, labelling studies with CD_3OD and CH_3OD confirm that the hydride ligands originate in the methyl group of methanol. Formation of **3a** implies that σ-π isomerization can compete with the second methanolysis step, with the product ratio being determined by the relative rates of these reactions. The high concentration of methanol associated with its use as co-solvent accounts for the high proportion of **2a** formed. While some contribution from reaction of **1a** with small amounts of methoxide generated directly via exchange with KOAr cannot be ruled out, co-production of decarbonylation and π-aryloxide products (**2a** and **3a**) in 20% MeOH-CH_2Cl_2 requires that the rates of reaction with KOAr and (putative) KOMe are at least comparable under these conditions, under which the Ru(σ-OAr) intermediate is available to participate in methanolysis as well as isomerization. Furthermore, reaction of **1b** with KOAr at higher MeOH concentrations (50%) yields a much *lower* proportion of **2a** versus **3a** (ratio 1:8; see Section 3.3). This observation, which is difficult to reconcile with reaction via free methoxide, is consistent with a $RuH(\sigma\text{-}OAr)(PPh_3)_3$ intermediate in which isomerization competes with alcoholysis.

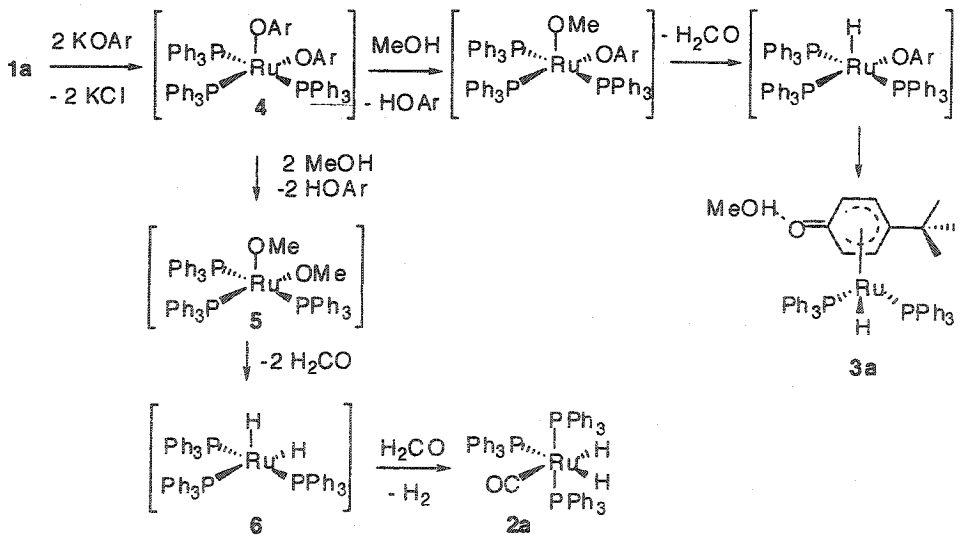

Scheme 3.3. Methanolysis vs. isomerization: generation of **2a** and **3a**.

3.2.2. Reaction of 1a with One Equivalent of Aryloxide

Analysis of the reaction of **1a** with one equivalent of KOAr was reexamined in light of the results above. A summary of the products is shown in Scheme 3.4, with a representative ^{31}P NMR spectrum in Figure 3.1. Signals are present for **2a** and **3a** (each 8%), as well as a small amount (3%) of unreacted **1a**. A major product is $RuHCl(PPh_3)_3$ **1b** (67%), identification of which was aided by its isolation from reactions in 3:1 MeOH-CH_2Cl_2.* Complex **1b** exhibits a hydride quartet at –17.7 ppm (Table 3.1), in agreement with the literature value.[33] (This upfield location suggests that the hydride ligand is trans to a vacant site.) A broad $^{31}P\{^1H\}$ NMR resonance centred at 57 ppm resolves into the reported A_2B pattern at 183 K.[33]

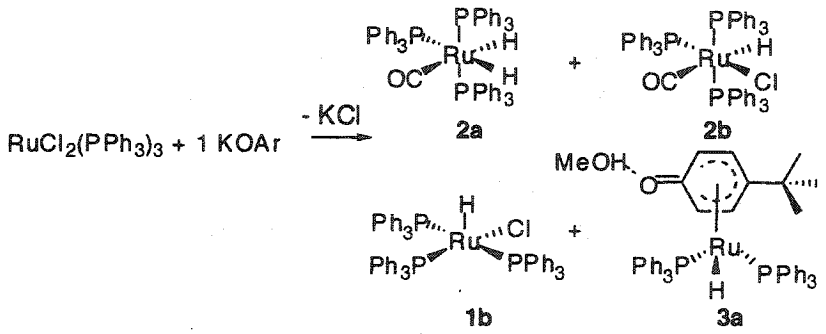

Scheme 3.4. Product mixture formed in reaction of **1a** + 1 KOAr (Ar = *p*-$C_6H_4{}^tBu$).

The last component of this mixture is $RuHCl(CO)(PPh_3)_3$ **2b** (14%), the hydridochloro analogue of **2a**. Identification of **2b** is supported by low-temperature $^{31}P\{^1H\}$ NMR experiments, in which the broad peaks at 40 and 14 ppm in the spectrum at room temperature are resolved into an A_2B pattern at 253 K. Selective decoupling experiments correlate these ^{31}P nuclei with a hydride signal at –7.3 ppm, which integrates to one proton. The multiplicity of this signal (a doublet of triplets) is consistent with splitting by one trans and two cis ^{31}P nuclei. The location and

coupling constants (Table 3.1) agree with the values reported,[30] as do IR data (ν(Ru-H) 2020 cm^{-1}; ν(C-O) 1922 cm^{-1}). Authentic samples of clean **2b** were prepared by treating **2a** with ethereal HCl.

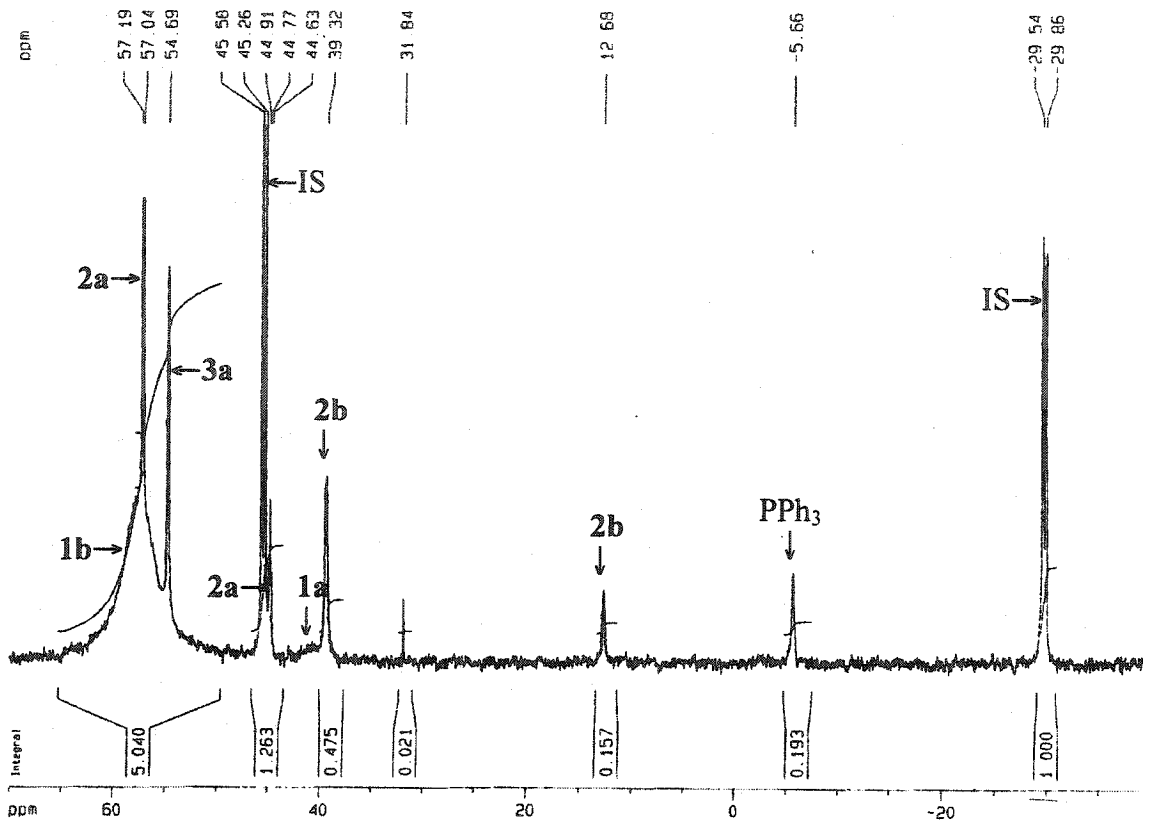

Figure 3.1. $^{31}P\{^{1}H\}$ NMR spectrum for reaction of **1a** with 1 equiv KOAr (Ar = $C_6H_4{}^tBu$) (15 min, RT). IS = internal standard; Ru(η^5-ArO)(*o*-$C_6H_4PPh_2$)(PPh_3) **9a**; see Section 3.5.

Formation of **2b** is presumed to proceed via RuCl(σ-OAr)(PPh_3)$_3$ 7 (Scheme 3.5), by a mechanism similar to that shown for **2a** in Fig. 3.3 above. Methanolyis and β-elimination of formaldehyde would in this case yield RuHCl(PPh_3)$_3$ **1b**, which can indeed be isolated from

---

* Complex **1b** is poorly soluble in this solvent system, and precipitates as a purple solid in ca. 90% yield, contaminated with ca. 10% **2a**. A protocol for synthesis of clean **1b** in quantitative yields (Section 3.4) was developed based on the mechanistic analysis in this section.

reactions in 3:1 MeOH-CH_2Cl_2, and which in separate experiments effected rapid decarbonylation of formaldehyde. Incomplete reaction of **1b** may indicate that yields of **2b** are limited by diffusion of gaseous formaldehyde into the headspace of the reaction vessel. In a closed system, higher conversions to **2b** were found. Observation of $RuH_2(CO)(PPh_3)_3$ **2a** and **3a** indicates that some double exchange of chloride occurs (Section 3.2.1).

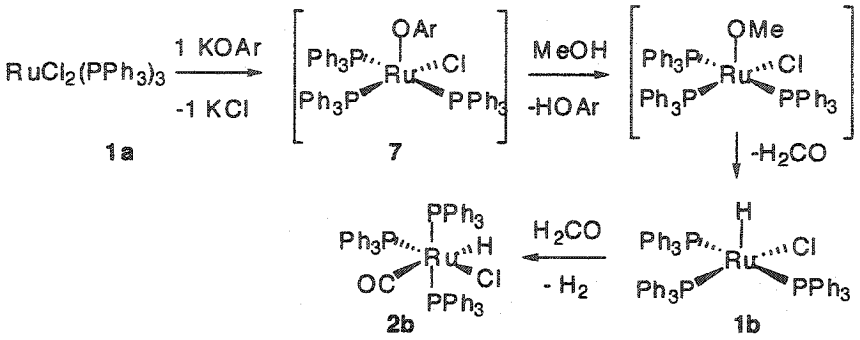

Scheme 3.5. Proposed mechanism for formation of **2b**.

Formation of carbonyl complexes **2a** and **2b** requires the presence of both aryloxide and methanol in the reaction medium. As remarked above, no evidence of decarbonylation is evident on refluxing $RuCl_2(PPh_3)_3$ **1a** in the presence of methanol. The presence of the aryloxide thus activates **1a** toward decarbonylation of methanol under mild conditions.

3.2.3. Molecular Structures of $RuH_2(CO)(PPh_3)_3$ 2a and $RuHCl(CO)(PPh_3)_3$ 2b

X-ray quality crystals of **2a** and **2b** were obtained from CH_2Cl_2 solutions, by evaporation or layering with hexanes, respectively. ORTEP diagrams are shown in Figure 3.2, bond lengths and angles in Table 3.2. The X-ray structure for **2a** has been previously reported,[34] but was obtained and reported subsequently by us[35] and is included here for comparison to **2b**. The geometry about ruthenium in both cases is distorted octahedral, with the equivalent phosphine ligands mutually trans. The cis-hydride ligands in **2a** were located; the hydride ligand for **2b** was

located from the difference map and refined with a riding model. The latter ligand is cis to chloride and trans to the CO ligand. In both **2a** and **2b**, cis-ligand bond angles deviate from the ideal 90° (**2a**: H(1)-Ru-P(1) = 79(2)°; H(1)-Ru-H(2) = 105(3)°; **2b**: P(1)-Ru-Cl = 84.7(3)°, C(1)-Ru-P(3) = 94.4(9)°), owing to the large cone angle[36] of PPh_3, vs. hydride.

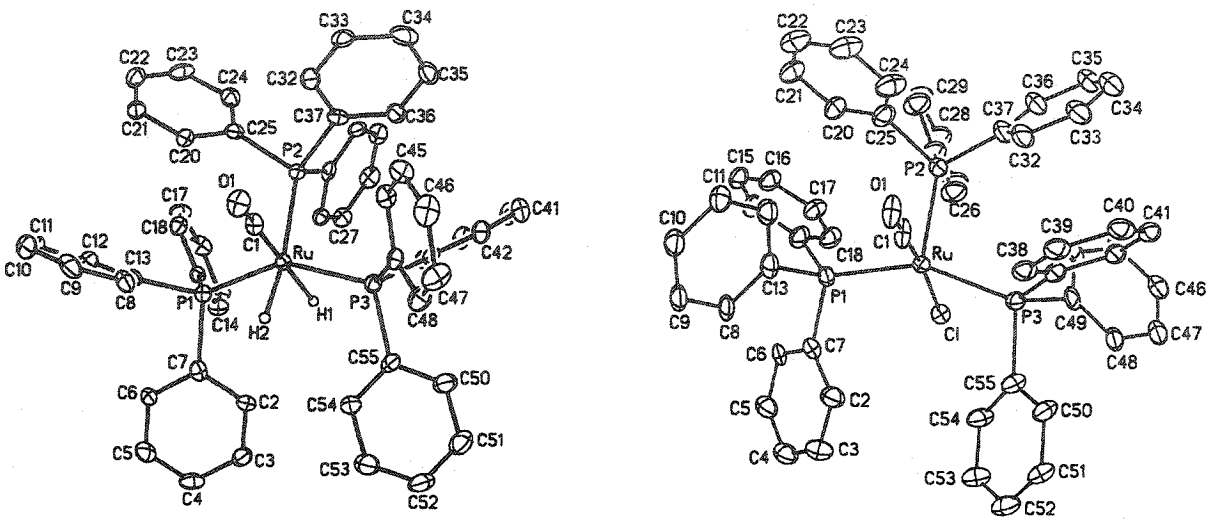

Figure 3.2. Molecular structures of $RuHX(CO)(PPh_3)_3$ (**2a**; X = H; left and **2b**; X = Cl; right). Thermal ellipsoids at 30% probability level; non-hydride hydrogen atoms and solvates omitted.

Table 3.2. Selected Bond Distances (Å) and Angles (°) for **2a** and **2b**.

Bond/Angle	**2a**	**2b**
Ru-X(1)	1.85(6)	2.459(8)
Ru-H(2)	1.84(6)	-
Ru-C(1)	1.920(11)	1.82(4)
Ru-P(1)	2.320(2)	2.371(8)
Ru-P(2)	2.398(2)	2.465(8)
Ru-P(3)	2.309(2)	2.411(9)
C(1)-O(1)	1.115(11)	1.06(3)
H(1)-Ru-X(1)	105(3)	-
Ru-C(1)-O(1)	175.5(8)	177(4)
P(1)-Ru-P(2)	101.39(8)	100.0(3)
P(2)-Ru-P(3)	102.75(8)	105.8(3)
P(1)-Ru-P(3)	147.95(9)	153.0(3)

3.3. Isomerization vs. Decarbonylation for Reaction of $RuHCl(PPh_3)_3$ with KOAr

Combining solutions of KOAr in methanol and **1b** in CH_2Cl_2 gave **3a**, accompanied by ca. 10% **2a** (Scheme 3.6), over the time of mixing.* The dominance of **3a** under these conditions indicates that $\sigma \rightarrow \pi$ isomerization within intermediate $RuH(OAr)(PPh_3)_3$ **8** out-competes methanolyis, in contrast with the behaviour of $Ru(OAr)_2(PPh_3)_3$ (Section 3.2.1). The strong σ-donor effect of the hydride ligand may contribute to this difference in reactivity, via enhanced filled-filled repulsions.

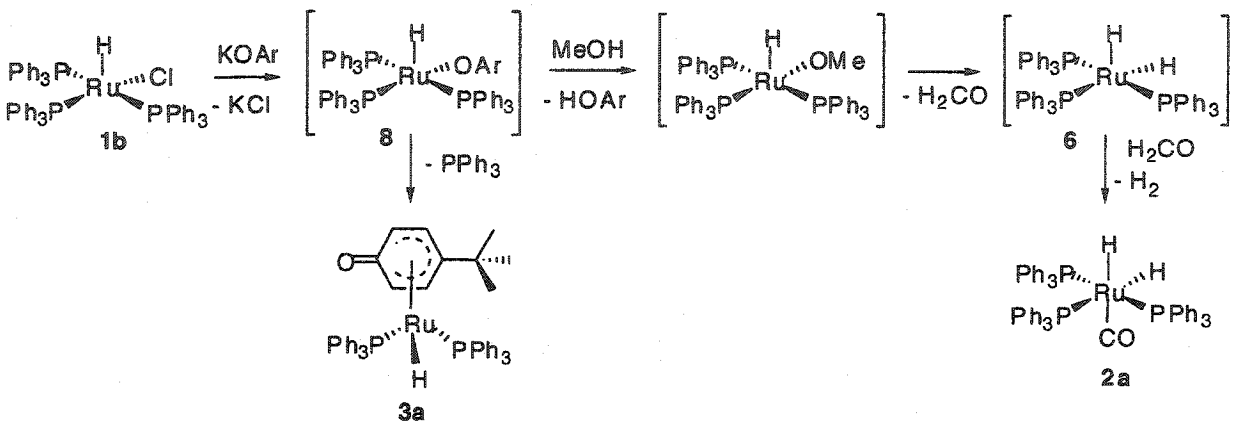

Scheme 3.6. Reaction of **1b** with one equivalent of aryloxide to form **3a** and **2a**.

3.4. A Clean, High-Yield Route to $RuHCl(PPh_3)_3$ 1b via Reaction with Isopropanol

The high reactivity of the Ru(σ-OAr) bond was exploited to develop a high-yield route to **1b**. Thus, alcoholysis of intermediate **7** (see Scheme 3.5) by addition of ^{i}PrOH generates a Ru-isopropoxide species. Subsequent β-elimination of acetone (which is not susceptible to decarbonylation) permits isolation of the desired **1b**.[37] Optimal yields are obtained for reactions in 4:1 benzene-^{i}PrOH. This solvent mixture gives a homogeneous solution of the starting

---

* The non-solvated product is formed over longer reaction times (2 h) in neat CH_2Cl_2, in which the aryloxide salt is poorly soluble. A phenol solvate is obtained if phenol is added.

materials at reflux, but **1b** precipitates as it is formed, facilitating quantitative isolation. Reactions at room temperature were less successful, owing to the limited solubility of **1a** in benzene; formation of **1b** was sluggish, reaching only 31% conversion after three days. While RT reaction occurs in 4:3 CH_2Cl_2-^{i}PrOH (which again affords a homogeneous solution), the increased solubility of **1b** in this solvent system led to partial formation of **3a**.

3.5. Reaction of $RuCl_2(PPh_3)_3$ with Aryloxide in the Absence of Alcohol

3.5.1. Formation of ortho-Metallated Complexes 9a and 9b

Investigations into the reactions of **1a** with KOAr or KOPh in neat toluene were carried out in parallel with the reactions described above. In the absence of alcohol, coordinatively saturated, ortho-metallated products of type **9** are obtained in *ca.* 60% isolated yield (Scheme 3.7).*

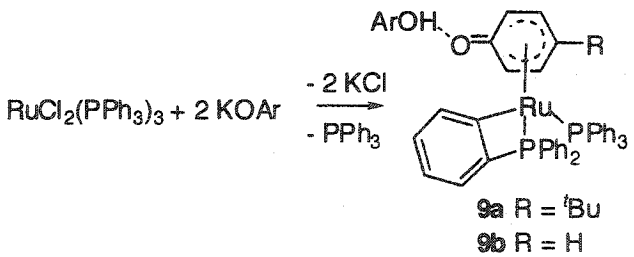

Scheme 3.7. Formation of ortho-metallated complex **9**.

$^{31}P\{^1H\}$ NMR analysis of **9** is diagnostic[38] for formation of a four-membered ring by ortho-metallation of PPh_3: two doublets are observed, with a chemical shift difference of nearly 80 ppm (Figure 3.3). π-Coordination of one aryloxide ligand is indicated by the distinctive upfield shifts of the arene signals in the ^1H NMR spectrum (Figure 3.4). These resonances are

---

* Variable amounts of a fine orange precipitate are also produced in THF (see above) and toluene. The extreme insolubility of this material in benzene, methylene chloride and DMSO precluded characterization.

found between 4.6 and 4.2 ppm for **9a**, and 5.1 to 4.3 ppm for **9b**; the latter values correspond well with data for related η^5-OPh systems.[19,39] Also evident in the aromatic region are signals for a solvating, hydrogen-bonded phenol. In the case of **9a**, two distinct *tert*-butyl singlets also appear, one due to π-bound aryloxide, the other to the solvating *t*-butyl phenol. A sharp singlet at ca. 9.0 ppm, which exchanges with D_2O, is assigned to the phenolic proton.

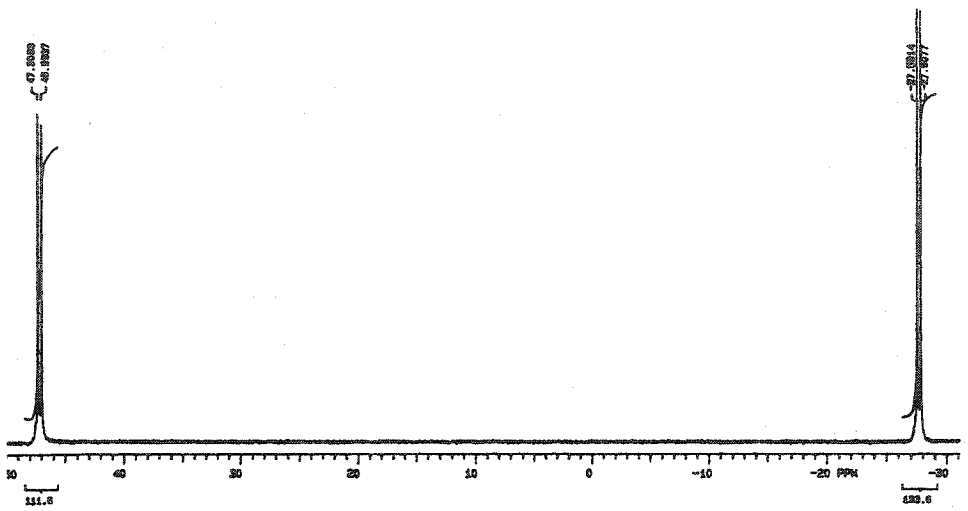

Figure 3.3. $^{31}P\{^1H\}$ NMR spectrum of Ru(η^5-ArO)(*o*-$C_6H_4PPh_2$)(PPh_3) **9a**.

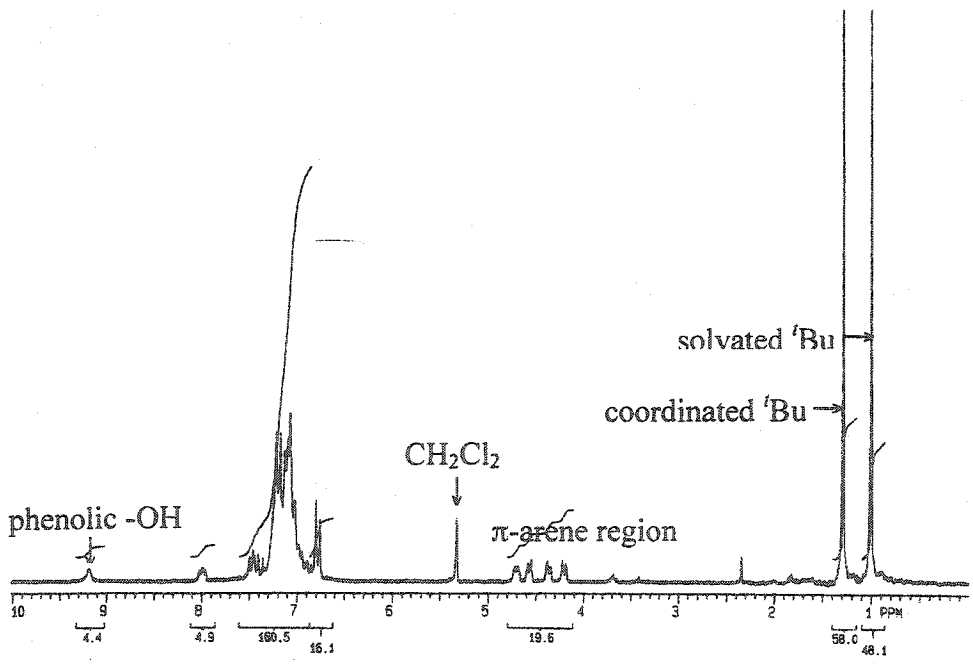

Figure 3.4. ^1H NMR spectrum of Ru(η^5-ArO)(*o*-$C_6H_4PPh_2$)(PPh_3) **9a**.

Infrared analysis of **9a** or **9b** reveals a medium-intensity band at *ca.* 1530 cm^{-1} (absent from the spectrum of the potassium salts), suggesting η^5-coordination of the aryloxide to give an oxocyclohexadienyl ligand with partial double-bond character of the C-O bond.[19] A broad, intense band at *ca.* 3100 cm^{-1} is assigned to the ν(O-H) stretching vibration of the phenol solvate. The strong propensity of π-phenoxide species for H-bonding, a manifestation of the basicity of the phenoxide oxygen, has been repeatedly noted.[40-42] Microanalytical and ^{1}H NMR integration data for bulk **9a** indicate a single solvating phenol, contrary to the X-ray evidence (see Section 3.5.2).

Complex **9** is thought to form via bis-phenoxide intermediate **4** (Scheme 3.8). The availability of three coordination sites, arising from the coordinative unsaturation of **4** and the lability of bound PPh_3, permits $\sigma \rightarrow \pi$ isomerization of an aryloxide ligand to give mixed σ,π-aryloxide species **10**. The basicity of the aryloxide oxygen within **10** facilitates abstraction of an ortho-proton from a phenyl group of a remaining PPh_3 ligand, resulting in ortho-metallation, concomitant elimination of phenol, and formation of solvated **9**. Elimination of alkane provides a driving force for ortho-metallation of PPh_3 in related Ru alkyl complexes.[20] Steric interactions within **10** may also be important, given the absence of ortho-metallation (via loss of H_2) in the reactions of $RuHCl(PPh_3)_3$ with aryloxide discussed in Section 3.3.

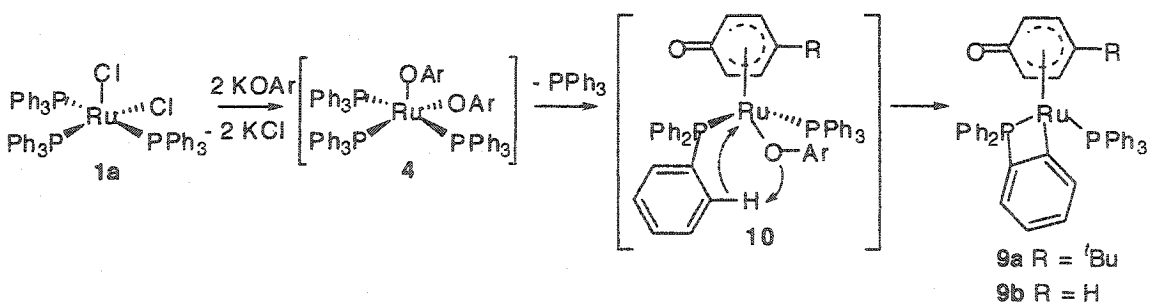

Scheme 3.8. Proposed mechanism for formation of **9**.

3.5.2. Molecular Structures of 9a•(HOAr)$_2$ and 9b•(HOPh)

X-ray quality crystals of **9a** were obtained by slow concentration of a $CDCl_3$ solution; of **9b**, by diffusion of hexanes into benzene. ORTEP plots are shown in Figure 3.5, bond lengths and angles in Table 3.3. A double solvate is found for **9a**•(HOAr)$_2$, presumably owing to incorporation of a second molecule of *p-tert*-butylphenol during crystallization. Retention of phenol solvates is very common in late-metal η^5-aryloxide systems,[40-42] in which the anionic charge on the oxygen atom is dispersed by hydrogen bonding.[41,43] Both **9a** and **9b** are distorted three-legged piano stools containing π-bound aryloxide and two PPh_3 ligands, one of which is η^1-bound and the other ortho-metallated. The four-membered ortho-metallated ring is highly strained. The bond angles of *ca.* 67, 109, 98, and 87° for P(1)-Ru-C(1), Ru-C(1)-C(6), C(1)-C(6)-P(1) and C(6)-P(1)-Ru, respectively, are significantly distorted from the idealized geometry about ruthenium (90°), carbon (120°), and phosphorus (109.5°). Cyclometallated angles and bond lengths are similar to those reported for K[RuH_2(*o*-$C_6H_4PPh_2$)(PPh_3)$_2$].[44] The phenol derivative **9b** reveals displacement of the Ru atom from the centroid of the ring toward C39, by >0.3 Å.

The aryloxy rings in **9a/b** possess partial η^5-oxocyclohexadienyl character, with C-O bond distances of 1.286(5) Å for **9a** and 1.260(4) Å for **9b**. Comparable values are reported for $Cp^*Ru(\eta^5$-2,6-*tert*-$Bu_2C_6H_3O$) (1.256(4) Å)[23] and $Cp^*Ru(\eta^5$-C_6H_5O)•(C_6H_5OH)$_2$ (1.284(7) Å).[40] All of these values are closer to the C-O bond distance of 1.22 Å described for the carbonyl group of benzoquinone than they are to the phenolic C-O bond distance of *ca.* 1.36 Å.[45] The carbon-carbon bond distances are generally shorter in the "hexadienyl" fragment of the ring as compared with the carbon bonds to C42. Puckering of the ring is evident in the rather long Ru-C42 bond distances (**9a** = 2.452(3) Å; **9b** = 2.478(4) Å) as compared to the Ru-C38 (**9a** =

2.253(4) Å; **9b** = 2.233(3) Å) and Ru-C41 (**9a** = 2.260(4) Å; **9b** = 2.270(3) Å).

Table 3.3. Selected Bond Lengths (Å) and Angles (°) for **9a** and **9b**. (Collection parameters and a complete list of bond lengths and angles are given in Appendices C and D).

Bond/Angle	9a	9b
Ru-C(1)	2.074(4)	2.083(4)
Ru-P(1)	2.3258(11)	2.3273(10)
Ru-P(2)	2.3313(12)	2.3060(10)
Ru-C(37)	2.273(4)	2.279(3)
Ru-C(38)	2.253(4)	2.233(3)
Ru-C(39)	2.357(4)	2.270(3)
Ru-C(40)	2.230(4)	2.220(3)
Ru-C(41)	2.260(4)	2.270(3)
Ru-C(42)	2.452(3)	2.478(4)
C(42)-O(1)	1.286(5)	1.260(4)
C(37)-C(38)	1.418(5)	1.396(5)
C938)-C(39)	1.415(5)	1.401(5)
C(39)-C(40)	1.409(5)	1.394(5)
C(40)-C(41)	1.405(5)	1.412(5)
C(41)-C(42)	1.428(5)	1.435(5)
C(42)-C(37)	1.425(5)	1.445(5)
P(1)-Ru-P(2)	95.18(4)	96.03(3)
P(1)-Ru-C(1)	66.60(11)	66.68(10)
P(2)-Ru-C(1)	87.13(11)	90.32(9)
Ru-C(1)-C(6)	108.7(3)	108.6(2)
C(1)-C(6)-P(1)	97.8(3)	98.1(2)
C(6)-P(1)-Ru	86.81(13)	86.64(11)
C(1)-C(2)-C(3)	119.3(4)	120.1(4)
C(2)-C(3)-C(4)	121.7(4)	121.9(4)
C(3)-C(4)-C(5)	102.2(4)	120.4(4)
C(4)-C(5)-C(6)	118.2(4)	117.0(3)
C(5)-C(6)-C(1)	123.3(4)	124.2(3)
C(6)-C(1)-C(2)	117.3(4)	116.4(3)
C(37)-C(38)-C(39)	122.3(4)	121.6(4)
C(38)-C(39)-C(40)	114.4(4)	117.2(4)
C(39)-C(40)-C(41)	123.6(4)	121.7(4)
C(40)-C(41)-C(42)	121.2(4)	122.1(3)
C(41)-C(42)-C(37)	114.3(4)	113.1(3)
C(42)-C(37)-C(38)	121.8(4)	122.6(4)

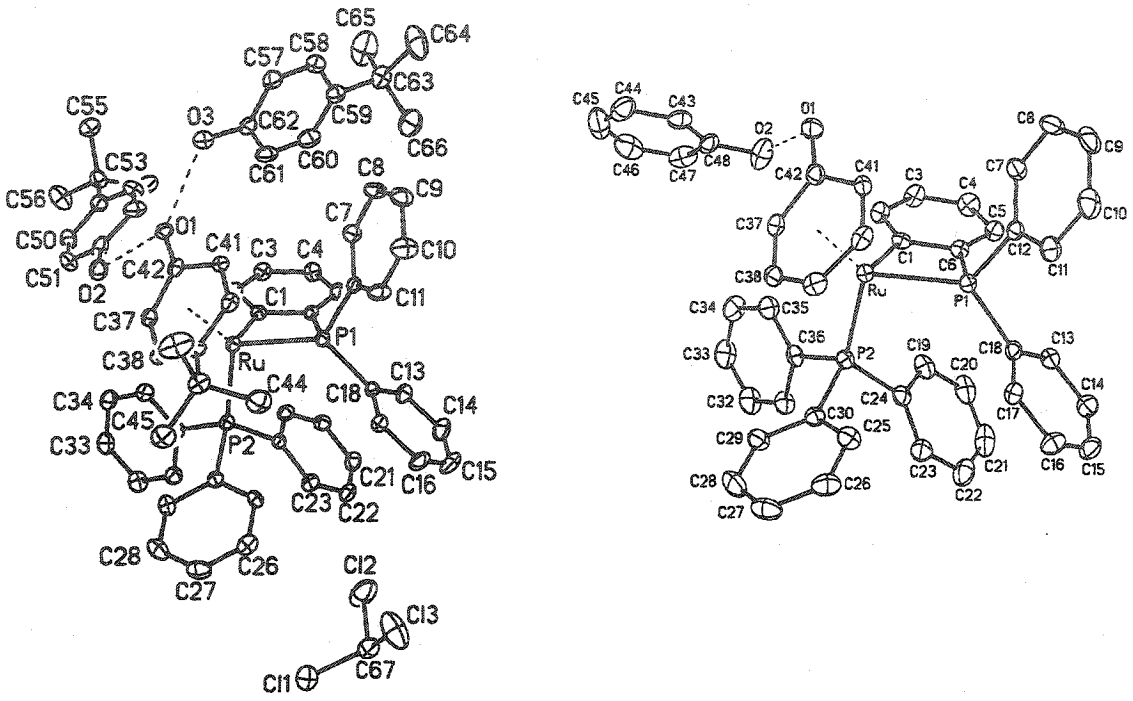

Figure 3.5. Molecular structures of **9a**•$(ArOH)_2(CHCl_3)$ (left) and **9b**•PhOH (right). Thermal ellipsoids depicted at 30% probability. Hydrogen atoms omitted for clarity.

3.6. Effect of Aryloxide Substitution on Product Formation

As indicated in Section 3.3, reaction of KOAr with **1b** results in hydride **3a**. However, reaction of **1b** with potassium *phenoxide* in CH_2Cl_2 does not afford the corresponding phenoxide derivative $RuH(\eta^5\text{-}OPh)(PPh_3)_2$ **3b**. Instead, complete conversion to chloride complex **11b** is found (Scheme 3.9). A ~30 ppm upfield shift is observed for the $^{31}P\{^1H\}$ NMR singlet (from 56 to 29 ppm), while neither a hydride NMR signal nor a ν(Ru-H) IR stretching band is evident. The identity of **11b** was confirmed by crystallographic analysis. Its formation is attributed to reaction with liberated KCl: Jay Conrad of this research group has noted that use of thallium phenoxide in this reaction yields **3b** and covalent, highly insoluble thallium chloride. Isolated **3b** can be converted to **11b** with sources of chloride ($CDCl_3$, ethereal HCl, KCl).

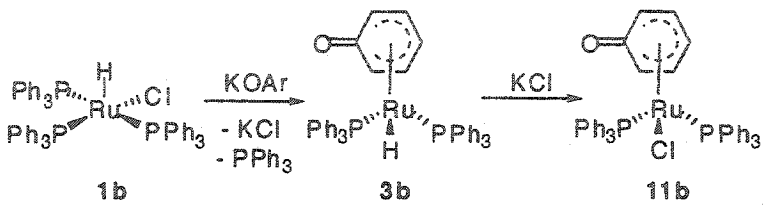

Scheme 3.9. Formation of $RuCl(\eta^5\text{-}OPh)(PPh_3)_3$ **11b**.

On the assumption that the *p-tert*-butylphenoxide analogue **11a** would likewise be accessible, **3a** was treated with ethereal HCl.[40] Surprisingly, the hydride ligand was not replaced by chloride. Instead, cationic **12a** was formed as the sole product: protonation of the η^5-OAr ligand transforms it into a η^6-phenol group, while the chloride group is present as a counter-ion (Scheme 3.10). The only spectroscopic indicator of change in this reaction is a 4 ppm upfield shift of the $^{31}P\{^1H\}$ NMR singlet. The identity of **12a** was unambiguously determined by X-ray analysis. The difference in reactivity between **3a** and **3b** may be due to the greater acidity of phenol than *p-tert*-butylphenol (pK_a values 9.99 and 10.31, respectively[46]). This would both facilitate protonation of the aryloxide ligand in **3a**, and enhance transfer of electron density to the metal center in **3b**, thus increasing the driving force for exchange of the strong σ- donor hydride with the weaker π-donor chloride.

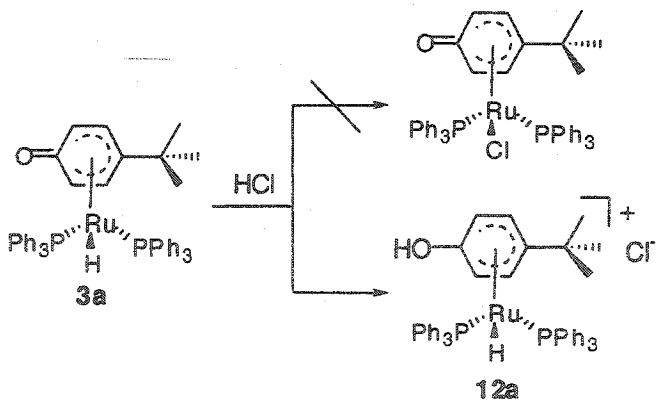

Scheme 3.10. Formation of $RuH(\eta^6\text{-}HOC_6H_4{}^tBu)(PPh_3)_2$ **12a** by reaction of **3a** with $HCl{\bullet}Et_2O$.

3.6.1. Molecular Structures of $RuCl(\eta^5\text{-}C_6H_5O)(PPh_3)_2$ 11b and $[RuH(\eta^6\text{-}C_6H_4{}^tBuOH)(PPh_3)_2]Cl$ 12a.

X-ray quality crystals of **11b** were obtained by slow diffusion of hexanes into a CD_2Cl_2 solution; of **12a**, by evaporation from $CDCl_3$. ORTEP diagrams are shown in Figure 3.6, with bond lengths and angles in Table 3.4. Both complexes are distorted three-legged piano stools, containing π-bound aryloxide, two PPh_3 ligands and a hydride ligand. A molecule of phenol is hydrogen-bonded to the phenoxide oxygen in **11b** (as previously seen for **9**). A molecule of *p-tert*-butylphenol is co-crystallized with **12a**, but is not associated via hydrogen bonding.

The P1-Ru-P2 angles in **11b** and **12a** (*ca.* 98°) are unstrained by comparison to those in **9a** and **9b**. Likewise, the P1-Ru-X angle (X = C(6) for **9a** and **9b**) is increased, by nearly 22° in the case of **11b**. In **12a**, a narrow splay of the "legs" of the piano stool (sum of angles around Ru = 257°, vs. 281° for **11b**) results from the combination of the steric demands of the phenolic *p-tert*-butyl substituent, and the minimal bulk of the hydride ligand. The corresponding value for $[Ru(\eta^6\text{-}C_6H_5CH_3)(PPh_3)_2Cl][BF_4]$[47] **13** is approximately 7° smaller than for **11b**, revealing a small but significant effect of a methyl substituent on the ring (its effect being amplified by the planarity of the ring in **13**). The Cl-Ru-P2 bond angle in **13** (85.3(1)°) is also approximately 9° smaller than the corresponding value of 93.81(9)° in **11b**. This may again be due to the planarity of the aromatic ring in **13**, which promotes interaction between the methyl group and the chloride ligand, compressing the Cl-Ru-P2 angle.

As in **9a** and **9b**, the aryloxy ring in **11b** possesses partial η^5-oxocyclohexadienyl character, with C-O bond distances of 1.248(11) Å, similar to the C-O bond distance cited for benzoquinone.[45] In comparison, the C-O bond distance in **12a** is 1.338(3) Å, much closer to the phenolic C-O value of 1.36 Å.[45] For the η^5-oxocyclohexadienyl derivatives, the carbon-carbon distances are likewise generally shorter in the "hexadienyl" fragment of the ring than in the

bonds to C42, and puckering of the ring is evident in the rather long Ru-C42 bond distances (reaching a maximum of 2.536(10) Å in the case of **11b**). These effects are much less marked for **12a**, although this complex shows some degree of non-planarity in the π-ArOH ring, as well as variation in the internal C-C angles from 116.8(3)° to 122.2(3)°. Elevation of C42 and C39 (the oxygen-functionalized and *para*-carbons, respectively) above the plane of the *ortho* and *meta* carbons is noted in **11b** (C42 = 0.2155 Å; C39 = 0.0142 Å), though these values are less dramatic than the elevations of 0.409 and 0.185 Å originally suggested[19] for **3b** (Table 3.5).

Table 3.4. Selected Bond Distances (Å) and Angles (°) for **11b** and **12a**. (Collection parameters and a complete list of bond lengths and angles are given in Appendices E and F).

Bond/Angle	**11b**	**12a**
Ru-X	X = Cl(1); 2.428(3)	X = H(1); 1.53(0.03)
Ru-P(1)	2.355(3)	2.3289(8)
Ru-P(2)	2.353(3)	2.3319(8)
Ru-C(37)	2.293(10)	2.329(3)
Ru-C(38)	2.210(10)	2.263(3)
Ru-C(39)	2.192(10)	2.302(3)
Ru-C(40)	2.235(10)	2.247(3)
Ru-C(41)	2.319(10)	2.255(3)
Ru-C(42)	2.536(10)	2.438(3)
C(42)-O(1)	1.248(11)	1.338(3)
C(37)-C(38)	1.392(14)	1.417(4)
C(38)-C(39)	1.415(14)	1.406(4)
C(39)-C(40)	1.376(14)	1.429(4)
C(40)-C(41)	1.425(14)	1.405(4)
C(41)-C(42)	1.417(14)	1.423(4)
C(42)-C(37)	1.453(15)	1.394(4)
P(1)-Ru-P(2)	98.44(10)	97.90(3)
P(1)-Ru-X	X = Cl(1); 88.70(9)	X = H(1); 84(1)
P(2)-Ru-X	X = Cl(1); 93.81(9)	X = H(1); 76(1)
C(37)-C(38)-C(39)	120.1(11)	122.2(3)
C(38)-C(39)-C(40)	119.7(11)	116.8(3)
C(39)-C(40)-C(41)	120.2(11)	120.4(3)
C(40)-C(41)-C(42)	121.7(11)	121.6(3)
C(41)-C(42)-C(37)	114.4(10)	117.1(3)
C(42)-C(37)-C(38)	121.5(11)	120.6(3)

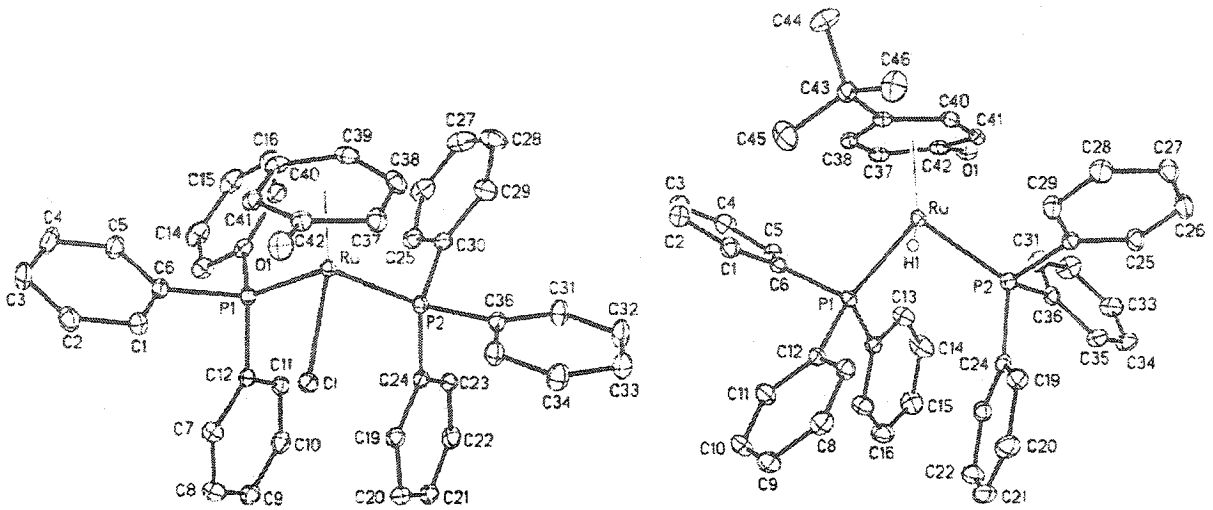

Figure 3.6. Molecular structures of $RuCl(\eta^5\text{-}C_6H_5O)(PPh_3)_2$ **11b** (left) and cation of $[RuH(\eta^6\text{-}C_6H_4{}^tBuOH)(PPh_3)_2]Cl$ **12a** (right). Thermal ellipsoids depicted at 30% probability level. Non-hydride hydrogen atoms omitted for clarity.

All of the C39 and C42 atoms in the arene complexes (**9a**, **9b**, **11b** and **12a**) show a deviation from the plane of the arene ring (Table 3.6) as well as some degree of displacement of the ruthenium atom from the centroid of the arene ring (illustrated for **11b** in Figure 3.7).

Table 3.5. Least-squares deviation from plane for **9a**, **9b**, **11b** and **12a** (relative to *ortho* and *meta* carbons (C37, C38, C40, C41).

	9a (Å)	**9b** (Å)	**11b** (Å)	**12a** (Å)
C39	0.094	0.049	0.0142	0.047
C42	0.168	0.164	0.2115	0.133

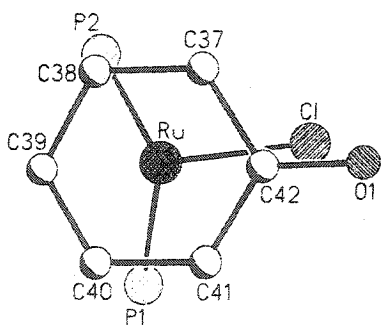

Figure 3.7. Displacement of Ru from the centroid of the arene ring **11b**.

3.7. Reaction of Aryloxide with a Coordinatively Saturated Ruthenium Complex

In the chemistry of Section 3.2, σ→π isomerization of aryloxide was facilitated by use of the coordinatively unsaturated precursors **1a** and **1b**. In order to probe the driving force for isomerization, a similar study was undertaken utilizing coordinatively saturated $RuCl_2(CO)_2(PPh_3)_2$ **14**. Despite itscoordinative saturatation, **14** has labile PPh_3 ligands, and could in principle support isomerization to $RuCl(\eta^5\text{-}OAr)(CO)_2$ (Scheme 3.11). The bis-CO piano-stool motif, although rare, has literature precedent.[48-50] If, however, the CO ligands sufficiently reduce the electron density on ruthenium, the η^1-aryloxide complex **15** may be stabilized by minimizing d_π-p_π repulsion.

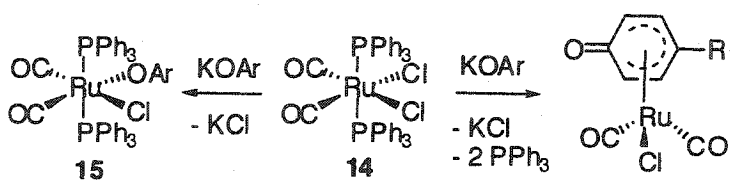

Scheme 3.11. Anticipated products from reaction of **14** with KOAr.

Treatment of $RuCl_2(CO)_2(PPh_3)_2$ **14** with one equivalent of KOAr in THF generated a ~1:1 mixture of starting material and product (subsequently identified as **15**), with ca. 2% of an additional product, tentatively identified as **16**. $^{31}P\{^1H\}$ NMR parameters are summarized in Table 3.6. Little structural insight could be gleaned from these data, however, as all of the peaks were singlets. Disproportionation, however, was clearly an issue, and reaction of **14** with excess KOAr was therefore undertaken. Three equivalents of aryloxide were required for complete consumption of **14**, affording **17** as the sole product in 77% yield. The ^1H NMR spectrum (consisting only of the aromatic signals for protons) was also uninformative, but X-ray analysis permitted identification of **17** as $K_2[Ru_2(CO)_4(OAr)_6(PPh_3)_2]$. The proposed reaction sequence is shown in Scheme 3.12.

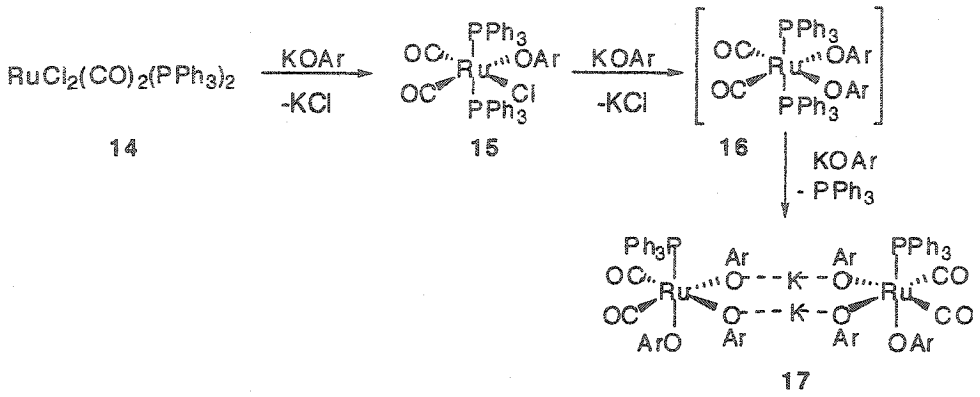

Scheme 3.12. Proposed reaction cascade leading to 17.

Table 3.6. Summary of ^{31}P (121 MHz) NMR data for CO complexes **14-17** [a]

Complex	δ_P (ppm)
14 $RuCl_2(CO)_2(PPh_3)_2$	18.2
15 $Ru(Cl)(\sigma\text{-}OAr)(CO)_2(PPh_3)_2$	14.8
16 $Ru(\sigma\text{-}OAr)_2(CO)_2(PPh_3)_2$	15.4
17 $K_2[Ru_2(CO)_4(OAr)_6(PPh_3)_2]$	33.2

[a] All spectra obtained at RT; samples dissolved in C_6D_6.
[b] Proposed intermediate.

Reaction of **14** with two equivalents of KOAr gave a mixture of unreacted **14** and all three substitution products, **15-17**, with mono-aryloxide **15** being formed in greatest amount (68%). Complex **15** was isolated, albeit in only 11% yield, by repeated recrystallization.The proposed structure contains two (equivalent) phosphine ligands, consistent with their appearance as a singlet in the 31P NMR spectrum; two inequivalent CO ligands are also present, which give rise to two ^{13}C NMR triplets at 195.5 and 190.0 ppm ($^2J_{CP}$ = 11 Hz in each case). Two strong infrared bands are also observed for the symmetrical and asymmetric ν(C-O) vibrations, at 2043 and 1977 cm^{-1}. ^1H NMR integration of the aromatic signals against the tert-butyl resonance also supports identification as **15**, as does microanalysis.

Following identification of **15** and **17**, three of the four singlets in the ^{31}P NMR spectrum of the reaction mixture could be assigned with confidence. The fourth, a singlet at 15.4 ppm,

never exceeded 10% of total integration, and the complex responsible could not be isolated. This signal is tentatively assigned to bis-aryloxide **16**, its low proportion providing some indication of the driving force for formation of the potassium-stabilized dimer **17**.

3.7.1. Crystal Structure Analysis of $K_2[Ru_2(CO)_4(OAr)_6(PPh_3)_2]$ 17

X-ray quality crystals of **17** were obtained by slow evaporation from benzene-hexanes. An ORTEP diagram is shown in Figure 3.8, with bond lengths and angles in Table 3.7. The complex is a dimer of octahedral Ru(II) centers linked by two potassium counter-ions that bind each aryloxide oxygen (O1-K1 = 2.581(4), O5-K1 = 2.577(4); O3-K2 = 2.678(4), O6-K2 = 2.644(4)).

Table 3.7. Selected Bond Lengths (Å) and Angles (°) for **17**.

Bond	Bond Length (Å)	Angle	Bond Angle (°)
Ru(1)-O(1)	2.083(4)	O(1)-Ru(1)-O(2)	82.35(14)
Ru(1)-O(2)	2.119(4)	O(1)-Ru(1)-O(3)	83.82(15)
Ru(1)-O(3)	2.075(4)	O(2)-Ru(1)-O(3)	78.76(14)
Ru(1)-P(1)	2.3617(15)	O(1)-Ru(1)-P(1)	168.85(11)
Ru(1)-C(61)	1.865(6)	O(2)-Ru(1)-C(62)	176.04(19)
Ru(1)-C(62)	1.868(6)	O(3)-Ru(1)-C(61)	174.3(2)
C(61)-O(7)	1.144(7)	Ru(1)-C(61)-O(7)	177.9(6)
C(62)-O(8)	1.141(7)	Ru(1)-C(62)-O(8)	175.9(6)
O(1)-K(1)	2.581(4)		
O(2)-K(1)	2.894(4)		
O(2)-K(2)	2.797(4)		
O(3)-K(2)	2.678(4)		

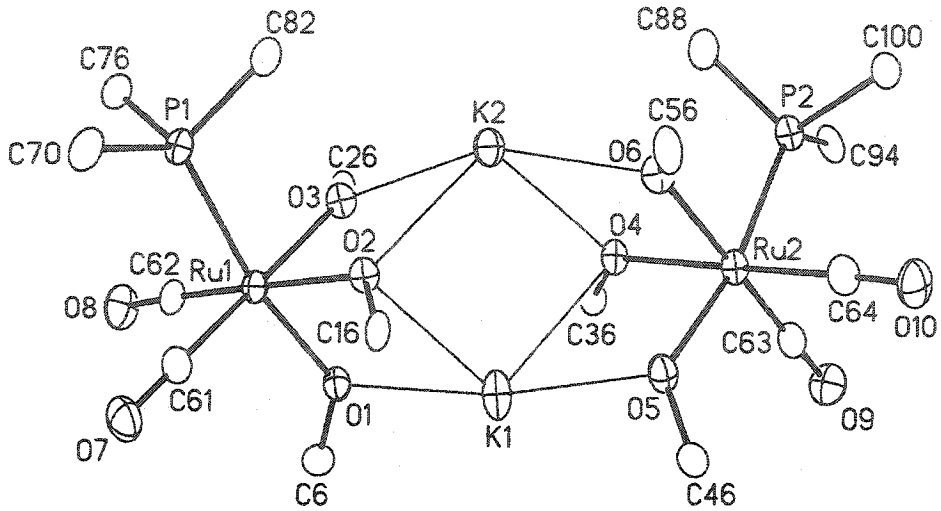

Figure 3.8. Molecular structure of $[K_2][Ru_2(CO)_4(OAr)_6(PPh_3)_2]$ **17**. Thermal ellipsoids depicted at 30% probability. Hydrogen atoms and full phenyl rings omitted for clarity.

Two of the three σ-bound aryloxide ligands are located trans to the CO ligands (O-Ru-C angles = 175.9(6) and 177.9(6)°). Trans-disposed CO and aryloxide ligands are also found in $RuH(\sigma\text{-}C_6H_4Me)(CO)(PMe_3)_3$ **19**.[25] The Ru-O bond lengths in **17** (ranging from 2.075(4) to 2.119(4) Å) agree well with the value of 2.108(6) Å reported for **19**.[13] These bond lengths are significantly shorter than those found in $RuH(\sigma\text{-}C_6H_4Me)(PMe_3)_4$ **18** (2.229(2)-2.364(2) Å), possibly owing to synergic push-pull donor-acceptor interactions between the aryloxide ligand and the trans CO group in **19**. Interestingly, **19** is formed by *selective* replacement of the PMe_3 ligand trans to the aryloxide group in **18** by CO (Scheme 3.13), further reinforcing the inference that d_π-p_π interactions play a key role in driving this chemistry.

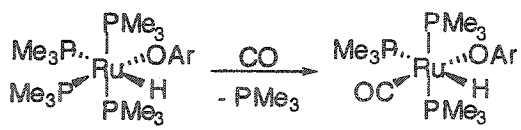

18 **19**

Scheme 3.13. Reaction of $RuH(\sigma\text{-}C_6H_4Me)(PMe_3)_4$ with CO.[13]

3.8. Conclusions

From the foregoing data, we conclude that reactions of chlororuthenium complexes with monodentate aryloxides show a pattern of high reactivity, in which the Ru-O bond strength is undermined by the accessibility of low-energy reaction pathways involving bond cleavage to afford coordinatively saturated, 18-electron π–complexes. Within coordinatively unsaturated ruthenium complexes containing labile ligands, π-bound aryloxide is thermodynamically preferred. Also accessible are pathways deriving from the basicity of the phenoxide oxygen. Thus, in the absence of alcohols, σ→π isomerization generates η^5-aryloxide products, including *ortho*-metallated Ru(η^5-ArO)(*o*-$C_6H_4PPh_2$)(PPh_3) **9** and RuH(η^5-ArO)(PPh_3)$_2$ **3a**. In the presence of methanol, alcoholysis of the σ-bound aryloxide liberates phenol, ultimately effecting decarbonylation of bound methoxide to afford **2a** or **2b**. Use of coordinatively saturated **14** permits isolation of σ-aryloxide complexes **15** and **17**, in which the trans CO ligands stabilize the σ-aryloxide ligands through a push-pull donor-acceptor interaction. Complexes **15** and **17** are the first isolated examples of Ru complexes containing monodentate, σ-aryloxide ligands and triphenylphosphine ligands. Of the reported Ru(σ-aryloxide) complexes, virtually all contain non-labile trialkylphosphine ligands.[18-23,40,41,51]

Coordinatively unsaturated Ru(σ-aryloxide) complexes containing labile PPh_3 ligands function as key intermediates in the chemistry described in this chapter, but their reactivity hampers observation or isolation. The electronic effects of substituents on the aryloxide ring can, however, affect the reaction chemistry. Indeed, subsequent work by Jay Conrad of this laboratory has built on this work to demonstrate that both isomerization and alcoholysis can be circumvented by use of electron-*poor* aryloxides, which can then function as effective pseudohalide ligands in coordinatively unsaturated complexes of ruthenium.[52]

3.9. References

(1) LeBras, J.; Amouri, H.; Viassermann, J. *Inorg. Chem.* **1998**, *37*, 5056 and references therein.
(2) Rees, W. M.; Churchill, M. R.; Fettinger, J. C.; Atwood, J. D. *Organometallics* **1985**, *4*, 2179.
(3) Dockter, D. W.; Fanwick, P. E.; Kubiak, C. P. *J. Am. Chem. Soc.* **1996**, *118*, 4846.
(4) Sanford, M. S.; Hanling, L. M.; Day, M. W.; Grubbs, R. H. *Angew. Chem. Int. Ed.* **2000**, *39*, 3451.
(5) Poulton, J. T.; Hauger, B. E.; Kuhlman, R. L.; Caulton, K. G. *Inorg. Chem.* **1994**, *33*, 3330.
(6) Johnson, T. J.; Huggman, J. C.; Caulton, K. G. *J. Am. Chem. Soc.* **1992**, *114*, 2725.
(7) Cámpora, J.; Reyes, M. L.; Mereiter, K. *Organometallics* **2002**, *21*, 1014.
(8) Cámpora, J.; Reyes, M. L.; Monge, T. H.; Ruiz, C. *Organometallics* **2000**, *19*, 2950 and references therein.
(9) DiBugno, C.; Pasquali, M.; P., L.; Sabatino, P.; Braga, D. *Inorg. Chem.* **1989**, *28*, 1390.
(10) Slough, G. A.; Bergman, R. G.; Heathcock, C. H. *J. Am. Chem. Soc.* **1989**, *111*, 938.
(11) Hartwig, J. F.; Bergman, R. G.; Andersen, R. A. *J. Organomet. Chem.* **1990**, *394*, 417.
(12) Hartwig, J. F.; Bergman, R. G.; Andersen, R. A. *Organometallics* **1991**, *10*, 3344.
(13) Hartwig, J. F.; Andersen, R. A.; Bergman, R. G. *Organometallics* **1991**, *10*, 1875.
(14) Trahanovsky, W. S.; Hall, R. A. *J. Am. Chem. Soc.* **1977**, *99*, 4850.
(15) Moulines, F.; Djakovitch, L.; Delville-Debois, M.-H.; Robert, F.; Gouzerh, P.; Astruc, D. *J. Chem. Soc., Chem. Commun.* **1995**, 463.
(16) LeBras, J.; Amouri, H.; Vaissermann, J. *Organometallics* **1996**, *15*, 5706.
(17) LeBras, L.; Rager, M. N.; Besace, Y.; Amouri, H.; Vaissermann, J. *Organometallics* **1997**, *16*, 1765.
(18) Rosete, R. O.; Cole-Hamilton, D. J.; Wilkinson, G. *J. Chem. Soc., Dalton Trans.* **1979**, 1618.
(19) Cole-Hamilton, D. J.; Young, R. J.; Wilkinson, G. *J. Chem. Soc., Dalton Trans.* **1976**, 1995.
(20) Cole-Hamilton, D. J.; Wilkinson, G. *New J. Chem.* **1977**, *1*, 141.
(21) Chaudret, B.; Xiaodong, H.; Huang, Y. *J. Chem. Soc., Chem. Commun.* **1989**, 1844.
(22) Christ, M. L.; Sabo-Etienne, S.; Chung, G.; Chaudret, B. *Inorg. Chem.* **1994**, *33*, 5316.
(23) Loren, S. D.; Campion, B. K.; Heyn, R. H.; Tilley, T. D.; Bursten, B. E.; Luth, K. W. *J. Am. Chem. Soc.* **1989**, *111*, 4712.
(24) Bryndza, H. E.; Tam, W. *Chem. Rev.* **1988**, *88*, 1163.
(25) Pearson, R. G. *J. Am. Chem. Soc.* **1963**, *85*, 3533.
(26) Caulton, K. G. *New J. Chem.* **1994**, *18*, 25.
(27) Hallman, P. S.; Stephenson, T. A.; Wilkinson, G. *Inorg. Synth.* **1970**, *12*, 237.
(28) Smith, T. A.; Apin, R. P.; Maitlis, P. M. *J. Organometal. Chem.* **1985**, C13.
(29) Hallman, P. S.; McGarvey, B. R.; Wilkinson, G. *J.Chem. Soc. A* **1968**, 3143.
(30) Levison, J. J.; Robinson, S. D. *J. Chem. Soc. A* **1970**, 2947.
(31) Van Der Sluys, L. S.; Kubas, G. J.; Caulton, K. G. *Organometallics* **1991**, *10*, 1033.
(32) Chaudret, B. N.; Cole-Hamilton, D. J.; Nohr, R. S.; Wilkinson, G. *J. Chem. Soc., Dalton Trans.* **1977**, 1546.
(33) Hoffman, P. R.; Caulton, K. G. *J. Am. Chem. Soc.* **1975**, *97*, 4221.
(34) Junk, P. C.; Steed, J. W. *J. Organomet. Chem.* **1999**, *587*, 191.
(35) Snelgrove, J. S.; Conrad, J. C.; Yap, G. P. A.; Fogg, D. E. *Inorg. Chim. Acta* **2003**, *345*, 268.

(36) Tolman, C. A. *Chem. Rev.* **1977**, *77*, 313.
(37) Aranyos, A.; Csjernyik, G.; Szabó, K. J.; Backväll, J.-E. *J. Chem. Soc., Chem. Commun.* **1999**, 351.
(38) Garrou, P. E. *Chem. Rev.* **1981**, *81*, 229.
(39) Yamamoto, T.; Miyashita, S.; Naito, Y.; Komiya, S.; Ito, T.; Yamamoto, A. *Organometallics* **1982**, *1*, 808.
(40) Koelle, U.; Wang, M. H.; Raabe, G. *Organometallics* **1991**, *10*, 2573.
(41) Bücken, K.; Koelle, U.; Pasch, R.; Ganter, B. *Organometallics* **1996**, *15*, 3095.
(42) Fulton, J. R.; Holland, A. W.; Fox, D. J.; Bergman, R. G. *Acc. Chem. Res.* **2000**, *35*, 44.
(43) Kegley, S. E.; Schaverien, C. J.; Freudenberger, J. H.; Bergman, R. G.; Nolan, S. P.; Hoff, C. D. *J. Am. Chem. Soc.* **1987**, *109*, 6563.
(44) Pez, G. P.; Grey, R. A.; Corsi, J. *J. Am. Chem. Soc.* **1981**, *103*, 7528.
(45) Allen, F. H.; Kennard, O.; Watson, D. G.; Brammer, L.; Orpen, A. G.; Taylor, R. *J. Chem. Soc., Perkin Trans. 2* **1987**, *2*, S1.
(46) Rived, F.; Roses, M.; Bosch, E. *Anal. Chem. Acta* **1998**, *374*, 309.
(47) Polam, J. R.; Porter, L. C. *Inorg. Chim. Acta* **1993**, *205*, 119.
(48) Roder, K.; Werner, H. *Chem. Ber.* **1989**, *112*, 833.
(49) Bohle, D. S.; Goodson, P. A. *J. Chem. Soc., Chem. Commun.* **1992**, 1205.
(50) Bohle, D. S.; Carron, K. T.; Christensen, A. N.; Goodson, P. A.; Powell, A. K. *Organometallics* **1994**, *13*, 1355.
(51) Bennett, M. A.; Matheson, T. W. *J. Organomet. Chem* **1979**, *175*, 87.
(52) Conrad, J. C.; Amoroso, D.; Czechura, P.; Yap, G. P. A.; Fogg, D. E. *Organometallics* **2003**, *22*, 3634.

CHAPTER 4

Can Chelation Inhibit σ-π Isomerization within Ru-Phenoxides? Exploration with a Heterobifunctional P, O-Chelating Ligand

4.1. Introduction

Chapter 3 described the kinetic instability of monodentate aryloxides toward σ→π isomerization within coordinatively unsaturated Ru complexes. However, a stable, *chelating* carbene-aryloxide ligand within a Ru alkylidene complex was recently reported (Figure 4.1).[1]

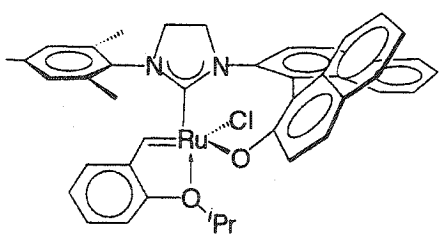

Figure 4.1. The "Hoveyda" catalyst[1] **20** contains a chelating carbene-aryloxide ligand.

While several examples of stable, η^2-P,O-chelated Ru-aryloxide complexes are known (Figure 4.2), these differ from **20** in that they are coordinatively saturated species containing no labile ligands. σ→π Isomerization is inhibited where the nonlability of ancillary ligands bars access to the three coordination sites required to accommodate the π-bound ring. Complex **20**, in contrast to **21-25**, is not only coordinatively unsaturated, but contains a labile bond between the ether oxygen and the metal center, which should in principle permit access to three coordination sites. The lability of the ether interaction is implied by the metathesis activity of **20**.[1]

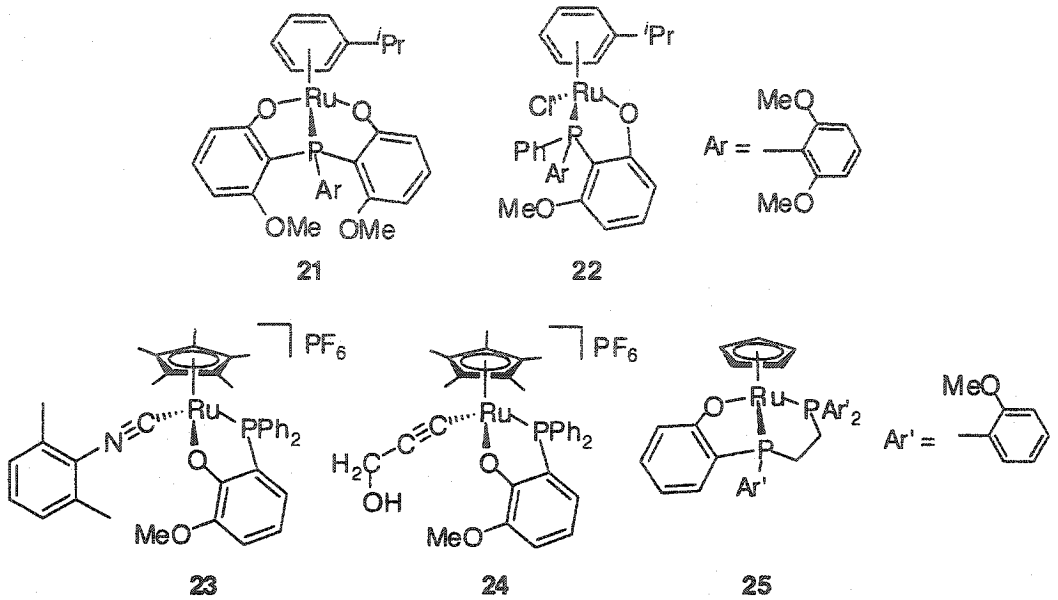

Figure 4.2. Reported examples of η^2-P,O complexes containing one or two Ru-aryloxide bonds (**21**, **22**,[2] **23**, **24**,[3] **25**[4])

We speculated that the stability of **20** might be due to the "extra" stabilization provided by the chelate effect. In order to probe this possibility, we examined the reaction of $RuCl_2(PPh_3)_3$ **1a** with the known[5] heterobifunctional phosphine-binaphtholate ligand **29** (2-(diphenylphosphino)-2'-hydroxy-1,1'-binaphthyl) which, by analogy to the structure of the well-known ligand binap, we term "binop" (Figure 4.3).

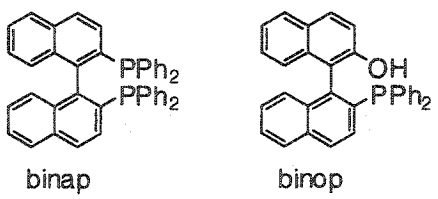

Figure 4.3. Heterobifunctional binap and "binop" ligands.

4.2. Preparation of (±)-2-(Diphenylphosphino)-2'-Hydroxy-1,1'-Binaphthyl (binop; 29)

Preparation of **29** was undertaken by the literature method,[5] involving conversion of binaphthol to the bis(triflate) **26**, followed by introduction of a diphenylphosphine group via Pd-

catalyzed cross-coupling to afford **27**. Conversion of **27** to phosphine oxide / phenol **28** is accomplished with $LiOH{\bullet}H_2O$, following which the phosphine oxide is reduced with trichlorosilane to afford **29** (Scheme 4.1, Path A). While an 88% overall yield was reported, total yields in our hands were only 34% following the literature protocols. The final reduction step was particularly problematic (45% yield, vs. the reported 94%), probably owing to the limited solubility of **28** in toluene. Indeed, use of chlorobenzene solvent at 120 °C (enabling complete dissolution) improved the yield of this step to 73%. Further improvements resulted from the observation that treating triflate-protected phosphine oxide **27** with trichlorosilane effects *both* reduction and deprotection: this tandem reaction proceeds in ca. 90% yield, shortening the total synthesis by one step (Scheme 4.1, Path B). Overall yields were thus ultimately increased to 82%.

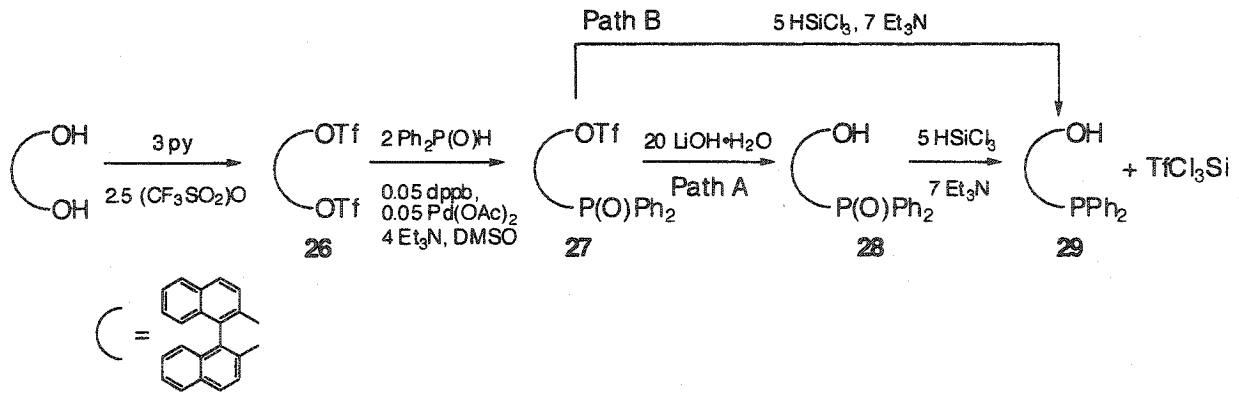

Scheme 4.1. Path A: Literature route to **29**. Path B: Optimized route to **29**.

4.3. Transformation of binop to its Alkali Metal Salts

Alkali metal salts of binop offer a convenient means of installing the binop ligand via transmetallation with, for example, $RuCl_2(PPh_3)_3$ **1a**. Binop is readily converted to its sodium

salt **30** on reaction with Na_2CO_3. Pure **30** is obtained (89%) by filtering off solid $NaHCO_3$ and unreacted Na_2CO_3, and removing the solvent under vacuum.

Use of *n*-butyllithium to abstract the phenolic proton was less successful. While no decomposition products were evident by ^{31}P NMR analysis, addition of ^{n}BuLi to a cold benzene solution of binop caused immediate discolouration of the solution. Reactions with **1a** indicated that an excess of Li-binop was required, in contrast with the 1:1 stoichiometry found for reactions using Na-binop (next section). In situ ^{31}P NMR analysis of a homogeneous solution, using dppb as an internal standard, confirmed loss of the integrated intensity for the Li-binop generated by this procedure, but not for the Na-binop generated from Na_2CO_3. Use of ^{n}BuLi may result in attack on the ring system of binop.

4.4. Reaction of $RuCl_2(PPh_3)_3$ 1a with Na-binop 30

Treatment of a CH_2Cl_2 solution of **1a** with one equivalent of Na-binop gives light orange RuCl(binop)(PPh_3) **31** (Scheme 4.2) in >90% yield.* Use of 2 equiv **30** did not yield the anticipated Ru(binop)$_2$ product: in contrast to the aryloxide reactions discussed in Chapter 3, in which both chloride ligands were readily displaced from **1a**, these reactions gave only **31**, with one equivalent of free **30** remaining (NMR evidence). The identity of **31** was established by detailed NMR and MALDI-MS analysis. Microanalytical data provided evidence for **31** with a molecule of hexane present. The presence of one equivalent of hexane was confirmed by the ^{1}H NMR integration. Crystallographic confirmation has proved troublesome, however.

---

* A byproduct (δ_P 52 ppm, s) was formed in various amounts depending on the reaction concentration: it was not observed in NMR scale reactions (0.01 mmol/mL), but at concentrations of **1a** in excess of 0.1 mmol/mL its integrated intensity ranged from 5-40%. It could not be separated from **31** except by chromatography, which caused it to decompose to a green, paramagnetic species that adhered to the silica gel.

The following sections are directed at unequivocal delineation of the proposed structure by NMR and MALDI-MS analyses. The σ,π-binop binding mode depicted finds precedent in Pregosin's reports of Ru(η^6:η^1-2-(diphenylphosphino)-1,1'-binaphthyl) complexes (Figure 4.4).[6] Related species that exhibit η^2-coordination to a C=C bond within the binaphthyl ring have also been described.[7] However, this coordination mode can be ruled out for **31** on the basis of chemical shift and other NMR data as discussed in Section 4.4.2.

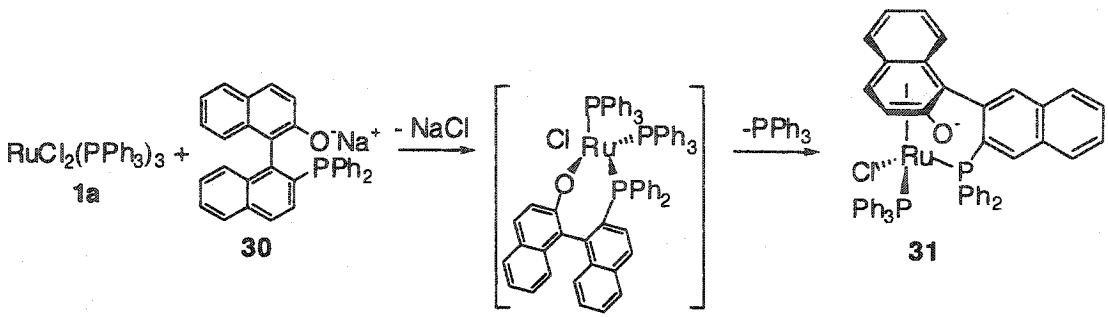

Scheme 4.2. Proposed reaction of $RuCl_2(PPh_3)_3$ **1a** with Na-Binop **30** .

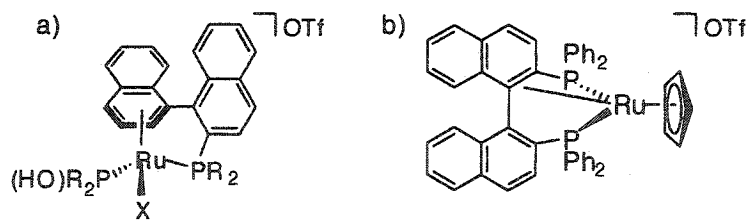

Figure 4.4. (a) η^6:η^1-bound Ru complexes of 2-(diphenylphosphino)-1,1'-binaphthyl (X = H, OTf; R = *i*-Pr, Cy)[6] and (b) CpRu(binap).[7]

4.4.1. Molecular Composition of 31

Strong evidence for formulation of **31** as RuCl(binop)(PPh_3) is provided by MALDI mass spectrometric analysis. The isotope pattern observed for the molecular ion by MALDI-MS (Figure 4.5) shows a peak-for-peak correspondence between theoretical and observed values (M^+ = m/z 852). A second pattern, at m/z 817, corresponds to [M^+-Cl], Ru(binop)(PPh_3)$^+$. The

complexity of these patterns is a function of the presence in ruthenium of seven naturally occurring isotopes, as well as the two naturally-occurring isotopes of chlorine.

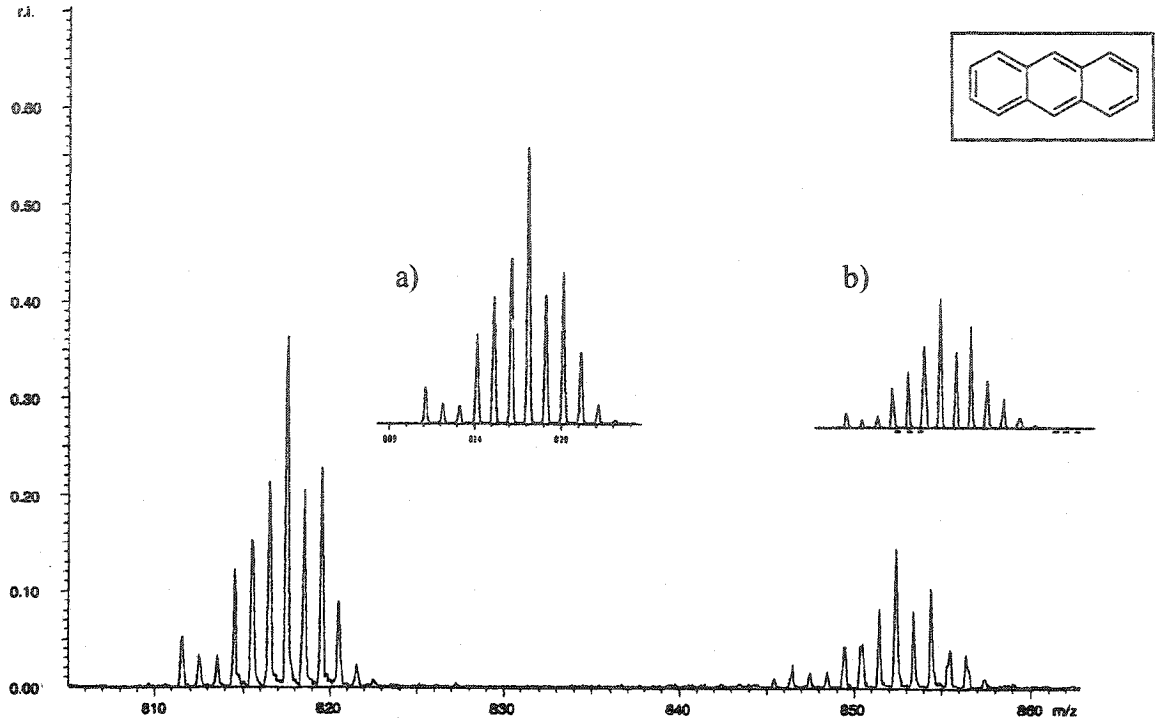

Figure 4.5. MALDI-MS spectrum for **31** (anthracene): (a) predicted isotope pattern for [M^+-Cl]; m/z 817; (b) predicted isotope pattern for [M^+]; m/z 852. The m/z value calculated corresponds to the exact mass of the isotopomer containing the highest-abundance isotope for each element.

The spectrum in Figure 4.5 was obtained on analysis in an anthracene matrix. Analysis in the more conventional, protic matrix dithranol results in a more complex pattern. Deviations from the theoretical isotope pattern we attribute to *partial* protonation of the molecular ion and its fragmentation products, as a result of the acidity of the dithranol. Competing ionization pathways (fragmentation and protonation) probably give rise to the isotope pattern seen.

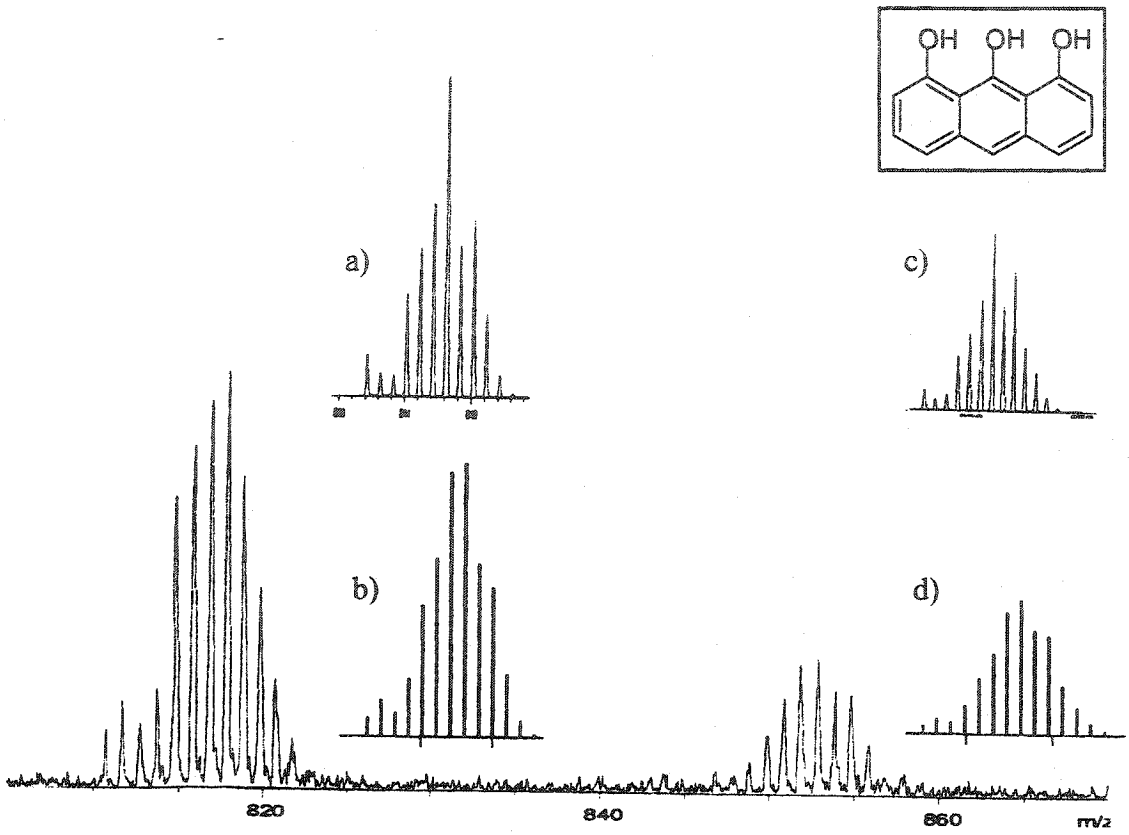

Figure 4.6. MALDI-MS spectrum for **31** (dithranol): (a) predicted isotope pattern for [M^+-Cl]; m/z 817; (b) predicted isotope pattern for [M^+-Cl]; m/z 817 with 60% protonation; c) predicted isotope pattern for [M^+]; m/z 852; d) predicted isotope pattern for [M^+]; m/z 852 with 60% protonation.

The proposed molecular composition is likewise supported by ^{1}H NMR integration data, which indicate a total of 37 aromatic protons. The presence of only two (inequivalent) ^{31}P nuclei is indicated by observation of an AB pattern in the $^{31}P\{^1H\}$ NMR spectrum (δ_P 48.1, 45.6; d, $^2J_{PP}$ = 58 Hz). In situ analysis confirms elimination of two PPh_3 ligands, both from the observed peak multiplicities (an A_2B pattern should be observed for $RuCl(binop)(PPh_3)_2$) and integration of the AB doublets against liberated PPh_3. Treatment with potential donors of minimal steric demand (CO, MeCN) shows no reaction at room temperature, implying coordinative saturation of **31**, and the non-lability of its ligands. (Under more forcing conditions (120 °C, 5 hours) the PPh_3 ligand

was partially (16%) displaced by CO, as judged by ^{31}P NMR analysis, resulting in unidentified products). The high stability of **31** is underlined by its successful purification by column chromatography on silica gel using "wet" solvents as eluants. In addition, solutions of **31** in C_6D_6 or $CDCl_3$ showed no decomposition on exposure to air for up to 3 days at RT.

4.4.2. Proposed Structure for RuCl(binop)(PPh_3) 31

The coordinatively saturated structure shown in Scheme 4.2, with its η^6:η^1-binop binding mode, is proposed on the basis of detailed ^1H, ^{13}C, and ^{31}P NMR experiments, including two-dimensional NMR experiments (for full series of spectra, see Appendix I).

The possibility of η^2-coordination of one C=C bond in the binop ligand (as in the binap complex of Fig 4.4b) was ruled out on the basis of ^1H and $^{13}C\{^1H\}$ NMR chemical shift data. η^2-Coordination of the aryl ring has a very minor effect on the chemical shift of the ^{13}C nuclei involved (145.2-125.9 ppm), whereas a significant upfield shift is found for several "aromatic" resonances in the $^{13}C\{^1H\}$ NMR spectrum for **31**. Also arguing against an η^2-C=C bonding mode is the absence of a ^{31}P NMR signal at low field (ca. 10 ppm[8]), characteristic of the four-membered Ru-P-C=C chelate ring.[9] Finally, the η^2-C=C coordination is rather easily displaced, even by a chloride available from CH_2Cl_2, whereas the π-binop ring is very nonlabile, as noted above.

^1H and ^{13}C NMR assignments for the π-bound binop ligand are summarized in Figure 4.7 and Table 4.1. The basis for these assignments is discussed in detail below.

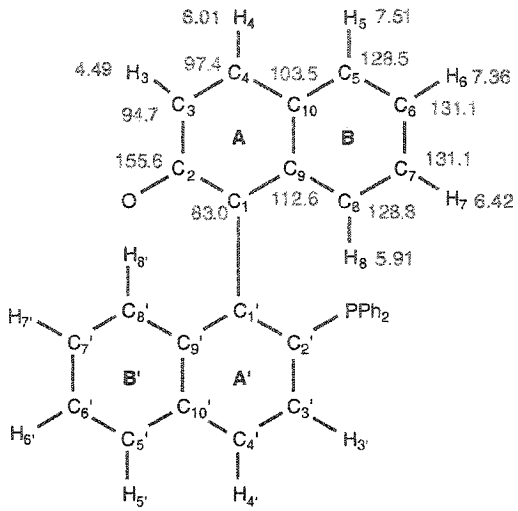

Figure 4.7. NMR peak assignments of carbon and hydrogen atoms for naphthol-based nuclei in **31**; unsaturation omitted for clarity. ^{1}H NMR values are red, ^{13}C NMR values are blue.

Table 4.1. $^{13}C\{^{1}H\}$ and ^{1}H NMR Assignments for **31**.[a]

C_n/H_n	δ_C	multiplicity	J_{CP} (Hz)	δ_H	multiplicity	J_{HH} (Hz)	J_{HP} (Hz)
1	83.0	s	-	-	-	-	-
2	155.8	s	-	-	-	-	-
3	97.3	d	9.6	4.49	dd	7.4	3.9
4	94.7	d	8.7	6.01	dd	7.4	2.6
5	128.5	s	-	7.51	d	7.4	-
6	131.1	br s	-	6.37[b]or 7.36	t	7.6	-
7	131.1	br s	-	6.37[b]or 7.36	t	7.6	-
8	128.9	s	-	5.93	d	8.4	-
9	112.6	s	-	-	-	-	-
10	103.5	s	-	-	-	-	-

[a] For atom numbering, see Figure 4.7. [b]Multiplet at 6.42 ppm at RT, overlapping with a non-naphthol doublet; resolved at 324 K (see text below and Figure 4.8c).

The ^{1}H NMR spectrum of **31** shows several aromatic signals shifted upfield of the 7-8 ppm region found for free binop (Figure 4.8). In Chapter 3, upfield shifts were demonstrated to be characteristic of protons on π-bound arene rings, with a range of 3.7-5.3 ppm being found for complexes $RuH(\eta^5\text{-}OAr)(PPh_3)_2$ **3a**, $Ru(\eta^5\text{-}OAr)(o\text{-}C_6H_4PPh_2)(PPh_3)$ **9**, $RuCl(\eta^5\text{-}OPh)(PPh_3)_2$ **11b**, and $[RuH(\eta^5\text{-}ArO)(PPh_3)_2]Cl$ **12a**.

The presence of one π-coordinated binop ligand in **31** was therefore suspected. Several NMR experiments (as detailed below), were carried out to confirm this and to identify which ring of the binop ligand was π-bound.

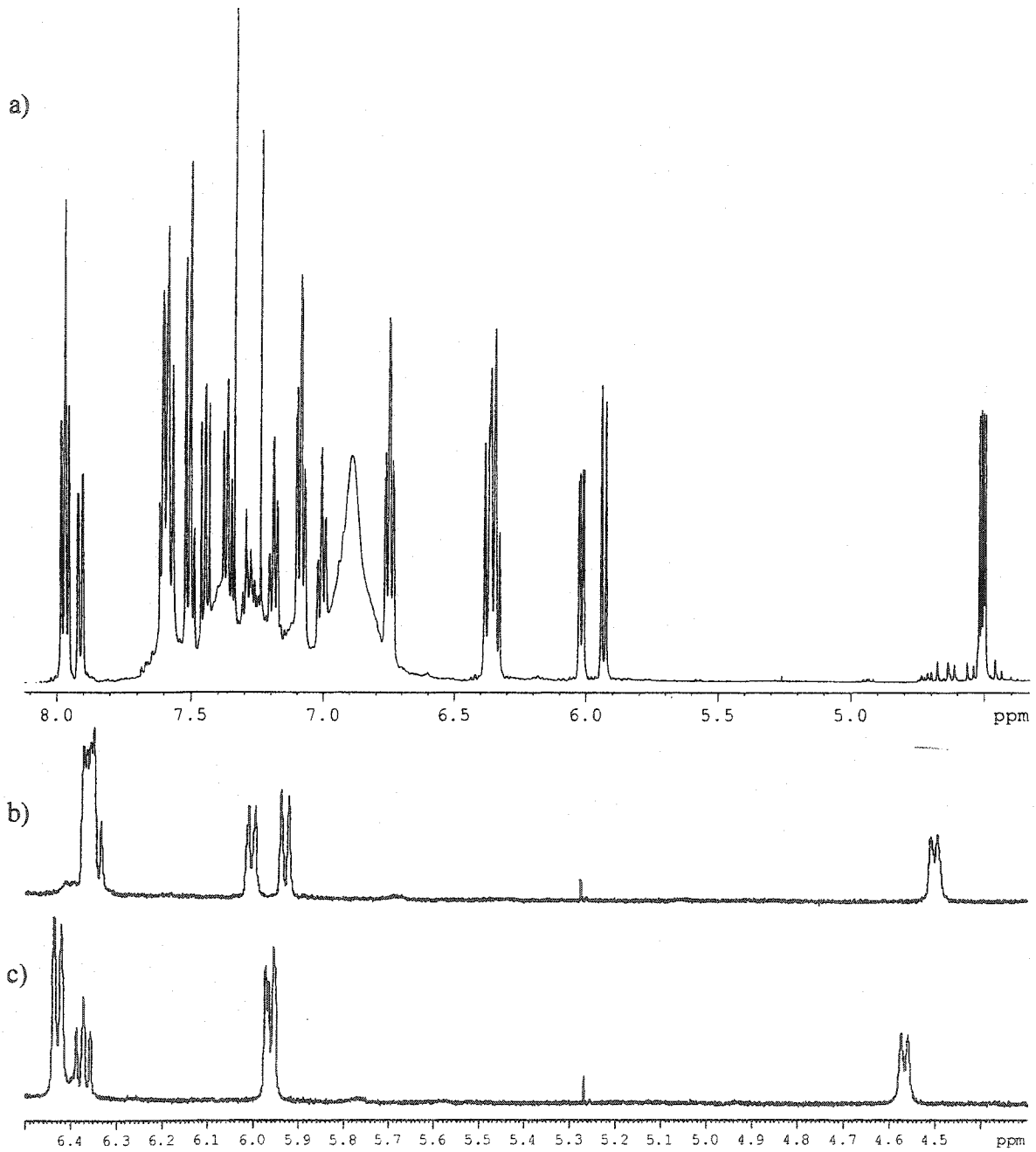

Figure 4.8. ^{1}H NMR spectrum for **31**: (a) full spectrum at 300K; (b) upfield region at 300K; (c) upfield region at 324K

The possibility of π-coordination of the ^{31}P-functionalized ring can be eliminated at the outset. $^{31}P\{^{1}H\}$ NMR spectra for η^2-binap complexes such as that shown in Figure 4.4 exhibit widely separated signals (e.g. 70.9 and 8.9 ppm), the upfield signal being due to the ^{31}P nucleus in the Ru-C-C-P chelate, α to the π-bound double bond as noted above.[10,11] The typical chemical shift values and small chemical shift difference of the ^{31}P signals for **31** (ca. 2 ppm) indicates that the two ^{31}P nuclei present occupy similar, strain-free donor environments. Simultaneous σ-coordination of the Ph_2P group, and π-coordination of the **B'** ring of the binaphthyl group is precluded by the rigidity of the ring system. π-Coordination must therefore be localized on the "naphthol" portion of the binop ring system.

Two sets of doublets of doublets are evident in the upfield portion of the ^{1}H NMR spectrum (4.49, 6.01 ppm). These correlate with each other (^{1}H-^{1}H COSY) and with two upfield doublets in the $^{13}C\{^{1}H\}$ NMR spectrum (94.7, 97.4 ppm; HMQC). The latter signals collapse to singlets on simultaneous ^{31}P and ^{1}H decoupling using a triple resonance probe. ^{31}P decoupling of the ^{1}H NMR spectrum likewise causes the peaks at 4.49 and 6.01 ppm to collapse to doublets. The magnitude of the upfield shift suggests that these protons are located on the ring that is π-bound to the metal center. Further, the multiplicities of the proton signals, as well as their mutual and exclusive correlation by COSY and TOCSY NMR spectroscopy, indicate that these signals are attributable to the "phenolate" ring.* The structure of **31** is thus analogous to that of $RuX(\eta^5\text{-}ArO)(PPh_3)_2$ (**3a**: X = H; **11b**: X = Cl). The only unexpected aspect of this finding is the apparent coupling to only *one* ^{31}P nucleus, rather than two, despite unequivocal ^{31}P NMR and MALDI-

* Unique assignment of H3/C3 and H4/C4 is not possible at this stage, but was made following more detailed analyses below: for clarity, however, the numbers ultimately assigned will be used in all discussions.

MS evidence for the presence of two phosphine ligands. This issue is addressed in more detail in Section 4.4.3.

Carbon connectivities could not be established by INADEQUATE ^{13}C NMR experiments, owing to the low solubility of **31**, exacerbated by the poor sensitivity of such experiments.* Indirect correlation methods were thus used, primarily ^{1}H-$^{13}C\{^{1}H\}$ HMBC and HMQC NMR experiments, supported by ^{1}H-^{1}H COSY and TOCSY analysis. The quaternary carbon signals of the naphthol ring, identified on the basis of their upfield location (with the exception of the phenolic carbon C2) and their disappearance on DEPT-135 analysis, provide a convenient entry point for analysis. The signal at 155.6 ppm is assigned to C2, by analogy to the value of 160.0 ppm for the C-O carbon in **3a**. The quaternary signals at 83.0, 103.5, and 112.6 ppm are assigned to C1, C10 and C9 respectively, on the basis of ^{1}H-^{13}C HMBC NMR data revealing $^{2}J_{HC}$ and $^{3}J_{HC}$ correlations (Figure 4.10). Predicted and found correlations are summarized in Table 4.2. A part of Figure 4.8, showing the naphthol portion of the binop ligand, is repeated below for convenient reference (Figure 4.9).

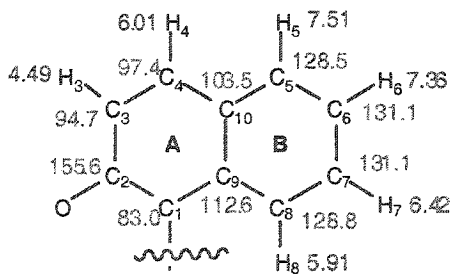

Figure 4.9. Naphthol portion of the binop ligand, showing numbering and chemical shifts (δ_H red, δ_C blue).

* $^{13}C\{^{1}H\}$ NMR INADEQUATE experiments require a signal-to-noise ratio of > 30:1 in a single scan. The S:N ratio for a saturated solution of **31** in $CDCl_3$ (100 mg in 0.75 mL) was only 3:1 after one scan.

Table 4.2. Anticipated and Observed ^{13}C-^{1}H Correlations for **31** from HMBC experiments.

	Predicted Couplings (H#)		Observed Couplings (H#)[a]
C# (δ_C)[b]	$^{2}J_{HC}$	$^{3}J_{HC}$ couplings	(δ_H ppm)
1 (83.0)	0	2 (H3, H8)	H3 (4.49), H8 (5.91)
2 (155.6)	1 (H3)	1 (H4)	H4 (6.01)
3 (97.4)	1 (H4)	0	H4 (6.01)
4 (94.7)	1 (H3)	1 (H5)	H3 (4.49), H5 (7.51)
5 (128.5)	1 (H6)	2 (H4, H7)	H4 (6.01), H6 (7.36), H7 (6.42)
6 (131.1)	2 (H5, H7)	1 (H8)	H5 (7.51), H7 (6.42), H8 (5.91)
7 (131.1)	2 (H6, H8)	1 (H5)	H5 (7.51), H6 (7.36), H8 (5.91)
8 (128.9)	1 (H7)	1 (H6)	H6 (7.36)
9 (112.6)	1 (H8)	3 (H4, H5, H7)	H4 (6.01), H5 (7.51), H7 (6.42), H8 (5.91)
10 (103.5)	2 (H4, H5)	3 (H3, H6, H8)	H3 (4.49), H4 (6.01), H5 (7.51), H6 (7.36), H8 (5.91)

[a] Two-bond and three-bond couplings are not distinguished by HMBC: the number of correlations is specified for ease of reference. [b] 4° carbons bold.

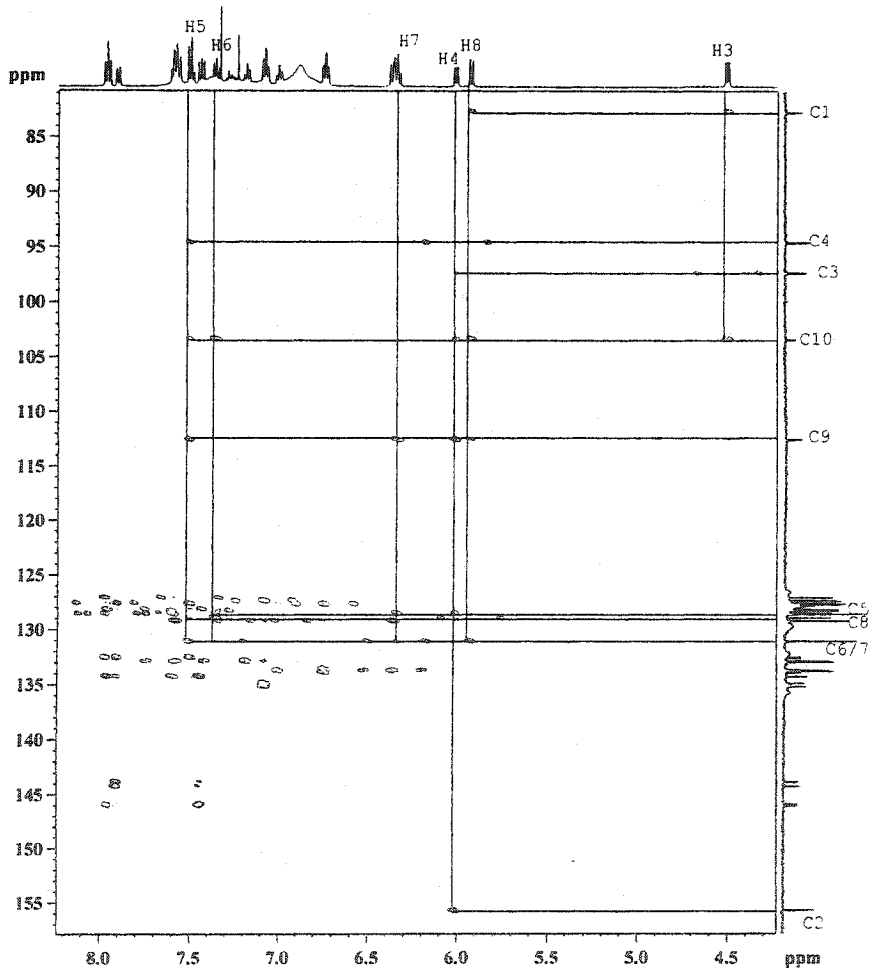

Figure 4.10. ^{1}H-^{13}C HMBC NMR spectrum for **31** (500 MHz, $CDCl_3$).

Unequivocal assignment of all quaternary carbon signals can be made on the basis of the unique number of total ($^2J_{HC}$ and $^3J_{HC}$) couplings for each resonance.* Thus, the signal at 103.5 ppm correlates to five protons (two $^2J_{HC}$ couplings to H4 and H5; three $^3J_{HC}$ bond couplings to H3, H6 and H8), and can therefore be assigned to C10. Similarly, the signal at 112.6 ppm correlates to four protons (one $^2J_{HC}$ coupling to H8; three $^3J_{HC}$ couplings to H4, H5, and H7) and can be assigned to C9. The signal at 83.0 ppm (two $^3J_{HC}$ couplings to H3 and H8) can be assigned to C1. The only correlations expected, but not observed for the quaternary carbons, are those between C2 and H3. While two correlations are expected ($^2J_{HC}$ and $^3J_{HC}$ couplings to H3 and H4, respectively), only the latter is observed in both cases. Anomalously small $^2J_{CH}$ coupling constants are not unprecedented: the ortho-couplings in benzene, for example, are between 0 and 5 Hz, while the meta-couplings are between 6 and 11 Hz.[12]

The ^{1}H-^{13}C correlations established above permit assignment of H3 and H4, on the basis of their correlation with (C1) and (C3, C5, C9), respectively. This deconvolutes the assignment of H3/C3 and H4/C4 that had been ambiguous in the COSY and HMQC analysis above. Assignment of H8 is made on the basis of the remaining correlation with C1, as well as correlation with C9 and C10. (Correlations with the non-quaternary carbons are ignored at this stage, as overlap with other signals adds complexity in this analysis). This permits identification of both C8 (HMQC) and H7 (COSY; see Figure 4.11). Assignment of H7 is confirmed by observation of the HMBC correlation with C9. Of the four HMBC correlations for C9, this leaves only one unassigned, and the signal for H5 can therefore be located as well. Finally, this leaves only one of the five correlations to C10 unassigned, and H6 can thus be located. Assignment of the corresponding ^{13}C nuclei is confirmed by HMQC correlations.

* HMBC spectra show contour spots due to $^1J_{HC}$ couplings, symmetrically disposed about the point of intersection of the ^{1}H and ^{13}C peaks. They can be recognized by the absence of a correlating peak in the ^{1}H NMR spectrum.

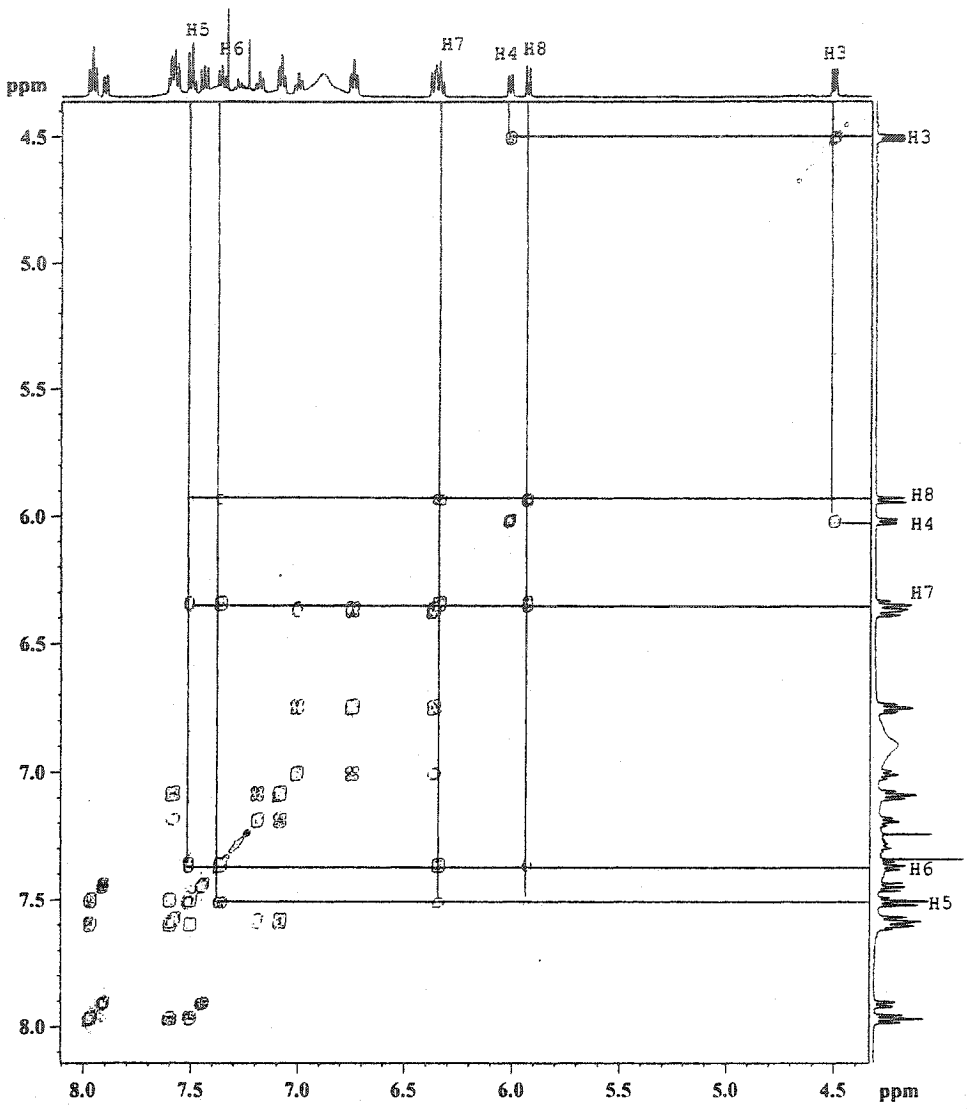

Figure 4.11. ^{1}H-^{1}H COSY NMR spectrum for **31** (500 MHz, $CDCl_3$).

These assignments, summarized in Figure 4.7 above, are supported by Boolean analysis, and by ^{1}H-^{1}H COSY and TOCSY NMR experiments directed at identification of one-bond, or two- and three-bond ^{1}H-^{1}H couplings, respectively. Protons H3 and H4 of Ring **A** (4.49 and 6.01 ppm) correlate only with each other, as expected. Of the protons in ring **B** (H8, 5.91; H7, 6.42; H6, 7.36; H5, 7.51 ppm), the triplet at 6.42 ppm overlaps with a doublet of doublets originating in a non-naphthol proton, from which it was

resolved at low temperature by ^{31}P decoupling. At 324K, the $^{1}H\{^{31}P\}$ NMR spectrum reveals a triplet for H7 at 6.37 ppm, and a doublet at 6.42 ppm (Figure 4.9c). The latter signal is probably due to H3' of the binaphthyl ring, coupled to the ^{31}P nucleus via a $^{3}J_{HP}$ coupling of 10.4 Hz.

As the binop ligand in **31** is π-coordinated through ring **A**, the possibility for η^5- or η^6-coordination exists. The arene ring within the monodentate phenoxide complexes of Chapter 3 is more precisely described as an oxocyclohexadienyl ligand (i.e. η^5-coordinated). The partial double-bond character of the C-O bond[13] in these complexes was manifested in an infrared ν(C=O) band at ca. 1530-1558 cm^{-1}. No such band is evident in the IR spectrum for **31**, implying that ring **A** of the binop ligand is η^6-coordinated, rather than η^5-coordinated.

4.4.3. ^{31}P Coupling Anomalies in NMR Data for 31

To discuss the ^{31}P-^{1}H coupling anomalies within **31** it is first necessary to identify peaks in the ^{31}P NMR spectrum (δ_P 45.6 and 48.1) as either the PPh_3 ligand or the PPh_2-tethered phosphine. Unambiguous identification of these phosphine ligands was determined using an ^{1}H-^{31}P HMQC NMR experiment optimized for 10 Hz coupling. The ^{31}P peak at 45.6 ppm showed strong P-H coupling to only H3 (4.49 ppm) of ring **A**, while the ^{31}P peak at 48.1 ppm showed couplings to H4 as well as to H3' as mentioned above, and several other aromatic protons located on rings **A'** and **B'**. From this, the ^{31}P peak at 48.1 ppm was determined to be the PPh_2-tethered phosphine and the peak at 45.6 ppm was therefore the PPh_3 ligand.

The unexpected appearance of protons H3 and H4 as doublets of doublets ($^{3}J_{HH}$ = 7.4 Hz, $^{3}J_{H(3)P}$ = 3.9; $^{3}J_{H(4)P}$ = 2.6 Hz), was noted at the beginning of the previous section. While this might suggest the presence of only *one* ^{31}P nucleus, rather than two, the ^{31}P NMR and MALDI-MS data provide unequivocal evidence for the presence of two phosphine ligands.

Closer examination of the coupling between the ^{31}P atoms and the ^{1}H nuclei located on ring **A** by ^{1}H-^{31}P HMQC NMR analysis reveals that H3, at 4.49 ppm, is split *only* by the ^{31}P NMR signal at 45.6 ppm, while the ^{31}P signal at 48.1 ppm is split *only* (and weakly) by H4, at 6.01 ppm. (Only very weak ^{31}P-^{1}H couplings were observed to protons H6 and H7 within ring **B**, again supporting the inference that the binop ligand is π-bound via the phenolic **A** ring of the naphthol group.) In **31**, the *lack* of coupling between H3 and PPh_2 provides information about the relative configurations of the two naphthyl ring systems. If the naphthyl rings of the binop ligand were *exactly* orthogonal to each other, the dihedral angle between H3 and PPh_2 would be 120° (Figure 4.12a) and ^{31}P-^{1}H coupling may be seen, however if the naphthyl rings were twisted 30° away from being orthogonal, the dihedral angle would approach 90° (Figure 4.12b) and no H3-PPh_2 coupling would be observed according to the Karplus relationship.

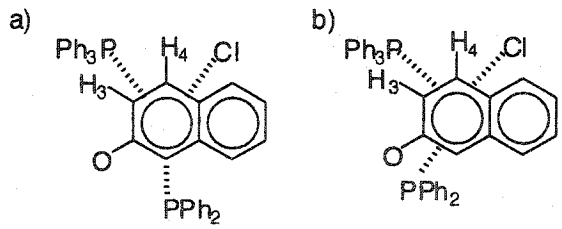

Figure 4.12. Top view of the predicted orientation of **31**, viewed from above the π-bound ring with the phosphine and chloride ligands below: a) with a H-C-Ru-PPh_2 dihedral angle of 120°; b) with a H-C-Ru-PPh_2 dihedral angle of 90°.

This 30° twist is plausible as no H3-PPh_2 splitting is observed. The orientation of the "seat" of the piano-stool complex must also put the H4-C4-Ru-PPh_3 angle at close to 90°, as no H4-PPh_3 splitting is observed. More surprising is the failure to observe splitting of the corresponding $^{13}C\{^{1}H\}$ NMR signals for C3 and C4 by coupling to the ^{31}P nuclei. Precedent for this is found in the σ,π-bound complexes of 2-(diphenylphosphino)-1,1'-binaphthyl, shown in Figure 4.4a above. In these complexes, C1 and C2 of the naphthyl ring couple to both ^{31}P nuclei (dd, J_{CP} = 9 and 1-3

Hz), but C3 and C4 couple to only one ^{31}P nucleus (d, J_{CP} = 4-8 Hz) (numbering as in Figure 4.7).[6]

4.5. Diastereomeric Bias within 31

Coordination of atropisomeric ligands within a piano-stool structure can give rise to diasteromers, owing to the combination of planar chirality and a sterogenic metal centre. Such behaviour is demonstrated by binaphthyl[6] and biphenyl[14,15] tethered-ligand compounds closely related to **31**. Two diastereomers are possible for **31**, each of which gives rise to two enantiomers (Figure 4.13), owing to the planar chirality of the binop ring. (A further element of complexity emerges if the PR_3 donor is *chiral*, four diastereomers and eight enantiomers then being present.[8]) In all isomers of **31**, a favourable interaction can be envisaged between the PPh_2 group and the oxygen atom of the binop ligand. Consistent with such an interaction is the observation of a strong IR stretching band at 1212 cm^{-1}, within the range characteristic of a P=O bond.

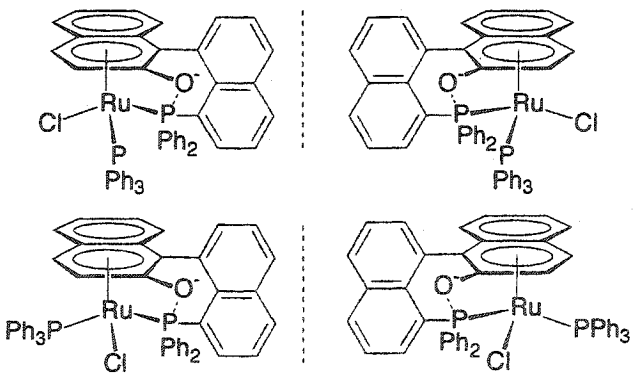

Figure 4.13. Stereoisomers of RuCl(binop)(PPh_3) **31**.

$^{31}P\{^1H\}$ NMR evidence suggests that **31** is formed as a single diastereomer: only one set of AB patterns is observed at room temperature. Low-temperature measurements were carried out to ensure that this was not an artifact of stereochemical nonrigidity, as noted in other

work.[8,16] Analysis of **31** (in $CDCl_3$ or CH_2Cl_2) showed no change in the AB pattern seen at room temperature down to -90 °C. This implies that either a single diastereomer is present, or that the equilibrium between diastereomers is too fast to be seen on the NMR timescale even at this low temperature. Rapid epimerization of the metal centre would require, however, facile loss and recoordination of the PPh_3 ligand. This possibility is ruled out by the extreme non-lability of the phosphine ligand noted above (Section 4.4.1) in reactions with carbon monoxide and acetonitrile.

Formation of a single diastereomer of a biphenyl tethered-ligand Ru complex has been reported by Faller and coworkers (Figure 4.14).[8] Low temperature NMR analysis showed no resolution of the single AB pattern into two distinct sets of resonances. Emergence of a very minor new pair of AB doublets was observed, but was attributed to slowing of a conformational interconversion (probably a conformational change in the PPh_3 ligand, as previously[17-19] noted). Crystallographic analysis of the Faller complex revealed the epimer in which the PPh_3 and NMe_2 groups was on opposite sides of the molecule. Preferential formation of this isomer was attributed to unfavourable steric interactions between the bulky PPh_3 ligand and the dimethylamino group in the η^6-ring. Interestingly, NMR and X-ray analysis of analogous complexes containing smaller phosphines (e.g. PMe_2Ph) reveal the presence of both diastereomers. The diastereomer in which the NMe_2 and PPh_3 groups lie on the same side of the molecule was presumed to be accessible in these cases because the phosphine conformation can adjust to minimize the unfavourable steric interaction with the NMe_2 group. The extent of diastereomeric bias in such systems is indeed commonly a function of the cone angle of the "L-donor" ligand.[8]

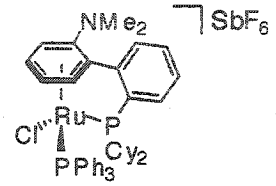

Figure 4.14. Literature example of a binaphthyl tethered-ligand Ru complex [8].

These arguments concerning the origin of diastereomeric bias can be extended to **31**, in which interactions between the bulky PPh_3 group and the oxygen of the binop ligand are conceivable. An unfavourable steric interaction would bias the system in favour of the isomer in which the PPh_3 and the dangling oxygen substituents are on opposite sides of the ring system. Sterically induced destabilization of the opposite isomer is difficult to reconcile, however, with the minimal interaction anticipated between the PPh_3 ligand and the binop oxygen. By analogy to the crystallographically characterized η^6-ArOH complex **12a** discussed in Chapter 3, the oxygen atom in **31** is presumed to be near-coplanar with the η^6-binaphthol ring; i.e. the "seat" of the piano stool. This would limit unfavourable steric interactions between the oxygen atom and the PPh_3 group. A more plausible explanation for the observed diastereomeric preference may be a *favourable, electronic* interaction between the binop oxygen and the PPh_3 ligand (Figure 4.13a), which would place the oxygen and PPh_3 groups on the *same* side of the molecule. Such an interaction would be facilitated by the 30° twist of the naphthyl rings (as discussed above), though a greater splay of the PPh_3 "leg" of the piano stool may also contribute.

Irrespective of the specific isomer preferred, the selectivity for a single diastereomer in **31** is potentially intriguing from the perspective of asymmetric catalysis. Should resolution of the two enantiomers be possible, **31** may be an interesting candidate for (e.g.) asymmetric Diels-Alder[8,20-23] or transfer hydrogenation[24-27] catalysis. η^1:η^6-Tethered complexes have been used in both of these reaction types, albeit with limited enantioselectivity to date. Abstraction of the

chloride ligand in **31** would provide a convenient means of generating the vacant site at the metal required for substrate binding.

4.5. Conclusions

Spectroscopic and experimental data for **31** indicate a coordinatively saturated $RuCl(binop)(PPh_3)$ complex, in which the binop ligand is σ-bound through phosphorus and π-bound via the aryloxide ring. Clearly, chelation does not inhibit σ→π isomerization of the Ru-OAr unit. As with the results of Chapter 3, this suggests that given sufficiently labile ancillary ligands (in this case PPh_3), ruthenium preferentially binds to carbon, rather than anionic oxygen, consistent with the Pearson 'hard-soft' formalism.[28]

The broader significance of this finding lies in its implications for the utility of such heterobifunctional P,O-ligands in late metal catalysts for which coordinative unsaturation is a prerequisite for activity. In this context, the apparent stability of the Hoveyda catalyst **20** against σ→π isomerization is of particular interest. Possible barriers to isomerization in **20** include the relatively low lability of the dative Ru-O (ether) bond (implied by the unusual stability and slow initiation[1] of this species), or the strong trans effect of the alkylidene ligand, which could prohibit formation of a coordinatively saturated piano-stool structure. Arguing against the latter possibility, however, is the recent report of a piano-stool type alkylidene complex $[RuCl(\eta^6\text{-}C_6Me_4H_2)(PMe_3)(=C(OMe)CH=CHC_6H_4CH=CHCO_2Me)]\ [PF_6]$.[29] The results outlined above suggest that the coordinatively unsaturated active species formed from **20** after one step of metathesis may likewise be susceptible to σ→π isomerization (Scheme 4.3), and short lifetimes may therefore be anticipated for this catalyst.

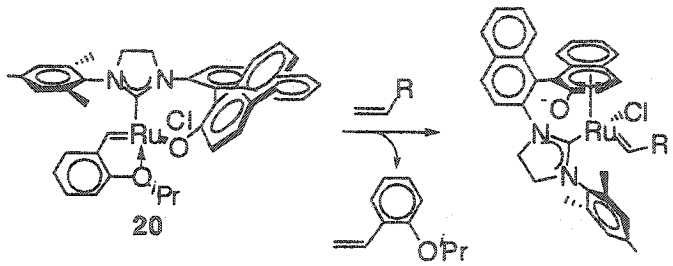

Scheme 4.3. Possible σ→π isomerization of the second-generation Hoveyda[1] catalyst **20**.

Although use of a chelating P,O-ligand did not enable stabilization of the Ru-O bond, the formation of only one diastereomer of **31** may have promise for asymmetric catalysis via piano-stool complexes.

4.6 References

(1) Van Veldhuizen, J. J.; Garber, S. B.; Kingsbury, J. S.; Hoveyda, A. H. *J. Am. Chem. Soc.* **2002**, *124*, 4954.
(2) Yamamoto, Y.; Sato, R.; Ohshima, M.; Matsuo, F.; Sudoh, C. *J. Organomet. Chem.* **1995**, *489*, C68.
(3) Yamamoto, Y.; Tanase, T.; Sudoh, C.; Turuta, T. *J. Organomet. Chem.* **1998**, *569*, 29.
(4) van der Drift, R. C.; Bouwman, E.; Drent, E.; Kooijman, H.; Spek, A. L.; van Oort, A. B.; Mul, W. P. *Organometallics* **2002**, *21*, 3401.
(5) Uozumi, Y.; Tanahashi, A.; Lee, S.-Y. H., T. *J. Org. Chem.* **1993**, *58*, 1945.
(6) Geldbach, T. J.; Pregosin, P. S.; Albinati, A. *Organometallics* **2003**, *22*, 1443.
(7) Pathak, D. D.; Adams, H.; Bailey, N. A.; King, P. J.; White, C. *J. Organomet. Chem.* **1994**, *479*, 237.
(8) Faller, J. W.; D'Alliessi, D. G. *Organometallics* **2003**, *22*, 2749.
(9) Garrou, P. E. *Chem. Rev.* **1981**, *81*, 229.
(10) Feiken, N.; Pregosin, P. S.; Trabesinger, G.; Scalone, M. *Organometallics* **1997**, *16*, 537.
(11) Feiken, N.; Pregosin, P. S.; Trabesinger, G.; Albinati, A.; Evoli, G. L. *Organometallics* **1997**, *16*, 5756.
(12) Breitmaier, E.; Voelter, W. In *Carbon-13 NMR Spectroscopy. High-Resolution Methods and Applications in Organic Chemistry and Biochemistry*; 3rd ed.; VCH Verlagsgesellschaft: New York, 1990, p 145.
(13) Cole-Hamilton, D. J.; Young, R. J.; Wilkinson, G. *J. Chem. Soc., Dalton Trans.* **1976**, 1995.
(14) Singewald, E. T.; Shi, X. B.; Mirkin, C. A.; Schofer, S. J.; Stern, C. L. *Organometallics* **1996**, *15*, 3062.
(15) Feiken, N.; Pregosin, P. S.; Trabesinger, G. *Organometallics* **1997**, *16*, 3735.
(16) Brunner, H.; Zwack, T. *Organometallics* **2000**, *19*, 2423.

(17) Davies, S. G.; Derome, A. E.; McNally, J. P. *J. Am. Chem. Soc.* **1991**, *113*, 2854.
(18) Costello, J. F.; Davies, S. G.; McNally, D. *J. Chem. Soc., Perkin Trans. 2* **1999**, 465.
(19) Dance, I.; Scudder, M. *J. Chem. Soc., Dalton Trans.* **2000**, *10*, 1579.
(20) Faller, J. W.; Lavoie, A. *J. Organomet. Chem.* **2001**, *630*, 17.
(21) Faller, J. W.; Grimmond, B. J. *Organometallics* **2001**, *20*, 2454.
(22) Faller, J. W.; Grimmond, B. J.; D'Alliessi, D. G. *J. Am. Chem. Soc.* **2001**, *123*, 2525.
(23) Faller, J. W.; Lavoie, A. R.; Grimmond, B. J. *Organometallics* **2002**, *21*, 1662.
(24) Faller, J. W.; Lavoie, A. R. *Organometallics* **2001**, *20*, 5245.
(25) Faller, J. W.; Lavoie, A. R. *Org. Lett.* **2001**, *3*, 3703.
(26) Faller, J. W.; Lavoie, A. R. *Organometallics* **2002**, *21*, 3493.
(27) Faller, J. W.; Lavoie, A. R. *Organometallics* **2002**, *21*, 2010.
(28) Pearson, R. G. *J. Am. Chem. Soc.* **1963**, *85*, 3533.
(29) Ulrich, K.; Guerchais, V.; Toupet, L.; LeBozec, H. *J. Organomet. Chem.* **2002**, *643-644*, 498.

CHAPTER 5

A New, General Precursor to Ruthenium Alkylidene Complexes, and an Investigation into Azine Coordination Chemistry

5.1. Introduction

In 1992, Grubbs reported the synthesis of **32a**, the first well-characterized ruthenium alkylidene complex (Scheme 5.1) capable of ring-opening metathesis polymerization (ROMP).[1] Compound **32a** is no longer used, as it must be prepared via a substituted cyclopropene whose preparation is synthetically challenging,[2] and it is less metathesis-active than the later-developed, electron-rich systems.[3,4] As this Chapter will show, however, complexes of type **32** have significant potential as an *entry point* to new metathesis catalysts.

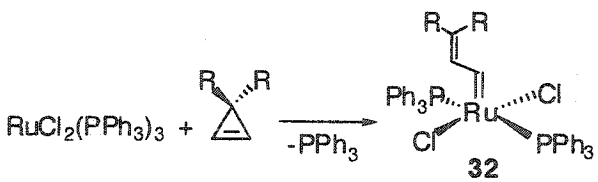

Scheme 5.1. Preparation of the first well-characterized ruthenium-alkylidene complex (**32a** R = Ph; **32b** R = Me).

An alternative means of installing an alkylidene ligand involves reaction of diazoalkanes with an appropriate ruthenium precursor. Of particular importance are the benzylidene derivatives obtained on use of phenyldiazomethane,[5,6] of which Grubbs' catalyst, $RuCl_2(PR_3)_2(CHPh)$ **33** is the prototypical example. Synthesis of **33** utilizes $RuCl_2(PPh_3)_3$ as a precursor. Other routes to Ru-alkylidene complexes rely on the use of ruthenium reagents that

are difficult to synthesize ($Ru(COD)(COT)$[7]), inherently unstable ($RuH_2(H_2)_2(PCy_3)_2$[8]), or stoichiometrically imprecise owing to low solubility ($[RuCl_2(COD)]_n$[9]). Indeed, such limitations have resulted in widespread use of Grubbs' catalyst itself as a precursor to the majority of new Ru alkylidenes,[4,10-15] despite the comparatively low lability of the PCy_3 ligands, the cost or multi-step syntheses required, and hazards associated with the use of toxic, unstable, and mutagenic phenyldiazomethane.[16] In addition, we have found that the azine byproduct formed during preparation of phenyldiazomethane can initiate undesired coordination chemistry (Section 5.3).

Surprisingly little attention has focused on the possibilities inherent in alkylidene installation via the known[17-20] insertion of alkynes into Ru-hydride bonds. Several years ago, Grubbs reported[21] such a reaction of $RuH(H_2)Cl(PCy_3)_2$ (Scheme 5.2). This system is limited, however, by the cumbersome synthesis of the precursor (including the need for H_2 gas), as well as the low lability of the phosphine ligands. We were interested in the possibility of utilizing this "propargyl chloride" chemistry to install the alkylidene moiety within an easily accessible, stable and soluble hydride complex. Incorporation of labile PPh_3 ligands was also targeted, as a means of facilitating ligand exchange within the Ru alkylidene complex. This chapter describes the development of such a convenient, general precursor to new Ru alkylidene complexes, as well as azine coordination chemistry. Parts of this chapter have been published.[22] Concurrent with our own efforts, a preliminary report appeared using this approach.[23]

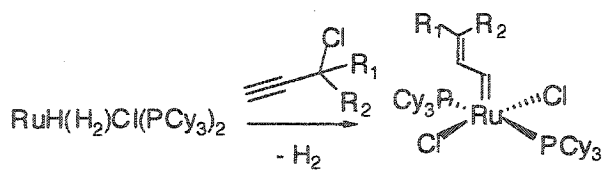

Scheme 5.2. Reaction of $RuH(H_2)Cl(PCy_3)_2$ with mono- or disubstituted and unsubstituted propargyl chlorides.

5.2. Preparation of a Versatile Precursor to New Ruthenium Alkylidene Complexes

$RuHCl(PPh_3)_3$ **1b** is an attractive entry point into this chemistry. This complex presents the two essential features noted above: a hydride ligand that serves as a handle for alkylidene installation, via reaction with 3-chloro-3-methyl-1-butyne,[21] and labile PPh_3 ligands that can subsequently be displaced. We have prepared $RuHCl(PPh_3)_3$ **1b** in quantitative yields by the reaction of $RuCl_2(PPh_3)_3$ **1a** with aryloxide in the presence of isopropanol;[22] it is also accessible by classical routes involving reaction of $RuCl_2(PPh_3)_3$ with Et_3SiH and base[24,25] or H_2 and NEt_3,[26,27] or reaction of $RuCl_3 \cdot H_2O$ with PPh_3 and NEt_3 under H_2.[28]

Addition of the chloro-alkyne effects conversion of **1b** into $RuCl_2(=CHCH=CMe_2)(PPh_3)_2$ **34** within *ca.* 30 min at room temperature in CH_2Cl_2 (Scheme 5.3). The broad $^{31}P\{^1H\}$ NMR resonance for **1b** is replaced by a sharp singlet at 30.0 ppm for **34**, and the upfield quartet for the hydride ligand of **1b** (δ_H –17.8, $^2J_{HP}$ = 25.8 Hz) gives way to a downfield quartet for H_α of the alkylidene (δ_H 18.20, $^3J_{HH} = {}^3J_{HP}$ = 9.4 Hz). Byproducts can be observed by in situ NMR analysis; identification of these was pursued by other researchers within the Fogg group, and is summarized in the next section for completeness.

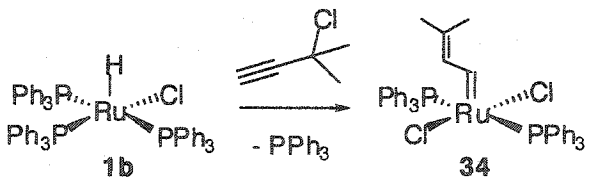

Scheme 5.3. Reaction of **1b** with 3-chloro-3-methyl-1-butyne.

5.2.1 Formation of Byproducts

Trace amounts of a second product (<5%) were observed by ^{31}P NMR analysis of the reaction of **1b** with 3-chloro-3-methyl-1-butyne in CH_2Cl_2. The new species gives rise to a ^{31}P

NMR singlet at 11.8 ppm. When the reaction is carried out on suspensions of **1b** in THF, the proportion of this byproduct sometimes exceeds that of **34**. It was isolated in 75% yield by Dino Amoroso of this group, on use of a fourfold excess of 3-chloro-3-methyl-1-butyne in THF (Scheme 5.4), and identified as Ru(IV) vinylcarbyne **35** on the basis of detailed spectroscopic and X-ray analysis.[22]

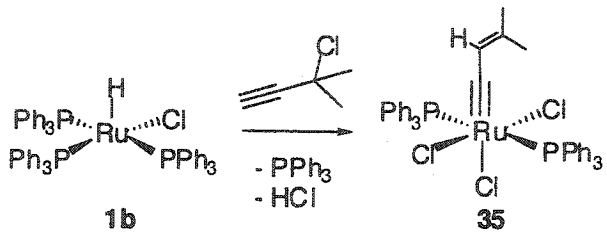

Scheme 5.4. Synthesis of vinylcarbyne **35**.

The stoichiometry of the reaction affording **34** can thus be critical. Subsequent work in this laboratory, however, has shown that formation of the carbyne byproduct can be suppressed by the simple expedient of adding base.[29] This implies that carbyne **35** is produced from HCl contamination of the chlorobutyne.

Another byproduct, characterized spectroscopically (Dino Amoroso),[22] is generated on attempted purification of **34**. Isolation and reprecipitation of **34** resulted in contamination by dinuclear $RuCl(PPh_3)_2(\mu\text{-}Cl)_3Ru(PPh_3)_2(=CHCH=CMe_2)$ **36**, formed by dimerization of **34** and extrusion of alkylidene (Scheme 5.5). It should be noted that dimerization occurs over a timescale that does not compete with phosphine exchange (see next section). In addition, **34** is stable in the solid state for months under inert atmosphere.

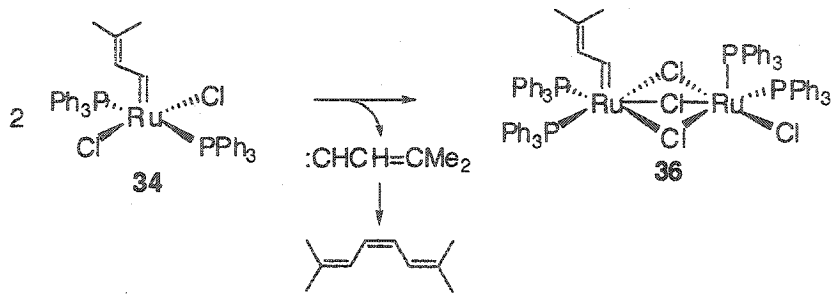

Scheme 5.5. Dimerization of **34** to **36** in solution.

5.2.2 Use of 34 as a Precursor

The PPh_3 ligands within **34** are displaced within minutes of adding PCy_3, and the reported[21] vinylcarbene $RuCl_2(=CHCH=CMe_2)(PCy_3)_2$ **37** can be isolated in 88% yield. More advantageously, **37** may also be generated in a one-pot procedure from **1b**, by successive addition of 3-chloro-3-methyl-1-butyne and PCy_3 in CH_2Cl_2 (Scheme 5.6). Within 40 minutes at room temperature, quantitative conversion is effected, as indicated by $^{31}P\{^1H\}$ NMR analysis.

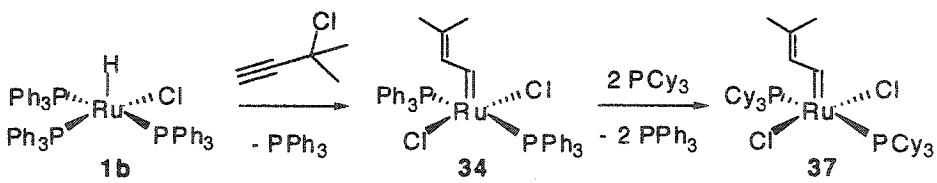

Scheme 5.6. One-pot synthesis of **37** from **1b**.

Complex **34** has now been used within the Fogg group as a precursor to novel "pincer" and N-heterocyclic carbene derivatives,[22] as well as **37**; other groups[23] have used it to gain entry to complexes of chelating diphosphines.

5.3. Azine Poisoning Studies

In situ installation of a benzylidene ligand using excess phenyldiazomethane is potentially complicated by the presence of contaminants in the diazoalkane reagent. The *Organic Synthesis* route to phenyldiazomethane[16] ($PhCHN_2$; **39**) involves condensation of tosyl hydrazine with benzaldehyde to yield benzaldehyde tosylhydrazone **38**, followed by deprotonation of the NH moiety and loss of the tosyl group.[30] The desired $PhCHN_2$ is formed on heating at 65 °C for only five minutes. Also present, however (^{1}H NMR evidence) are the starting material **38** and the "over-reaction" product *t,t*-benzaldehyde azine **40**, the latter being generated by condensation of **38** with a second molecule of benzaldehyde.[31] Conversion to **40** is complete on heating for 24 h (Scheme 5.7). Samples of $PhCHN_2$ are thus invariably contaminated with the azine, but purification is impossible, owing to the instability of the diazoalkane. We suspected that issues of $PhCHN_2$ purity might be problematic in the synthesis of Ru benzylidene complexes, and of particular concern for in situ synthesis of new Ru metathesis catalysts.[32-36] The effects of azine on metathesis, and the potential for azine to coordinate to the metal, were therefore investigated.

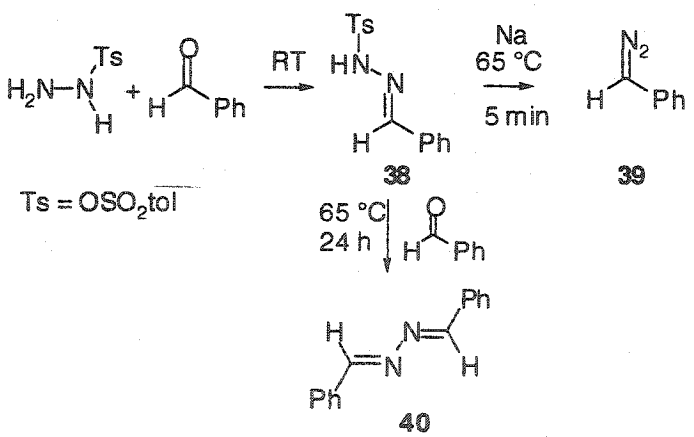

Scheme 5.7. Preparation of phenyldiazomethane **39** or *t,t*-benzaldehyde azine **40**.

5.3.1 Formation of an Azine Adduct of Ruthenium

Parallel work in the Fogg group focused on the metathesis activity of catalysts prepared in situ from Ru diphosphine species and $PhCHN_2$. The ability of azine **40** to coordinate to one such Ru species, $Ru_2Cl_4(dppb)_2$ **41a**, was therefore investigated. This complex is generated on dissolving $Ru_2Cl_4(dppb)_2(\mu\text{-}H_2O)$ **41** in organic solvents (Scheme 5.8, ^{31}P NMR spectrum Figure 5.1a).[37] Under an atmosphere of nitrogen, the N_2-coordinated dimer **41b** is also present.

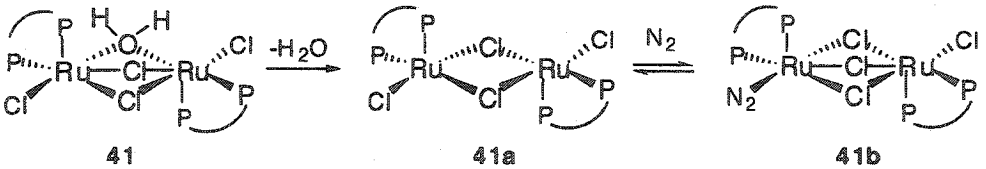

Scheme 5.8. Preparation of $Ru_2Cl_4(dppb)_2$ **41a** in solution.

Initial reactions were carried out on NMR scale in $CDCl_3$. A solution of **41** and azine **40** was freeze-pump-thaw degassed under Ar, to avoid formation of **41b** (which would complicate the ^{31}P NMR spectrum). After 24 h, a new ^{31}P NMR pattern was evident (Figure 5.1b).* The spectrum includes two sets of AB systems, in a pattern characteristic of unsymmetrically substituted $RuCl(dppb)(\mu\text{-}Cl)_3Ru(dppb)(L)$ systems[37] (δ_P 53.2, 52.1, $^2J_{PP}$ = 43 Hz; 47.9, 47.5, $^2J_{PP}$ = 37 Hz). Such complexes are readily generated by reaction of **41a** with a wide range of L-donors (L = NEt_3, NH^nBu_2, acetone, CO, DMA and DMSO (**45**)).[37] These signals are assigned to product **42** (Scheme 5.9) in which the azine is bound via a single N-donor. The ^{31}P NMR signals on the 'chloride' end of such dimers typically display a narrow range of chemical shifts and coupling constants, and indeed one of the AB patterns for **42** agrees well with values reported for

* The same product is formed over four days at RT on use of one equiv azine. In either case, ^1H NMR analysis was uninformative.

other $Ru_2Cl_4(dppb)_2(L)$ type complexes (**42**: δ_P 53.2, 52.1, $^2J_{PP}$ = 43 Hz; L = CO: δ_P 53.8, 53.3, $^2J_{PP}$ = 45 Hz; L = DMA: δ_P 53.5, 52.2, $^2J_{PP}$ = 43 Hz). The signals due to the phosphorus groups on the "L-end" of the dimer vary more widely, depending on the type of donor ligand employed, but these are typically within the 40-50 ppm range found for **42**.

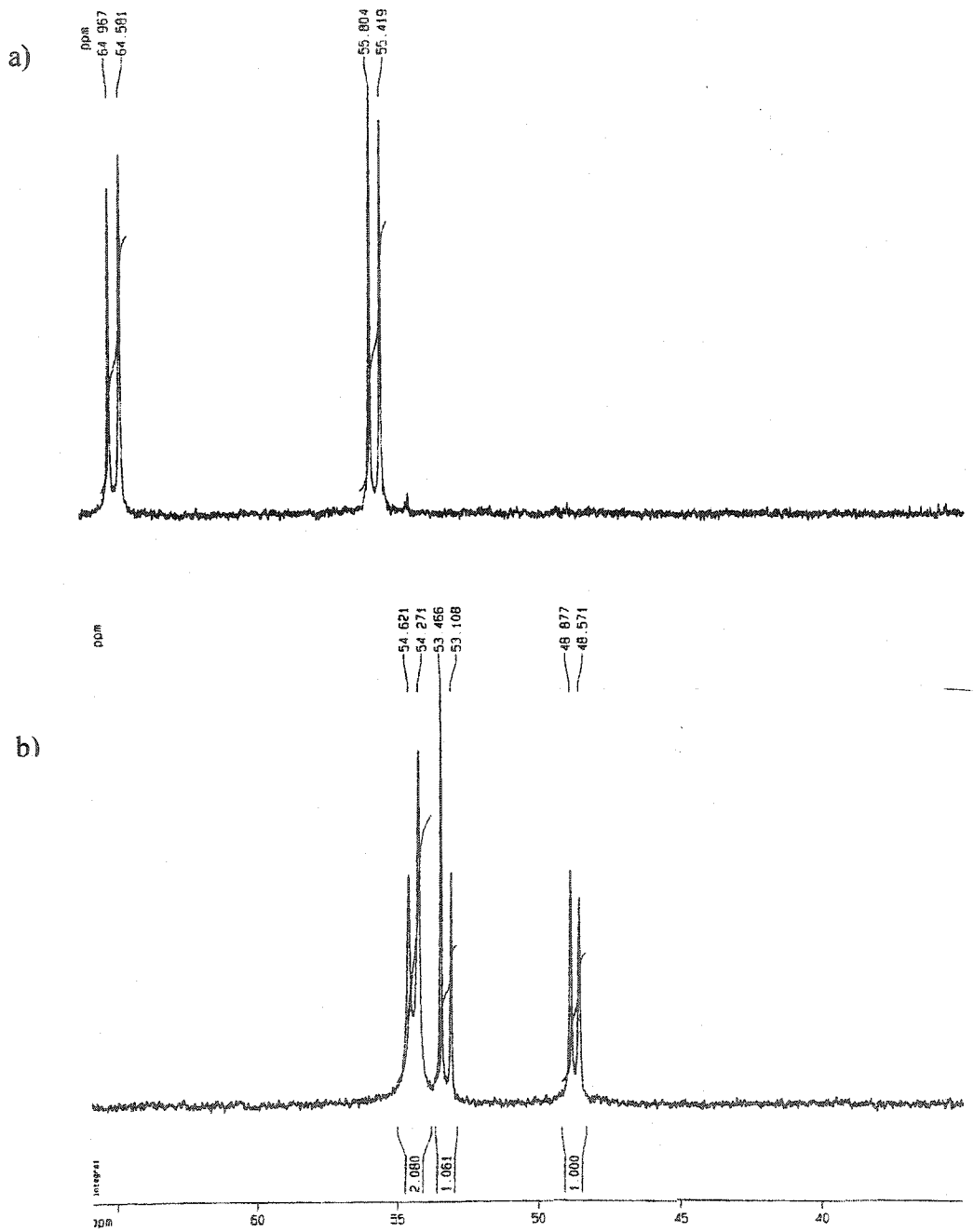

Figure 5.1. $^{31}P\{^1H\}$ NMR spectrum of a) starting material **41a** ; b) **42**.

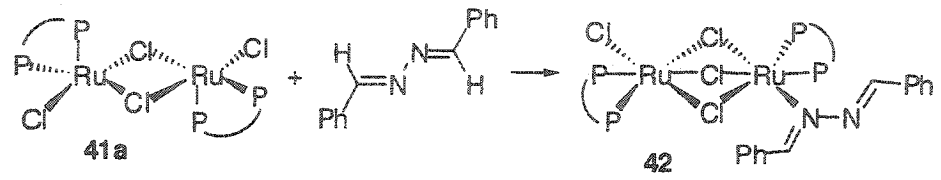

Scheme 5.9. Coordination of azine to **41a**.

Azines typically bind to transition metals through both nitrogen atoms (as reported for a $C_pV(CO)_2$(azine) cationic complex).[38] In recent work, however, the complex $Fe(CO)_3$(PhCH=CHCH=NN=CHR) was found to exhibit azine binding via a single nitrogen donor, with auxiliary binding through an adjacent site of unsaturation.[39] In complex **42**, chelation of the azine is presumably inhibited by the coordinative saturation of the dimer, enforced by the high thermodynamic stability of the face-bridged $Ru_2(\mu\text{-}Cl)_3$ structure. η^1-Coordination of *t,t*-benzaldehyde azine via nitrogen was recently proposed within a PCP-pincer complex of rhodium.[40] The complex was not isolated, however, its structure being proposed on the basis of in situ $^{31}P\{^1H\}$, ^1H, $^{13}C\{^1H\}$, ^{15}N-^1H, heteronuclear ^{13}C-^1H correlation and ^{13}C DEPT-135 experiments.[40]

To gain information regarding the electronic requirements necessary for N-N cleavage of a Ru coordinated azine, coordination of the *t,t*-benzaldehyde azine **40** to electron-rich $Ru_2Cl_4(dcypb)_2(N_2)$ (dcypb = 1,4-bis(dicyclohexylphophino)butane) was attempted. If the heterolytic N-N cleavage requires an electron-deficient metal centre, the reaction should be inhibited using $Ru_2Cl_4(dcypb)_2(N_2)$. Preliminary attempts to coordinate azine to $Ru_2Cl_4(dcypb)_2(N_2)$ showed no evidence for coordination. The dcypb dimer has a very low solubility in C_6H_6, however, which could have impeded coordination.

5.3.2. Azine Activation Products

In an attempt to force chelation, thermolysis of **42** was undertaken at 50 °C. After 2 days, only two new species (**43** and **44**; ratio 1:1) remained, as shown in Figure 5.2. The structure of the two products is clearly analogous, given the strong correspondence of the chemical shifts, patterns, and coupling constants evident in Table 5.1. Again, the pattern of two AB quartets observed for each suggests a diruthenium, face-bridged structure, similar to that found for **42**. These are formulated as nitrile and imine adducts formed by activation of bound azine (Scheme 5.10), as discussed below.

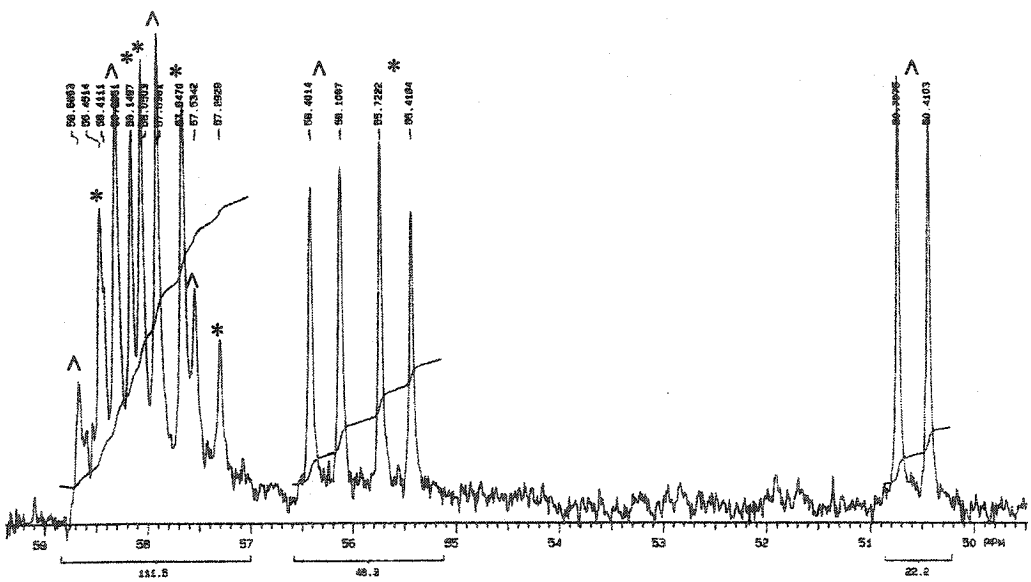

Figure 5.2. $^{31}P\{^{1}H\}$ NMR spectrum of **43** (∧) and **44** (*).

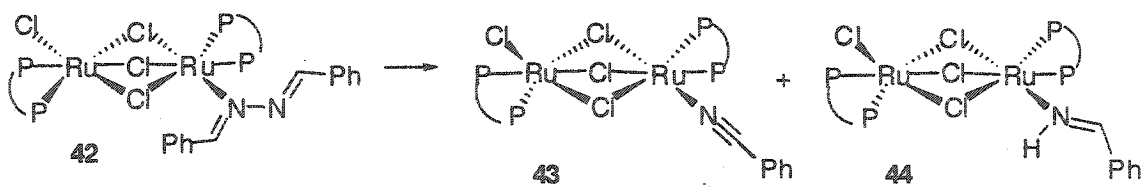

Scheme 5.10. Thermolysis of **42** to yield **43** and **44**.

Table 5.1. $^{31}P\{^{1}H\}$ NMR data (C_6D_6) for **42** under Ar, **43** and **44** under N_2

Complex	δ_P $^{31}P\{^{1}H\}$ NMR Data	
42	53.2, 52.1 ($^{2}J_{PP}$ = 43 Hz)	47.9, 47.5 ($^{2}J_{PP}$ = 37 Hz)
43	58.5, 57.7 ($^{2}J_{PP}$ = 44 Hz)	56.3, 50.6 ($^{2}J_{PP}$ = 36 Hz)
44	58.3, 55.6 ($^{2}J_{PP}$ = 37 Hz)	58.2, 57.5 ($^{2}J_{PP}$ = 43 Hz)

NMR and IR analysis of the mixture permits identification of **43** as known[41] PhCN complex $Ru_2Cl_4(dppb)_2(N{\equiv}Ph)$ (an assignment confirmed by crystallographic analysis), and of **44** as the isostructural imine derivative. An infrared stretching band at 2232 cm^{-1} is assigned to $\nu(C{\equiv}N)$ (**43**), a medium band at 1571 cm^{-1} to $\nu(C{=}N)$ (**44**), and a broad band at *ca.* 3200 cm^{-1} to $\nu(N\text{-}H)$ (**44**). The location of the nitrile stretching band is in agreement with the value of 2230 cm^{-1} reported for $Ru_2Cl_4(dppb)_2(L)$ (L = PhCN) (originally obtained on treatment of **41a** with benzonitrile[41]). A value of 1570 cm^{-1} was reported[42] for the $\nu(C{=}N)$ stretching vibration for $Mo(\eta^6\text{-}C_6H_6)$ $(MeC{=}NPh)(CO)_2(P)OMe)_3$.

Characterization of **44** was further enabled by ^{1}H NMR analysis which reveals a doublet at 9.37 ppm ($^{3}J_{HH}$ = 21 Hz); the azine -C*H*N signal originally observed at 8.65 ppm is no longer present. The COSY spectrum shows a correlation between the doublet at 9.37 ppm and a signal at 8.18 ppm (several overlapping resonances). No ^{1}J coupling to a ^{13}C nucleus is observed by HMQC analysis, supporting assignment of this signal to the NH proton. Consistent with this, a $^{15}N\text{-}^{1}H$ HSQC experiment reveals a ^{1}J correlation with a broad ^{15}N NMR singlet at 434 ppm (referenced to NH_3 as external standard). A value of 392 ppm was reported for the nitrogen nucleus in Rh(PCP)(NH=CHPh) (PCP = $[2,6\text{-}(^{i}Pr_2PCH_2)_2C_6H_3]$).[40] Long-range coupling between the NH proton and a carbon singlet at 172 ppm is observed (HMBC); the latter signal in turn correlates to the proton resonance at 8.18 ppm (HMQC), and to two aromatic signals at 7.3 and

7.7 ppm (HMBC). These data provide strong evidence for the presence of a HN=CHPh entity. On this basis, complex **44** is proposed to be the benzylidene imine analogue of **43**.

5.3.3. Mechanism of Formation of 43 and 44

A possible sequence of azine coordination events is shown in Scheme 5.11. Coordination of the intact azine at room temperature yields azine adduct **42**, following which thermolysis enables nucleophilic attack of the "dangling" azine nitrogen on the benzylidene proton. This triggers cleavage of the N-N bond, liberating HN=CHPh and forming one equivalent of the benzonitrile adduct **43**. Surprisingly, the 1:1 stoichiometry between **43** and imine adduct **44** is retained *irrespective* of the proportion of azine added (from 1-10 equiv), implying that the coordinating power of the imine is considerably superior to that of azine. The possible involvement of free **41** is ruled out by obervation of a 1:1 product ratio on thermolysis of isolated **42**.

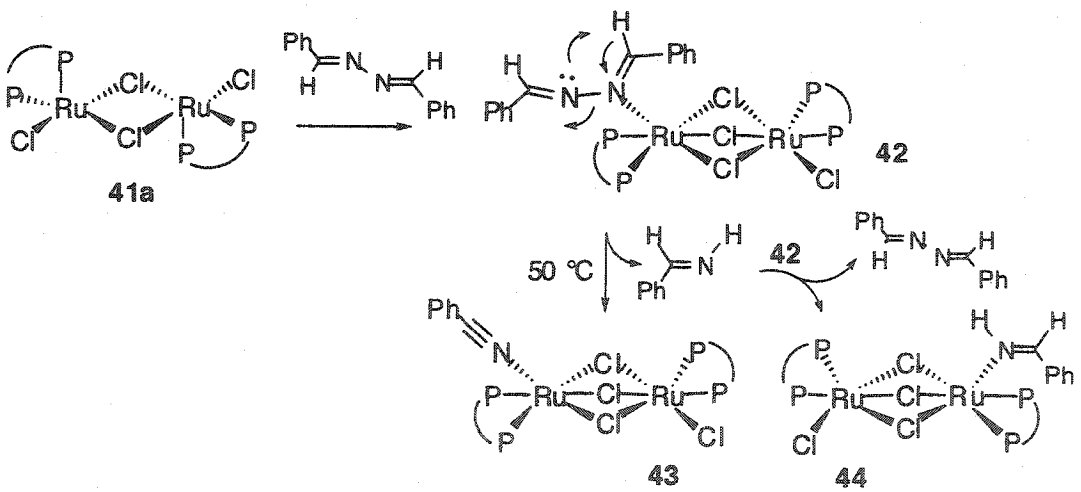

Scheme 5.11. Proposed mechanism for overall reaction of azine **40** with $Ru_2Cl_4(dppb)_2$ **41a**.

Homolytic N-N bond cleavage of azines to form transition metal imide derivatives is effected by Ti,[43] Zr,[44] Co,[44] and Fe[45] complexes. Contributing to the symmetrical cleavage may be the usual η^2-coordination mode of azine donors, in which both nitrogens are bound to the metal.[46-49] Only one previous example of heterolytic azine activation is reported in the literature.[40] Catalytic N-N bond activation of *t,t*-benzaldehyde azine was effected by Rh(η^3-PCP)(N_2) affording nitrile and imine complexes as the final inorganic products. The Rh(azine) complex could not be isolated, but was characterized spectroscopically (see Section 5.3.1). In the present case, the lower reactivity of the Ru(II) center in **42** permits interception of the azine derivative, with its novel η^1-coordination mode. Coordination of a single nitrogen to the metal appears to play a critical role, enabling the non-coordinated nitrogen to function as a nucleophile. Thermolysis of isolated **42** resulted in the formation of **43** and **44**, showing unambiguously that the N-N heterolytic cleavage of **42** occurs in an intramolecular, rather than intermolecular, fashion.

5.3.4. Hydrolysis of Imine Complex 44

Addition of H_2O to a C_6D_6 solution of **43** and **44** gave rise to a new singlet at 10.32 ppm within 1 hour at room temperature. This correlates (HMQC) to a $^{13}C\{^1H\}$ NMR singlet at 192 ppm. Both values are consistent with data for benzaldehyde. The high hydrolytic sensitivity of bound imine was noted previously[50] in complexes of the type $Ru_2Cl_4(dppb)_2(RN{=}CHPh)$ (R = Ph, CH_2): sequential dehydrogenation of a secondary amine to (bound) imine was followed by hydrolysis to yield a complex containing a primary amine.[50] In the present case, the reaction is presumed to culminate in ammine derivative $Ru_2Cl_4(dppb)_2(NH_3)$, with liberation of benzaldehyde (Scheme 5.12). Oxidation of the liberated benzaldehyde to benzoic acid by trace

oxygen would account for the observation of a broad ^{1}H NMR singlet at 12.6 ppm after prolonged heating. Detailed analysis of the $^{31}P\{^{1}H\}$ NMR spectrum was prohibited by the complexity of the spectrum: the presence of three closely related ruthenium species causes considerable peak congestion in the region 52-58 ppm.

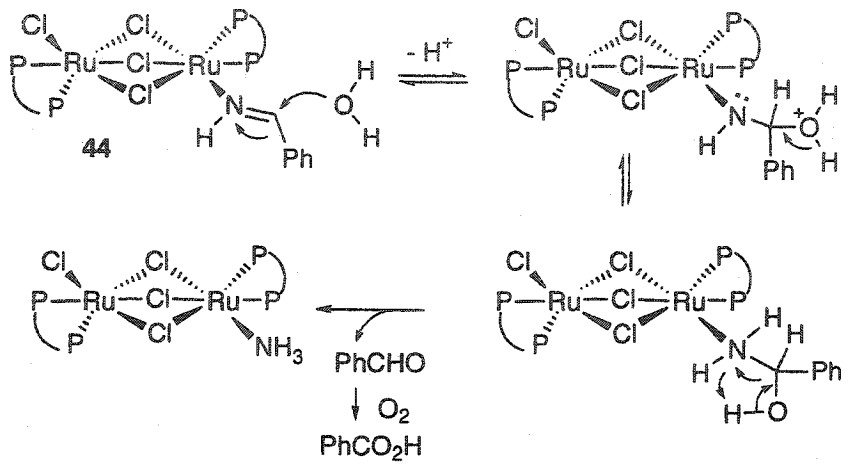

Scheme 5.12. Proposed mechanism for hydrolysis of **44** by residual H_2O.

5.3.5. Molecular Structure of $Ru_2Cl_4(dppb)_2(NCPh)$ 43

X-ray quality crystals of **43** were obtained by evaporation of a $CDCl_3$ solution of the sample that had been heated for 140 h at 50 °C. The mass of crystals from which the crystal subjected to X-ray analysis was selected consisted of a 1:1 ratio of **43** and **44**, as judged by ^{31}P NMR analysis. The molecular structure of the dimer is shown in Figure 5.3, with selected bond lengths and angles in Table 5.2.

Table 5.2. Selected Bond Lengths (Å) and Angles (°) for **43** and **45**. (Collection parameters and a complete table of bond lengths and angles for **43** is in Appendix H).

Bond	**43**	**45**[37]
Ru(1)-Cl(1)	2.4804(18)	2.468(1)
Ru(1)-Cl(2)	2.4747(19)	2.495(1)
Ru(1)-Cl(3)	2.4007(19)	2.429(1)
Ru(1)-P(1)	2.274(2)	2.305(1)
Ru(1)-P(2)	2.266(2)	2.305(1)
Ru(2)-Cl(1)	2.4189(18)	2.418(1)
Ru(2)-Cl(2)	2.5359(18)	2.517(1)
Ru(2)-Cl(3)	2.5348(19)	2.492(1)
Ru(2)-Cl(4)	2.4120(19)	2.399(1)
Ru(2)-P(3)	2.2695(19)	2.261(1)
Ru(2)-P(4)	2.239(2)	2.257(1)
Ru(1)-X	X = N(1); 2.009(7)	X = S(1); 2.244(1)
N(1)-C(7)	1.105(11)	----
Cl(1)-Ru(1)-Cl(2)	78.77(6)	78.25(3)
Cl(1)-Ru(1)-Cl(3)	84.81(6)	78.46(3)
Cl(1)-Ru(1)-P(1)	171.56(7)	172.23(4)
Cl(1)-Ru(1)-P(2)	92.66(7)	93.62(4)
Cl(1)-Ru(1)-X	X = N; 88.77(18)	X = S; 91.86(4)
Cl(2)-Ru(1)-Cl(3)	80.65(6)	80.80(3)
Cl(2)-Ru(1)-P(1)	93.78(7)	94.73(4)
Cl(2)-Ru(1)-P(2)	170.98(7)	169.35(4)
Cl(2)-Ru(1)-X	X = N; 88.72(18)	X = S; 91.94(4)
Cl(3)-Ru(1)-P(1)	90.10(7)	97.29(4)
Cl(3)-Ru(1)-P(2)	95.90(7)	90.90(4)
Cl(3)-Ru(1)-X	X = N; 168.47(18)	X = S; 168.87(4)
P(1)-Ru(1)-P(2)	94.56(8)	92.93(4)
P(1)-Ru(1)-X	X = N; 95.08(18)	X = S; 91.68(4)
P(2)-Ru(1)-X	X = N; 93.95(18)	X = S; 95.23(4)
Ru(1)-Cl(1)-Ru(2)	82.20(6)	86.69(3)
Ru(1)-Cl(2)-Ru(2)	84.49(6)	84.01(3)
Ru(1)-Cl(3)-Ru(2)	83.69(6)	85.93(3)
N(1)-C(7)-C(6)	161.6(18)	------

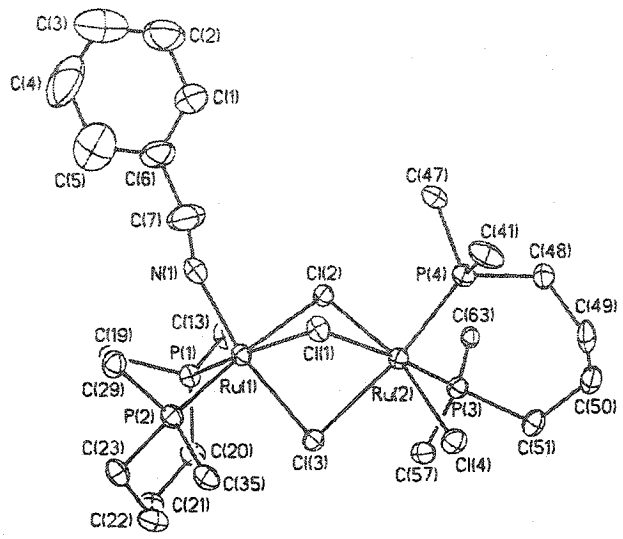

Figure 5.3. Molecular structure of $Ru_2Cl_4(dppb)_2(NCPh)$ **43**. Hydrogen atoms and dppb phenyl rings omitted for clarity.

The dinuclear, trichloro-bridged structure exhibits a slightly distorted octahedral geometry around both ruthenium atoms. Its molecular structure closely resembles that of $Ru_2Cl_4(dppb)_2(DMSO)$ (**45**).[37] All of the bond lengths and angles are comparable, though not statistically equivalent, presumably owing to the difference in L-donor. Chloride atoms trans to phosphorus in **43** display distinctly longer Ru-Cl bond distances (av. 2.48 Å) compared to the Ru-Cl distance trans to the L donor ligand (2.40 Å), as expected from the strong trans influence of PR_3. The average bridging angle (Ru(1)-Cl-Ru(2)) in **43** (av. 83.46°) is nearly 13° larger than the ideal value of 70.5° for two regular face-sharing octahedral.[51] This indicates that the Ru centers are further apart than expected for a regular cofacial bioctahedron, though they are closer than in **45** (av. 85.55°). The N(1)-C(7) bond distance (1.105(11) Å) is statistically equivalent[52] to values found for bound nitrile in $Ru(dppb)(MeCN)_4^{+2}$ (N-C = 1.129(4), 1.126(3), 1.135(3) and 1.131(3) Å) and *t*-$RuCl_2(MeCN)_4$ (N-C = 1.119(3) and 1.129(3) Å).[52] Imine bond lengths are typically significantly longer, as indicated by the values in $PtI(MeC{=}NH(C_6H_{11}))(PMe_2Ph)$ (N-C

= 1.287(13) Å)[53] and Mo(η^6-C_6H_6)(MeC=NPh)$(CO)_2(P(OMe)_3)$ (N-C = 1.266(12) Å).[42] The short N(1)-C(7) bond length is consistent with identification of the crystal structure as nitrile **43**. Unexpectedly, however, the N-C(7)-C(6) bond angle of 161.6(18)° shows a strong deviation from the expected value of 180° for the *sp* hybridized carbon of **43**. A search of the Cambridge Structural Database (CSD v 2.23)[54] for all Ru-N≡C-C segments revealed 248 compounds, of which the smallest reported N≡C-C angle was ca. 164.20° (for $[Ru(MeCN)_3)(ETP)](CF_3SO_3)_2$; ETP = tris(MeCN)-bis(2-(diphenylphosphino)ethyl)phenyl-phosphine).[55] The error associated with this value is not reported in the database and the angle is not reported nor discussed in the paper, but the R value of 6.3 for the complex is reasonable, suggesting that typical error is associated with the value. The typical N≡C-C angle is between 175 and 180° according to the number of N≡C-C angles reported in this range in the database, but there are four compounds given that have N≡C-C bond angles of less than 170°. The N-C(7)-C(6) bond angle (161.6(18)°) in the crystal structure of **43**, while remarkable, is thus not without precedent. Given the "normal" location of the infrared ν(C≡N) stretching band, the distortion of the N-C(7)-C(6) bond angle may be imposed by crystal packing forces.

5.4. Conclusions

$RuHCl(PPh_3)_3$ **1b** was identified as an attractive, accessible precursor to new Ru-alkylidenes via the versatile intermediate $Ru(=CHCH=CMe_2)(PPh_3)_2$ **34**. The lability of the PPh_3 ligands in **34** permit facile phosphine exchange, as demonstrated by the one-pot reaction with PCy_3 to produce $RuCl_2(=CHCH=CMe_2)(PCy_3)_2$ **37**.[21] Exchange for alternative neutral donor ligands affords convenient access to a range of new and known olefin metathesis catalysts.[22] Formation of byproduct **35** is readily suppressed by addition of base, while dimerization to give

36 does not occur on the timescale of phosphine exchange. Dimerization does occur over hours in solution, however, and (given the bimolecular nature of the reaction) proceeds more rapidly as the concentration of **34** increases, hampering isolation of pure **34**.

Coordination and N-N bond activation of azine was demonstrated in the azine poisoning studies. While addition of excess azine showed no deleterious effect on ROMP at room temperature via the $PhCHN_2$ / $Ru_2Cl_4(dppb)_2$ (**41a**; dppb = 1,4-bis(phenylphosphino)butane) catalyst system,[32] the coordination chemistry described may complicate ROMP using unreactive catalysts or monomers, polymerizations at high temperatures, or those requiring use of phenyldiazomethane in large excess. For highly active catalysts, however, the timescale for azine coordination is much slower than the rate of polymerization.[32] More fundamentally, however, these results suggest the very interesting potential of Ru catalysts for N-N, C-H, and C-N bond activation.

5.5. References

(1) Nguyen, S. T.; Johnson, L. K.; Grubbs, R. H.; Ziller, J. W. *J. Am. Chem. Soc.* **1992**, *114*, 3974.
(2) Trnka, T. M.; Grubbs, R. H. *Acc. Chem. Res.* **2001**, *34*, 18.
(3) Weskamp, T.; Koh, F. J.; Hieringer, W.; Gleich, D.; Herrmann, W. A. *Angew, Chem. Int. Ed.* **1999**, *38*, 2416.
(4) Scholl, M.; Ding, S.; Lee, C. W.; Grubbs, R. H. *Org. Lett.* **1999**, *1*, 953.
(5) Schwab, P.; France, M. B.; Ziller, J. W.; Grubbs, R. H. *Angew. Chem. Int. Ed.* **1995**, *34*, 2039.
(6) Schwab, P.; Grubbs, R. H.; Ziller, J. W. *J. Am. Chem. Soc.* **1996**, *118*, 100.
(7) Belderrain, T. R.; Grubbs, R. H. *Organometallics* **1997**, *16*, 4001.
(8) Olivan, M.; Caulton, K. G. *Inorg. Chem.* **1999**, *38*, 566.
(9) van der Schaaf, P. A.; Kolly, R.; Hafner, A. *J. Chem. Soc., Chem. Commun.* **2000**, 1045.
(10) Zhang, J.; Gunnoe, T. B. *Organometallics* **2003**, *22*, 2291.
(11) Garber, S. B.; Kingsbury, J. S.; Gray, B. L.; Hoveyda, A. H. *J. Am. Chem. Soc.* **2000**, *122*, 8168.
(12) Huang, J.; Stevens, E. D.; Nolan, S. P.; Petersen, J. L. *J. Am. Chem. Soc.* **1999**, *121*, 2674.

(13) Sanford, M. S.; Hanling, L. M.; Day, M. W.; Grubbs, R. H. *Angew. Chem. Int. Ed.* **2000**, *39*, 3451.
(14) Sanford, M. S.; Love, J. A.; Grubbs, R. H. *Organometallics* **2001**, *20*, 5314.
(15) Trnka, T. M.; Morgan, J. P.; Sanford, M. S.; Wilhelm, T. E.; Scholl, M.; Choi, T.-L.; Ding, S.; Day, M. W.; Grubbs, R. H. *J. Am. Chem. Soc.* **2003**, *125*, 2546.
(16) Creary, X. In *Organic Syntheses*; Wiley & Sons: Toronto, 1990; Vol. VII, p 438.
(17) Xia, H. P.; Jia, G. *Organometallics* **1997**, *16*, 1.
(18) Esteruelas, M. A.; Lahoz, F. J.; Oñate, E.; Oro, L. A.; Zeier, B. *Organometallics* **1994**, *13*, 4258.
(19) Grünwald, C.; Gevert, O.; Wolf, J.; Gonzáles-Herrero, P.; Werner, H. *Organometallics* **1996**, *15*, 1960.
(20) Burrow, T.; Sabo-Etienne, S.; Chaudret, B. *Inorg. Chem.* **1995**, *34*, 2470.
(21) Wilhelm, T. E.; Belderrain, T. R.; Brown, S. N.; Grubbs, R. H. *Organometallics* **1997**, *16*, 3867.
(22) Amoroso, D.; Snelgrove, J. L.; Conrad, J.; Drouin, S. D.; Yap, G. P. A.; Fogg, D. E. *Adv. Synth. Catal.* **2002**, *344*, 757.
(23) Volland, M. A. O.; Rominger, F.; Eisenträger, F.; Hofmann, P. *J. Organomet. Chem.* **2002**, *641*, 220.
(24) Eaborn, C.; Odell, K.; A., P. *J. Organomet. Chem.* **1973**, *63*, 93.
(25) Kono, H.; Wakao, N.; Ito, K.; Nagai, Y. *J. Organomet. Chem.* **1977**, *132*, 53.
(26) Schunn, R. A.; Wonchoba, E. R. *Inorg. Synth.* **1971**, *13*, 131.
(27) Hallman, P. S.; McGarvey, B. R.; Wilkinson, G. *J.Chem. Soc. A* **1968**, 3143.
(28) Candlin, J. P.; Jennings, J. R.; Todd, P. F.: GB 1246123, 1971.
(29) Conrad, J. C.; Yap, G. P. A.; Fogg, D. E. *Organometallics* **2003**, *22*, 1986.
(30) Smith, M. B.; March, J. *March's Advanced Organic Chemistry: Reactions, Mechanisms, and Structure*; 5th ed.; Wiley-Interscience: Toronto, 2001.
(31) Pouchert, J. J.; Behnke, J. In *Aldrich Library of NMR Data*; Aldrich Chemical Co.: Milwaukee, WI, 1993; Vol. 3, p 546(A).
(32) Amoroso, D.; Fogg, D. E. *Macromolecules* **2000**, *33*, 2815.
(33) Amoroso, D.; Yap, G. P. A.; Fogg, D. E. *Can. J. Chem.* **2001**, *79*, 958.
(34) Amoroso, D.; Yap, G. P. A.; Fogg, D. E. *Organometallics* **2002**, *21*, 3335.
(35) Demonceau, A.; Stumpf, A. W.; Saive, E.; Noels, A. F. *Macromolecules* **1997**, *30*, 3127.
(36) Delaude, L.; Demonceau, A.; Noels, A. F. *Macromolecules* **1999**, *32*, 2091.
(37) Joshi, A. M.; Thorburn, I. S.; Rettig, S. J.; James, B. R. *Inorg. Chim. Acta* **1992**, *198-200*, 283.
(38) Woitha, C.; Behrens, U.; Vergopoulos, V.; Rehder, D. *J. Organomet. Chem.* **1990**, *393*, 97.
(39) Son, S. U.; Park, K. H.; Jung, I. G.; Chung, Y. K.; Lah, M. S. *Organometallics* **2002**, *21*, 5366.
(40) Cohen, R.; Rybtchinski, B.; Gandelman, M.; Shimon, L. J. W.; Martin, J. M. L.; Milstein, D. *Angew. Chem. Int. Ed.* **2003**, *42*, 1949.
(41) Fogg, D. E. *Ph.D. Thesis*; The Univerisity of British Columbia: Vancouver, 1994.
(42) Adams, R. D.; Chodosh, D. F. *Inorg. Chem.* **1978**, *17*, 41.
(43) Rep, M.; Kaagman, J.-W. F.; Elsevier, C. J.; Sedmera, P.; Hiller, J.; Thewalt, U.; Horacek, M.; Mach, K. *J. Organomet. Chem.* **2000**, *597*, 146.
(44) Zippel, T.; Arndt, P.; Ohff, A.; Spannenberg, A.; Kempe, R.; Rosenthal, U. *Organometallics* **1998**, *17*, 4429.

(45) Zimniak, A.; Bakalarski, G. *J. Mol. Struct.* **2001**, *597*, 211.
(46) Weiss, K.; Kindl, P. *Angew. Chem. Int. Ed.* **1984**, *13*, 629.
(47) Bright, D.; Mills, O. S. *J. Chem. Soc., Chem. Commun.* **1967**, 245.
(48) Lin, C.-J.; Hwang, W.-S.; Chiang, M. Y. *J. Organomet. Chem.* **2001**, *640*, 85.
(49) Cotton, F. A.; Duraj, S. A.; Roth, W. J. *J. Am. Chem. Soc.* **1984**, *106*, 4749.
(50) Fogg, D. E.; James, B. R. *Inorg. Chem.* **1995**, *34*, 2557.
(51) Chioccala, G.; Daly, J. J. *J. Chem. Soc. A* **1968**, 1981.
(52) Fogg, D. E.; Rettig, S. J.; James, B. R. *Can. J. Chem.* **1995**, *73*, 1084.
(53) Wagner, K. P.; Treichel, P. M.; Calabrese, J. C. *J. Organomet. Chem.* **1974**, *71*, 299.
(54) Allen, F. H.; Kennard, O. *Chemical Design Automation News* **1993**, *8*, 1 & 31.
(55) Albinati, A.; Jiang, Q.; Rüegger, H.; Venanzi, L. M. *Inorg. Chem.* **1993**, *32*, 4940.

CHAPTER 6

The Effect of Tacticity on Macroscopic Polymer Structure: Stereoselective ROMP via Molybdenum Biphenolate Catalysts

6.1. Introduction

The effect of tacticity on the tertiary structure of ROMP polymers is expected to be dramatic. Of particular interest is the possibility of a helical tertiary structure. Polymers that retain a stable helical structure in solution are rare,[1-3] being confined to a few classes (poly(isocyanides),[4-7] poly(isocyanates),[8] poly(guanidines),[9] and poly(acrylates);[10] Figure 6.1). Helicity is constrained in these polymers by the bulky side groups, which restrict rotation around the single bonds in the backbone. In consequence, however, these materials are limited in their potential for variations in helical parameters such as pitch and radius.

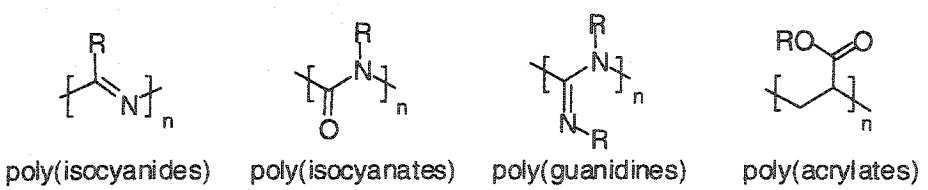

Figure 6.1. Literature examples of helical polymers.

Modelling studies in the Fogg group suggest that helical ROMP polymers have potential for tunable pitch and radius.[11] Such a well-defined three-dimensional polymer structure may necessitate a highly regular microstructure. While a helical structure has been posited for ROMP polymers prepared using ill-defined or non-stereoselective metathesis catalysts ($RuCl_3$,

$RuCl_2(PCy_3)_2(CHPh)$), the experimental evidence for helicity is inconclusive.[12] Wide and small angle X-ray scattering data indicated the presence of crystalline microdomains in ROMP polymers **46** (Figure 6.2), for which molecular modelling at low levels of theory (CSC Chem3D; Cambridge Scientific Computing) suggested that the bulky substituents could impose a helical structure on an otherwise flexible polymer backbone. The X-ray measurements were repeated on *oriented* polymer films (a key experiment in which the lattice periodicity associated with crystal packing is eradicated, leaving only the periodicity associated with the tertiary structure), from which a periodicity of 4.4 Å was determined. This corresponded to the periodicity modelled for a *cis* extended conformation (though the polymer was determined to have 63% *trans* linkages). The periodicity calculated for a trans conformation was 6.0 Å. On this basis, as well as complexation of Li^+ (as $LiSO_3CF_3$), a columnar structure was proposed.[12]

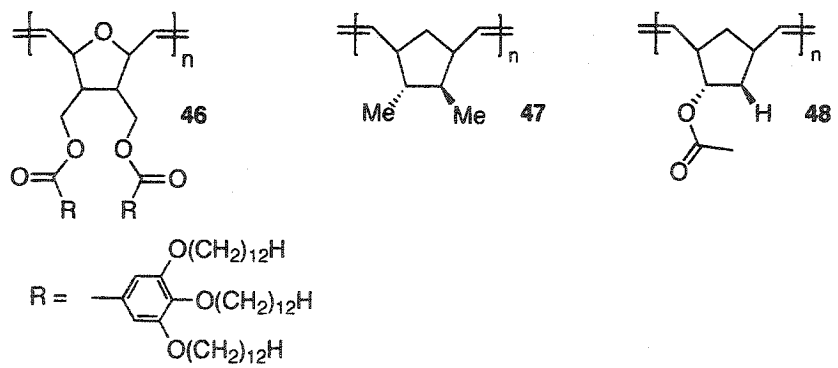

Figure 6.2. ROMP polymers for which a helical structure has been proposed.

A further suggestion of helicity came from analysis of chiral ROMP polymers **47**[13] and **48**,[14] prepared using the well-defined catalyst $Mo(=NAr)(OR)_2(=CHCMe_2Ph)$ (Ar = 2,6-diisopropylphenyl, R = O-*tert*-Bu, $OCMe_2(CF_3)$, $OCMe(CF_3)_2$). A helical structure was proposed for polymer **47**, initially on the basis of discrepancies between theoretical molecular weights, and those found by gel permeation chromatography (GPC) using viscometry as the detection method.

Given the living nature of the polymerization, it was suggested that the observation of higher-than-expected molecular weights was due to deviations from a random coil conformation.[13] No efforts at confirmation by methods such as light scattering were made, but circular dichroism (CD) measurements showed a transition identical to that for the monomer, implying that either the three-dimensional polymer structure was achiral (i.e. a random coil), or that it was racemic (i.e. both "hands" of the helix were formed). The CD data are of limited utility, however, given that the material was obtained using an achiral catalyst. Helicity in both **47** and **48** was not experimentally verified, though again, low-level molecular modelling suggested that it was possible.

We sought to clarify whether helical ROMP polymers could be constructed, by undertaking the synthesis of highly tactic ROMP polymers using well-defined, stereoselective metathesis catalysts. Pending development of *robust,* Ru-based enantioselective catalysts, we utilized the known, highly selective molybdenum aryloxide (biphenolate) initiators **49a-c**.[15-17] Also studied, for the purposes of comparison, was achiral bis-O^{t}Bu catalyst **49d**[18] (Figure 6.3).

Monomer selection was guided by earlier molecular mechanics calculations (Cerius 2) directed at optimizing interactions leading to helicity in the polymers. The molecular modeling studies suggested that helicity was most favoured for cis, isotactic ROMP polymers of disubstituted-poly(norbornadienes).[11] Low-level calculations (MM2, CAChe system) for the four regular structures of poly(NBDF6) (Chapter 1, Section 1.5) likewise suggested that only the cis, isotactic microstructure could adopt a helical structure.[19] We chose to study substituted norbornadienes, in order to maximize steric interactions between the substituents (Figure 6.4). Such interactions can potentially force the polymer backbone to twist to alleviate steric repulsion, thus constraining helicity.

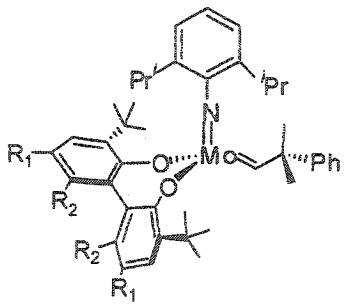

49a: R_1 = ^{t}Bu; R_2 = H
49b: R_1 = Me; R_2 = Me
49c: R_1 = ^{t}Bu; R_2 = Me

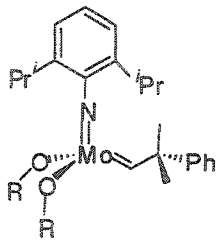

49d: R = -OCMe$_3$
49e: R = -OCMe(CF$_3$)$_2$
49f: R = -OC(CF$_3$)$_3$
49g: R = -OC(CF$_3$)$_2$(CF$_2$CF$_2$CF$_3$)

Figure 6.3. ROMP catalysts used: biphenolates **49a-c** and alkoxide **49d**.

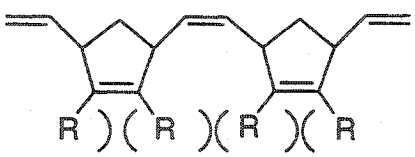

Figure 6.4. Steric repulsion between bulky substituents in a norbornadiene polymer

Chiral biphenolate catalysts of the type shown in Fig. 6.3 are reported to yield highly cis, tactic ROMP polymers of both 2,3-dicarbomethoxynorbornadiene and 2,3-bis(trifluoromethyl)norbornadiene (NBDF6) (Table 6.1). In preliminary work, however, we found that this level of selectivity was not general across all norbornadiene monomers, but varied for a given monomer with a given catalyst / ligand combination. A systematic investigation of ROMP of 2,3-disubstituted norbornadienes by three Mo-biphenolate catalysts was undertaken in order to assess the microstructure and tacticity imparted in each case. Thermal properties of the polymers were investigated using differential scanning calorimetry (DSC), thermal gravimetric analysis (TGA) and high temperature infrared (IR) spectroscopy. Preliminary studies of tertiary polymer structure were also undertaken.

Table 6.1. Summary of Literature Microstructure Data for Highly Tactic ROMP Polymers

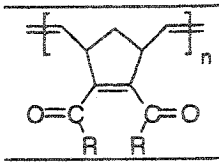	Catalyst	Reported selectivity, tacticity	Found[a] selectivity, tacticity	Reference
R = OMe	**49a**	>99% cis, 96% iso	99% cis, 99% iso	16
	49d	Trans Syndio[b]	20% cis 20% iso	20
	49e	98% cis, 60% iso	-	21
	49f	97% cis, 61% iso	-	21
	49g	99% cis, 54% iso	-	21
	49c' (NAr = N-2-*t*-BuC_6H_4)	54% cis -	-	15
R = O^{t}Bu	**49e**	99% cis, 88% iso	-	21
	49f	99% cis, 95% iso	-	21
	49g	99% cis, 90% iso	-	21
R = OMen[c]	**49a**	99% cis, 99% iso	76% cis 99% iso	19
	49d	6% trans, 0% *iso*[d]	0% cis 0% iso[d]	19

[a] Remeasured; this work. [b] Not quantified. [c] Men = menthyl [d] Determined by ^{1}H-^{1}H COSY and ^{1}H NMR instead of ^{13}C{^{1}H} NMR analysis

6.2. Preparation of Biphenolate ROMP Catalysts

Synthesis of **49a-c** required preparation of both the molybdenum precursors and the biphenolate ligand. The molybdenum precursors were generated by the literature procedures (Scheme 6.1).[22,23] Addition of solid biphenolate (1 equiv) or LiO^{t}Bu (2 equiv) to THF solutions of triflate **50** gave alkylidenes **49a-d**, respectively, in ca. 85% yield (Figure 6.5).[15-17]

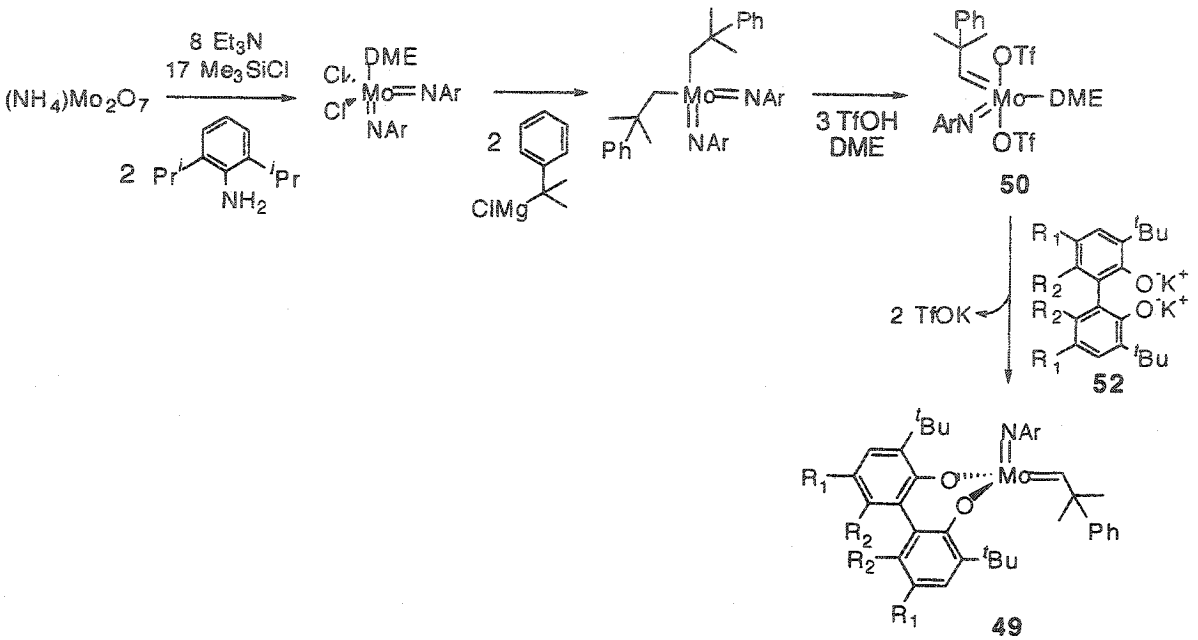

Scheme 6.1. Synthesis of Mo ROMP catalysts used.[15-17,20,22,23]

Biphenol ligands that were not commercially available (**51a**, **51c**: Figure 6.5) were prepared by the general method reported,[15,24] involving oxidative coupling of the corresponding substituted phenol. This procedure generated biphenol **51a** in 75% yield; yields of **51c**, however, were limited to ca. 22% by formation of the yellow 2-methyl-5-*tert*-butylquinone side product[21] (40%). Deprotonation of the phenols using benzyl potassium[25] generated the biphenolate ligands **52a-c**.*

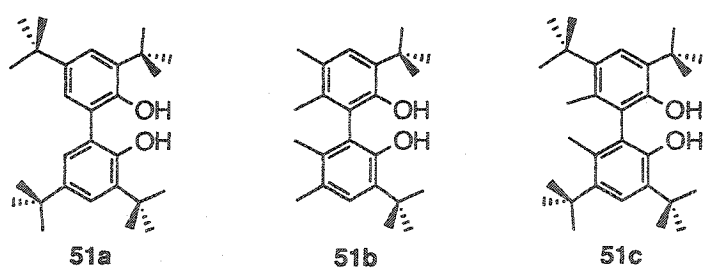

Figure 6.5. Biphenol ligands used in this thesis work.

*This reaction was carried out by the reported method,[19] prior to our discovery (Chapter 4) that deprotonation of binop using a strong base (*n*-butyllithium) can cause undesired side-reactions. No ill effects were noted in the present work.

6.3. Synthesis of Norbornadiene Monomers

2,3-Dicarbomethoxynorbornadiene **53** was prepared by the reported Diels-Alder reaction of cyclopentadiene and dimethylacetylene dicarboxylate.[26] The corresponding *tert*-butyl and menthoxy esters (**54**, **55**) were then readily prepared by transesterification of **53**, as shown in Scheme 6.2 (in preference to, e.g., the Diels-Alder route described[21] for **54**). Thus, addition of LiOR or KOR to a THF solution of **53** liberated the lithium/potassium methoxide as a white precipitate within five minutes. Workup with aqueous acid, chromatography on silica gel, and recrystallization from hot hexanes or methanol gave the desired monomers (**54**: 98% yield; **55**: 70% yield).

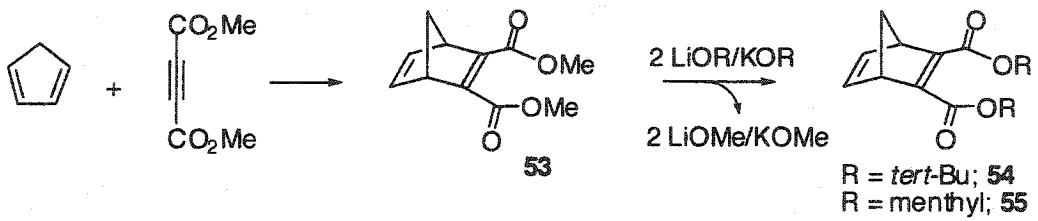

Scheme 6.2. Preparation of 2,3-dicarbomethoxynorbornadiene **53** and transesterification generating **54** and **55**.

This transesterification route to dimenthyl monomer **54** was much more efficient than the diacid chloride route[19] we initially pursued. In a modification of the latter method, we chose to generate the acid chloride in situ, in order to limit hydrolysis. Thus, norborna-2,5-diene-2,3-dicarboxylic acid was treated with the Vilsmeier reagent, followed by menthoxide (Scheme 6.3). Workup as above afforded **55** in 54% overall yield.

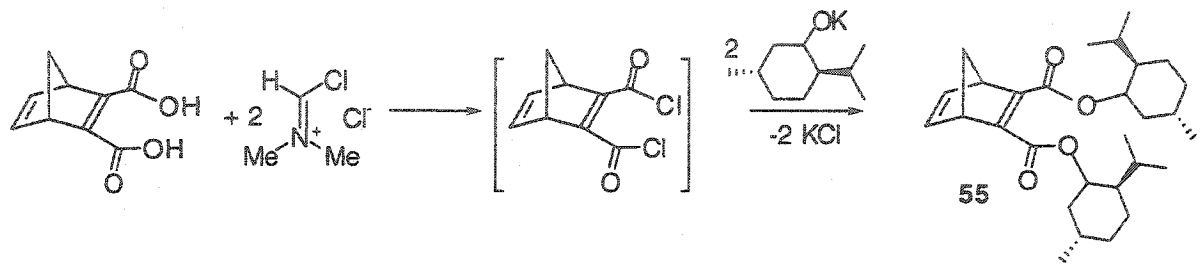

Scheme 6.3. In situ preparation of diacid chloride en route to **55**.

Novel, diphenylamide monomer **56** (Scheme 6.4) was prepared from 2,3-dicarbomethoxy monomer **53** in a manner analogous to the transesterification route, using $LiNPh_2$ in place of the lithium alkoxides. Workup as above and reprecipitation from hot toluene/hexanes afforded **56** as a white powder in 90% yield. Its identity was confirmed by ^1H and $^{13}C\{^1H\}$ NMR analysis, mass spectrometry, and microanalysis.

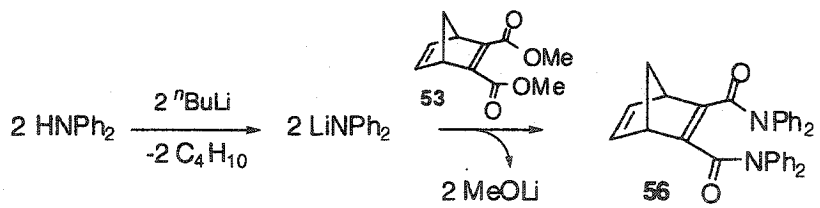

Scheme 6.4. Preparation of diphenylamide monomer **56**.

6.4. ROMP of Norbornadiene Monomers with Molybdenum Biphenolate Catalysts

The extreme sensitivity of the Mo catalysts requires stringent reaction conditions. All polymerizations were carried out in the glovebox using meticulously dried and degassed solvents, with monomers distilled or recrystallized under N_2. In most cases, THF was used as the

reaction solvent, given its suggested* ability to enhance cis-selectivities by poisoning the anti-rotamer of alkoxide catalysts (**49e-g**; Scheme 6.5), thus leaving only the syn-rotamer available for ROMP.[21] *Tactic* ester polymers (generated using the biphenolate catalysts) were insoluble in THF, while all polymers generated using Mo-O'Bu catalyst **49d** (and polymers of diphenylamide **56**) were soluble. Likewise, 99% cis, tactic poly(NBDF6) was THF-insoluble, while samples of lower tacticity (88%; all-cis) were completely soluble.[16] This circumstantial evidence suggests a low degree of tacticity in the diphenylamide polymer, irrespective of catalyst used. NMR analyses described in the following section support this inference.

Scheme 6.5. Syn- and anti-rotamers of molybdenum imido complexes.

After ROMP was complete (as judged by ^{1}H NMR analysis), CH_2Cl_2 was added to redissolve any precipitated polymer, in order to facilitate quenching with benzaldehyde. (Quenching *without* dilution gave materials characterized by multimodal GPC traces). With the exception of the diphenylamide polymer, ROMP polymers prepared via biphenolate catalysts **49a-c** were isolated as powders by dropwise addition of the concentrated polymer solution to rapidly stirring methanol, followed by centrifugation. Polymers of diphenylamide **56** were isolated as a solid mass, rather than a powder, as were polymers prepared via *tert*-butoxide catalyst **49d**. The latter is the first example of a diamide-functionalized poly(norbornadiene).

* A ^{1}H NMR study of the syn/anti relationship for **49b**[17] showed that THF binds more strongly to the anti isomer than to the more abundant syn isomer.[17,27,28] It may be noted, however (Table 6.3) that high selectivities were in some cases observed for polymers prepared in CH_2Cl_2 solvent, implying that the relative reactivities of the syn and anti rotamers of biphenolate-based initiators is not simply controlled by solvent, but depends on the nature of both ligands and substrate.[17]

Few examples have been reported of ROMP of amide monomers by Mo catalysts, and the reported cases invariably utilize amide functionalized *norbornenes.*[29,30]

GPC data for all polymers are summarized in Table 6.2. Experimentally determined molecular weights are generally greater than the theoretical values. This may be due to poisoning of the anti-rotamer by THF (though see comment above), which would reduce the overall amount of active (syn) catalyst available, affecting the reaction stoichiometry. If this is the case, the relatively narrow PDIs found suggest that the syn rotamer of the propagating species must not isomerize to the "poisoned" anti form.[31] The only polymer for which the actual molecular weight is less than that calculated is that obtained by ROMP of **53** via catalyst **49c**.

Polymerization of **53** with **49b** in non-coordinating solvents (CH_2Cl_2 and toluene) resulted in bimodal GPC traces, suggesting that both syn and anti rotamers are present, and that they propagate at different rates. Indeed, similar results in earlier work have been attributed to different rates of growth of two non-interconvertible enantiomers of the catalyst.[15,19] PDI values were generally high* relative to those reported for ROMP via catalyst **49d**, though values for ester polymers prepared via **49d** itself were within the reported range.[16] Selectivities and tacticities were in excellent agreement with literature values (see Table 6.1 above). The consistently high PDI value for polymers prepared from *tert*-butyl ester **54** appears to be intrinsic, as it is independent of catalyst or monomer batch (monomer was exhaustively recrystallized), and the glovebox atmosphere, solvent and catalyst purities were checked by probe reactions using monomer **53**, for which GPC results were comparable to those reported in Table 6.2.

* Polydispersities appear to be generally higher for initiators with chelating aryloxide ligands; PDI values up to 2.38 have been reported.[16]

Table 6.2. Solution Properties of Polymers of **53-56** Prepared using Catalyst **49** in THF.[a]

Monomer 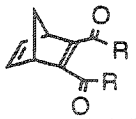	Catalyst	PDI	M_n(Theoretical)	M_n(Found)	Difference	Slope of r_g vs. M_w
53 (R = OMe)	**49a**	1.3	104,125	129,000	24,875	0.45
		1.49[b]	104,125	344,300	240,175	-
	49b	1.5	104,125	161,200	57,075	0.28
		1.6[b,c]	41,650	139,000	97,350	
		1.50[d,e]	41,650	1,313,000	1,271,350	-
				150,100	108,450	
		1.48				
	49c	1.6	104,125	80,180	-23,945	0.40
	49d	1.1[b]	41,650	156,700	115,050	0.22
54 (R = O^{t}Bu)	**49a**	1.7	146,190	172,600	26,410	-
	49b	1.9	146,190	290,100	143,910	0.38
55 (R = OMen)	**49a**	1.5	228, 335	322,700	94,365	-
	49b	1.2	228, 335	353,000	124,665	0.33
	49d	1.1[b]	228,335	462,200	233,865	0.42
56 (R = NPh_2)	**49a**	1.5	241,300	263,100	21,800	0.42
	49b	1.2	241,300	325,100	83,800	0.18
	49c	1.3	241, 300	311,200	69,900	0.36
	49d	1.2,[b,e]	96,520	432,300,	335,780	0.38
		1.1		248,000	151,480	

[a] GPC data obtained in CH_2Cl_2 versus polystyrene standards. [b] Polymerization carried out in CH_2Cl_2. [c] PDI and M_n found for a broad peak containing 2 peaks. [d] Polymerization carried out in toluene. [e] Bimodal GPC trace

Light scattering measurements permit evaluation of the solution conformation of polymer chains, via assessment of the average distance between the two chain ends. The conformation is deduced from the slope of a log-log plot of the radius of gyration (r_g) versus M_w. (A random coil yields a slope of 0.5-0.6, whereas a rigid rod yields a slope of 1, and a sphere yields a slope of 0.33).[11] Observed values ranging from 0.22 - 0.45 (Table 6.2), are consistent with a morphology between spherical and random coil. This implies that none of the polymers prepared give rise to a *stable* helical structure in solution, for which a rigid-rod morphology would be observed.

6.4.1. Cis/Trans Selectivity and Tacticity Determination

As discussed in Chapter 1, ROMP of norbornene or norbornadiene monomers gives rise to polymers with several stereochemical features. The first is the stereochemistry of the olefinic bonds (cis or trans). Formation of cis or trans double bonds is dependent upon the orientation in which the norbornene or norbornadiene monomer 'docks' to the homogeneous catalyst.* Schrock[31] has proposed that monomer binds via attack on the CNO face of the catalyst. This places the monomer cis to alkylidene, such that the bridge carbon (C7) of the norbornene lies over the planar arylimido ring (Scheme 6.6). The orientation of the alkylidene ligand (syn or anti) determines the final configuration of the double bond. If the initiator is trapped as the anti rotamer, a trans metallacycle is formed, and subsequent ring opening yields a trans double bond. Conversely, if the syn rotamer is trapped, the resulting double bond is cis.

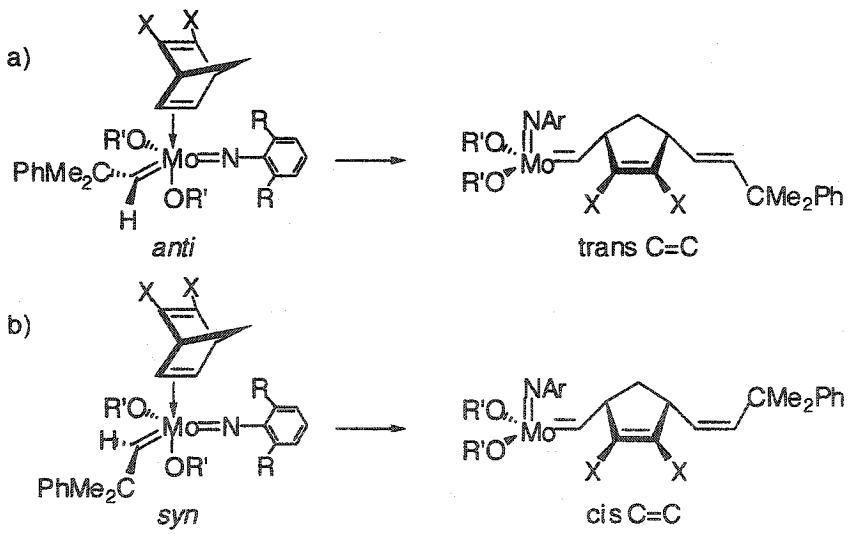

Scheme 6.6. Monomer docking orientations leading to (a) trans; (b) cis double bonds.

* An alternative and contradictory, stereochemical model initially proposed for heterogeneous catalysts is outlined in Appendix J. However, experimental data (particularly 2D NMR data) presented by Schrock strongly support the model outlined in the text, and our analysis is therefore predicated on the latter.

Cis / trans ratios for ROMP polymers can be determined from the relative integration values of the allylic carbon signals (values for norbornadiene polymers: $\delta_{C1,4}$ trans ~50 ppm, cis ~45 ppm) (Figure 6.6; Appendix K). These ratios can be confirmed by integration of the olefinic carbon signals ($\delta_{C\ 5,6}$ trans ~132.5 ppm, $\delta_{C\ 5,6}$ cis ~132 ppm).[15,16,19,20] Assessments of cis/trans ratios by ^{1}H NMR analysis is hampered (for norbornadiene polymers of **53**, **54**, **55**, and **56**) by poor resolution and peak overlap.

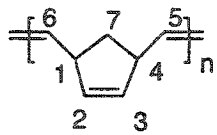

Figure 6.6. Numbering system for polynorbornadienes.

For polymers synthesized from symmetrical monomers, relative tacticities can be determined from the chemical shift of the C_7 signal (δ_{C7} ~40 ppm). The chemical shift of the C_7 carbon is sensitive to two neighbouring repeat units (triads), such that $\delta_{mm} > \delta_{mr/rm} > \delta_{rr}$ (see Section 1.1, Figure 1.3).[32] The integrated intensity of these signals is used to estimate the tacticity of a given polymer. To establish a basis for comparison, *tert*-butoxide catalyst **49d** was used to prepare atactic ROMP polymers of monomers **53-56**. This enabled location of the olefinic carbons for both cis and trans polymers, and all three C_7 peaks (*mm*, *mr/rm*, and *rr*).

Experimentally measured cis/trans ratios and tacticities are summarized in Table 6.3. Both are independent of polymer chain length (entries 1-3). There is, however, a difference in catalyst selectivity for a given monomer. For methyl ester **53**, catalyst **49a** produces essentially all cis, isotactic polymer, whereas catalysts **49b** and **49c** are much less selective (entries 3, 6 and 7). For menthyl ester monomer **55**, complex **49b** gives highly cis, isotactic polymer (entry 15), but **49a** is rather unselective (entry 14). None of the catalysts used show extremely high

selectivity in ROMP of *tert*-butyl ester **54** (entries 9-13), though catalyst **49a** affords 97% cis, 91% isotactic polymer (entry 9). Observation of high selectivities in CH_2Cl_2 solvent (up to 99% cis, isotactic; Entries 4 and 15) argues against the rationale noted earlier concerning a role for the coordinating solvent THF in controlling selectivity.

Table 6.3. Polymer tacticity and cis content from $^{13}C\{^1H\}$ NMR analysis.[a]

Entry	monomer 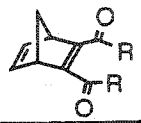	Equiv. monomer	Solvent	Catalyst	% cis[b]	Tacticity[b]
1	**53** (R = OMe)	50	THF	**49a**	99	99% iso
2		200			99	99% iso
3		500			99	99% iso
4		500	CH_2Cl_2		99	99% iso
5		500		**49b**	78	71% iso
6		500	THF		77	66% iso
7		500		**49c**	68	57% iso
8		200	CH_2Cl_2	**49d**	20	20% iso
9	**54** (R = O^{t}Bu)	200	THF	**49a**	95	89% iso
10		500			97	91% iso
11		500		**49b**	73	61% iso
12		500		**49c**	69	53% iso
13		200		**49d**	2	20% syndio
14	**55** (R = OMen)	500	CH_2Cl_2	**49a**	76	99% iso[c]
15		500		**49b**	99	99% *iso*[c]
16		200		**49d**	0	0% iso[c]
17	**56** (R = NPh_2)	500	THF	**49a**	25	28% iso, 35% syndio
18		500		**49b**	1	16% iso, 46% syndio
19		500		**49c**	8	13% iso, 40% syndio
20		200	CH_2Cl_2	**49d**	1	73% iso

[a] For representative $^{13}C\{^1H\}$ NMR spectra, see Appendix K. [b] Determined by $^{13}C\{^1H\}$ NMR analysis except where indicated. [c] Determined by ^1H-^1H COSY and ^1H NMR[19]

$^{13}C\{^1H\}$ NMR spectra of polymers prepared from phenylamide **56** (Entries 17-20) exhibited peak broadening associated with restricted rotation about the amide bond at room

temperature.[33] Analysis was therefore carried out at 100 °C in 1,3-dichlorobenzene. Predominantly trans linkages were found for this monomer, irrespective of catalyst used. Syndiotactic biases were seen with the biphenolate catalysts, while the *tert*-butoxide catalyst **49d** gave predominantly isotactic polymer. Indeed, the latter result exhibits the highest tacticity observed for this monomer. The selectivity may arise from some degree of chain end control.[34] The trans geometry is consistent with propagation via the anti rotamer,[18,31,35] perhaps owing to steric crowding by the phenyl rings in the syn rotamer.

6.5. Solution Analysis of Polymer Tertiary Structure

Circular dichroism (CD) can reveal the presence of a chiral, helical polymer if only a single 'hand' of the helix is present in solution. We were therefore interested in carrying out CD analysis on the polymers which displayed maximum stereoselectivity (and thus the highest probability of helicity). Polymers of methyl ester monomer **53** prepared via racemic biphenolate catalyst **49a** showed >99% cis, isotactic microstructures (see above). However, this catalyst cannot be resolved, because (owing to the lack of 6,6'-substituents on the ligand)[10] the biphenolate rings readily twist past each other. Lanthanum complexes containing the biphenolate ligand used in catalyst **49a** have been observed to racemize on the NMR timescale.[36] In contrast, the 6,6'-functionalized biphenol present in catalyst **49b** (Figure 6.3) is not only configurationally stable, but commercially available (although this catalyst gave lower cis, isotacticity). *Enantiopure* (R)-(+)-**49** was prepared with chiral (R)-(+)-biphenol,[17] and used to effect ROMP of **53**, **54**, and **56** in THF. NMR analysis showed, for polymers of **53**, 77% cis, 77% isotactic microstructures; for polymers of **54**: 73% cis, 61% iso; for polymers of **56**: 1% cis, 16% iso (i.e. in fair agreement with the data in Table 6.3). The isolated polymers were dissolved in CH_2Cl_2 and the optical

rotation measured. As the polymers themselves contain no chiral moieties, any rotation observed would be due to a chiral tertiary structure. No optical rotation was noted, however, possibly because helix "unwinding" occurs in solution (as indeed suggested by molecular dynamics simulations.[11]) Alternatively, defects in the backbone of polymers of **53** and **54** may cause twisting and deformation of the polymer chains, as earlier proposed for amylose (Figure 6.7).

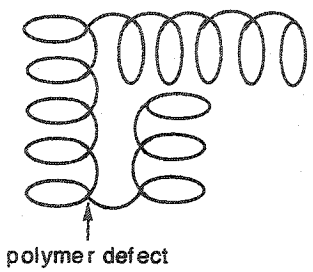

Figure 6.7. Proposed structure of amylose, showing deformed helical regions caused by polymer defects.

Increases in the size of the polymer substituent, as seen in polymers of **55** and **56**, impede alignment of the polymer chains, and an amorphous morphology results. An increase in helical pitch may also result, and thus could promote dynamic helical behaviour. Alternatively, the structures may simply not be helical, though the possibility remains that the limited microstructure control seen with (R)-(+)-**49b** may promote introduction of helix defects that hamper or obscure a helical superstructure.

6.6. TGA and DSC Results for Polymers of 53-56.

The possibility of dynamic helix formation in solution prompted us to investigate the *solid-state* structure by X-ray methods. These methods require comparison of diffraction patterns from non-oriented and oriented polymer films, in the latter of which the periodicities associated with the polymer crystal lattice are removed. Film orientation, in turn, requires "annealing" of the

polymer films. The thermal stability of the polymers of **53**, **54**, **55**, and **56** was therefore examined by DSC and TGA. Samples chosen corresponded to the most ordered microstructure (highest tacticity) in each case, except for the polymer of **56**, for which all samples were analyzed for comparison. Glass transition (T_g), melting (T_m), crystallization (T_c) and decomposition (T_d)* temperatures, where applicable, are summarized in Table 6.4. Representative DSC thermograms and plots of relative percent mass loss vs. temperature (TGA data) are presented in Appendix L.

Table 6.4. Summary of Thermal Transitions from TGA and DSC Data.

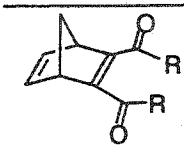	Catalyst	Micro-structure	T_g (DSC; °C)	T_d (% loss) (TGA; °C)	$T_{c/m}$ (DSC; °C)
53 (R = OMe)	**49a**	99% cis, 99% iso	-	114 (5%) 300 (25%)	T_c = 300 T_m = >350
54 (R = O^{t}Bu)	**49a**	97% cis, 91% iso	68	135 (33%); 225 (5%)	T_m = 170 T_c = 245
55 (R = OMen)	**49b**	99% cis, 99% iso	107	269 (47%)	T_m = 300
56 (R = NPh_2)	**49a**	25% cis 28% iso	231	158 (5%), 275 (43%)	T_m = >350 T_c = 335
	49b	1% cis 16% iso	230	159 (5%) 270(43%)	T_m = >350 T_c = 335
	49d	1 % cis 73% iso	228	156(5%) 274(43%)	T_m = >350 T_c = 335

The polymer derived from methyl ester **53** exhibits a T_d onset of 114 °C, with a total weight loss of 30% occurring in the temperature range from 114-400 °C. This corresponds, within experimental error, to loss of one $-CO_2Me$ substituent (a 28% weight loss). The DSC thermogram shows a broad exothermic transition at a temperature of 300 °C: despite the semi-

* T_d is defined as the temperature at which 5% of the mass has been lost.[37]

crystallinity of the sample evident from X-ray diffraction studies (Section 6.5.3), no endothermic melting transition was observed, likely due to decomposition prior to reaching the melting point. No T_g was observed, perhaps owing to conformational restriction of the polymer chains.

A *broad* exothermic transition (T_c) at or above 300 °C for the polymers of **53**, **54** and **56** is found at or above the decomposition temperature (T_d). We speculate that the breadth of the exotherm (in conjunction with the decomposition observed at these temperatures) may be due to partial decomposition of the polymer and crystallization of the resulting shorter chain polymer segments.

The polymer derived from *tert*-butyl ester **54** undergoes a two-stage weight loss (i.e., a weight loss, then a plateau followed by a second weight loss). Approximately 33% of its weight, corresponding to one -$CO_2{}^t$Bu substituent (35% of total mass), was lost rapidly between 135 °C and 175 °C. A further 5% weight loss occurred beginning at ~225 °C, coinciding with the onset of an exothermic transition (T_c) in the DSC thermogram as discussed above. The glass transition temperature is 68 °C. An endothermic melting point transition was observed at 170 °C, suggesting that the sample is crystalline (consistent with the stereoregularity evident from NMR analysis). However, no crystallization temperature (T_c) was noted upon cooling. While decomposition at higher temperatures could be responsible, no clear T_c transition could be observed even where precautions were taken to prevent decomposition, either by arresting the temperature increase above the T_m but below the second T_d, or by increasing the temperature quickly (30 °C/min vs. 10 °C/min) to limit total heating time. In view of this, the endothermic transition cannot be conclusively identified as T_m. Attempts to measure the melting point by conventional 'organic' methods resulted in sample decomposition only: at 135 °C, the beige powder began to darken, becoming steadily darker until ~170 °C, by which point the sample was

black. The transition at 170 °C may be due to melting of one of the decomposition products in the sample.

The polymer derived from menthyl ester **55** is much more thermally stable, with the onset of decomposition at 269 °C, and loss of 47% of its mass from 269-400 °C. Loss of one $-CO_2$menthyl group accounts for a weight loss of 40%. The DSC thermogram shows a relatively sharp endothermic transition at 300 °C corresponding to T_m. Again no T_c is noted, probably because decomposition of the sample occurs prior to crystallization. The T_g is 107 °C.

For the polymers derived from diphenylamide **56**, a two-stage weight loss was again observed: a minimal (5%) loss occurred at ca. 158 °C, with major mass loss (43%) occurring at ca. 275 °C. Loss of one $-C(O)NPh_2$ substituent accounts for a mass loss of 40%. Again, a broad DSC exothermic transition (T_c) was observed at 335 °C.

The glass transition temperature is associated with increases in long-range molecular motion and greater rotational freedom within the polymer chain.[38] The lower T_g seen for polymers derived from **54** and **55** (ca. 68 °C and 107 °C, respectively), as compared to **56** (231 °C), indicates a greater rotational freedom in the ester polymers vs. the amide polymer. Large differences in T_g for polynorbornenes with different substituents has been noted previously.[39] The absence of a glass transition temperature for the polymer derived from **53** was unexpected given the comparable crystallinities of the polymers of **54** and **53** (see Section 6.6.1); again, such "missing" T_g values have been noted by others.[40] An estimated T_g value of ~140 °C, associated with an irreversible thermal transition, was suggested for polymers of **53**.[40]

Investigations into the thermal properties of ROMP polymers suggest that the glass transition temperature T_g can also be a function of the cis content of the polymer.[13,20] Schrock has reported differential scanning calorimetry (DSC) data, as well as thermal gravimetric

black. The transition at 170 °C may be due to melting of one of the decomposition products in the sample.

The polymer derived from menthyl ester **55** is much more thermally stable, with the onset of decomposition at 269 °C, and loss of 47% of its mass from 269-400 °C. Loss of one $-CO_2$menthyl group accounts for a weight loss of 40%. The DSC thermogram shows a relatively sharp endothermic transition at 300 °C corresponding to T_m. Again no T_c is noted, probably because decomposition of the sample occurs prior to crystallization. The T_g is 107 °C.

For the polymers derived from diphenylamide **56**, a two-stage weight loss was again observed: a minimal (5%) loss occurred at ca. 158 °C, with major mass loss (43%) occurring at ca. 275 °C. Loss of one $-C(O)NPh_2$ substituent accounts for a mass loss of 40%. Again, a broad DSC exothermic transition (T_c) was observed at 335 °C.

The glass transition temperature is associated with increases in long-range molecular motion and greater rotational freedom within the polymer chain.[38] The lower T_g seen for polymers derived from **54** and **55** (ca. 68 °C and 107 °C, respectively), as compared to **56** (231 °C), indicates a greater rotational freedom in the ester polymers vs. the amide polymer. Large differences in T_g for polynorbornenes with different substituents has been noted previously.[39] The absence of a glass transition temperature for the polymer derived from **53** was unexpected given the comparable crystallinities of the polymers of **54** and **53** (see Section 6.6.1); again, such "missing" T_g values have been noted by others.[40] An estimated T_g value of ~140 °C, associated with an irreversible thermal transition, was suggested for polymers of **53**.[40]

Investigations into the thermal properties of ROMP polymers suggest that the glass transition temperature T_g can also be a function of the cis content of the polymer.[13,20] Schrock has reported differential scanning calorimetry (DSC) data, as well as thermal gravimetric

analyses (TGA), for ROMP polymers of NBDF6 prepared using four different catalysts ($WCl_6/SnMe_4$, $RuCl_3/SnMe_4$, $MoCl_5/SnMe_4$ and Mo(CH-*tert*-Bu)(NAr)(O-*tert*-Bu)$_2$).[20] T_g values for poly(NBDF6) decreased with an increasing proportion of trans olefinic units. For example, a predominantly trans sample of poly(NBDF6) (98% trans) had a T_g of 97 °C; a sample with 54% trans linkages had a T_g of 125 °C.

6.6.1. Polymer Crystallinity: X-Ray Powder and Thin Film Diffraction Analyses

Polymer samples were assessed for crystallinity before and after annealing below their decomposition temperature (as determined from TGA). Samples chosen again corresponded to polymers with the most ordered microstructure, though a sample of monomer **53** polymerized with *tert*-butoxide catalyst **49d** was also studied for comparison. Percent crystallinity values (Table 6.5) were determined from X-ray powder diffraction plots, in which the integrated intensity of the "amorphous" band was subtracted from the total integrated intensity. The spacing between periodic elements (*d* spacings) were obtained from the powder diffraction trace (Figure 6.8).

Films of semi-crystalline poly(NBDF6) can be drawn into fibers from a melt.[5] In contrast, thin films of polymers derived from ROMP of **53** using catalyst **49a** were semi-crystalline, brittle films that crumbled to a powder when manipulated. This suggests that the polymer has a highly stereoregular structure, with very regular packing of the polymer chains. Surprisingly, however, X-ray powder diffraction data show a crystallinity of only ca. 8%, which *decreased* on annealing, presumably owing to decomposition (despite choice of an annealing temperature below T_d (300 °C (25% mass loss)) This initially perplexing observation is clarified by the sensitivity to cross-linking evident from the IR study below. The corresponding polymer

prepared from achiral *tert*-butoxide catalyst **49d** was amorphous, and showed no induced crystallinity when annealed at 140 °C for two or four hours.

Polymers derived from *tert*-butyl ester **54** using catalyst **49a** were also semi-crystalline, while polymers of menthyl ester **55** and diphenylamide **56** were essentially amorphous. The amorphous nature of the menthyl ester polymers is notable, given their high tacticity: the large menthyl substituents may inhibit regular packing of the polymer chains.

Table 6.5. Percent Crystallinity for Polymers of **53** and **54** Before and After Annealing.

Polymer	Catalyst	% Crystallinity	Annealing Temperature	% Crystallinity
53	**49a**	8	170	7
53	**49d**	0	140	0
54	**49a**	12	125	26

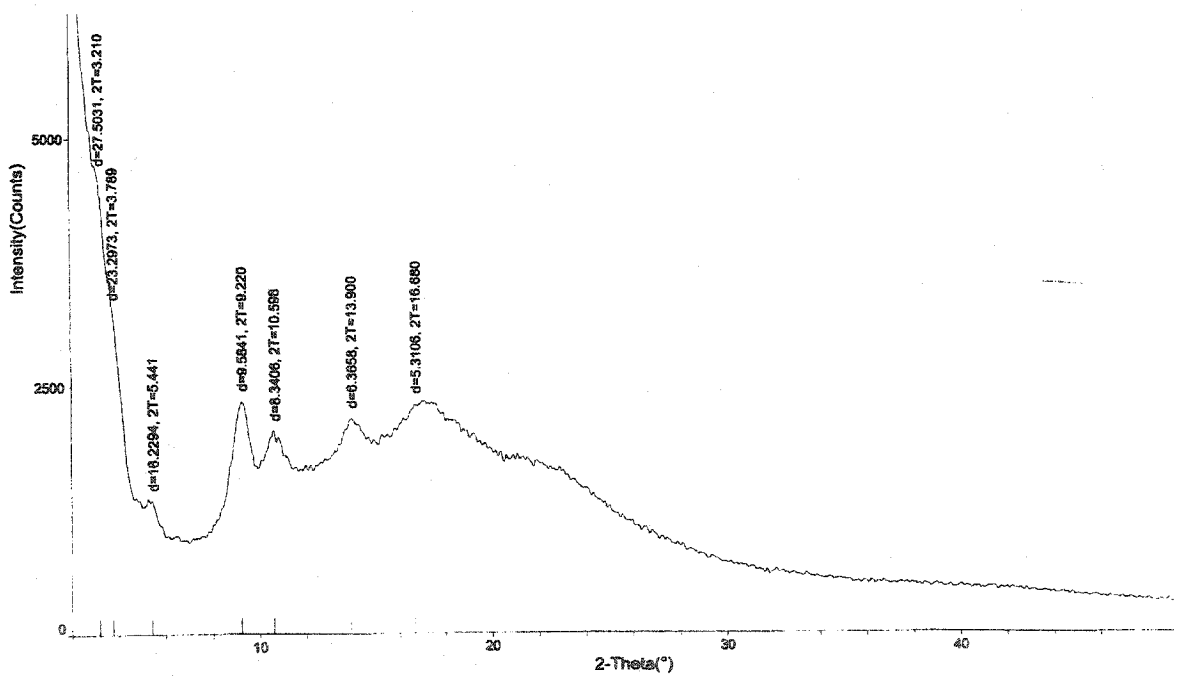

Figure 6.8. Powder diffraction trace of polymer **57a**.

Wide-angle X-ray analysis of thin films (Figure 6.9), in which *d* spacings are more readily observed than in powder diffraction, was undertaken on polymers of **53** exhibiting the maximum order (>99% cis, 99% isotactic; prepared via racemic **49a**). The extreme fragility of thin films of this polymer impeded analysis, however. With the intention of obtaining films that could be manipulated, copolymerization of **53** with methyltetracyclodecene (MTD) was undertaken. Poly(MTD) is amorphous; it has a high T_g (>200 °C), and forms well-behaved, amorphous thin films.[31] Block copolymers of **53** with varying amounts of MTD were therefore prepared in THF (this solvent assuring both solubility and, possibly, stereospecific ROMP). Block copolymers were made with ratios of **53**:MTD of 4:1, 1:1, and 1:4 (**57a-b**). Tractable thin films were obtained for all copolymers, enabling wide-angle XRD analysis. The periodicity measured for the unoriented films was in fair agreement with powder diffraction results (Table 6.6): in general, *d* spacings observed in the powder diffraction study were also seen in the thin film study, though as the proportion of amorphous MTD increases, the number of *d* spacings drops off dramatically.

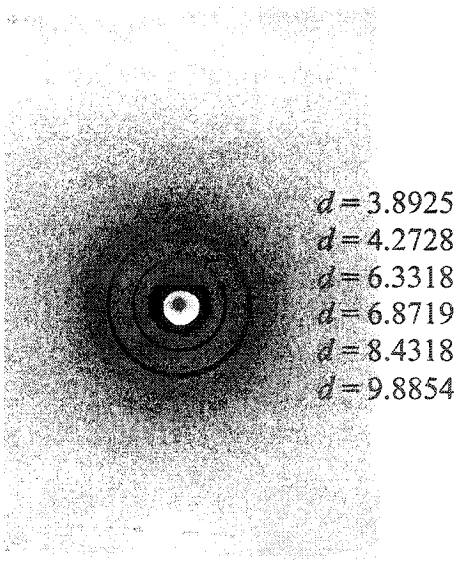

Figure 6.9. Wide angle X-ray film diffraction of polymer **57a**.

Table 6.6. Powder and Film X-Ray Diffraction *d* Spacings for Polymers of **53** and **57**.

Polymer	*d* spacings (Å, powder diffraction)	*d* spacings (Å, film diffraction)
53	9.6679	-
	8.3859	
	6.3749	
	5.2980	
	4.1759	
57a	16.2294	-
	9.5841	9.8854
	8.3406	8.4318
	6.3658	6.8719
	5.3106	6.3318
	-	4.2728
	-	3.8925
57b	9.6255	9.7725
	8.2767	8.3504
57c	9.4207	9.6081

With the X-ray data for the *unoriented* thin films in hand, solid-state analysis was attempted on the *oriented* copolymer films of **53**, in order to determine whether a helical bias exists in the solid state.*

Attempts at orienting the film failed, as noted above, because the film crumbled when manipulated. Although the copolymer films of **57a-c** did not disintegrate when handled, they cracked when stretching was attempted at 80 °C. For this reason the solid-state analyses could not be completed.

* X-ray diffraction patterns of oriented thin films can provide insight into the tertiary structure of a polymer, as noted earlier, by eradication of periodicity associated with crystal packing, leaving only the periodicity associated with the tertiary structure in the diffraction pattern. Polymer samples obtained using a racemic catalyst can be used for analysis, as the 'handedness' of a polymer is irrelevant: the pitch, radius and other periodicities associated with the polymer should be identical irrespective of twist sense.

6.5.2. Infrared Analysis

The anomalous powder diffraction results noted above (suggesting lower crystallinity than apparent from T_g or mechanical observation) inspired a more detailed study of the thermal degradation processes in these polymers, using IR spectroscopy. For each sample, a KBr plate containing the polymer was heated to 80 °C, and the spectrum was monitored for 4 h for evidence of decomposition. The stretching bands for the C=O and C=C groups, in particular, were examined. Integration of these bands saw a decrease in area, attributed to the degradation of the functional group.

Polymers of **53-55**, containing ester substituents, showed minimal degradation in the intensity of the ν(C=O) band as compared to that observed for the ν(C=C) band. Intensity loss for the latter, however, exhibited a first order exponential decay, with loss of up to 20% of the original band area within 4 hours (Figure 6.10). All plots of IR band integration vs. time are presented in Appendix L.

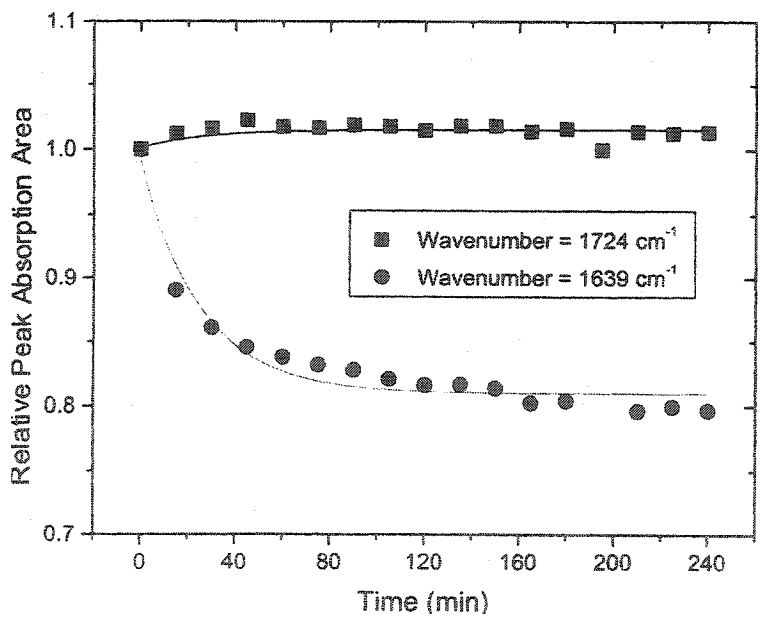

Figure 6.10. Representative plot of IR band area vs. time for polymer **53**.

This points toward cross-linking or oxidation of the C=C double bond at 80 °C, over the timescale of analysis. A corresponding study of diphenylamide polymer of **56** showed no appreciable degradation. This was surprising, given that the C=C bond is identical in every polymer sample, irrespective of ester or amide substitution. One explanation for this thermal stability at 80 °C is that the large phenyl groups shield the double bonds from degradation by oxidation or cross-linking.

In all other cases, however, an inordinate (and unsuspected) thermal sensitivity was observed. This has fundamental implications for the broader use of ROMP polymers, as well as the development of helical polymer materials.

6.7. Conclusions

The work summarized in this chapter illustrates that selectivity and tacticity are determined by the match between catalyst and monomer. For example, while catalyst **49a** gives 99% cis, isotactic polymers of **53**, the closely related catalyst **49c** gives only a 68% cis, 57% isotactic polymer. Control experiments with the *tert*-butoxide catalyst **49d** gave unselective, atactic polymers with all monomers except the diphenylamide derivative, for which this catalyst produced an essentially all-trans polymer. This may be due to the presence of the anti rotamer, which can more readily accommodate the large diphenyl amide substituents; steric crowding must substantially limit the reactivity of the syn rotamer.

CD investigations of tertiary structure indicate that a stable helical structure is not present in solution. Consistent with this, light-scattering measurements indicate an approximately spherical structure, rather than the rigid-rod morphology expected for a helical polymer. The possibility of a *dynamic* helical structure which collapses in solution cannot be ruled out,

however, and is indeed supported by molecular dynamics simulations.[11] The morphology may resemble that proposed for the natural polymer amylose, which has a helical structure in the solid state,[41] but is thought to exist as a deformed helix in solution.[42] Those polymers with relatively small substituents (-CO_2Me and –$CO_2{}^t$Bu) were semi-crystalline, while their congeners with larger substituents (-CO_2menthyl and –C(O)NPh_2) were amorphous. This is presumably due to the ability of the polymer chains to align effectively in the semi-crystalline polymers. The diamide polymer of **56** has a glass transition temperature of 231 °C, significantly higher than that observed for norbornadiene polymers (T_g <150 °C).[40]

TGA, DSC and IR studies were used to investigate the thermal properties of the ROMP polymers. All difunctionalized polymers, including the diphenylamide polymer **56**, decomposed at elevated temperatures (>135 °C), while the ester-functionalized polymers **53**, **54** and **55** were seen by IR analysis to decompose (more slowly) even at lower temperatures (20% loss, 80 °C, < 4 h). IR analysis suggests that the C=C double bonds are thermally sensitive, but the carbonyl units remain essentially undisturbed. Polymers of **56** show greater stability at 80 °C, perhaps because the bulky phenyl groups remain on the periphery of the polymer mass, effectively shielding the C=C double bonds until high temperatures are reached.

Orientation of polymer films for solid-state tertiary structure determination was hampered because of the brittleness of the polymer films, which cracked on attempted orientation. The thermal instability of the polymers prevents solid-state analysis, because orientation of the polymer films requires heating the film below its glass transition temperature, which causes significant crosslinking and hence morphological deformation.

Polymers of 5-alkyl-2-norbornenes have been described[43] as having poor oxidative stability, even at ambient temperature, due to unsaturation in the polymer backbone. This can be

eliminated by hydrogenation of the materials, which then show excellent thermal and oxidative stability. This suggests that hydrogenated polymers of **53-56** will be more robust, though appropriate substitution would be required in order to overcome the lower solubility of hydrogenated polymers. Alternatively, the greater thermal stability seen with polymer of **56** points toward substituent-induced stabilization against thermal degradation. In either case, introduction of appropriate functionality onto the monomer may contribute both toward thermal stability, and a helical tertiary structure. Despite the problems outlined in this chapter, therefore, helical ROMP polymers may still be attainable.

6.8. References

(1) Okamoto, Y.; Nakano, T. *Chem. Rev.* **1994**, *94*, 349.
(2) Okamoto, Y. *Macromol. Symp.* **1996**, *101*, 343.
(3) Okamoto, Y.; Nakano, T.; Habaue, S.; Shiohara, K.; Maeda, K. *Pure Appl. Chem.* **1997**, *A34*, 1771.
(4) Nolte, R. J. M.; van Beijnen, A. J. M.; Drenth, W. *J. Am. Chem. Soc.* **1974**, *96*, 6932.
(5) Nolte, R. J. M. *Chem. Soc. Rev.* **1994**, 11.
(6) Deming, T. J.; Novak, B. M. *J. Am. Chem. Soc.* **1992**, *114*, 7926.
(7) van Beijnen, A. J. M.; Nolte, R. J. M.; Drenth, W.; Hezemans, A. M. F. *Tetrahedron* **1976**, *32*, 2017.
(8) Goodman, M.; Chem, S. C. *Macromolecules* **1970**, *3*, 398.
(9) Nieh, M. P.; Goodwin, A. A.; Stewart, J. R.; Novak, B. M.; Hoagland, D. A. *Macromolecules* **1998**, *31*, 3151.
(10) Nakano, T.; Mori, M.; Okamoto, Y. *Macromolecules* **1993**, *26*, 867.
(11) Mainville-Dale, R. M. E. *M.Sc. Thesis*; University of Ottawa: Ottawa, 2002.
(12) Percec, V.; Schlueter, D.; Ronda, J. C.; Johansson, G.; Ungar, G.; Zhou, J. P. *Macromolecules* **1996**, *29*, 1464.
(13) Sunaga, T.; Ivin, K. J.; Hofmeister, G. E.; Oskam, J. H.; Schrock, R. R. *Macromolecules* **1994**, *27*, 4043.
(14) Stelzer, F.; Schitter, R.; Steinhausler, T. In *Metathesis Polymerizations of Olefins and Polymerization of Alkynes*; Imamoglu, Y., Ed.; Kluwer Academic Publishers: Netherlands, 1998, p 243.
(15) Totland, K. M.; Boyd, T. J.; Lavoie, G. G.; Davis, W. M.; Schrock, R. R. *Macromolecules* **1996**, *29*, 6614.
(16) McConville, D. H.; Wolf, J. R.; Schrock, R. R. *J. Am. Chem. Soc.* **1993**, *115*, 4413.

(17) Alexander, J. B.; Schrock, R. R.; Davis, W. M.; Hultzsch, K. C.; Hoveyda, A. H.; Houser, J. H. *Organometallics* **2000**, *19*, 3700.
(18) Schrock, R. R. *Acc. Chem. Res.* **1990**, *23*, 158.
(19) O'Dell, R.; McConville, D. H.; Hofmeister, G. E.; Schrock, R. R. *J. Am. Chem. Soc.* **1994**, *116*, 3414.
(20) Bazan, G. C.; Khosravi, E.; R., S. R.; Feast, W. J.; Gibson, V. C.; O'Regan, M. B.; Thomas, J. D.; Davis, W. M. *J. Am. Chem. Soc.* **1990**, *112*, 8378.
(21) Schrock, R. R.; Lee, J. K.; O'Dell, R.; Oskam, J. H. *Macromolecules* **1995**, *28*, 5933.
(22) Schrock, R. R.; Murzdek, J. S.; Bazan, G. C.; Robbins, J.; DiMare, M.; O'Reagan, M. *J. Am. Chem. Soc.* **1990**, *112*, 3875.
(23) Fox, H. H.; Yap, K. B.; Robbins, J.; Cai, S.; Schrock, R. R. *Inorg. Chem.* **1992**, *31*, 2287.
(24) Albert, H. E. *J. Am. Chem. Soc.* **1954**, *76*, 4983.
(25) Schlosser, R. R.; Hartmann, J. *Angew. Chem. Int. Ed.* **1973**, *12*, 508.
(26) Tabor, D. C.; White, F. H.; Collier, L. W.; Evans, S. A. *J. Org. Chem.* **1983**, *48*, 1638.
(27) Zhu, S. S.; Cefalo, D. R.; La, D. S.; Jamieson, J. Y.; Davis, W. M.; Hoveyda, A. H.; Schrock, R. R. *J. Am. Chem. Soc.* **1999**, *121*, 8251.
(28) Schrock, R. R.; Crowe, W. E.; Bazan, G. C.; DiMare, M.; O'Regan, M. B.; Schofield, M. H. *Organometallics* **1991**, *10*, 1832.
(29) Sinner, F.; Buchmeiser, M. R.; Tessadri, R.; Mupa, M.; Wurst, K.; Bonn, G. K. *J. Am. Chem. Soc.* **1998**, *120*, 2790.
(30) Buchmeiser, M. B.; Wurst, K. *J. Am. Chem. Soc.* **1999**, *121*, 11101.
(31) Schrock, R. R. *Topics in Organometallic Chem.* **1998**, *1*, 1.
(32) Amir-Ebrahimi, V.; Corry, D. A. K.; Hamilton, J. G.; Rooney, J. J. *J. Mol. Catal. A* **1998**, *133*, 115.
(33) Jarek, R. L.; Flesher, R. J.; Shin, S. K. *J. Chem. Ed.* **1997**, *74*, 978.
(34) Ivin, K. J.; Rooney, J. J. *Olefin Metathesis and Metathesis Polymerization*; Academic Press Ltd.: Toronto, 1997.
(35) Schrock, R. R. In *Metathesis Polymerization and Olefins and Polymerization of Alkynes*; Imamoglu, Y., Ed.; Kluwer Academic Publishers: Netherlands, 1998; Vol. 23, p 1991.
(36) Schaverien, C. J.; Meijboom, N.; Orpen, A. G. *J. Chem. Soc., Chem. Commun.* **1992**, 124.
(37) Peetz, R. M.; Moustafa, A. F.; Kennedy, J. P. *J. Polym. Sci., Part A: Polym. Chem.* **2003**, *41*, 732.
(38) Stevens, M. P. *Polymer Chemistry. An Introduction*; 2nd ed.; Oxford University Press: New York, 1990.
(39) Contreras, A. P.; Pineda, A. M.; Tlenkopatchev, M. A. *Macromol. Chem. Phys.* **2002**, *203*, 1811.
(40) Bazan, G. C.; Oskam, J. H.; Cho, H. N.; Park, L. Y.; Schrock, R. R. *J. Am. Chem. Soc.* **1991**, *112*, 6899.
(41) Rundle, R. E.; Daasch, L.; French, D. *J. Am. Chem. Soc.* **1944**, *66*, 130.
(42) Rao, V. S. R.; Foster, J. F. *Biopolymers* **1963**, *1*, 527.
(43) Hatjopoulos, J. D.; Register, R. A. *Abstracts, 36th Middle Atlantic Regional Meeting of the Am. Chem. Soc.*, Washington, D.C, June, 2003.

CHAPTER 7

Summary and Recommendations for Future Work

The work summarized in this thesis demonstrates a pattern of heightened reactivity for σ-aryloxide species containing direct or incipient coordinative unsaturation. The strength of the Ru-O bond in such complexes is compromised by the accessibility of low-energy reaction pathways involving Ru-O bond cleavage, and leading to stable 18-electron products. These low-energy pathways arise from the basicity of the aryloxide oxygen, in conjunction with the availability of π electrons in the aromatic system. Thus, reaction of $RuCl_2(PPh_3)_3$ **1a** with aryloxide in the presence of methanol results in decarbonylation to afford $RuH_2(CO)(PPh_3)_3$ **2a** and $RuHCl(CO)(PPh_3)_3$ **2b**. (This reaction was exploited to develop a convenient, high-yield route to $RuHCl(PPh_3)_3$ **1b**.) In the *absence* of methanol, η^5-aryloxide products are obtained on treating **1a** or $RuHCl(PPh_3)_3$ **1b** with aryloxide. The high reactivity of the putative bis(aryloxide) or mixed aryloxide/methoxide intermediates may arise from electrostatic repulsion between the filled oxygen p orbitals and one or more filled ruthenium d orbitals.

Investigations with the chelating, heterobifunctional P,O-chelating ligand binop (±)-2-(diphenylphosphino)-2'-hydroxy-1,1'-binaphthyl; Chapter 4) indicate that the chelate effect is insufficient to prevent σ→π isomerization. Instead, $RuCl(binop)(PPh_e)$ **31** was obtained, in which the binop ligand was σ-bound through the phosphorus donor, and π-bound via the naphthol ring. This finding points toward a probable deactivation pathway for ruthenium catalysts containing aryloxide ligands: σ→π isomerization must be considered as long as catalysis proceeds via an inner sphere mechanism, such that the three coordination sites required

for isomerization can be accessed during the normal catalytic cycle. The active catalyst formed by metathesis of the second-generation Hoveyda[1] catalyst provides one example of such a species.

Incorporation of a CO ligand may offer some stabilization against isomerization, as indicated by the accessibility (Chapter 3) of a stable, Ru(σ-ArO) entity in complexes containing two labile triphenylphosphine ligands (i.e. $RuCl(OAr)(CO)_2(PPh_3)_2$ **15** and $K_2[Ru(OAr)(CO)_2(PPh_3)]_2$ **17**). The trans orientation of the aryloxide and carbon monoxide ligand may help to stabilize the Ru-O bond against isomerization, alleviating filled-filled metal d-orbital / aryloxide p-orbital repulsions via a push-pull interaction between the CO and OR orbitals. This possibility should be explored by installation of aryloxide within the recently-prepared[2] $RuHCl(CO)(IMes)(PPh_3)$ (IMes = 1,3-bis(2,4,6-trimethylphenyl)imidazol-2-ylidene) (Scheme 7.1).

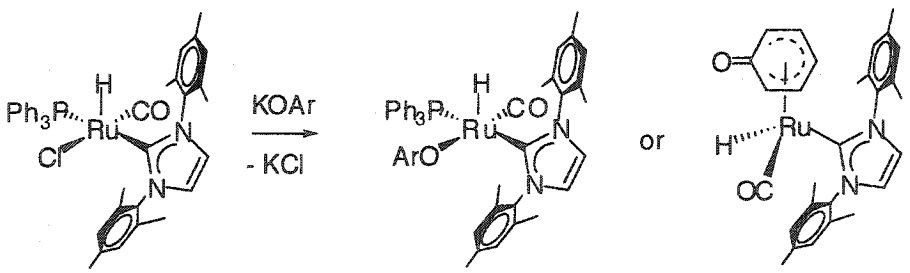

Scheme 7.1. Stabilization of the Ru-O σ-bond by a trans CO ligand.

The importance of electronic parameters in limiting isomerization has been established in subsequent work in the Fogg group. Insights from the chemistry described above laid the groundwork for the development of olefin metathesis catalysts containing *electron-deficient* aryloxide and biphenolate ligands, in which d_π-p_π repulsion is minimized.[3] Promising results with chelating, chiral fluoroaryloxide ligands may open the way for stereoselective ring-opening metathesis.

Other findings (Chapter 5) include the synthesis of a versatile ruthenium alkylidene precursor $RuCl_2(=CH=CHMe_2)(PPh_3)_2$ **34** on treatment of $RuHCl(PPh_3)_3$ **1b** with 3-chloro-3-methyl-1-butyne. A carbyne byproduct is formed by reaction of **34** with excess 3-chloro-3-methyl-1-butyne, but this has been avoided by the use of base in the reaction.[4] Reaction of isolated **34** with HCl would clarify the potential role of HCl (a potential contaminant in the alkyne reagent) in formation of **35**. The ease of phosphine exchange reactions of **34** was demonstrated by reaction with PCy_3, generating $RuCl(=CH=CHMe_2)(PCy_3)_2$ **37**.

The potential for coordination of *t,t*-benzaldehyde azine **40**, a contaminant invariably present in phenyldiazomethane **39**, was also explored in Chapter 5. Reaction of Ru precursors with azine is slow at room temperature. N-N bond activation was found at 50 °C, with formation of Ru-nitrile and -imine products. The metal center may function as an electron sink in this reaction, depleting electron density on the bound nitrogen and activating it toward nucleophilic attack by the "dangling" nitrogen. To gain information about the electronics of this reaction coordination of *t,t*-benzaldehyde azine **40** to electron-rich $Ru_2Cl_4(dcypb)_2(N_2)$ (dcypb = 1,4-bis(dicyclohexylphosphino)butane) was used attempted, but was unsuccessful due to the insolubility of the dcypb dimer in the chosen solvent system. The coordination of **40** should be further investigated in different solvent systems (including CH_2Cl_2) to see if heterolytic N-N cleavage is inhibited by an electron-rich metal center.

Finally, Chapter 6 describes investigations of the effect of tacticity on polymer properties, using three Mo biphenolate alkylidene catalysts **49** for ROMP of a range of 2,3-disubstituted norbornadiene monomers. Both biphenolate and monomer substituents affected tacticity. No obvious trends emerged, but with the very bulky monomer substituent $-C(O)NPh_2$, solely trans polymer was obtained, probably because the trans-producing anti rotamer was sterically

favoured. Conformation plots from light-scattering data showed that all of the polymers had an approximately spherical conformation in solution. Optical rotation experiments with polymers prepared with enantiopure biphenolate initiator (R)-(+)-**49b**, showed no chiral (helical) tertiary structure in solution. The solid-state tertiary structure of a 99% cis, isotactic polymer was investigated. The brittleness of the homopolymer of **53** as well as block copolymers prepared using MTD to amplify flexibility, prevented orientation of the thin films. Tertiary structure periodicities could not be obtained, in consequence.

All of the ROMP polymers underwent thermal decomposition above 300 °C; notably, however, 2,3-dicarboalkoxynorbornadiene polymers showed significant decomposition by IR analysis, even at 80 °C, while diphenylamide-functionalized polymer was more robust. This instability should be investigated at ambient temperatures in order to establish the susceptibility to oxidative degradation in these polymers in the solid state. The effect of substituents on the polymer on polymer stability should also be studied in more detail to determine if this is a viable way to stabilize polynorbornadiene polymers. Thermal instability has been noted for polynorbornene based materials, and overcome by hydrogenation. Molecular modelling calculations should be carried out on hydrogenated polymers of **53-56** to predict whether or not reduced polymers adopt a helical conformation.

References

(1) Van Veldhuizen, J. J.; Garber, S. B.; Kingsbury, J. S.; Hoveyda, A. H. *J. Am. Chem. Soc.* **2002**, *124*, 4954.
(2) Prepared by U. Dharmasena of the Fogg lab group.
(3) Conrad, J. C.; Amoroso, D.; Czechura, P.; Yap, G. P. A.; Fogg, D. E. *Organometallics* **2003**, *22*, 3634.
(4) Conrad, J. C.; Yap, G. P. A.; Fogg, D. E. *Organometallics* **2003**, *22*, 1986.

APPENDICES

Appendix A. Crystallographic Information for $RuH_2(CO)(PPh_3)_3 \cdot CH_2Cl_2$ (2a).

Table A.1. Crystal data and structure refinement for $RuH_2(CO)(PPh_3)_3 \cdot CH_2Cl_2$ (2a).

Empirical formula	C56 H49 Cl2 O P3 Ru
Formula weight	1002.83
Temperature	203(2) K
Wavelength	0.71073 A
Crystal system, space group	Orthorhombic, Pbca
Unit cell dimensions	a = 19.173(2) Å $\alpha = 90°$ b = 18.322(2) Å $\beta = 90°$ c = 26.758(3) Å $\gamma = 90°$
Volume	9400(2) A^3
Z, Calculated density	8, 1.417 Mg/m^3
Absorption coefficient	0.590 mm^{-1}
F(000)	4128
Crystal size	0.40 x 0.10 x 0.05 mm
Theta range for data collection	1.52 to 20.81 deg.
Limiting indices	0<=h<=19, 0<=k<=18, 0<=l<=26
Reflections collected / unique	4926 / 4926 [R(int) = 0.0792]
Completeness to theta = 20.81	99.9 %
Absorption correction	Semi-empirical from equivalents
Max. and min. transmission	0.928079 and 0.332762
Refinement method	Full-matrix least-squares on F^2
Data / restraints / parameters	4926 / 1 / 575
Goodness-of-fit on F^2	1.085
Final R indices [I>2sigma(I)]	R1 = 0.0763, wR2 = 0.1656
R indices (all data)	R1 = 0.1032, wR2 = 0.1828
Extinction coefficient	0.00068(12)
Largest diff. peak and hole	0.772 and -0.739 $e.A^{-3}$

Table A.2. Bond lengths [Å] and angles [°] for $RuH_2(CO)(PPh_3)_3 \cdot CH_2Cl_2$ (2a).

Ru-C(1)	1.920(11)
Ru-P(3)	2.309(2)
Ru-P(1)	2.320(2)
Ru-P(2)	2.398(2)
Ru-H(1)	1.85(6)
Ru-H(2)	1.84(6)
P(1)-C(13)	1.849(9)
P(1)-C(19)	1.852(8)
P(1)-C(7)	1.852(9)
P(2)-C(31)	1.842(8)
P(2)-C(37)	1.842(9)
P(2)-C(25)	1.846(9)
P(3)-C(43)	1.842(9)
P(3)-C(49)	1.843(9)
P(3)-C(55)	1.845(9)
O(1)-C(1)	1.115(11)
C(2)-C(3)	1.367(14)
C(2)-C(7)	1.386(13)
C(3)-C(4)	1.370(14)
C(4)-C(5)	1.369(15)
C(5)-C(6)	1.395(14)
C(6)-C(7)	1.379(12)
C(8)-C(13)	1.394(13)
C(8)-C(9)	1.400(15)
C(9)-C(10)	1.378(15)
C(10)-C(11)	1.387(16)
C(11)-C(12)	1.373(14)
C(12)-C(13)	1.386(13)
C(14)-C(15)	1.372(13)
C(14)-C(19)	1.396(13)
C(15)-C(16)	1.384(14)
C(16)-C(17)	1.371(15)
C(17)-C(18)	1.392(13)
C(18)-C(19)	1.386(12)
C(20)-C(21)	1.378(13)
C(20)-C(25)	1.397(13)
C(21)-C(22)	1.360(14)
C(22)-C(23)	1.380(15)
C(23)-C(24)	1.384(14)
C(24)-C(25)	1.374(13)
C(26)-C(27)	1.393(13)
C(26)-C(31)	1.408(13)
C(27)-C(28)	1.368(14)
C(28)-C(29)	1.364(15)
C(29)-C(30)	1.403(14)

C(30)-C(31)	1.372(13)
C(32)-C(33)	1.387(14)
C(32)-C(37)	1.418(14)
C(33)-C(34)	1.387(16)
C(34)-C(35)	1.368(16)
C(35)-C(36)	1.381(14)
C(36)-C(37)	1.386(13)
C(38)-C(39)	1.387(13)
C(38)-C(43)	1.403(13)
C(39)-C(40)	1.370(14)
C(40)-C(41)	1.370(15)
C(41)-C(42)	1.400(14)
C(42)-C(43)	1.374(13)
C(44)-C(45)	1.369(14)
C(44)-C(49)	1.403(13)
C(45)-C(46)	1.370(15)
C(46)-C(47)	1.388(16)
C(47)-C(48)	1.380(15)
C(48)-C(49)	1.380(13)
C(50)-C(55)	1.391(14)
C(50)-C(51)	1.395(15)
C(51)-C(52)	1.390(16)
C(52)-C(53)	1.347(16)
C(53)-C(54)	1.393(14)
C(54)-C(55)	1.385(13)
C(56)-Cl(1)	1.692(16)
C(56)-Cl(2)	1.751(16)

C(1)-Ru-P(3)	96.3(3)
C(1)-Ru-P(1)	104.1(3)
P(3)-Ru-P(1)	147.95(9)
C(1)-Ru-P(2)	90.8(3)
P(3)-Ru-P(2)	102.75(8)
P(1)-Ru-P(2)	101.39(8)
H(1)-Ru-H(2)	105(3)
H(1)-Ru-P(1)	79(2)
H(1)-Ru-P(2)	94(2)
H(1)-Ru-P(3)	78(2)
H(1)-Ru-C(1)	173(2)
H(2)-Ru-P(1)	85(2)
H(2)-Ru-P(2)	160(2)
H(2)-Ru-P(3)	79(2)
H(2)-Ru-C(1)	69(2)
C(13)-P(1)-C(19)	104.3(4)
C(13)-P(1)-C(7)	101.2(4)
C(19)-P(1)-C(7)	99.0(4)

C(13)-P(1)-Ru	117.6(3)
C(19)-P(1)-Ru	118.0(3)
C(7)-P(1)-Ru	113.9(3)
C(31)-P(2)-C(37)	102.7(4)
C(31)-P(2)-C(25)	101.8(4)
C(37)-P(2)-C(25)	99.6(4)
C(31)-P(2)-Ru	119.7(3)
C(37)-P(2)-Ru	115.0(3)
C(25)-P(2)-Ru	115.2(3)
C(43)-P(3)-C(49)	102.4(4)
C(43)-P(3)-C(55)	101.6(4)
C(49)-P(3)-C(55)	100.0(4)
C(43)-P(3)-Ru	117.0(3)
C(49)-P(3)-Ru	117.3(3)
C(55)-P(3)-Ru	115.8(3)
O(1)-C(1)-Ru	175.5(8)
C(3)-C(2)-C(7)	120.1(8)
C(2)-C(3)-C(4)	121.7(9)
C(5)-C(4)-C(3)	119.4(9)
C(4)-C(5)-C(6)	119.2(9)
C(7)-C(6)-C(5)	121.4(9)
C(6)-C(7)-C(2)	118.2(8)
C(6)-C(7)-P(1)	120.3(7)
C(2)-C(7)-P(1)	121.1(6)
C(13)-C(8)-C(9)	120.7(9)
C(10)-C(9)-C(8)	120.0(10)
C(9)-C(10)-C(11)	119.0(9)
C(12)-C(11)-C(10)	121.1(10)
C(11)-C(12)-C(13)	120.9(10)
C(12)-C(13)-C(8)	118.2(8)
C(12)-C(13)-P(1)	125.5(7)
C(8)-C(13)-P(1)	116.3(7)
C(15)-C(14)-C(19)	121.3(9)
C(14)-C(15)-C(16)	120.0(9)
C(17)-C(16)-C(15)	119.8(9)
C(16)-C(17)-C(18)	120.3(9)
C(19)-C(18)-C(17)	120.7(9)
C(18)-C(19)-C(14)	117.9(8)
C(18)-C(19)-P(1)	121.4(7)
C(14)-C(19)-P(1)	120.3(6)
C(21)-C(20)-C(25)	121.3(9)
C(22)-C(21)-C(20)	120.3(9)
C(21)-C(22)-C(23)	119.7(9)
C(22)-C(23)-C(24)	119.7(9)
C(25)-C(24)-C(23)	121.7(9)
C(24)-C(25)-C(20)	117.2(8)

C(24)-C(25)-P(2)	123.1(7)
C(20)-C(25)-P(2)	119.7(6)
C(27)-C(26)-C(31)	119.0(8)
C(28)-C(27)-C(26)	121.4(9)
C(29)-C(28)-C(27)	119.9(9)
C(28)-C(29)-C(30)	119.9(9)
C(31)-C(30)-C(29)	120.8(9)
C(30)-C(31)-C(26)	119.0(8)
C(30)-C(31)-P(2)	124.7(7)
C(26)-C(31)-P(2)	116.3(6)
C(33)-C(32)-C(37)	119.8(9)
C(34)-C(33)-C(32)	120.9(10)
C(35)-C(34)-C(33)	118.8(9)
C(34)-C(35)-C(36)	121.6(10)
C(35)-C(36)-C(37)	120.6(9)
C(36)-C(37)-C(32)	118.2(8)
C(36)-C(37)-P(2)	122.6(7)
C(32)-C(37)-P(2)	118.9(7)
C(39)-C(38)-C(43)	119.8(9)
C(40)-C(39)-C(38)	120.7(9)
C(41)-C(40)-C(39)	119.6(9)
C(40)-C(41)-C(42)	120.8(9)
C(43)-C(42)-C(41)	119.8(9)
C(42)-C(43)-C(38)	119.2(8)
C(42)-C(43)-P(3)	123.1(7)
C(38)-C(43)-P(3)	117.7(7)
C(45)-C(44)-C(49)	121.0(8)
C(44)-C(45)-C(46)	120.8(10)
C(45)-C(46)-C(47)	118.8(9)
C(48)-C(47)-C(46)	120.9(9)
C(49)-C(48)-C(47)	120.5(10)
C(48)-C(49)-C(44)	118.0(8)
C(48)-C(49)-P(3)	123.7(7)
C(44)-C(49)-P(3)	118.3(6)
C(55)-C(50)-C(51)	120.9(10)
C(52)-C(51)-C(50)	119.5(10)
C(53)-C(52)-C(51)	119.6(10)
C(52)-C(53)-C(54)	121.6(10)
C(55)-C(54)-C(53)	120.1(9)
C(54)-C(55)-C(50)	118.3(8)
C(54)-C(55)-P(3)	120.4(7)
C(50)-C(55)-P(3)	120.9(7)
Cl(1)-C(56)-Cl(2)	115.0(10)

Symmetry transformations used to generate equivalent atoms:

Appendix B. Crystallographic Information for $RuHCl(CO)(PPh_3)_3$ (2b).

Table B.1. Crystal data and structure refinement for $RuHCl(CO)(PPh_3)_3$ (2b).

Empirical formula	C55 H46 Cl O P3 Ru
Formula weight	952.35
Temperature	203(2) K
Wavelength	0.71073 A
Crystal system, space group	Trigonal, P3(2)
Unit cell dimensions	a = 12.664(5) Å $\alpha = 90°$ b = 12.664(5) Å $\beta = 90°$ c = 26.301(13) Å $\gamma = 120°$
Volume	3653(3) A^3
Z, Calculated density	3, 1.299 Mg/m^3
Absorption coefficient	0.513 mm^{-1}
F(000)	1470
Crystal size	0.1 x 0.1 x 0.1 mm
Theta range for data collection	2.01 to 20.80 deg.
Limiting indices	-12<=h<=6, 0<=k<=12, 0<=l<=24
Reflections collected / unique	10815 / 2501 [R(int) = 0.1365]
Completeness to theta = 20.80	98.1 %
Absorption correction	Semi-empirical from equivalents
Max. and min. transmission	0.978266 and 0.713690
Refinement method	Full-matrix least-squares on F^2
Data / restraints / parameters	2501 / 501 / 443
Goodness-of-fit on F^2	1.105
Final R indices [I>2sigma(I)]	R1 = 0.0838, wR2 = 0.2282
R indices (all data)	R1 = 0.1024, wR2 = 0.2473
Absolute structure parameter	-0.05(15)
Largest diff. peak and hole	1.785 and -0.628 $e.A^{-3}$

Table B.2. Bond lengths [Å] and angles [°] for $RuHCl(CO)(PPh_3)_3$ (2b).

Ru-C(1)	1.82(4)
Ru-P(1)	2.371(8)
Ru-P(3)	2.411(9)
Ru-Cl	2.459(8)
Ru-P(2)	2.465(8)
O(1)-C(1)	1.06(3)
P(1)-C(13)	1.821(15)
P(1)-C(19)	1.840(15)
P(1)-C(7)	1.863(15)
P(2)-C(37)	1.810(18)
P(2)-C(31)	1.877(18)
P(2)-C(25)	1.880(17)
P(3)-C(43)	1.848(15)
P(3)-C(49)	1.867(16)
P(3)-C(55)	1.891(15)
C(2)-C(3)	1.3900
C(2)-C(7)	1.3900
C(3)-C(4)	1.3900
C(4)-C(5)	1.3900
C(5)-C(6)	1.3900
C(6)-C(7)	1.3900
C(8)-C(9)	1.3900
C(8)-C(13)	1.3900
C(9)-C(10)	1.3900
C(10)-C(11)	1.3900
C(11)-C(12)	1.3900
C(12)-C(13)	1.3900
C(14)-C(15)	1.3900
C(14)-C(19)	1.3900
C(15)-C(16)	1.3900
C(16)-C(17)	1.3900
C(17)-C(18)	1.3900
C(18)-C(19)	1.3900
C(20)-C(21)	1.3900
C(20)-C(25)	1.3900
C(21)-C(22)	1.3900
C(22)-C(23)	1.3900
C(23)-C(24)	1.3900
C(24)-C(25)	1.3900
C(26)-C(27)	1.3900
C(26)-C(31)	1.3900
C(27)-C(28)	1.3900
C(28)-C(29)	1.3900

C(29)-C(30)	1.3900
C(30)-C(31)	1.3900
C(32)-C(33)	1.3900
C(32)-C(37)	1.3900

Symmetry transformations used to generate equivalent atoms:

Appendix C. Crystallographic Information for Ru(η^5-ArO)(*o*-$C_6H_4PPh_2$)(PPh_3)•(2ArOH)($CHCl_3$) (9a).

Table C.1. Crystal data and structure refinement for Ru(η^5-ArO)(*o*-$C_6H_4PPh_2$)(PPh_3)•(2ArOH)($CHCl_3$) (9a).

Empirical formula	C67 H71 Cl3 O3 P2 Ru
Formula weight	1193.60
Temperature	203(2) K
Wavelength	0.71073 A
Crystal system, space group	Monoclinic, P2(1)/n
Unit cell dimensions	a = 13.721(2) Å α = 90° b = 25.215(3) Å β = 97.471(2)° c = 17.372(2) Å γ = 90°
Volume	5959(1) $A^3$3
Z, Calculated density	4, 1.330 Mg/m^3
Absorption coefficient	0.497 mm^{-1}
F(000)	2488
Crystal size	0.2 x 0.2 x 0.2 mm
Theta range for data collection	1.70 to 24.71 deg.
Limiting indices	-16<=h<=16, 0<=k<=29, 0<=l<=20
Reflections collected / unique	47562 / 10154 [R(int) = 0.1332]
Completeness to theta = 24.71	100.0 %
Absorption correction	Semi-empirical from equivalents
Max. and min. transmission	0.928079 and 0.786416
Refinement method	Full-matrix least-squares on F^2
Data / restraints / parameters	10154 / 0 / 685
Goodness-of-fit on F^2	1.010
Final R indices [I>2sigma(I)]	R1 = 0.0470, wR2 = 0.0795
R indices (all data)	R1 = 0.1010, wR2 = 0.0883
Largest diff. peak and hole	0.774 and -0.608 $e.A^{-3}$

Table C.2. **Bond lengths [Å] and angles [°] for $Ru(\eta^5\text{-}ArO)(o\text{-}C_6H_4PPh_2)(PPh_3)\cdot(2ArOH)(CHCl_3)$ (9a).**

Ru-C(1)	2.074(4)
Ru-C(40)	2.230(4)
Ru-C(38)	2.253(4)
Ru-C(41)	2.260(4)
Ru-C(37)	2.273(3)
Ru-P(1)	2.3258(11)
Ru-P(2)	2.3312(11)
Ru-C(39)	2.357(4)
Ru-C(42)	2.452(4)
P(1)-C(6)	1.792(4)
P(1)-C(18)	1.823(4)
P(1)-C(12)	1.825(4)
P(2)-C(30)	1.831(4)
P(2)-C(36)	1.845(4)
P(2)-C(24)	1.846(4)
O(1)-C(42)	1.285(5)
O(2)-C(52)	1.369(5)
O(3)-C(62)	1.377(5)
Cl(1)-C(67)	1.755(5)
Cl(2)-C(67)	1.744(5)
Cl(3)-C(67)	1.743(5)
C(1)-C(2)	1.406(5)
C(1)-C(6)	1.408(5)
C(2)-C(3)	1.390(5)
C(3)-C(4)	1.393(5)
C(4)-C(5)	1.375(5)
C(5)-C(6)	1.389(5)
C(7)-C(8)	1.375(5)
C(7)-C(12)	1.397(5)
C(8)-C(9)	1.365(6)
C(9)-C(10)	1.376(6)
C(10)-C(11)	1.385(6)
C(11)-C(12)	1.382(5)
C(13)-C(14)	1.374(5)
C(13)-C(18)	1.390(5)
C(14)-C(15)	1.370(6)
C(15)-C(16)	1.384(6)
C(16)-C(17)	1.395(5)
C(17)-C(18)	1.389(5)
C(19)-C(20)	1.384(5)
C(19)-C(24)	1.395(5)
C(20)-C(21)	1.374(5)
C(21)-C(22)	1.376(5)
C(22)-C(23)	1.400(5)

C(23)-C(24)	1.382(5)
C(25)-C(26)	1.383(5)
C(25)-C(30)	1.404(5)
C(26)-C(27)	1.359(6)
C(27)-C(28)	1.374(6)
C(28)-C(29)	1.378(6)
C(29)-C(30)	1.404(5)
C(31)-C(32)	1.382(5)
C(31)-C(36)	1.400(5)
C(32)-C(33)	1.379(6)
C(33)-C(34)	1.369(6)
C(34)-C(35)	1.386(5)
C(35)-C(36)	1.384(5)
C(37)-C(38)	1.418(5)
C(37)-C(42)	1.425(5)
C(38)-C(39)	1.415(5)
C(39)-C(40)	1.409(5)
C(39)-C(43)	1.522(5)
C(40)-C(41)	1.405(5)
C(41)-C(42)	1.428(5)
C(43)-C(45)	1.528(6)
C(43)-C(46)	1.534(5)
C(43)-C(44)	1.542(6)
C(47)-C(48)	1.377(6)
C(47)-C(52)	1.406(6)
C(48)-C(49)	1.406(6)
C(49)-C(50)	1.388(6)
C(49)-C(53)	1.530(6)
C(50)-C(51)	1.407(6)
C(51)-C(52)	1.332(6)
C(53)-C(56)	1.525(6)
C(53)-C(55)	1.544(6)
C(53)-C(54)	1.548(6)
C(57)-C(62)	1.374(6)
C(57)-C(58)	1.379(6)
C(58)-C(59)	1.389(6)
C(59)-C(60)	1.395(6)
C(59)-C(63)	1.521(6)
C(60)-C(61)	1.374(6)
C(61)-C(62)	1.374(6)
C(63)-C(64)	1.508(7)
C(63)-C(65)	1.513(7)
C(63)-C(66)	1.514(6)

C(1)-Ru-C(40)	126.48(15)
C(1)-Ru-C(38)	140.80(15)

C(40)-Ru-C(38)	63.95(14)
C(1)-Ru-C(41)	94.49(15)
C(40)-Ru-C(41)	36.46(13)
C(38)-Ru-C(41)	76.07(15)
C(1)-Ru-C(37)	105.06(15)
C(40)-Ru-C(37)	75.67(13)
C(38)-Ru-C(37)	36.51(13)
C(41)-Ru-C(37)	63.82(14)
C(1)-Ru-P(1)	66.60(11)
C(40)-Ru-P(1)	93.70(10)
C(38)-Ru-P(1)	151.30(11)
C(41)-Ru-P(1)	96.92(11)
C(37)-Ru-P(1)	159.12(11)
C(1)-Ru-P(2)	87.13(11)
C(40)-Ru-P(2)	145.86(11)
C(38)-Ru-P(2)	94.81(11)
C(41)-Ru-P(2)	167.41(11)
C(37)-Ru-P(2)	103.69(10)
P(1)-Ru-P(2)	95.18(4)
C(1)-Ru-C(39)	159.30(14)
C(40)-Ru-C(39)	35.65(14)
C(38)-Ru-C(39)	35.65(13)
C(41)-Ru-C(39)	64.95(14)
C(37)-Ru-C(39)	64.78(13)
P(1)-Ru-C(39)	116.07(11)
P(2)-Ru-C(39)	112.38(11)
C(1)-Ru-C(42)	86.76(14)
C(40)-Ru-C(42)	63.42(14)
C(38)-Ru-C(42)	63.59(14)
C(41)-Ru-C(42)	34.98(13)
C(37)-Ru-C(42)	34.84(13)
P(1)-Ru-C(42)	124.30(11)
P(2)-Ru-C(42)	132.97(10)
C(39)-Ru-C(42)	74.95(13)
C(6)-P(1)-C(18)	112.71(18)
C(6)-P(1)-C(12)	105.20(18)
C(18)-P(1)-C(12)	101.82(17)
C(6)-P(1)-Ru	86.81(13)
C(18)-P(1)-Ru	131.86(13)
C(12)-P(1)-Ru	115.31(12)
C(30)-P(2)-C(36)	101.33(18)
C(30)-P(2)-C(24)	105.49(18)
C(36)-P(2)-C(24)	97.22(17)
C(30)-P(2)-Ru	111.70(12)
C(36)-P(2)-Ru	119.47(13)
C(24)-P(2)-Ru	119.14(13)

C(2)-C(1)-C(6)	117.3(4)
C(2)-C(1)-Ru	133.8(3)
C(6)-C(1)-Ru	108.7(3)
C(3)-C(2)-C(1)	119.3(4)
C(2)-C(3)-C(4)	121.7(4)
C(5)-C(4)-C(3)	120.2(4)
C(4)-C(5)-C(6)	118.2(4)
C(5)-C(6)-C(1)	123.2(4)
C(5)-C(6)-P(1)	138.4(3)
C(1)-C(6)-P(1)	97.8(3)
C(8)-C(7)-C(12)	121.3(4)
C(9)-C(8)-C(7)	119.6(4)
C(8)-C(9)-C(10)	120.7(4)
C(9)-C(10)-C(11)	119.7(4)
C(12)-C(11)-C(10)	120.8(4)
C(11)-C(12)-C(7)	117.9(4)
C(11)-C(12)-P(1)	122.1(3)
C(7)-C(12)-P(1)	119.9(3)
C(14)-C(13)-C(18)	120.6(4)
C(15)-C(14)-C(13)	120.9(4)
C(14)-C(15)-C(16)	119.7(4)
C(15)-C(16)-C(17)	119.7(4)
C(18)-C(17)-C(16)	120.4(4)
C(17)-C(18)-C(13)	118.6(4)
C(17)-C(18)-P(1)	120.1(3)
C(13)-C(18)-P(1)	121.2(3)
C(20)-C(19)-C(24)	121.4(4)
C(21)-C(20)-C(19)	120.1(4)
C(20)-C(21)-C(22)	119.6(4)
C(21)-C(22)-C(23)	120.3(4)
C(24)-C(23)-C(22)	120.6(4)
C(23)-C(24)-C(19)	117.9(3)
C(23)-C(24)-P(2)	124.9(3)
C(19)-C(24)-P(2)	117.2(3)
C(26)-C(25)-C(30)	120.5(4)
C(27)-C(26)-C(25)	120.6(4)
C(26)-C(27)-C(28)	120.0(5)
C(27)-C(28)-C(29)	120.9(4)
C(28)-C(29)-C(30)	120.2(4)
C(25)-C(30)-C(29)	117.7(4)
C(25)-C(30)-P(2)	119.5(3)
C(29)-C(30)-P(2)	122.6(3)
C(32)-C(31)-C(36)	120.4(4)
C(33)-C(32)-C(31)	120.4(4)
C(34)-C(33)-C(32)	119.8(4)
C(33)-C(34)-C(35)	120.4(4)

C(36)-C(35)-C(34)	120.8(4)
C(35)-C(36)-C(31)	118.3(4)
C(35)-C(36)-P(2)	122.8(3)
C(31)-C(36)-P(2)	118.9(3)
C(38)-C(37)-C(42)	121.8(4)
C(38)-C(37)-Ru	71.0(2)
C(42)-C(37)-Ru	79.5(2)
C(39)-C(38)-C(37)	122.3(4)
C(39)-C(38)-Ru	76.2(2)
C(37)-C(38)-Ru	72.5(2)
C(40)-C(39)-C(38)	114.4(4)
C(40)-C(39)-C(43)	121.2(4)
C(38)-C(39)-C(43)	123.8(4)
C(40)-C(39)-Ru	67.2(2)
C(38)-C(39)-Ru	68.1(2)
C(43)-C(39)-Ru	141.7(3)
C(41)-C(40)-C(39)	123.6(4)
C(41)-C(40)-Ru	73.0(2)
C(39)-C(40)-Ru	77.1(2)
C(40)-C(41)-C(42)	121.2(4)
C(40)-C(41)-Ru	70.6(2)
C(42)-C(41)-Ru	79.8(2)
O(1)-C(42)-C(37)	123.4(4)
O(1)-C(42)-C(41)	122.0(4)
C(37)-C(42)-C(41)	114.3(4)
O(1)-C(42)-Ru	135.5(3)
C(37)-C(42)-Ru	65.7(2)
C(41)-C(42)-Ru	65.2(2)
C(39)-C(43)-C(45)	112.5(4)
C(39)-C(43)-C(46)	106.5(3)
C(45)-C(43)-C(46)	108.9(4)
C(39)-C(43)-C(44)	111.8(4)
C(45)-C(43)-C(44)	108.0(4)
C(46)-C(43)-C(44)	109.0(4)
C(48)-C(47)-C(52)	118.7(4)
C(47)-C(48)-C(49)	123.0(5)
C(50)-C(49)-C(48)	116.0(4)
C(50)-C(49)-C(53)	122.8(4)
C(48)-C(49)-C(53)	121.2(4)
C(49)-C(50)-C(51)	121.0(4)
C(52)-C(51)-C(50)	121.5(4)
C(51)-C(52)-O(2)	118.9(5)
C(51)-C(52)-C(47)	119.8(4)
O(2)-C(52)-C(47)	121.3(4)
C(56)-C(53)-C(49)	112.5(4)
C(56)-C(53)-C(55)	107.7(4)

C(49)-C(53)-C(55)	109.4(4)
C(56)-C(53)-C(54)	109.1(4)
C(49)-C(53)-C(54)	109.3(4)
C(55)-C(53)-C(54)	108.7(4)
C(62)-C(57)-C(58)	120.2(4)
C(57)-C(58)-C(59)	122.2(4)
C(58)-C(59)-C(60)	115.4(4)
C(58)-C(59)-C(63)	122.2(4)
C(60)-C(59)-C(63)	122.4(4)
C(61)-C(60)-C(59)	123.2(5)
C(60)-C(61)-C(62)	119.3(5)
C(57)-C(62)-C(61)	119.6(5)
C(57)-C(62)-O(3)	117.6(4)
C(61)-C(62)-O(3)	122.7(4)
C(64)-C(63)-C(65)	109.0(5)
C(64)-C(63)-C(66)	106.4(4)
C(65)-C(63)-C(66)	109.0(5)
C(64)-C(63)-C(59)	112.2(4)
C(65)-C(63)-C(59)	109.0(4)
C(66)-C(63)-C(59)	111.2(4)
Cl(3)-C(67)-Cl(2)	111.1(3)
Cl(3)-C(67)-Cl(1)	110.6(2)
Cl(2)-C(67)-Cl(1)	109.7(2)

Symmetry transformations used to generate equivalent atoms:

Appendix D. Crystallographic Information for Ru(η^5-PhO)(*o*-$C_6H_4PPh_2$)(PPh_3)•(2PhOH) (9b).

Table D.1. Crystal data and structure refinement for Ru(η^5-PhO)(*o*-$C_6H_4PPh_2$)(PPh_3)•(2PhOH)(9b).

Empirical formula	C48 H40 O2 P2 Ru
Formula weight	811.81
Temperature	203(2) K
Wavelength	0.71073 A
Crystal system, space group	Orthorhombic, Pbcn
Unit cell dimensions	a = 35.692(3) Å α = 90° b = 12.157(1) Å β = 90° c = 17.925(2) Å γ = 90°
Volume	7778(1) A^3
Z, Calculated density	8, 1.387 Mg/m^3
Absorption coefficient	0.525 mm^{-1}
F(000)	3344
Crystal size	0.10 x 0.10 x 0.02 mm
Theta range for data collection	2.10 to 24.71 deg.
Limiting indices	0<=h<=41, 0<=k<=14, 0<=l<=21
Reflections collected / unique	61494 / 6631 [R(int) = 0.1395]
Completeness to theta = 24.71	99.9 %
Absorption correction	Semi-empirical from equivalents
Max. and min. transmission	0.928078 and 0.725343
Refinement method	Full-matrix least-squares on F^2
Data / restraints / parameters	6631 / 2 / 482
Goodness-of-fit on F^2	1.017
Final R indices [I>2sigma(I)]	R1 = 0.0371, wR2 = 0.0693
R indices (all data)	R1 = 0.0778, wR2 = 0.0771
Largest diff. peak and hole	0.485 and -0.684 $e.A^{-3}$

Table D.2. Bond lengths [Å] and angles [°] for Ru(η^5-PhO)(*o*-$C_6H_4PPh_2$)(PPh_3)•(2PhOH)(9b).

Ru-C(1)	2.083(3)
Ru-C(40)	2.220(3)
Ru-C(38)	2.233(3)
Ru-C(41)	2.270(3)
Ru-C(39)	2.270(3)
Ru-C(37)	2.279(3)
Ru-P(2)	2.3060(10)
Ru-P(1)	2.3273(9)
Ru-C(42)	2.478(4)
P(1)-C(6)	1.799(3)
P(1)-C(18)	1.822(4)
P(1)-C(12)	1.832(4)
P(2)-C(30)	1.837(4)
P(2)-C(36)	1.836(4)
P(2)-C(24)	1.843(4)
O(1)-C(42)	1.260(4)
C(1)-C(2)	1.404(5)
C(1)-C(6)	1.402(5)
C(2)-C(3)	1.383(5)
C(3)-C(4)	1.377(5)
C(4)-C(5)	1.390(5)
C(5)-C(6)	1.394(4)
C(7)-C(8)	1.385(5)
C(7)-C(12)	1.394(5)
C(8)-C(9)	1.367(6)
C(9)-C(10)	1.376(6)
C(10)-C(11)	1.380(5)
C(11)-C(12)	1.386(5)
C(13)-C(14)	1.384(5)
C(13)-C(18)	1.387(5)
C(14)-C(15)	1.372(5)
C(15)-C(16)	1.382(5)
C(16)-C(17)	1.381(5)
C(17)-C(18)	1.387(5)
C(19)-C(20)	1.380(5)
C(19)-C(24)	1.397(5)
C(20)-C(21)	1.373(6)
C(21)-C(22)	1.371(6)
C(22)-C(23)	1.397(5)
C(23)-C(24)	1.386(5)
C(25)-C(26)	1.378(5)
C(25)-C(30)	1.404(5)
C(26)-C(27)	1.373(6)
C(27)-C(28)	1.371(6)

C(28)-C(29)	1.380(5)
C(29)-C(30)	1.385(5)
C(31)-C(32)	1.378(5)
C(31)-C(36)	1.406(5)
C(32)-C(33)	1.391(6)
C(33)-C(34)	1.378(6)
C(34)-C(35)	1.396(5)
C(35)-C(36)	1.375(5)
C(37)-C(38)	1.396(5)
C(37)-C(42)	1.445(5)
C(38)-C(39)	1.401(5)
C(39)-C(40)	1.394(5)
C(40)-C(41)	1.412(5)
C(41)-C(42)	1.435(5)
O(2)-C(48)	1.326(5)
O(2')-C(43)	1.321(6)
C(43)-C(48)	1.341(5)
C(43)-C(44)	1.356(6)
C(44)-C(45)	1.331(7)
C(45)-C(46)	1.355(7)
C(46)-C(47)	1.389(7)
C(47)-C(48)	1.380(6)

C(1)-Ru-C(40)	132.85(14)
C(1)-Ru-C(38)	138.33(14)
C(40)-Ru-C(38)	64.80(14)
C(1)-Ru-C(41)	100.18(13)
C(40)-Ru-C(41)	36.65(13)
C(38)-Ru-C(41)	76.23(13)
C(1)-Ru-C(39)	164.54(14)
C(40)-Ru-C(39)	36.15(13)
C(38)-Ru-C(39)	36.24(12)
C(41)-Ru-C(39)	65.35(13)
C(1)-Ru-C(37)	104.62(13)
C(40)-Ru-C(37)	76.03(14)
C(38)-Ru-C(37)	36.02(12)
C(41)-Ru-C(37)	63.75(13)
C(39)-Ru-C(37)	64.89(13)
C(1)-Ru-P(2)	90.32(9)
C(40)-Ru-P(2)	135.98(10)
C(38)-Ru-P(2)	89.64(10)
C(41)-Ru-P(2)	165.87(9)
C(39)-Ru-P(2)	103.11(10)
C(37)-Ru-P(2)	104.60(10)
C(1)-Ru-P(1)	66.68(10)
C(40)-Ru-P(1)	94.82(10)

C(38)-Ru-P(1)	154.50(10)
C(41)-Ru-P(1)	96.80(9)
C(39)-Ru-P(1)	118.50(10)
C(37)-Ru-P(1)	157.82(10)
P(2)-Ru-P(1)	96.03(3)
C(1)-Ru-C(42)	89.54(13)
C(40)-Ru-C(42)	63.76(13)
C(38)-Ru-C(42)	63.61(12)
C(41)-Ru-C(42)	34.82(12)
C(39)-Ru-C(42)	75.43(13)
C(37)-Ru-C(42)	35.05(12)
P(2)-Ru-C(42)	137.18(9)
P(1)-Ru-C(42)	122.80(9)
C(6)-P(1)-C(18)	114.27(16)
C(6)-P(1)-C(12)	106.36(17)
C(18)-P(1)-C(12)	101.41(16)
C(6)-P(1)-Ru	86.64(11)
C(18)-P(1)-Ru	129.88(11)
C(12)-P(1)-Ru	116.16(11)
C(30)-P(2)-C(36)	103.09(16)
C(30)-P(2)-C(24)	104.57(17)
C(36)-P(2)-C(24)	98.98(16)
C(30)-P(2)-Ru	109.69(12)
C(36)-P(2)-Ru	118.30(13)
C(24)-P(2)-Ru	120.10(12)
C(2)-C(1)-C(6)	116.4(3)
C(2)-C(1)-Ru	134.8(3)
C(6)-C(1)-Ru	108.6(2)
C(3)-C(2)-C(1)	120.1(4)
C(4)-C(3)-C(2)	121.9(4)
C(3)-C(4)-C(5)	120.4(4)
C(4)-C(5)-C(6)	117.0(3)
C(5)-C(6)-C(1)	124.2(3)
C(5)-C(6)-P(1)	137.3(3)
C(1)-C(6)-P(1)	98.1(2)
C(8)-C(7)-C(12)	120.2(4)
C(9)-C(8)-C(7)	121.0(4)
C(8)-C(9)-C(10)	119.2(4)
C(9)-C(10)-C(11)	120.6(4)
C(10)-C(11)-C(12)	120.8(4)
C(11)-C(12)-C(7)	118.2(3)
C(11)-C(12)-P(1)	122.4(3)
C(7)-C(12)-P(1)	119.4(3)
C(14)-C(13)-C(18)	120.5(4)
C(15)-C(14)-C(13)	119.6(4)
C(14)-C(15)-C(16)	120.6(4)

C(17)-C(16)-C(15)	119.9(4)
C(16)-C(17)-C(18)	120.1(3)
C(17)-C(18)-C(13)	119.3(3)
C(17)-C(18)-P(1)	119.8(3)
C(13)-C(18)-P(1)	120.8(3)
C(20)-C(19)-C(24)	119.6(4)
C(21)-C(20)-C(19)	121.1(5)
C(22)-C(21)-C(20)	119.7(4)
C(21)-C(22)-C(23)	120.4(5)
C(24)-C(23)-C(22)	119.9(4)
C(23)-C(24)-C(19)	119.3(4)
C(23)-C(24)-P(2)	123.5(3)
C(19)-C(24)-P(2)	117.2(3)
C(26)-C(25)-C(30)	121.1(4)
C(27)-C(26)-C(25)	120.4(4)
C(28)-C(27)-C(26)	119.0(4)
C(27)-C(28)-C(29)	121.4(4)
C(28)-C(29)-C(30)	120.6(4)
C(29)-C(30)-C(25)	117.5(4)
C(29)-C(30)-P(2)	124.2(3)
C(25)-C(30)-P(2)	118.1(3)
C(32)-C(31)-C(36)	121.1(4)
C(31)-C(32)-C(33)	120.0(4)
C(34)-C(33)-C(32)	119.2(4)
C(33)-C(34)-C(35)	121.0(4)
C(36)-C(35)-C(34)	120.3(4)
C(35)-C(36)-C(31)	118.5(4)
C(35)-C(36)-P(2)	122.1(3)
C(31)-C(36)-P(2)	119.4(3)
C(38)-C(37)-C(42)	122.6(4)
C(38)-C(37)-Ru	70.2(2)
C(42)-C(37)-Ru	80.0(2)
C(37)-C(38)-C(39)	121.6(4)
C(37)-C(38)-Ru	73.82(19)
C(39)-C(38)-Ru	73.3(2)
C(40)-C(39)-C(38)	117.2(4)
C(40)-C(39)-Ru	70.0(2)
C(38)-C(39)-Ru	70.42(19)
C(39)-C(40)-C(41)	121.7(4)
C(39)-C(40)-Ru	73.9(2)
C(41)-C(40)-Ru	73.6(2)
C(40)-C(41)-C(42)	122.1(3)
C(40)-C(41)-Ru	69.8(2)
C(42)-C(41)-Ru	80.6(2)
O(1)-C(42)-C(41)	123.3(3)
O(1)-C(42)-C(37)	123.5(4)

C(41)-C(42)-C(37)	113.1(3)
O(1)-C(42)-Ru	136.4(3)
C(41)-C(42)-Ru	64.6(2)
C(37)-C(42)-Ru	64.9(2)
O(2')-C(43)-C(48)	124.3(7)
O(2')-C(43)-C(44)	113.2(6)
C(48)-C(43)-C(44)	121.5(4)
C(45)-C(44)-C(43)	120.3(5)
C(44)-C(45)-C(46)	120.3(5)
C(45)-C(46)-C(47)	120.0(5)
C(48)-C(47)-C(46)	118.7(5)
O(2)-C(48)-C(43)	123.0(5)
O(2)-C(48)-C(47)	117.9(4)
C(43)-C(48)-C(47)	119.1(4)

Symmetry transformations used to generate equivalent atoms:

Appendix E. Crystallographic Information for $RuCl(\eta^5\text{-}PhO)(PPh_3)_2 \cdot CH_2Cl_2$ (11b).

Table E.1. Crystal data and structure refinement for $RuCl(\eta^5\text{-}PhO)(PPh_3)_2 \cdot CH_2Cl_2$ (11b).

Empirical formula	C48 H41 Cl O2 P2 Ru
Formula weight	848.27
Temperature	203(2) K
Wavelength	0.71073 A
Crystal system, space group	Monoclinic, P2(1)/c
Unit cell dimensions	a = 12.412(2) Å $\alpha = 90°$ b = 10.470(2) Å $\beta = 101.954(2)°$ c = 29.962(6) Å $\gamma = 90°$
Volume	3809(1) A^3
Z, Calculated density	4, 1.479 Mg/m^3
Absorption coefficient	0.607 mm^{-1}
F(000)	1744
Crystal size	0.12 x 0.10 x 0.03 mm
Theta range for data collection	1.68 to 20.81 deg.
Limiting indices	-12<=h<=12, 0<=k<=10, 0<=l<=29
Reflections collected / unique	60061 / 3992 [R(int) = 0.0841]
Completeness to theta = 20.81	99.9 %
Absorption correction	Semi-empirical from equivalents
Max. and min. transmission	0.928081 and 0.012889
Refinement method	Full-matrix least-squares on F^2
Data / restraints / parameters	3992 / 490 / 487
Goodness-of-fit on F^2	1.052
Final R indices [I>2sigma(I)]	R1 = 0.0658, wR2 = 0.1392
R indices (all data)	R1 = 0.0991, wR2 = 0.1465
Largest diff. peak and hole	0.961 and -0.939 $e.A^{-3}$

Table E.2. Bond lengths [Å] and angles [°] for $RuCl(\eta^5\text{-}PhO)(PPh_3)_2 \cdot CH_2Cl_2$ (11b).

Ru-C(39)	2.192(10)
Ru-C(38)	2.210(10)
Ru-C(40)	2.235(10)
Ru-C(37)	2.293(10)
Ru-C(41)	2.319(10)
Ru-P(2)	2.353(3)
Ru-P(1)	2.355(3)
Ru-Cl	2.428(3)
Ru-C(42)	2.536(10)
P(1)-C(6)	1.834(10)
P(1)-C(18)	.841(10)
P(1)-C(12)	1.846(10)
P(2)-C(24)	1.804(10)
P(2)-C(30)	1.839(10)
P(2)-C(36)	1.864(10)
O(1)-C(42)	1.248(11)
C(1)-C(2)	1.401(14)
C(1)-C(6)	1.416(14)
C(2)-C(3)	1.349(14)
C(3)-C(4)	1.375(14)
C(4)-C(5)	1.392(14)
C(5)-C(6)	1.378(13)
C(7)-C(8)	1.391(13)
C(7)-C(12)	1.398(13)
C(8)-C(9)	1.396(14)
C(9)-C(10)	1.345(14)
C(10)-C(11)	1.356(12)
C(11)-C(12)	1.366(13)
C(13)-C(18)	1.391(14)
C(13)-C(14)	1.394(13)
C(14)-C(15)	1.387(14)
C(15)-C(16)	1.354(14)
C(16)-C(17)	1.393(13)
C(17)-C(18)	1.386(13)
C(19)-C(24)	1.385(13)
C(19)-C(20)	1.392(12)
C(20)-C(21)	1.398(13)
C(21)-C(22)	1.383(14)
C(22)-C(23)	1.401(13)
C(23)-C(24)	1.390(13)
C(25)-C(30)	1.365(13)
C(25)-C(26)	1.394(13)
C(26)-C(27)	1.369(14)
C(27)-C(28)	1.355(14)

C(28)-C(29)	1.391(14)
C(29)-C(30)	1.409(13)
C(31)-C(36)	1.384(13)
C(31)-C(32)	1.387(13)
C(32)-C(33)	1.379(13)
C(33)-C(34)	1.380(14)
C(34)-C(35)	1.373(14)
C(35)-C(36)	1.376(13)
C(37)-C(38)	1.392(14)
C(37)-C(42)	1.453(15)
C(38)-C(39)	1.415(14)
C(39)-C(40)	1.376(14)
C(40)-C(41)	1.425(14)
C(41)-C(42)	1.417(14)
O(2)-C(48)	1.351(12)
C(43)-C(48)	1.394(15)
C(43)-C(44)	1.415(15)
C(44)-C(45)	1.378(14)
C(45)-C(46)	1.375(15)
C(46)-C(47)	1.386(14)
C(47)-C(48)	1.340(14)

C(39)-Ru-C(38)	37.5(4)
C(39)-Ru-C(40)	36.2(4)
C(38)-Ru-C(40)	65.7(4)
C(39)-Ru-C(37)	65.6(4)
C(38)-Ru-C(37)	35.9(4)
C(40)-Ru-C(37)	76.2(4)
C(39)-Ru-C(41)	65.0(4)
C(38)-Ru-C(41)	76.1(4)
C(40)-Ru-C(41)	36.4(3)
C(37)-Ru-C(41)	63.1(4)
C(39)-Ru-P(2)	99.8(3)
C(38)-Ru-P(2)	86.2(3)
C(40)-Ru-P(2)	133.1(3)
C(37)-Ru-P(2)	103.1(3)
C(41)-Ru-P(2)	162.2(3)
C(39)-Ru-P(1)	109.0(3)
C(38)-Ru-P(1)	146.0(3)
C(40)-Ru-P(1)	87.7(3)
C(37)-Ru-P(1)	158.4(3)
C(41)-Ru-P(1)	95.4(3)
P(2)-Ru-P(1)	98.44(10)
C(39)-Ru-Cl	155.6(3)
C(38)-Ru-Cl	124.8(3)
C(40)-Ru-Cl	132.9(3)

C(28)-C(29)	1.391(14)
C(29)-C(30)	1.409(13)
C(31)-C(36)	1.384(13)
C(31)-C(32)	1.387(13)
C(32)-C(33)	1.379(13)
C(33)-C(34)	1.380(14)
C(34)-C(35)	1.373(14)
C(35)-C(36)	1.376(13)
C(37)-C(38)	1.392(14)
C(37)-C(42)	1.453(15)
C(38)-C(39)	1.415(14)
C(39)-C(40)	1.376(14)
C(40)-C(41)	1.425(14)
C(41)-C(42)	1.417(14)
O(2)-C(48)	1.351(12)
C(43)-C(48)	1.394(15)
C(43)-C(44)	1.415(15)
C(44)-C(45)	1.378(14)
C(45)-C(46)	1.375(15)
C(46)-C(47)	1.386(14)
C(47)-C(48)	1.340(14)

C(39)-Ru-C(38)	37.5(4)
C(39)-Ru-C(40)	36.2(4)
C(38)-Ru-C(40)	65.7(4)
C(39)-Ru-C(37)	65.6(4)
C(38)-Ru-C(37)	35.9(4)
C(40)-Ru-C(37)	76.2(4)
C(39)-Ru-C(41)	65.0(4)
C(38)-Ru-C(41)	76.1(4)
C(40)-Ru-C(41)	36.4(3)
C(37)-Ru-C(41)	63.1(4)
C(39)-Ru-P(2)	99.8(3)
C(38)-Ru-P(2)	86.2(3)
C(40)-Ru-P(2)	133.1(3)
C(37)-Ru-P(2)	103.1(3)
C(41)-Ru-P(2)	162.2(3)
C(39)-Ru-P(1)	109.0(3)
C(38)-Ru-P(1)	146.0(3)
C(40)-Ru-P(1)	87.7(3)
C(37)-Ru-P(1)	158.4(3)
C(41)-Ru-P(1)	95.4(3)
P(2)-Ru-P(1)	98.44(10)
C(39)-Ru-Cl	155.6(3)
C(38)-Ru-Cl	124.8(3)
C(40)-Ru-Cl	132.9(3)

C(37)-Ru-Cl	91.7(3)
C(41)-Ru-Cl	97.5(3)
P(2)-Ru-Cl	93.81(9)
P(1)-Ru-Cl	88.70(9)
C(39)-Ru-C(42)	74.2(4)
C(38)-Ru-C(42)	62.6(4)
C(40)-Ru-C(42)	62.3(4)
C(37)-Ru-C(42)	34.5(3)
C(41)-Ru-C(42)	33.6(3)
P(2)-Ru-C(42)	136.5(3)
P(1)-Ru-C(42)	124.5(3)
Cl-Ru-C(42)	82.0(3)
C(6)-P(1)-C(18)	100.8(5)
C(6)-P(1)-C(12)	103.3(5)
C(18)-P(1)-C(12)	100.0(5)
C(6)-P(1)-Ru	109.8(3)
C(18)-P(1)-Ru	120.0(4)
C(12)-P(1)-Ru	120.2(3)
C(24)-P(2)-C(30)	105.3(5)
C(24)-P(2)-C(36)	97.8(5)
C(30)-P(2)-C(36)	105.2(5)
C(24)-P(2)-Ru	123.3(4)
C(30)-P(2)-Ru	109.6(3)
C(36)-P(2)-Ru	113.9(3)
C(2)-C(1)-C(6)	119.9(10)
C(3)-C(2)-C(1)	120.0(11)
C(2)-C(3)-C(4)	120.9(12)
C(3)-C(4)-C(5)	120.2(12)
C(6)-C(5)-C(4)	120.5(11)
C(5)-C(6)-C(1)	118.2(10)
C(5)-C(6)-P(1)	122.5(8)
C(1)-C(6)-P(1)	119.0(8)
C(8)-C(7)-C(12)	119.6(10)
C(7)-C(8)-C(9)	118.9(10)
C(10)-C(9)-C(8)	121.6(10)
C(9)-C(10)-C(11)	118.1(11)
C(10)-C(11)-C(12)	124.2(11)
C(11)-C(12)-C(7)	117.5(9)
C(11)-C(12)-P(1)	121.6(8)
C(7)-C(12)-P(1)	121.0(8)
C(18)-C(13)-C(14)	121.2(11)
C(15)-C(14)-C(13)	118.2(11)
C(16)-C(15)-C(14)	121.4(11)
C(15)-C(16)-C(17)	120.2(11)
C(18)-C(17)-C(16)	120.1(10)
C(17)-C(18)-C(13)	118.6(10)

C(17)-C(18)-P(1)	121.3(8)
C(13)-C(18)-P(1)	120.0(8)
C(24)-C(19)-C(20)	121.8(10)
C(19)-C(20)-C(21)	121.6(10)
C(22)-C(21)-C(20)	117.0(10)
C(21)-C(22)-C(23)	120.6(10)
C(24)-C(23)-C(22)	122.6(10)
C(19)-C(24)-C(23)	116.1(9)
C(19)-C(24)-P(2)	118.5(8)
C(23)-C(24)-P(2)	124.4(8)
C(30)-C(25)-C(26)	120.0(11)
C(27)-C(26)-C(25)	119.7(11)
C(28)-C(27)-C(26)	121.5(11)
C(27)-C(28)-C(29)	119.6(11)
C(28)-C(29)-C(30)	119.5(11)
C(25)-C(30)-C(29)	119.5(10)
C(25)-C(30)-P(2)	119.9(8)
C(29)-C(30)-P(2)	120.4(8)
C(36)-C(31)-C(32)	119.7(10)
C(33)-C(32)-C(31)	120.6(11)
C(32)-C(33)-C(34)	118.2(11)
C(35)-C(34)-C(33)	122.3(11)
C(34)-C(35)-C(36)	118.9(10)
C(35)-C(36)-C(31)	120.2(10)
C(35)-C(36)-P(2)	118.3(8)
C(31)-C(36)-P(2)	120.9(8)
C(38)-C(37)-C(42)	121.5(11)
C(38)-C(37)-Ru	68.8(6)
C(42)-C(37)-Ru	81.9(6)
C(37)-C(38)-C(39)	120.1(11)
C(37)-C(38)-Ru	75.3(6)
C(39)-C(38)-Ru	70.6(6)
C(40)-C(39)-C(38)	119.7(11)
C(40)-C(39)-Ru	73.6(6)
C(38)-C(39)-Ru	71.9(6)
C(39)-C(40)-C(41)	120.2(11)
C(39)-C(40)-Ru	70.2(6)
C(41)-C(40)-Ru	75.0(6)
C(42)-C(41)-C(40)	121.7(11)
C(42)-C(41)-Ru	81.7(6)
C(40)-C(41)-Ru	68.6(6)
O(1)-C(42)-C(41)	124.4(10)
O(1)-C(42)-C(37)	120.9(11)
C(41)-C(42)-C(37)	114.4(10)
O(1)-C(42)-Ru	138.6(8)
C(41)-C(42)-Ru	64.8(6)

C(37)-C(42)-Ru	63.5(6)
C(48)-C(43)-C(44)	118.5(11)
C(45)-C(44)-C(43)	119.0(11)
C(46)-C(45)-C(44)	121.0(11)
C(45)-C(46)-C(47)	119.5(11)
C(48)-C(47)-C(46)	120.7(11)
C(47)-C(48)-O(2)	125.4(11)
C(47)-C(48)-C(43)	121.3(11)
O(2)-C(48)-C(43)	113.3(10)

Symmetry transformations used to generate equivalent atoms:

Appendix F. Crystallographic Information for [RuH(η^6-ArOH)(PPh_3)$_2$]Cl•ArOH (12a).

Table F.1. Crystal data and structure refinement for [RuH(η^6-ArOH)(PPh_3)$_2$]Cl•ArOH (12a).

Empirical formula	C56 H59 Cl O2 P2 Ru
Formula weight	962.49
Temperature	203(2) K
Wavelength	0.71073 A
Crystal system, space group	Monoclinic, P2(1)/n
Unit cell dimensions	a = 14.0684(11) Å α = 90° b = 23.3999(19) Å β = 107.7270 (10) ° c = 14.8621(12) Å γ = 90°
Volume	4660.3(6) A^3
Z, Calculated density	4, 1.372 Mg/m^3
Absorption coefficient	0.505 mm^{-1}
F(000)	2008
Crystal size	0.1 x 0.1 x 0.1 mm
Theta range for data collection	1.68 to 28.78 deg.
Limiting indices	-18<=h<=17, 0<=k<=31, 0<=l<=20
Reflections collected / unique	41617 / 11188 [R(int) = 0.0755]
Completeness to theta = 20.81	92.2 %
Absorption correction	Semi-empirical from equivalents
Max. and min. transmission	0.928076 and 0.771026
Refinement method	Full-matrix least-squares on F^2
Data / restraints / parameters	11188 / 0 / 562
Goodness-of-fit on F^2	1.006
Final R indices [I>2sigma(I)]	R1 = 0.0428, wR2 = 0.0822
R indices (all data)	R1 = 0.0879, wR2 = 0.0903
Largest diff. peak and hole	0.532 and -0.459 $e.A^{-3}$

Table F.2. **Bond lengths [Å] and angles [°] for [RuH(η^6-ArOH)(PPh_3)$_2$]Cl•ArOH (12a).**

Ru-C(40)	2.247(3)
Ru-C(41)	2.255(3)
Ru-C(38)	2.263(3)
Ru-C(39)	2.302(3)
Ru-C(37)	2.329(3)
Ru-P(1)	2.3289(8)
Ru-P(2)	2.3319(8)
Ru-C(42)	2.438(3)
P(1)-C(12)	1.834(3)
P(1)-C(6)	1.844(3)
P(1)-C(18)	1.844(3)
P(2)-C(36)	1.834(3)
P(2)-C(24)	1.838(3)
P(2)-C(30)	1.850(3)
O(1)-C(42)	1.338(3)
O(2)-C(52)	1.364(4)
C(1)-C(6)	1.391(4)
C(1)-C(2)	1.398(4)
C(2)-C(3)	1.372(5)
C(3)-C(4)	1.376(5)
C(4)-C(5)	1.386(4)
C(5(-C(6)	1.386(4)
C(7)-C(12)	1.385(4)
C(7)-C(8)	1.397(4)
C(8)-C(9)	1.368(4)
C(9)-C(10)	1.383(5)
C(10)-C(11)	1.380(4)
C(11)-C(12)	1.396(4)
C(13)-C(14)	1.383(4)
C(13)-C(18)	1.389(4)
C(14)-C(15)	1.373(5)
C(15)-C(16)	1.382(5)
C(16)-C(17)	1.379(4)
C(17)-C(18)	1.384(4)
C(19)-C(24)	1.394(4)
C(19)-C(20)	1.398(4)
C(20)-C(21)	1.374(5)
C(21)-C(22)	1.372(4)
C(22)-C(23)	1.391(4)
C(23)-C(24)	1.389(4)
C(25)-C(26)	1.380(4)
C(25)-C(30)	1.393(4)
C(26)-C(27)	1.371(4)

C(27)-C(28)	1.369(4)
C(28)-C(29)	1.384(4)
C(29)-C(30)	1.383(4)
C(31)-C(36)	1.381(4)
C(31)-C(32)	1.391(4)
C(32)-C(33)	1.375(4)
C(33)-C(34)	1.376(4)
C(34)-C(35)	1.388(4)
C(35)-C(36)	1.387(4)
C(37)-C(42)	1.394(4)
C(37)-C(38)	1.417(4)
C(38)-C(39)	1.406(4)
C(39)-C(40)	1.429(4)
C(39)-C(43)	1.538(4)
C(40)-C(41)	1.405(4)
C(41)-C(42)	1.423(4)
C(43)-C(45)	1.528(4)
C(43)-C(44)	1.531(4)
C(43)-C(46)	1.531(4)
C(47)-C(52)	1.368(5)
C(47)-C(48)	1.410(5)
C(48)-C(49)	1.400(5)
C(49)-C(50)	1.411(4)
C(49)-C(53)	1.543(5)
C(50)-C(51)	1.345(4)
C(51)-C(52)	1.384(4)
C(53)-C(55)	1.502(5)
C(53)-C(54)	1.507(5)
C(53)-C(56)	1.533(5)

C(40)-Ru-C(41)	36.36(10)
C(40)-Ru-C(38)	64.74(10)
C(41)-Ru-C(38)	75.74(10)
C(40)-Ru-C(39)	36.61(10)
C(41)-Ru-C(39)	65.30(10)
C(38)-Ru-C(39)	35.87(10)
C(40)-Ru-C(37)	75.71(10)
C(41)-Ru-C(37)	62.21(10)
C(38)-Ru-C(37)	35.92(10)
C(39)-Ru-C(37)	64.53(10)
C(40)-Ru-P(1)	157.17(7)
C(41)-Ru-P(1)	151.57(8)
C(38)-Ru-P(1)	94.49(7)
C(39)-Ru-P(1)	120.59(7)
C(37)-Ru-P(1)	93.13(7)
C(40)-Ru-P(2)	103.89(7)

C(41)-Ru-P(2)	90.45(8)
C(38)-Ru-P(2)	166.19(7)
C(39)-Ru-P(2)	137.00(7)
C(37)-Ru-P(2)	136.58(8)
P(1)-Ru-P(2)	97.90(3)
C(40)-Ru-C(42)	63.44(10)
C(41)-Ru-C(42)	35.03(10)
C(38)-Ru-C(42)	62.44(10)
C(39)-Ru-C(42)	74.66(10)
C(37)-Ru-C(42)	33.90(10)
P(1)-Ru-C(42)	116.83(7)
P(2)-Ru-C(42)	106.11(7)
C(12)-P(1)-C(6)	100.52(13)
C(12)-P(1)-C(18)	103.92(13)
C(6)-P(1)-C(18)	102.67(13)
C(12)-P(1)-Ru	121.76(10)
C(6)-P(1)-Ru	110.35(9)
C(18)-P(1)-Ru	115.13(9)
C(36)-P(2)-C(24)	101.59(13)
C(36)-P(2)-C(30)	102.35(13)
C(24)-P(2)-C(30)	102.34(13)
C(36)-P(2)-Ru	119.69(10)
C(24)-P(2)-Ru	119.19(9)
C(30)-P(2)-Ru	109.19(9)
C(6)-C(1)-C(2)	120.7(3)
C(3)-C(2)-C(1)	119.9(3)
C(2)-C(3)-C(4)	120.0(3)
C(3)-C(4)-C(5)	120.1(3)
C(6)-C(5)-C(4)	121.2(3)
C(5)-C(6)-C(1)	118.0(3)
C(5)-C(6)-P(1)	122.0(2)
C(1)-C(6)-P(1)	119.7(2)
C(12)-C(7)-C(8)	120.8(3)
C(9)-C(8)-C(7)	119.8(3)
C(8)-C(9)-C(10)	120.2(3)
C(9)-C(10)-C(11)	120.2(3)
C(10)-C(11)-C(12)	120.5(3)
C(7)-C(12)-C(11)	118.5(3)
C(7)-C(12)-P(1)	121.8(2)
C(11)-C(12)-P(1)	119.7(2)
C(14)-C(13)-C(18)	120.8(3)
C(14)-C(15)-C(13)	120.3(3)
C(14)-C(15)-C(16)	119.3(3)
C(15)-C(16)-C(17)	120.6(3)
C(18)-C(17)-C(16)	120.6(3)
C(17)-C(18)-C(13)	118.4(3)

C(17)-C(18)-P(1)	124.1(2)
C(13)-C(18)-P(1)	117.5(2)
C(24)-C(19)-C(20)	120.4(3)
C(21)-C(20)-C(19)	119.8(3)
C(22)-C(21)-C(20)	120.4(3)
C(21)-C(22)-C(23)	120.4(3)
C(22)-C(23)-C(24)	120.3(3)
C(23)-C(24)-C(19)	118.8(3)
C(23)-C(24)-P(2)	119.3(2)
C(19)-C(24)-P(2)	121.9(2)
C(26)-C(25)-C(30)	120.5(3)
C(27)-C(26)-C(25)	121.2(3)
C(26)-C(27)-C(28)	118.9(3)
C(27)-C(28)-C(29)	120.4(3)
C(28)-C(29)-C(30)	121.4(3)
C(29)-C(30)-C(25)	117.6(3)
C(29)-C(30)-P(2)	119.6(2)
C(25)-C(30)-P(2)	122.9(2)
C(36)-C(31)-C(32)	121.5(3)
C(33)-C(32)-C(31)	119.5(3)
C(34)-C(33)-C(32)	119.9(3)
C(33)-C(34)-C(35)	120.3(3)
C(34)-C(35)-C(36)	120.7(3)
C(31)-C(36)-C(35)	118.1(3)
C(31)-C(36)-P(2)	118.5(2)
C(35)-C(36)-P(2)	123.3(2)
C(42)-C(37)-C(38)	120.6(3)
C(42)-C(37)-Ru	77.31(17)
C(38)-C(37)-Ru	69.50(16)
C(39)-C(38)-C(37)	122.2(3)
C(39)-C(38)-Ru	73.56(16)
C(37)-C(38)-Ru	74.58(16)
C(38)-C(39)-C(40)	116.8(3)
C(38)-C(39)-C(43)	121.3(3)
C(40)-C(39)-C(43)	121.8(3)
C(38)-C(39)-Ru	70.57(16)
C(40)-C(39)-Ru	69.60(15)
C(43)-C(39)-Ru	133.50(19)
C(41)-C(40)-C(39)	120.4(3)
C(41)-C(40)-Ru	72.15(15)
C(39)-C(40)-Ru	73.79(16)
C(40)-C(41)-C(42)	121.6(3)
C(40)-C(41)-Ru	71.50(15)
C(42)-C(41)-Ru	79.50(16)
O(1)-C(42)-C(37)	125.4(3)
O(1)-C(42)-C(41)	117.5(3)

C(37)-C(42)-C(41)	117.1(3)
O(1)-C(42)-Ru	137.45(19)
C(37)-C(42)-Ru	68.79(16)
C(41)-C(42)-Ru	65.47(15)
C(45)-C(43)-C(44)	110.4(3)
C(45)-C(43)-C(39)	111.8(2)
C(44)-C(43)-C(39)	106.5(3)
C(45)-C(43)-C(46)	108.2(3)
C(44)-C(43)-C(46)	108.0(3)
C(39)-C(43)-C(46)	111.9(2)
C(52)-C(47)-C(48)	117.4(3)
C(49)-C(48)-C(47)	123.7(3)
C(48)-C(49)-C(50)	114.9(3)
C(48)-C(49)-C(53)	123.0(3)
C(50)-C(49)-C(53)	122.1(3)
C(51)-C(50)-C(49)	122.1(3)
C(50)-C(51)-C(52)	121.4(3)
O(2)-C(52)-C(47)	166.6(3)
O(2)-C(52)-C(51)	123.0(3)
C(47)-C(52)-C(51)	120.5(3)
C(55)-C(53)-C(54)	107.7(4)
C(55)-C(53)-C(56)	107.2(4)
C(54)-C(53)-C(56)	108.5(3)
C(55)-C(53)-C(49)	108.7(3)
C(54)-C(53)-C(49)	111.7(3)
C(56)-C(53)-C(49)	112.8(3)

Symmetry transformations used to generate equivalent atoms:

Appendix G. Crystallographic Information for $2K[Ru(OAr)_3(CO)_2(PPh_3)]_2$ (17)

Table G.1. Crystal data and structure refinement for $2K[Ru(OAr)_3(CO)_2(PPh_3)]_2$ (17)

Empirical formula	C108.73 H108 K2 O10 P2 Ru2
Formula weight	1916.96
Temperature	203(2) K
Wavelength	0.71073 A
Crystal system, space group	Monoclinic, P2(1)/n
Unit cell dimensions	a = 17.3604(13) Å $\alpha = 90°$ b = 28.575(2) Å $\beta = 93.5510(10)°$ c = 23.3644(17) Å $\gamma = 90°$
Volume	11568.4(15) A^3
Z, Calculated density	4, 1.101 Mg/m^3
Absorption coefficient	0.409 mm^{-1}
F(000)	3985
Crystal size	0.2 x 0.12 x 0.08 mm
Theta range for data collection	1.13 to 28.77 deg.
Limiting indices	-22<=h<=22, 0<=k<=38, 0<=l<=30
Reflections collected / unique	90770 / 27631 [R(int) = 0.0730]
Completeness to theta = 24.71	91.8 %
Absorption correction	Semi-empirical from equivalents
Max. and min. transmission	0.928077 and 0.644708
Refinement method	Full-matrix least-squares on F^2
Data / restraints / parameters	27631 / 216 / 1151
Goodness-of-fit on F^2	1.027
Final R indices [I>2sigma(I)]	R1 = 0.0749, wR2 = 0.2189
R indices (all data)	R1 = 0.1396, wR2 = 0.2504
Largest diff. peak and hole	1.088 and –1.724 $e.A^{-3}$

Table G.2. Bond lengths [Å] and angles [°] for $2K[Ru(OAr)_3(CO)_2(PPh_3)]_2$ (17)

Ru(1)-C(61)	1.865(6)
Ru(1)-C(62)	1.868(6)
Ru(1)-O(3)	2.075(4)
Ru(1)-O(1)	2.083(4)
Ru(1)-O(2)	2.119(4)
Ru(1)-P(1)	2.3617(15)
Ru(1)-K(1)	3.9286(15)
Ru(1)-K(2)	4.0089(13)
Ru(2)-C(63)	1.851(6)
Ru(2)-C(64)	1.868(6)
Ru(2)-O(6)	2.084(4)
Ru(2)-O(5)	2.082(4)
Ru(2)-O(4)	2.102(4)
Ru(2)-P(2)	2.3678(15)
Ru(2)-K(1)	3.9679(15)
Ru(2)-K(2)	4.0054(13)
K(1)-O(5)	2.577(4)
K(1)-O(1)	2.581(4)
K(1)-O(2)	2.896(4)
K(1)-O(4)	2.955(4)
K(1)-C(36)	3.096(5)
K(1)-C(16)	3.099(5)
K(1)-C(35)	3.235(6)
K(1)-C(46)	3.245(6)
K(1)-C(15)	3.265(5)
K(1)-C(6)	3.277(6)
K(1)-C(41)	3.307(7)
K(1)-C(5)	3.332(6)
K(2)-O(6)	2.644(4)
K(2)-O(3)	2.678(4)
K(2)-O(2)	2.797(4)
K(2)-O(4)	2.813(4)
K(2)-C(56)	3.369(5)
K(2)-C(81)	3.422(6)
K(2)-C(80)	3.444(7)
K(2)-C(83)	3.471(7)
K(2)-C(26)	3.474(5)
P(1)-C(82)	1.809(6)
P(1)-C(76)	1.822(6)
P(1)-C(70)	1.827(6)
P(2)-C(88)	1.811(6)
P(2)-C(100)	1.831(6)
P(2)-C(94)	1.831(6)
O(1)-C(6)	1.341(6)

O(2)-C(16)	1.365(6)
O(3)-C(26)	1.345(6)
O(4)-C(36)	1.340(6)
O(5)-C(46)	1.339(7)
O(6)-C(56)	1.339(6)
O(7)-C(61)	1.144(7)
O(8)-C(62)	1.141(7)
O(9)-C(63)	1.154(7)
O(10)-C(64)	1.136(7)
C(1)-C(2)	1.373(9)
C(1)-C(6)	1.390(8)
C(2)-C(3)	1.377(11)
C(3)-C(4)	1.388(11)
C(3)-C(7)	1.552(9)
C(4)-C(5)	1.390(8)
C(5)-C(6)	1.402(8)
C(7)-C(9)	1.481(18)
C(7)-C(10)	1.535(17)
C(7)-C(8)	1.506(17)
C(11)-C(12)	1.394(8)
C(11)-C(16)	1.402(7)
C(12)-C(13)	1.377(9)
C(13)-C(14)	1.371(8)
C(13)-C(17)	1.541(8)
C(14)-C(15)	1.403(7)
C(15)-C(16)	1.349(8)
C(17)-C(19)	1.502(8)
C(17)-C(18)	1.531(8)
C(17)-C(20)	1.540(9)
C(21)-C(26)	1.389(8)
C(21)-C(22)	1.405(8)
C(22)-C(23)	1.378(9)
C(23)-C(24)	1.392(9)
C(23)-C(27)	1.542(8)
C(24)-C(25)	1.388(8)
C(25)-C(26)	1.395(8)
C(27)-C(29)	1.499(9)
C(27)-C(28)	1.503(9)
C(27)-C(30)	1.522(10)
C(31)-C(32)	1.382(8)
C(31)-C(36)	1.397(7)
C(32)-C(33)	1.377(8)
C(33)-C(34)	1.398(8)
C(33)-C(37)	1.539(8)
C(34)-C(35)	1.402(8)
C(35)-C(36)	1.408(8)

C(37)-C(39)	1.474(9)
C(37)-C(38)	1.511(8)
C(37)-C(40)	1.539(9)
C(41)-C(42)	1.377(9)
C(41)-C(46)	1.398(8)
C(42)-C(43)	1.395(9)
C(43)-C(44)	1.394(9)
C(43)-C(47)	1.523(9)
C(44)-C(45)	1.372(9)
C(45)-C(46)	1.401(8)
C(47)-C(49)	1.484(9)
C(47)-C(48)	1.516(9)
C(47)-C(50)	1.543(9)
C(51)-C(52)	1.393(9)
C(51)-C(56)	1.394(9)
C(52)-C(53)	1.384(12)
C(53)-C(54)	1.372(12)
C(53)-C(57)	1.531(10)
C(54)-C(55)	1.382(9)
C(55)-C(56)	1.390(8)
C(57)-C(59)	1.440(12)
C(57)-C(58)	1.487(12)
C(57)-C(60)	1.516(13)
C(65)-C(70)	1.390(9)
C(65)-C(66)	1.403(9)
C(66)-C(67)	1.377(11)
C(67)-C(68)	1.351(11)
C(68)-C(69)	1.409(9)
C(69)-C(70)	1.386(8)
C(71)-C(76)	1.390(8)
C(71)-C(72)	1.396(9)
C(72)-C(73)	1.381(10)
C(73)-C(74)	1.364(9)
C(74)-C(75)	1.387(8)
C(75)-C(76)	1.395(8)
C(77)-C(82)	1.382(9)
C(77)-C(78)	1.388(10)
C(78)-C(79)	1.385(11)
C(79)-C(80)	1.342(11)
C(80)-C(81)	1.377(9)
C(81)-C(82)	1.388(8)
C(83)-C(88)	1.381(9)
C(83)-C(84)	1.418(11)
C(84)-C(85)	1.355(14)
C(85)-C(86)	1.341(14)
C(86)-C(87)	1.412(11)

C(87)-C(88)	1.387(10)
C(89)-C(90)	1.366(9)
C(89)-C(94)	1.395(8)
C(90)-C(91)	1.365(11)
C(91)-C(92)	1.357(10)
C(92)-C(93)	1.385(8)
C(93)-C(94)	1.368(9)
C(95)-C(100)	1.381(8)
C(95)-C(96)	1.388(9)
C(96)-C(97)	1.393(10)
C(97)-C(98)	1.345(9)
C(98)-C(99)	1.401(8)
C(99)-C(100)	1.396(8)
C(200)-C(216)	1.15(3)
C(200)-C(208)	1.31(3)
C(201)-C(208)	1.92(4)
C(202)-C(214)	1.31(3)
C(202)-C(205)	1.40(3)
C(203)-C(206)	1.30(3)
C(204)-C(207)	1.39(3)
C(205)-C(218)	1.16(4)
C(207)-C(213)	1.33(3)
C(209)-C(215)	1.17(4)
C(209)-C(217)	1.48(5)
C(210)-C(212)	1.07(5)
C(211)-C(215)	1.75(5)
C(212)-C(218)	1.65(5)
C(213)-C(213)#1	1.47(4)

C(61)-Ru(1)-C(62)	87.1(3)
C(61)-Ru(1)-O(3)	174.3(2)
C(62)-Ru(1)-O(3)	98.5(2)
C(61)-Ru(1)-O(1)	97.2(2)
C(62)-Ru(1)-O(1)	94.6(2)
O(3)-Ru(1)-O(1)	83.82(15)
C(61)-Ru(1)-O(2)	95.7(2)
C(62)-Ru(1)-O(2)	176.04(19)
O(3)-Ru(1)-O(2)	78.76(14)
O(1)-Cru(1)-O(2)	82.35(14)
C(61)-Ru(1)-P(1)	93.42(19)
C(62)-Ru91)-P(1)	89.33(17)
O(3)-Ru(1)-P(1)	85.27(11)
O(1)-Ru(1)-P(1)	168.85(11)
O(2)-Ru(1)-P(1)	93.25(11)
C(61)-Ru(1)-K(1)	103.89(18)
C(62)-Ru(1)-K(1)	130.46(16)

O(3)-RU(1)-K(1)	73.57(11)
O(1)-Ru(1)-K(1)	36.76(10)
O(2)-Ru(1)-K(1)	46.14(10)
P(1)-Ru(1)-K(1)	136.53(4)
C(61)-Ru(1)-K(2)	136.94(18)
C(62)-Ru(1)-K(2)	135.92(19)
O(3)-Ru(1)-K(2)	37.45(10)
O(1)-Ru(1)-K(2)	83.48(10)
O(2)-Ru(1)-K(2)	41.43(9)
P(1)-Ru(1)-K(2)	86.45(4)
K(1)-Ru(1)-K(2)	53.88(3)
C(63)-Ru(2)-C(64)	87.7(3)
C(63)-Ru(2)-O(6)	176.0(2)
C(64)-Ru(2)-O(6)	96.2(2)
C(63)-Ru(2)-O(5)	96.0(2)
C(64)-Ru(2)-O(5)	93.7(2)
O(6)-Ru92)-O(5)	84.96(16)
C(63)-Ru(2)-O(4)	97.9(2)
C(64)-Ru(2)-O(4)	173.4(2)
O(6)-Ru(2)-O(4)	78.34(14)
O(5)-Ru(2)-O(4)	82.27(15)
C(63)-Ru(2)-P(2)	94.14(18)
C(64)-Ru(2)-P(2)	90.79(18)
O(6)-Ru(2)-P(2)	84.65(11)
O(5)-Ru(2)-P(2)	169.07(12)
O(4)-Ru(2)-P(2)	92.30(11)
C(63)-Ru(2)-K(1)	100.92(17)
C(64)-Ru(2)-K(1)	128.83(18)
O(6)-Ru(2)-K(1)	77.59(11)
O(5)-Ru(2)-K(1)	35.59(10)
O(4)-Ru(2)-K(1)	46.75(11)
P(2)-Ru(2)-K(1)	137.66(4)
C(63)-Ru(2)-K(2)	139.69(17)
C(64)-Ru(2)-K(2)	132.38(19)
O(6)-Ru(2)-k92)	36.63(10)
O(5)-Ru(2)-K(2)	79.44(11)
O(4)-Ru(2)-K(2)	41.83(10)
P(2)-Ru(2)-K(2)	90.18(4)
K(1)-Ru(2)-K(2)	53.62(3)
O(5)-K(1)-O(1)	169.32(15)
O(5)-K(1)-O(2)	110.30(13)
O(1)-K(1)-O(2)	60.35(11)
O(5)-K(1)-O(4)	59.20(11)
O(1)-K(1)-O(4)	115.23(12)
O(2)-K(1)-O(4)	99.29(11)
O(5)-K(1)-C(36)	75.87(13)

O(1)-K(1)-C(36)	102.43(14)
O(2)-K(1)-C(36)	113.12(13)
O(4)-K(1)-C(36)	25.45(12)
O(5)-K(1)-C(16)	98.55(14)
O(1)-K(1)-C(16)	74.96(13)
O(2)-K(1)-C(16)	26.05(12)
O(4)-K(1)-C(16)	114.01(14)
C(36)-K(1)-C(16)	134.49(16)
O(5)-K(1)-C(35)	74.57(13)
O(1)-K(1)-C(35)	108.55(14)
O(2)-K(1)-C(35)	138.17(14)
O(4)-K(1)-C(35)	45.82(13)
C(35)-K(1)-C(35)	25.58(14)
C(16)-K(1)-C(35)	159.55(16)
O(5)-K(1)-C(46)	23.16(13)
O(1)-K(1)-C(46)	163.96(14)
O(2)-K(1)-C(46)	118.15(13)
O(4)-K(1)-C(46)	80.76(12)
C(36)-K(1)-C(46)	92.79(14)
C(16)-K(1)-C(46)	98.02(14)
C(35)-K(1)-C(46)	83.15(14)
O(5)-K(1)-C(15)	106.32(14)
O(1)-K(1)-C(15)	71.27(13)
O(2)-K(1)-C(15)	45.27(12)
O(4)-K(1)-C(15)	137.90(14)
C(36)-K(1)-C(15)	158.15(16)
C(16)-K(1)-C(15)	24.29(15)
C(35)-K(1)-C(15)	176.15(17)
C(46)-K(1)-C(15)	96.30(14)
O(5)-K(1)-C(6)	167.93(15)
O(1)-K(1)-C(6)	22.73(13)
O(2)-K(1)-C(6)	80.89(12)
O(4)-K(1)-C(6)	124.98(13)
C(36)-K(1)-C(6)	104.42(15)
C(16)-K(1)-C(6)	89.78(14)
C(35)-K(1)-C(6)	100.35(15)
C(46)-K(1)-C(6)	147.01(15)
C(15)-K(1)-C(6)	78.03(15)
O(5)-K(1)-C(41)	44.78(13)
O(1)-K(1)-C(41)	139.71(15)
O(2)-K(1)-C(41)	105.80(14)
O(4)-K(1)-C(41)	103.97(13)
C(36)-K(1)-C(41)	117.37(15)
C(16)-K(1)-C(41)	81.19(15)
C(35)-K(1)-C(41)	105.14(15)
C(46)-K(1)-C(41)	24.62(13)

C(15)-K(1)-C(41)	73.63(14)
C(6)-K(1)-C(41)	129.20(16)
O(5)-K(1)-C(5)	145.05(15)
O(1)-K(1)-C(5)	44.48(13)
O(2)-K(1)-C(5)	104.63(13)
O(4)-K(1)-C(5)	114.22(13)
C(36)-K(1)-C(5)	89.52(15)
C(16)-K(1)-C(5)	113.83(15)
C(35)-K(1)-C(5)	79.73(15)
C(46)-K(1)-C(5)	131.94(15)
C(15)-K(1)-C(5)	98.95(16)
C(6)-K(1)-C(5)	24.47(14)
C(41)-K(1)-C(5)	125.57(16)
O(6)-K(2)-O(3)	154.57(13)
O(6)-K(2)-O(2)	107.56(12)
O(3)-K(2)-O(2)	58.11(11)
O(6)-K(2)-O(4)	57.86(11)
O(3)-K(2)-O(4)	103.17(12)
O(2)-K(2)-O(4)	105.27(12)
O(6)-K(2)-C(56)	21.74(12)
O(3)-K(2)-C(56)	154.94(13)
O(2)-K(2)-C(56)	97.07(12)
O(4)-K(2)-C(56)	78.59(12)
O(6)-K(2)-C(81)	114.04(13)
O(3)-K(2)-C(81)	77.52(13)
O(2)-K(2)-C(81)	57.38(14)
O(4)-K(2)-C(81)	159.64(14)
C(56)-K(2)-C(81)	92.32(13)
O(6)-K(2)-C(80)	97.91(14)
O(3(0K(2)-C(80)	98.61(14)
O(2)-K(2)-C(80)	76.96(15)
O(4)-K(2)-C(80)	155.49(14)
C(56)-K(2)-C(80)	76.93(15)
C(81)-K(2)-C(80)	23.13(15)
O(6)-K(2)-C(83)	72.43(13)
O(3)-K(2)-C(83)	113.60(14)
O(2)-K(2)-C(83)	160.47(16)
O(4)-K(2)-C(83)	57.50(15)
C(56)-K(2)-C(83)	88.71(14)
C(81)-K(2)-C(83)	141.31(18)
C(80)-K(2)-C(83)	122.56(19)
O(6)-K(2)-C(26)	150.81(13)
O(3)-K(2)-C(26)	20.46(11)
O(2)-K(2)-C(26)	77.68(12)
O(4)-K(2)-C(26)	92.96(12)
C(56)-K(2)-C(26)	168.63(15)

C(81)-K(2)-C(26)	93.22(13)
C(80)-K(2)-C(26)	111.17(15)
C(83)-K(2)-C(26)	93.15(14)
O(6)-K(2)-K(1)	79.72(9)
O(3)-K(2)-K(1)	75.02(9)
O(2)-K(1)-K(2)	52.06(8)
O(4)-K(2)-K(1)	53.21(8)
C(56)-K(2)-K(1)	86.99(11)
C(81)-K(2)-K(1)	108.67(12)
C(80)-K(2)-K(1)	124.03(14)
C(83)-K(2)-K(1)	110.01(14)
C(26)-K(2)-K(1)	81.83(10)
O(6)-K(2)-Ru(2)	28.05(8)
O(3)-K(2)-Ru(2)	130.40(9)
O(2)-K(2)-Ru(2)	107.22(8)
O(4)-K(2)-Ru(2)	29.89(7)
C(56)-K(2)-Ru(2)	48.77(10)
C(81)-K(2)-Ru(2)	138.55(11)
C(80)-K(2)-Ru(2)	125.68(12)
C(83)-K(2)-Ru(2)	63.20(11)
C(26)-K(2)-Ru(2)	122.77(9)
K(1)-K(2)-Ru(2)	62.65(3)
O(6)-K(2)-Ru(1)	135.24(10)
O(3)-K(2)-Ru(1)	28.10(8)
O(2)-K(2)-Ru(1)	30.09(7)
O(4)-K(2)-Ru(1)	107.90(8)
C(56)-K(2)-Ru(1)	127.16(10)
C(81)-K(2)-Ru(1)	63.28(10)
C(80)-K(2)-Ru(1)	86.40(12)
C(83)-K(2)-Ru(1)	140.07(12)
C(26)-K(2)-Ru(1)	48.13(9)
K(1)-K(2)-Ru(1)	61.92(3)
Ru(2)-K(2)-Ru(1)	124.58(4)
C(82)P(1)-C(76)	105.6(3)
C(82)-P(1)-C(70)	104.4(3)
C(76)-P(1)-C(70)	102.4(2)
C(82)-P(1)-Ru(1)	109.87(18)
C(76)-P(1)-Ru(1)	115.27(18)
C(70)-P(1)-Ru(1)	118.0(2)
C(88)-P(2)-C(100)	104.3(3)
C(88)-P(2)-C(94)	105.0(3)
C(100)-P(2)-C(94)	101.9(2)
C(88)-P(2)-Ru(2)	110.6(2)
C(100)-P(2)-Ru(2)	114.62(18)
C(94)-P(2)-Ru(2)	119.0(2)
C(6)-O(1)-Ru(1)	132.2(3)

C(6)-O(1)-K(1)	109.2(3)
Ru(1)-O(1)-K(1)	114.37(16)
C(16)-O(2)-Ru(1)	128.8(3)
C(16)-O(2)-K(2)	125.4(3)
Ru(1)-O(2)-K(2)	108.48(13)
C(16)-O(2)-K(1)	85.3(3)
Ru(1)-O(2)-K(1)	102.01(13)
K(2)-O(2)-K(1)	78.33(10)
C(26)-O(3)-Ru(1)	128.1(3)
C(26)-O(3)-K(2)	115.4(3)
Ru(1)-O(3)-K(2)	114.45(15)
C(36)-O(4)-Ru(2)	129.1(3)
C(36)-O(4)-K(2)	122.0(3)
Ru(2)-O(4)-K(2)	108.27(14)
C(36)-O(4)-K(1)	83.2(3)
Ru(2)-O(4)-K(1)	102.04(14)
K(2)-O(4)-K(1)	77.10(10)
C(46)-O(5)-Ru(2)	131.6(3)
C(46)-O(5)-K(1)	107.6(3)
Ru(2)-O(5)-K(1)	116.37(16)
C(56)-O(6)-Ru(2)	128.5(4)
C(56)-O(6)-K(2)	111.3(3)
Ru(2)-O(6)-K(2)	115.32(15)
C(2)-C(1)-C(6)	120.7(7)
C(1)-C(2)-C(3)	123.4(7)
C(4)-C(3)-C(2)	116.1(6)
C(4)-C(3)-C(7)	119.7(8)
C(2)-C(3)-C(7)	124.2(8)
C(3)-C(4)-C(5)	121.9(7)
C(4)-C(5)-C(6)	120.8(6)
C(4)-C(5)-K(1)	142.5(4)
C(6)-C(5)-K(1)	75.6(3)
O(1)-C(6)-C(1)	125.7(5)
O(1)-C(6)-C(5)	117.4(5)
C(1)-C(6)-C(5)	116.9(5)
O(1)-C(6)-K(1)	48.0(2)
C(1)-C(6)-K(1)	144.9(4)
C(5)-C(6)-K(1)	80.0(3)
(9)-C(7)-C(3)	106(10)
C(9)-C(7)-C(10)	109(3)
C(3)-C(7)-C(10)	113(10)
C(9)-C(7)-C(8)	112.(3)
C(3)-C(7)-C(8)	112(10)
C(10)-C(7)-C(8)	105(2)
C(12)-C(11)-C(16)	119.2(5)
C(13)-C(12)-C(11)	123.2(5)

C(14)-C(13)-C(12)	116.3(5)
C(14)-C(13)-C(17)	123.6(6)
C(12)-C(13)-C(17)	120.2(5)
C(13)-C(14)-C(15)	121.4(6)
C(16)-C(15)-C(14)	122.0(5)
C(16)-C(15)-K(1)	70.9(3)
C(14)-C(15)-K(1)	125.8(4)
C(15)-C(16)-o92)	123.9(5)
C(15)-C(16)-C(11)	117.9(5)
O(2)-C(16)-C(11)	118.1(5)
C(15)-C(16)-K(1)	84.8(3)
O(2)-C(16)-K(1)	68.7(2)
C(11)-C(16)-K(1)	116.2(3)
C(19)-C(17)-C(13)	109.0(5)
C(19)-C(17)-C(18)	109.7(6)
C(13)-C(17)-C(18)	109.9(5)
C(19)-C(17)-C(20)	109.6(6)
C(13)-C(17)-C(20)-	111.0(5)
C(18)-C(17)-C(20)	107.6(6)
C(26)-C(21)-C(22)	120.9(5)
C(23)-C(22)-C(21)	121.6(6)
C(22)-C(23)-C(24)	117.4(5)
C(22)-C(23)-C(27)	123.6(6)
C(24)-C(23)-C(27)	119.0(6)
C(23)-C(24)-C(25)	121.4(6)
C(24)-C(25)-C(26)	121.5(6)
O(3)-C(26)-C(21)	124.6(5)
O(3)-C(26)-C(25)	118.2(5)
C(21)-C(26)-C(25)	117.2(5)
O(3)-C(26)-K(2)	44.1(2)
C(21)-C(26)-K(2)	143.1(4)
C(25)-C(26)-K(2)	86.3(3)
C(29)-C(27)-C(28)	111.7(7)
C(29)-C(27)-C(23)	110.7(6)
C(28)-C(27)-C(23)	110.8(6)
C(29)-C(27)-C(30)	107.6(8)
C(28)-C(27)-C(30)	107.7(7)
C(23)-C(27)-C(30)	108.8(6)
C(32)-C(31)-C(36)	121.7(5)
C(31)-C(32)-C(33)	122.6(5)
C(32)-C(33)-C(34)	116.6(5)
C(32)-C(33)-C(37)	122.7(5)
C(34)-C(33)-C(37)	120.8(6)
C(33)-C(34)-C(35)	121.8(6)
C(34)-C(35)-C(36)	120.7(5)
C(34)-C(35)-K(1)	123.2(4)

C(36)-C(35)-K(1)	71.7(3)
O(4)-C(36)-C(31)	119.7(5)
O(4)-C(36)-C(35)	123.7(5)
C(31)-C(36)-C(35)	116.4(5)
O(4)-C(36)-K(1)	71.4(3)
C(31)-C(36)-K(1)	114.2(4)
C(35)-C(36)-K(1)	82.7(3)
C(39)-C(37)-C(38)	111.2(7)
C(39)-C(37)-C(33)	110.7(6)
C(38)-C(37)-C(33)	109.6(5)
C(39)-C(37)-C(40)	109.5(8)
C(38)-C(37)-C(40)	105.0(7)
C(33)-C(37)-C(40)	110.7(6)
C(42)-C(41)-C(46)	120.9(6)
C(42)-C(41)-K(1)	141.2(5)
C(46)-C(41)-K(1)	75.2(3)
C(41)-C(42)-C(43)	123.5(6)
C(42)-C(43)-C(44)	114.4(6)
C(42)-C(43)-C(47)	121.8(6)
C(44)-C(43)-C(47)	123.8(6)
C(45)-C(44)-C(43)	123.6(6)
C(44)-C(45)-C(46)	121.1(6)
O(5)-C(46)-C(41)	117.5(5)
O(5)-C(46)-C(45)	126.0(5)
C(41)-C(46)-C(45)	116.4(5)
O(5)-C(46)-K(1)	49.9(2)
C(41)-C(46)-K(1)	80.2(4)
C(45)-C(46)-K(1)	143.0(4)
C(49)-C(47)-C(43)	109.0(6)
C(49)-C(47)-C(48)	110.1(8)
C(43)-C(47)-C(48)	112.1(6)
C(49)-C(47)-C(50)	110.5(8)
C(43)-C(47)-C(50)	111.2(6)
C(48)-C(47)-C(50)	103.9(7)
C(52)-C(51)-C(56)	121.3(7)
C(53)-C(52)-C(51)	121.7(8)
C(54)-C(53)-C(52)	115.8(6)
C(54)-C(53)-C(57)	122.0(9)
C(52)-C953)-C(57)	122.3(9)
C(53)-C(54)-C955)	124.2(7)
C(54)-C(55)-C(56)	119.8(7)
O(6)-C(56)-C(55)	124.6(6)
O(6)-C(56)-C(51)	118.2(5)
C(55)-C(56)-C(51)	117.2(5)
O(6)-C(56)-K(2)	47.0(2)
C(55)-C(56)-K(2)	133.6(4)

C(51)-C(56)-K(2)	89.0(4)
C(59)-C(57)-C(58)	117.6(13)
C(59)-C(57)-C(60)	109.0(14)
C(58)-C(57)-C(60)	101.3(11)
C(59)-C(57)-C(53)	108.5(8)
C(58)-C(57)-C(53)	112.5(9)
C(60)-C(57)-C(53)	107.3(9)
O(7)-C(61)-Ru(1)	177.9(6)
O(8)-C(62)-Ru(1)	175.9(6)
O(9)-C(63)-Ru(2)	178.2(5)
O(10)-C(64)-Ru(2)	177.7(6)
C(70)-C(65)-C(66)	120.2(7)
C(67)-C(66)-C(65)	120.4(7)
C(68)-C(67)-C(66)	119.5(6)
C(67)-C(68)-C(69)	121.4(7)
C(70)-C(69)-C(68)	119.7(7)
C(69)-C(70)-C(65)	118.8(6)
C(69)-C(70)-P(1)	122.9(5)
C(65)-C(70)-P(1)	118.1(5)
C(76)-C71)-C(72)	120.4(6)
C(73)-C(72)-C(71)	120.6(6)
C(74)-C(73)-C(72)	119.3(6)
C(73)-C(740-C(75)	120.8(6)
C(74)-C(75)-C(76)	120.9(6)
C(71)-C(76)-C(75)	118.0(5)
C(71)-C(76)-P(1)	121.1(4)
C(75)-C(76)-P(1)	121.0(4)
C(82)-C(77)-C(78)	120.0(6)
C(79)-C(78)-C(77)	120.4(7)
C(80)-C(79)-C(78)	119.7(7)
C(79)-C(80)-C(81)	120.6(7)
C(79)-C(80)-K(2)	85.3(5)
C(81)-C(80)-K(2)	77.6(4)
C(80)-C(81)-C(82)	121.3(6)
C(80)-C(81)-K(2)	79.3(4)
C(82)-C(81)-K(2)	85.3(3)
C(77)-C(82)-C(81)	118.1(6)
C(77)-C(82)-P(1)	122.8(5)
C(81)-C(82)-P(1)	119.1(5)
C(88)-C(83)-C(84)	119.3(8)
C(88)-C(83)-K(2)	93.0(4)
C(84)-C(83)-K(2)	82.3(4)
C(85)-C(84)-C(83)	121.6(8)
C(86)-C(85)-C(84)	118.8(9)
C(85)-C(86)-C(87)	121.9(10)
C(88)-C(87)-C(86)	119.5(8)

C(83)-C(88)-C(87)	118.7(7)
C(83)-C(88)-P(2)	119.4(6)
C(87)-C(88)-P(2)	121.9(5)
C(90)-C(89)-C(94)	121.4(7)
C(91)-C(90)-C(89)	120.5(7)
C(90)-C(91)-C(92)	118.8(6)
C(91)-C(92)-C(93)	121.3(7)
C(94)-C(93)-C(92)	120.7(7)
C(93)-C(94)-C(89)	117.3(6)
C(93)-C(94)-P(2)	118.6(5)
C(89)-C(94)-P(2)	123.9(5)
C(100)-C(95)-C(96)	120.6(6)
C(97)-C(96)-C(95)	120.0(7)
C(98)-C(97)-C(96)	119.8(6)
C(97)-C(98)-C(99)	121.0(6)
C(100)-C(99)-C(98)	119.7(6)
C(95)-C(100)-C(99)	118.8(5)
C(95)-C(100)-P(2)	122.2(4)
C(99)-C(100)-P(2)	119.0(4)
C(216)-C(200)-C(208)	122(3)
C(214)-C(202)-C(205)	112(3)
C(218)-C(205)-C(202)	132(4)
C(213)-C(207)-C(204)	137(3)
C(200)-C(208)-C(201)	94(2)
C(215)-C(209)-C(217)	127(4)
C(210)-C(212)-C(218)	132(5)
C(207)-C(213)-C(213)#1	135(3)
C(209)-C(215)-C(211)	133(4)
C(205)-C(218)-C(212)	145(4)

Symmetry transformations used to generate equivalent atoms: #1 –x-1, -y+1, -z+1

Appendix H. Crystallographic Information for $Ru_2Cl_4(dppb)_2(N{\equiv}CPh)$ (43).

Table H.1. Crystal data and structure refinement for $Ru_2Cl_4(dppb)_2(N{\equiv}CPh)$ (43).

Empirical formula	C67 H71 Cl4 N O P4 Ru2
Formula weight	1374.07
Temperature	203(2) K
Wavelength	0.71073 A
Crystal system, space group	Orthorhombic, Pca2(1)
Unit cell dimensions	a = 26.699(2) Å $\alpha = 90°$ b = 18.830(1) Å $\beta = 90°$ c = 13.226(1) Å $\gamma = 90°$
Volume	6649.4(8) A^3
Z, Calculated density	4, 1.373 Mg/m^3
Absorption coefficient	0.752 mm^{-1}
F(000)	2816
Crystal size	0.2 x 0.1 x 0.1 mm
Theta range for data collection	2.03 to 24.71 deg.
Limiting indices	0<=h<=31, 0<=k<=22, -15<=l<=15
Reflections collected / unique	52378 / 11270 [R(int) = 0.0980]
Completeness to theta = 24.71	99.6 %
Absorption correction	Semi-empirical from equivalents
Max. and min. transmission	0.801532 and 0.727277
Refinement method	Full-matrix least-squares on F^2
Data / restraints / parameters	11270 / 10 / 579
Goodness-of-fit on F^2	1.054
Final R indices [I>2sigma(I)]	R1 = 0.0477, wR2 = 0.1113
R indices (all data)	R1 = 0.0747, wR2 = 0.1194
Absolute structure parameter	0.00(4)
Largest diff. peak and hole	0.933 and -0.459 $e.A^{-3}$

Table H.2. Bond lengths [Å] and angles [°] for $Ru_2Cl_4(dppb)_2(N{\equiv}CPh)$ (43).

Ru(1)-N(1)	2.009(7)
Ru(1)-P(2)	2.266(2)
Ru(1)-P(1)	2.274(2)
Ru(1)-Cl(3)	2.4007(19)
Ru(1)-Cl(2)	2.4747(19)
Ru(1)-Cl(4)	2.4804(18)
Ru(2)-P(3)	2.239(2)
Ru(2)-P(4)	2.2695(19)
Ru(2)-Cl(1)	2.4120(19)
Ru(2)-Cl(4)	2.4189(18)
Ru(2)-Cl(3)	2.5348(19)
Ru(2)-Cl(2)	2.5359(18)
N(1)-C(7)	1.105(11)
P(1)-C(13)	1.836(5)
P(1)-C(19)	1.844(4)
P(1)-C(20)	1.848(8)
P(2)-C(23)	1.815(8)
P(2)-C(29)	1.837(4)
P(2)-C(35)	1.855(4)
P(3)-C(47)	1.822(4)
P(3)-C(48)	1.837(8)
P(3)-C(41)	1.854(4)
P(4)-C(51)	1.838(7)
P(4)-C(57)	1.852(5)
P(4)-C(63)	1.857(4)
C(1)-C(2)	1.3900
C(1)-C(6)	1.3900
C(2)-C(3)	1.3900
C(3)-C(4)	1.3900
C(4)-C(5)	1.3900
C(5)-C(6)	1.3900
C(6)-C(7)	1.431(13)
C(8)-C(9)	1.3900
C(8)-C(13)	1.3900
C(9)-C(10)	1.3900
C(10)-C(11)	1.3900
C(11)-C(12)	1.3900
C(12)-C(13)	1.3900
C(14)-C(15)	1.3900
C(14)-C(19)	1.3900
C(15)-C(16)	1.3900
C(16)-C(17)	1.3900
C(17)-C(18)	1.3900
C(18)-C(19)	1.3900
C(20)-C(21)	1.518(11)

C(21)-C(22)	1.532(11)
C(22)-C(23)	1.521(11)
C(24)-C(25)	1.3900
C(24)-C(29)	1.3900
C(25)-C(26)	1.3900
C(26)-C(27)	1.3900
C(27)-C(28)	1.3900
C(28)-C(29)	1.3900
C(30)-C(31)	1.3900
C(30)-C(35)	1.3900
C(31)-C(32)	1.3900
C(32)-C(33)	1.3900
C(33)-C(34)	1.3900
C(34)-C(35)	1.3900
C(36)-C(37)	1.3900
C(36)-C(41)	1.3900
C(37)-C(38)	1.3900
C(38)-C(39)	1.3900
C(39)-C(40)	1.3900
C(40)-C(41)	1.3900
C(42)-C(43)	1.3900
C(42)-C(47)	1.3900
C(43)-C(44)	1.3900
C(44)-C(45)	1.3900
C(45)-C(46)	1.3900
C(46)-C(47)	1.3900
C(48)-C(49)	1.559(11)
C(49)-C(50)	1.518(12)
C(50)-C(51)	1.559(10)
C(52)-C(53)	1.3900
C(52)-C(57)	1.3900
C(53)-C(54)	1.3900
C(54)-C(55)	1.3900
C(55)-C(56)	1.3900
C(56)-C(57)	1.3900
C(58)-C(59)	1.3900
C(58)-C(63)	1.3900
C(59)-C(60)	1.3900
C(60)-C(61)	1.3900
C(61)-C(62)	1.3900
C(62)-C(63)	1.3900
O(1)-C(64)	1.22(3)
O(1)-C(66)	1.27(3)
C(64)-C(65)	1.64(3)
C(66)-C(67)	1.62(3)

N(1)-Ru(1)-P(2)	93.95(18)
N(1)-Ru(1)-P(1)	95.08(18)
P(2)-Ru(1)-P(1)	94.56(8)
N(1)-Ru(1)-Cl(3)	168.47(18)
P(2)-Ru(1)-Cl(3)	95.90(7)
P(1)-Ru(1)-Cl(3)	90.10(7)
N(1)-Ru(1)-Cl(2)	88.77(18)
P(2)-Ru(1)-Cl(2)	92.66(7)
P(1)-Ru(1)-Cl(2)	171.56(7)
Cl(3)-Ru(1)-Cl(2)	84.81(6)
N(1)-Ru(1)-Cl(4)	88.72(18)
P(2)-Ru(1)-Cl(4)	170.98(7)
P(1)-Ru(1)-Cl(4)	93.78(7)
Cl(3)-Ru(1)-Cl(4)	80.65(6)
Cl(2)-Ru(1)-Cl(4)	78.77(6)
P(3)-Ru(2)-P(4)	92.99(7)
P(3)-Ru(2)-Cl(1)	96.12(7)
P(4)-Ru(2)-Cl(1)	89.46(7)
P(3)-Ru(2)-Cl(4)	95.31(7)
P(4)-Ru(2)-Cl(4)	99.96(6)
Cl(1)-Ru(2)-Cl(4)	164.78(7)
P(3)-Ru(2)-Cl(3)	171.45(7)
P(4)-Ru(2)-Cl(3)	88.23(6)
Cl(4)-Ru(2)-Cl(3)	79.21(6)
P(3)-Ru(2)-Cl(2)	91.69(7)
P(4)-Ru(2)-Cl(2)	175.24(7)
Cl(1)-Ru(2)-Cl(2)	90.90(7)
Cl(4)-Ru(2)-Cl(2)	78.73(6)
Cl(3)-Ru(2)-Cl(2)	80.86(6)
Ru(1)-Cl(2)-Ru(2)	82.20(6)
Ru(1)-Cl(3)-Ru(2)	83.69(6)
Ru(2)-Cl(4)-Ru(1)	84.49(6)
C(7)-N(1)-Ru(1)	157.9(11)
C(13)-P(1)-C(19)	99.8(3)
C(13)-P(1)-C(20)	101.6(4)
C(19)-P(1)-C(20)	102.4(3)
C(13)-P(1)-Ru(1)	111.3(2)
C(19)-P(1)-Ru(1)	122.15(19)
C(20)-P(1)-Ru(1)	116.5(3)
C(23)-P(2)-C(29)	103.6(3)
C(23)-P(2)-C(35)	99.6(3)
C(29)-P(2)-C(35)	99.7(3)
C(23)-P(2)-Ru(1)	118.6(3)
C(29)-P(2)-Ru(1)	113.0(2)
C(35)-P(2)-Ru(1)	119.53(18)
C(47)-P(3)-C(48)	101.0(3)

C(47)-P(3)-C(41)	101.0(3)
C(48)-P(3)-C(41)	100.1(4)
C(47)-P(3)-Ru(2)	115.3(2)
C(48)-P(3)-Ru(2)	118.5(3)
C(41)-P(3)-Ru(2)	118.0(2)
C(51)-P(4)-C(57)	97.4(3)
C(51)-P(4)-C(63)	103.5(3)
C(57)-P(4)-C(63)	100.9(3)
C(51)-P(4)-Ru(2)	117.8(3)
C(57)-P(4)-Ru(2)	110.8(2)
C(63)-P(4)-Ru(2)	122.43(18)
C(2)-C(1)-C(6)	120.0
C(1)-C(2)-C(3)	120.0
C(2)-C(3)-C(4)	120.0
C(5)-C(4)-C(3)	120.0
C(4)-C(5)-C(6)	120.0
C(5)-C(6)-C(1)	120.0
C(5)-C(6)-C(7)	118.8(10)
C(1)-C(6)-C(7)	121.2(10)
N(1)-C(7)-C(6)	161.6(18)
C(9)-C(8)-C(13)	120.0
C(10)-C(9)-C(8)	120.0
C(11)-C(10)-C(9)	120.0
C(10)-C(11)-C(12)	120.0
C(13)-C(12)-C(11)	120.0
C(12)-C(13)-C(8)	120.0
C(12)-C(13)-P(1)	119.5(4)
C(8)-C(13)-P(1)	120.2(4)
C(15)-C(14)-C(19)	120.0
C(14)-C(15)-C(16)	120.0
C(17)-C(16)-C(15)	120.0
C(16)-C(17)-C(18)	120.0
C(19)-C(18)-C(17)	120.0
C(18)-C(19)-C(14)	120.0
C(18)-C(19)-P(1)	120.7(3)
C(14)-C(19)-P(1)	119.2(3)
C(21)-C(20)-P(1)	119.1(6)
C(20)-C(21)-C(22)	117.7(7)
C(23)-C(22)-C(21)	116.1(7)
C(22)-C(23)-P(2)	113.5(6)
C(25)-C(24)-C(29)	120.0
C(26)-C(25)-C(24)	120.0
C(25)-C(26)-C(27)	120.0
C(28)-C(27)-C(26)	120.0
C(29)-C(28)-C(27)	120.0
C(28)-C(29)-C(24)	120.0

C(28)-C(29)-P(2)	118.4(3)
C(24)-C(29)-P(2)	121.4(3)
C(31)-C(30)-C(35)	120.0
C(30)-C(31)-C(32)	120.0
C(33)-C(32)-C(31)	120.0
C(32)-C(33)-C(34)	120.0
C(33)-C(34)-C(35)	120.0
C(34)-C(35)-C(30)	120.0
C(34)-C(35)-P(2)	117.6(3)
C(30)-C(35)-P(2)	122.3(3)
C(37)-C(36)-C(41)	120.0
C(38)-C(37)-C(36)	120.0
C(37)-C(38)-C(39)	120.0
C(40)-C(39)-C(38)	120.0
C(41)-C(40)-C(39)	120.0
C(40)-C(41)-C(36)	120.0
C(40)-C(41)-P(3)	118.0(3)
C(36)-C(41)-P(3)	121.9(3)
C(43)-C(42)-C(47)	120.0
C(44)-C(43)-C(42)	120.0
C(45)-C(44)-C(43)	120.0
C(46)-C(45)-C(44)	120.0
C(45)-C(46)-C(47)	120.0
C(46)-C(47)-C(42)	120.0
C(46)-C(47)-P(3)	117.9(3)
C(42)-C(47)-P(3)	122.1(3)
C(49)-C(48)-P(3)	114.7(6)
C(50)-C(49)-C(48)	112.7(7)
C(49)-C(50)-C(51)	115.9(7)
C(50)-C(51)-P(4)	119.4(6)
C(53)-C(52)-C(57)	120.0
C(52)-C(53)-C(54)	120.0
C(53)-C(54)-C(55)	120.0
C(54)-C(55)-C(56)	120.0
C(57)-C(56)-C(55)	120.0
C(56)-C(57)-C(52)	120.0
C(56)-C(57)-P(4)	117.8(3)
C(52)-C(57)-P(4)	122.2(3)
C(59)-C(58)-C(63)	120.0
C(58)-C(59)-C(60)	120.0
C(61)-C(60)-C(59)	120.0
C(62)-C(61)-C(60)	120.0
C(61)-C(62)-C(63)	120.0
C(62)-C(63)-C(58)	120.0
C(62)-C(63)-P(4)	119.7(3)
C(58)-C(63)-P(4)	120.2(3)

C(64)-O(1)-C(66)	116(2)
O(1)-C(64)-C(65)	103(2)
O(1)-C(66)-C(67)	99(2)

Symmetry transformations used to generate equivalent atoms:

Appendix I. NMR Spectroscopic Data for 31

Figure I.1. $^{31}P\{^{1}H\}$ NMR spectrum of 31 ($CDCl_3$)

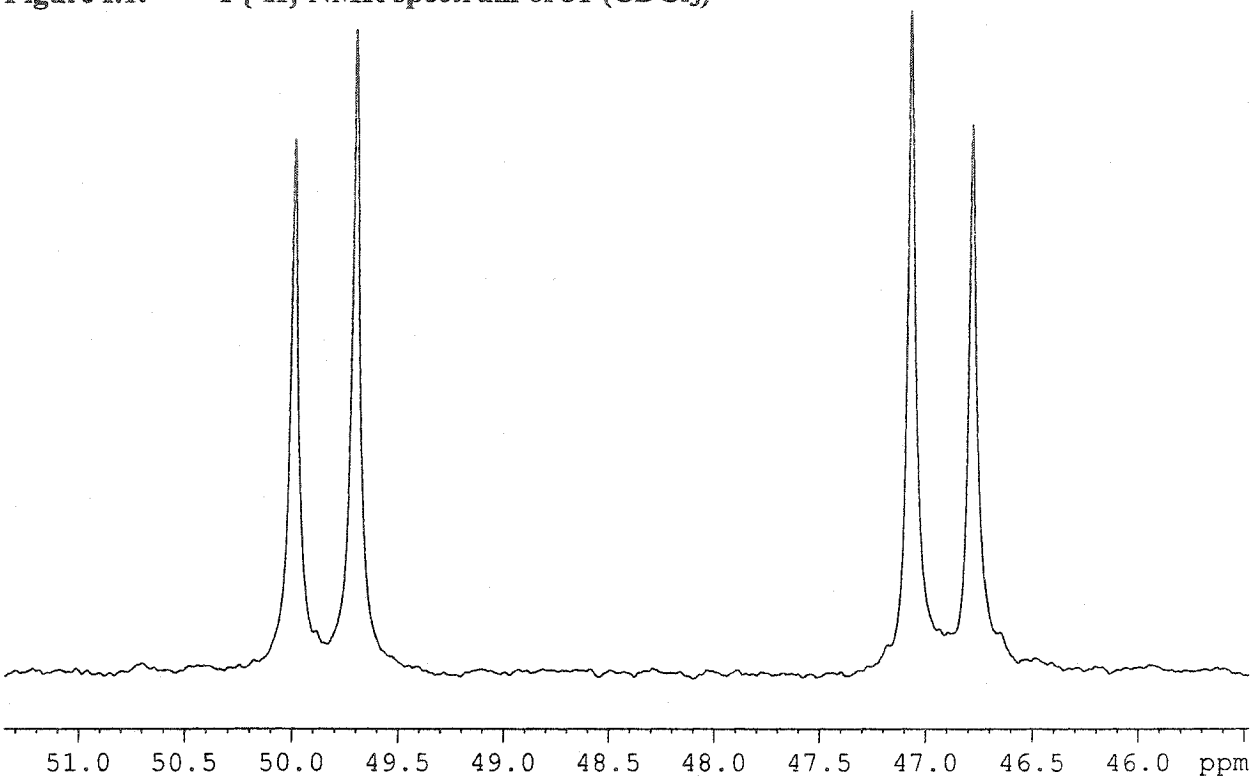

Figure I.2. **Expansion of Upfield Region of the ^{1}H NMR Spectrum of 31 ($CDCl_3$) at a) 300K and b) 324K**

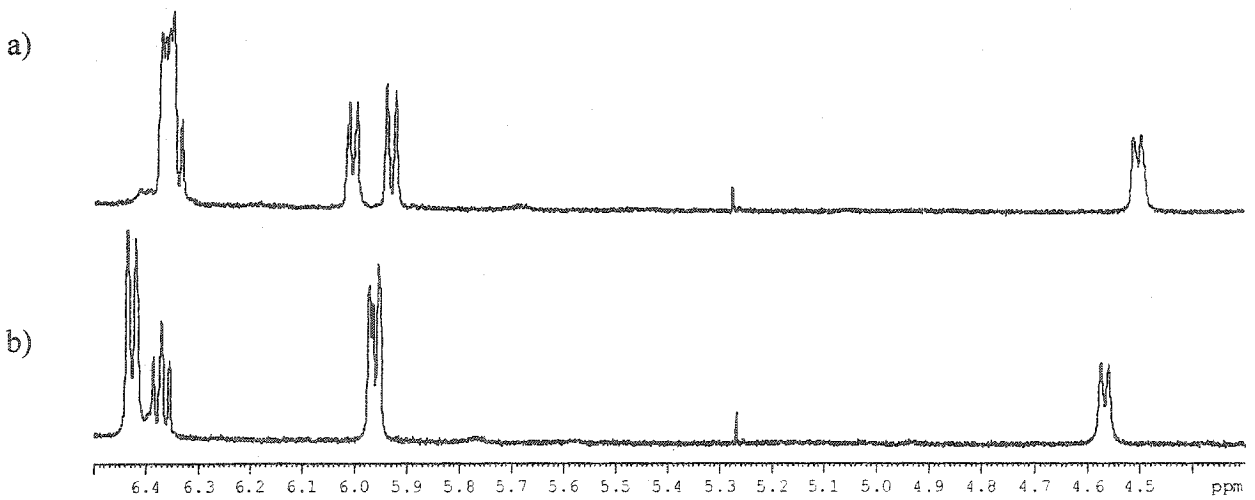

Figure I.3. a) $^{13}C\{^{1}H\}$ NMR Spectrum of 31 ($CDCl_3$)

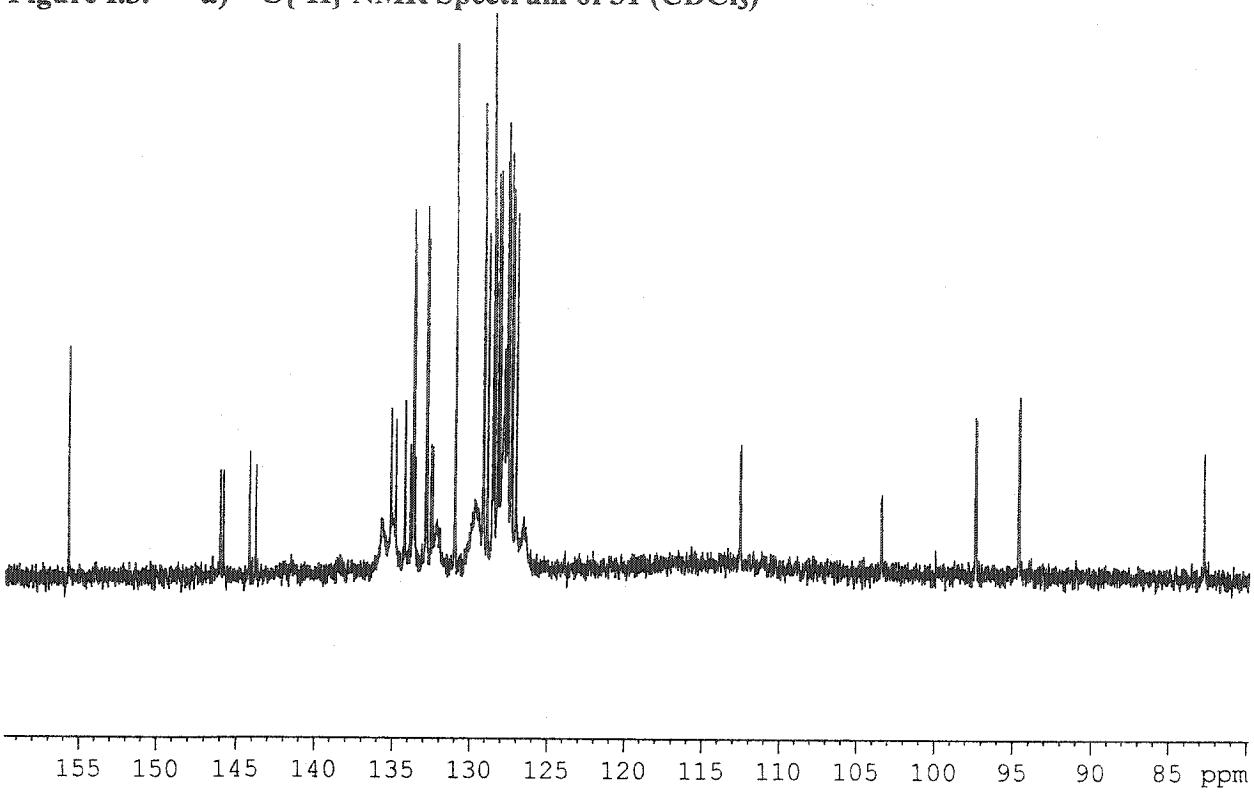

Figure I.4. $^{13}C\{^{1}H\}$ DEPT 135 Spectrum of 31 ($CDCl_3$)

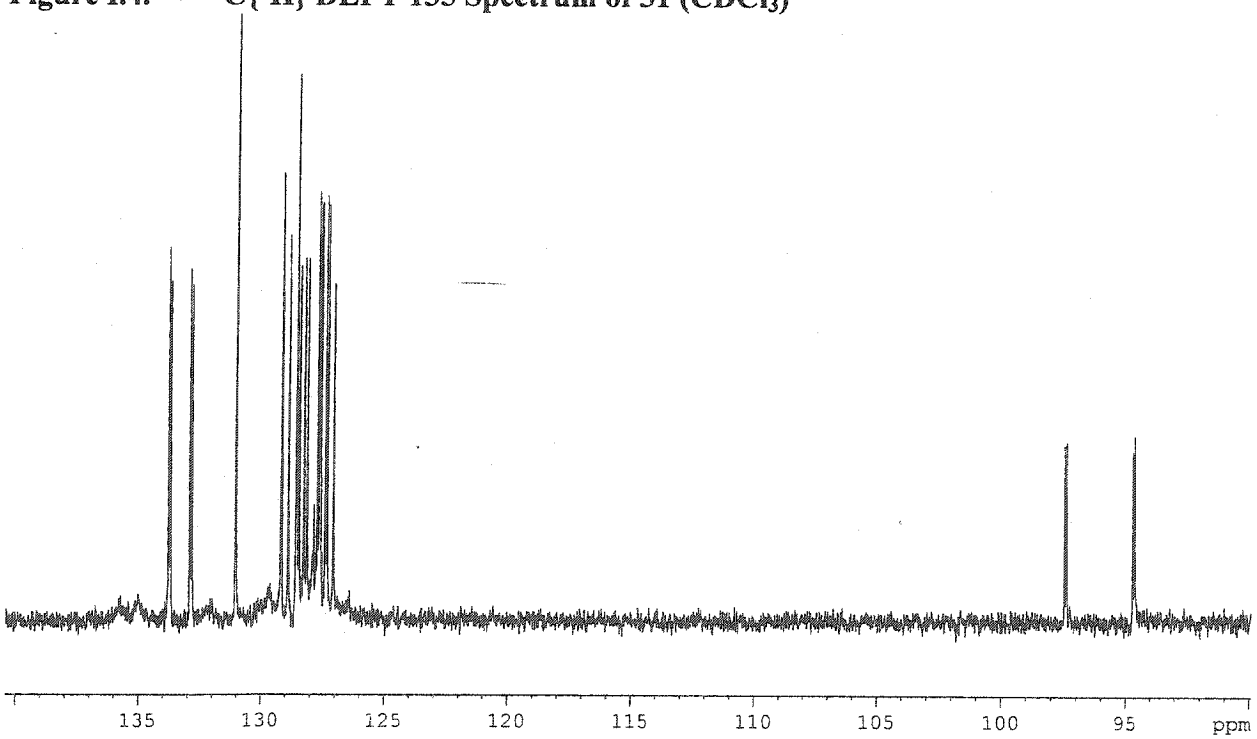

Figure I.5. **^{1}H-^{1}H COSY NMR Spectrum for 31 ($CDCl_3$; unsaturation omitted in numbered figure for clarity)**

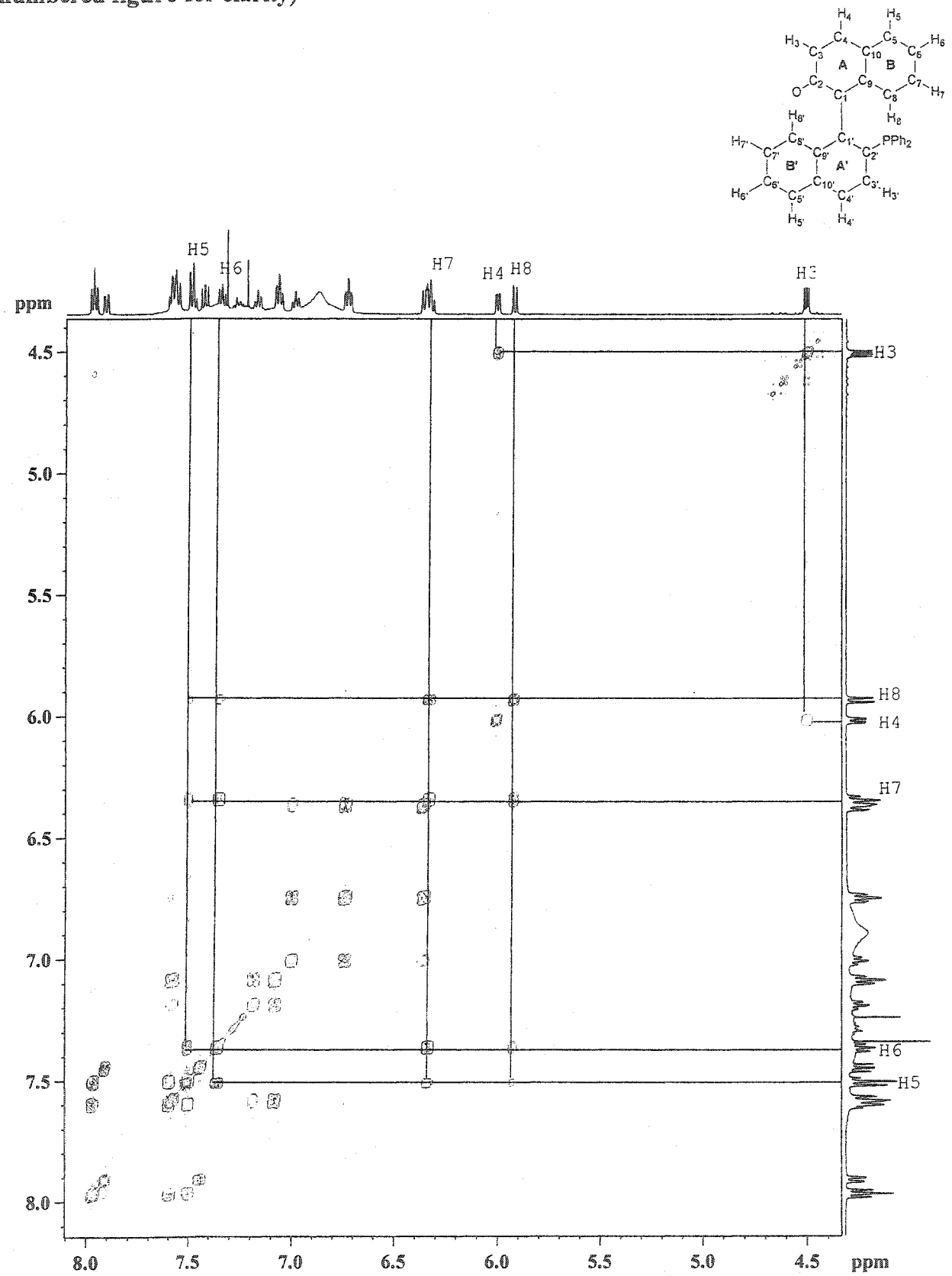

Figure I.6. ^{1}H-$^{13}C\{^{1}H\}$ HMQC NMR Spectrum of 31 ($CDCl_3$; unsaturation omitted in numbered figure for clarity)

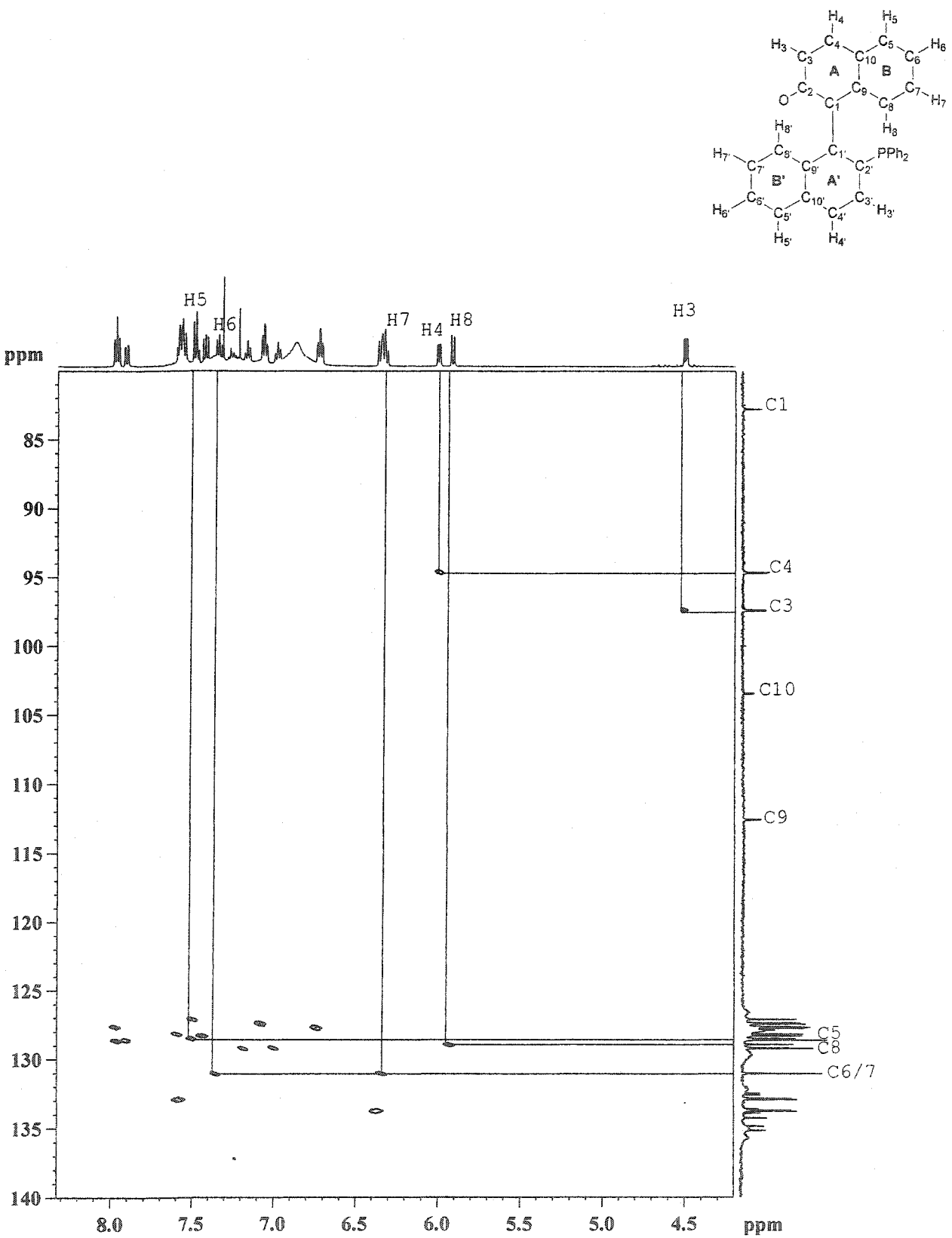

Figure I.7. **^{1}H-^{1}H TOCSY NMR Spectrum of 31 ($CDCl_3$; unsaturation omitted in numbered figure for clarity)**

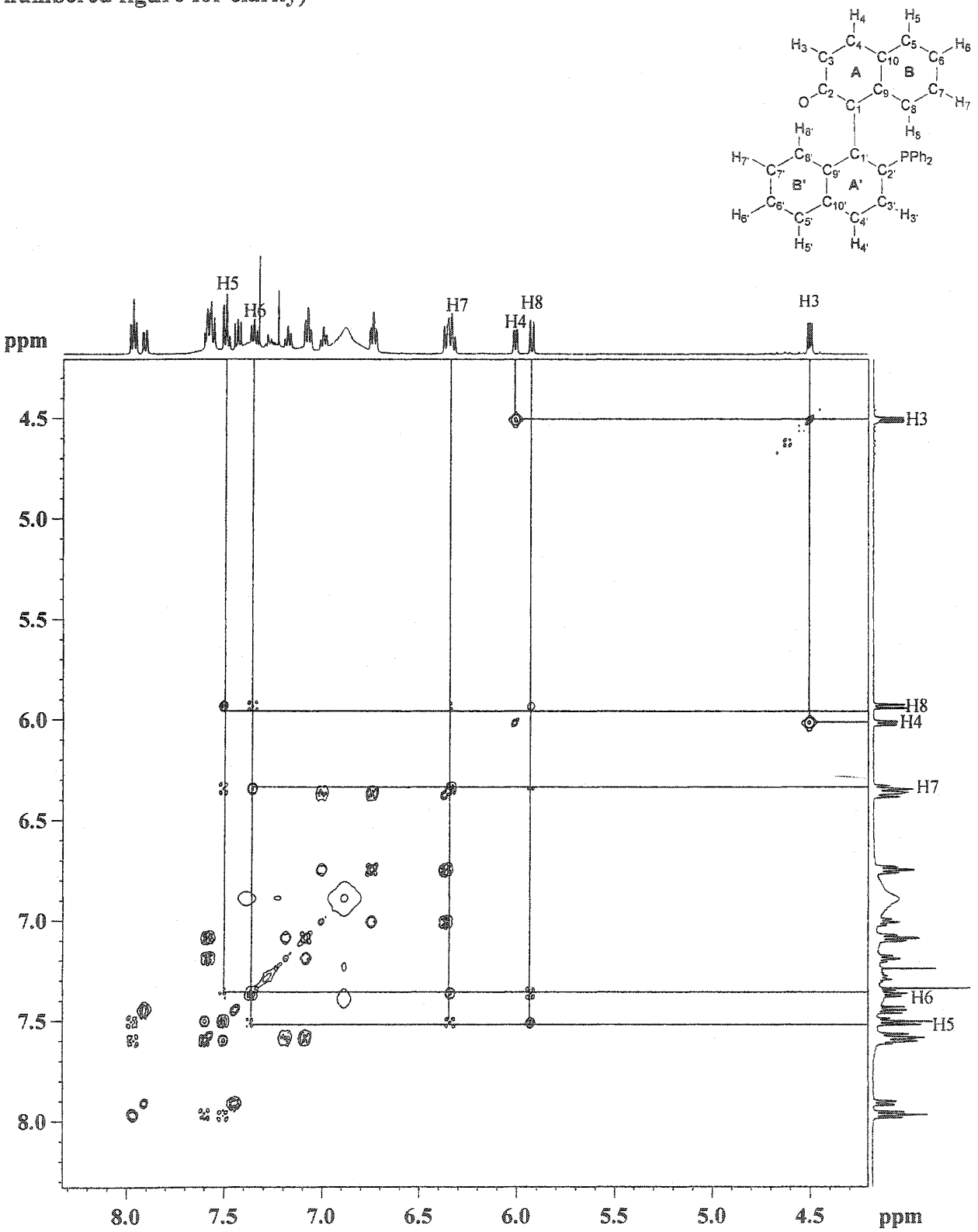

Figure I.8. **^{1}H-^{13}C HMBC NMR Spectrum for 31 ($CDCl_3$; unsaturation omitted in numbered figure for clarity)**

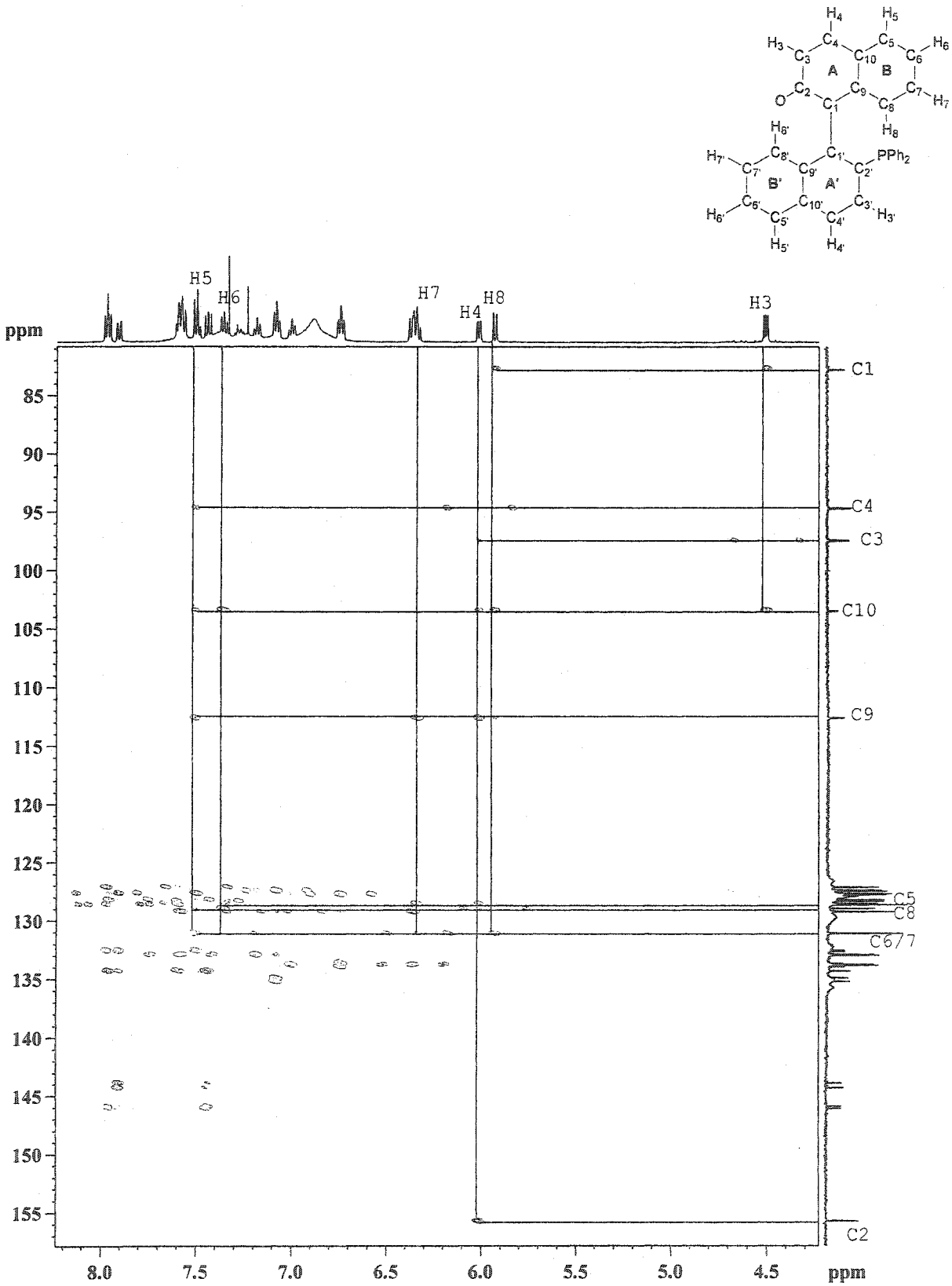

Figure I.9. ^{1}H-^{31}P HMQC NMR Spectrum for 31 optimized for 10 Hz coupling ($CDCl_3$; unsaturation omitted in numbered figure for clarity)

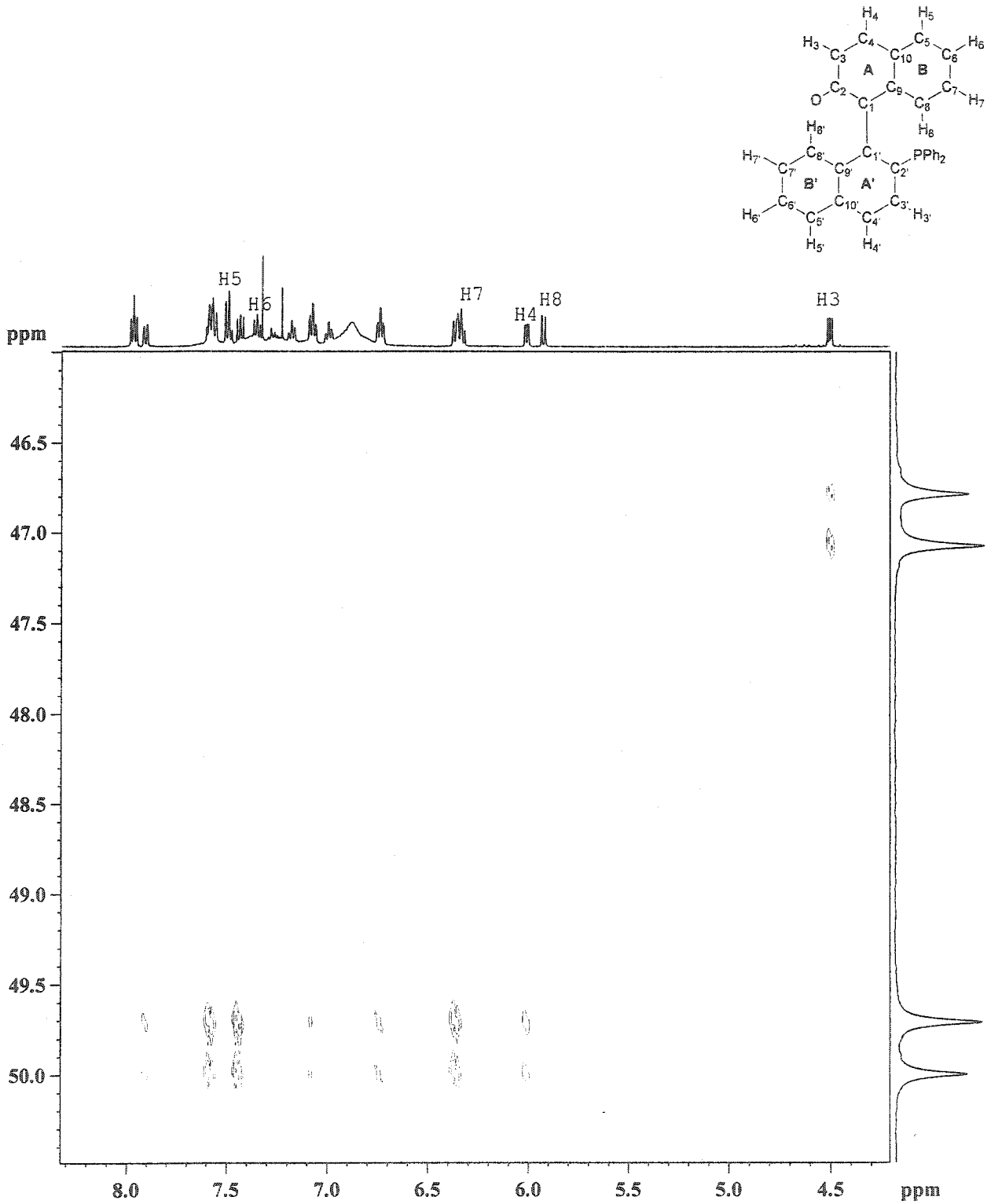

Figure I.10. **^{1}H-^{31}P HMQC NMR Spectrum for 31 optimized for 5 Hz coupling ($CDCl_3$; unsaturation omitted in numbered figure for clarity)**

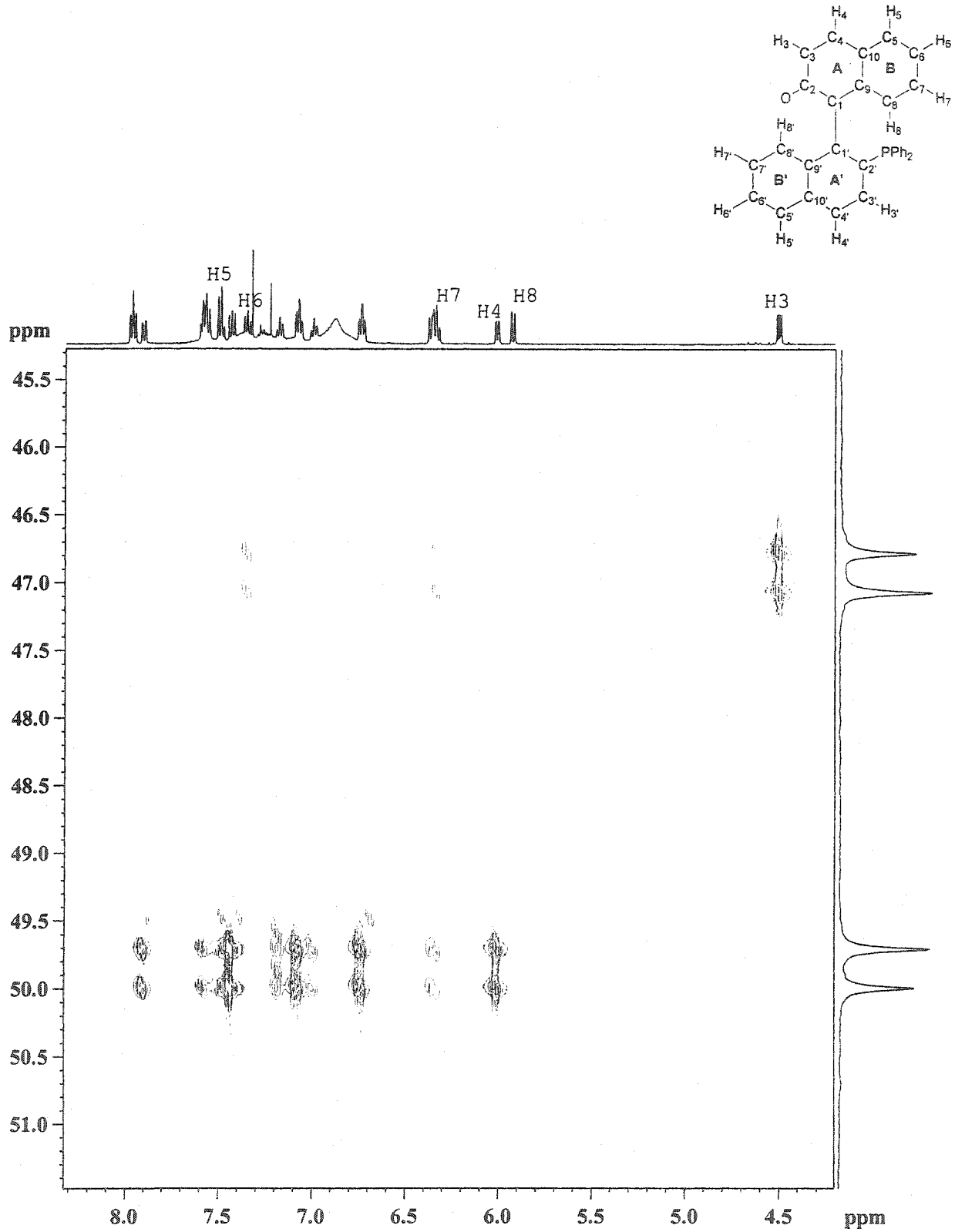

Appendix J: Ivin and Rooney ROMP Mechanism.

There are two schools of thought on how the monomer approaches the metal center to generate a stereoselective polymer. Ivin and Rooney make several assumptions in their model (Figure J).[1] First, it is assumed that the propagating species may have left- or right-handed forms (P_l or P_r) with one vacant site available for monomer coordination. Second, the bicycle presents its less hindered *exo* face to the metal center. Third, the M=C and C=C double bonds are in a parallel alignment as they approach each other which is dependent upon the alignment of the filled and unfilled orbitals on the M=C and C=C bonds, and fourth, the configuration of P_l or P_r is maintained; there is no ligand migration or rotation about the M=C bond between successive propagation steps.

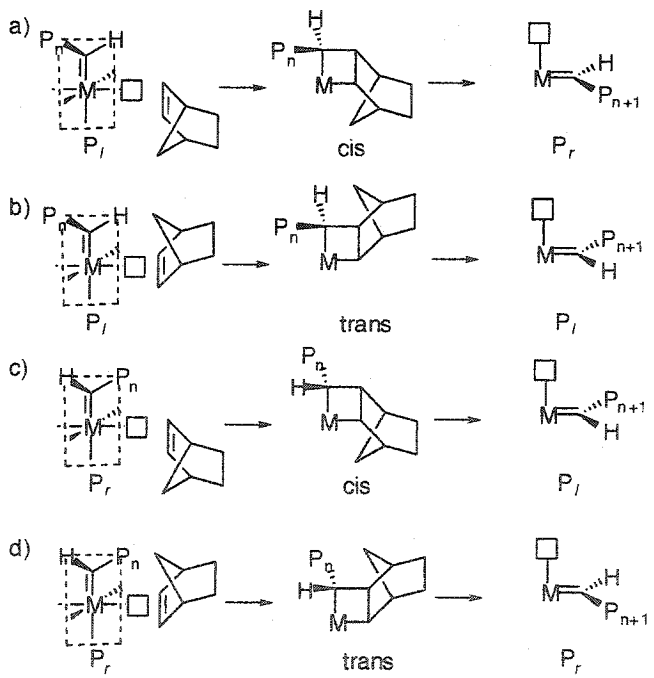

Figure J. Ivin and Rooney stereochemical model.

[1] Ivin, K. J.; Rooney, J. C. *Olefin Metathesis and Metathesis Polymerization*; Academic Press, Ltd.: Toronto, 1997, p 253

Appendix K. $^{13}C\{^{1}H\}$ **NMR ($CDCl_3$, 125 MHz) Spectra For Polymers of a) 53 b) 54 c) 55 and d) 56.**

a)

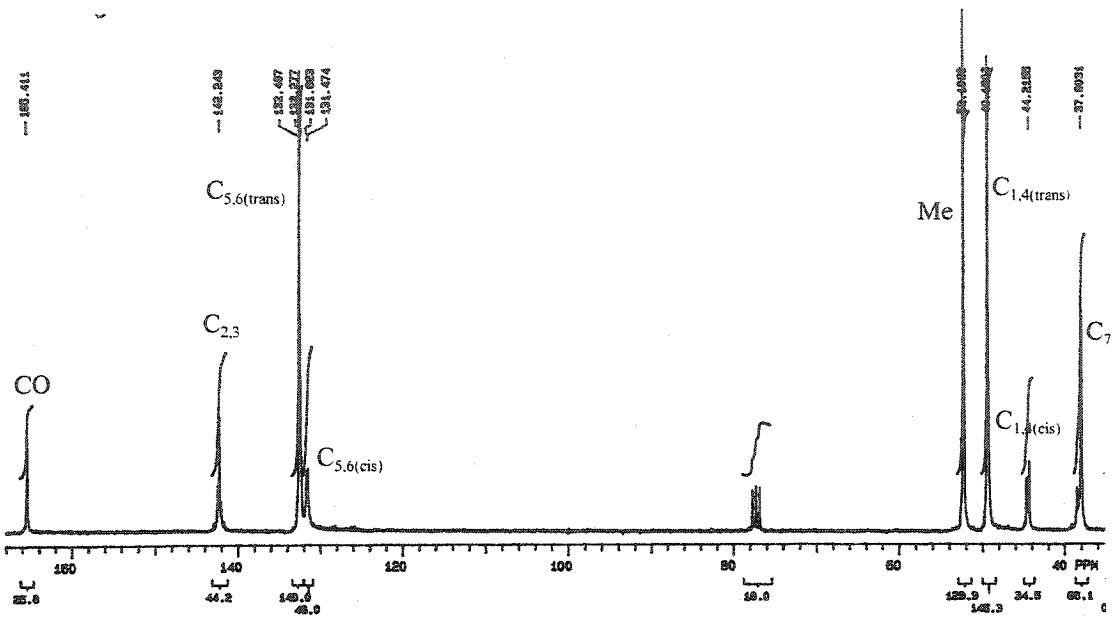

b)

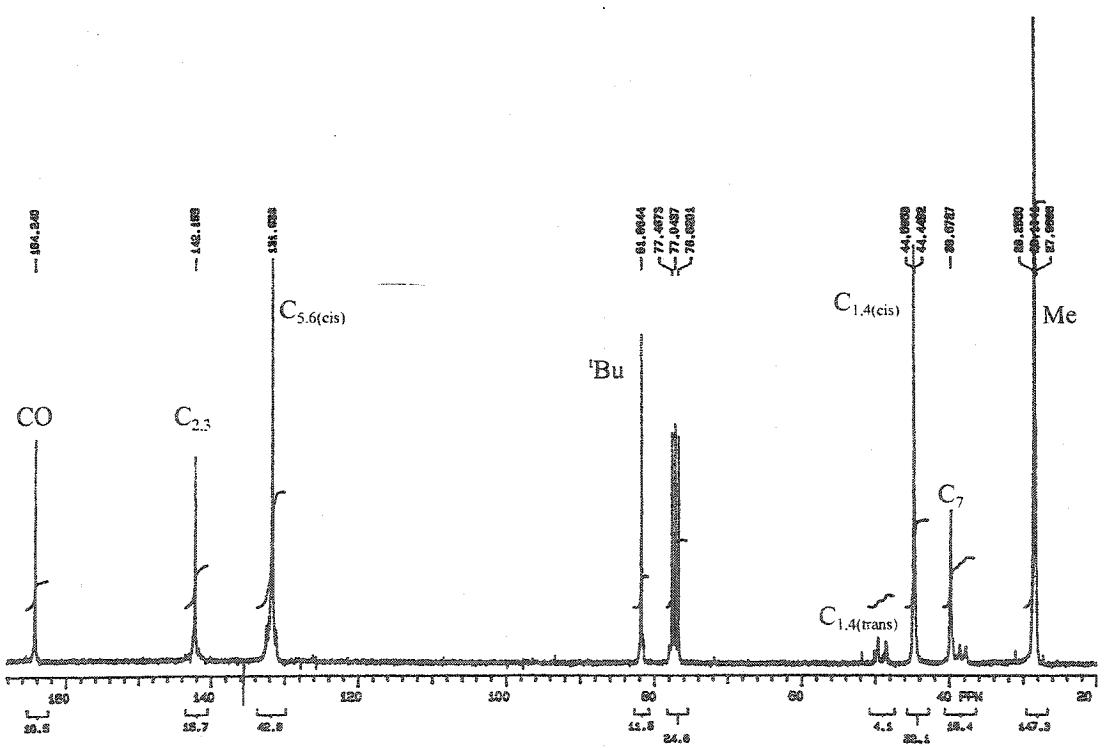

c)

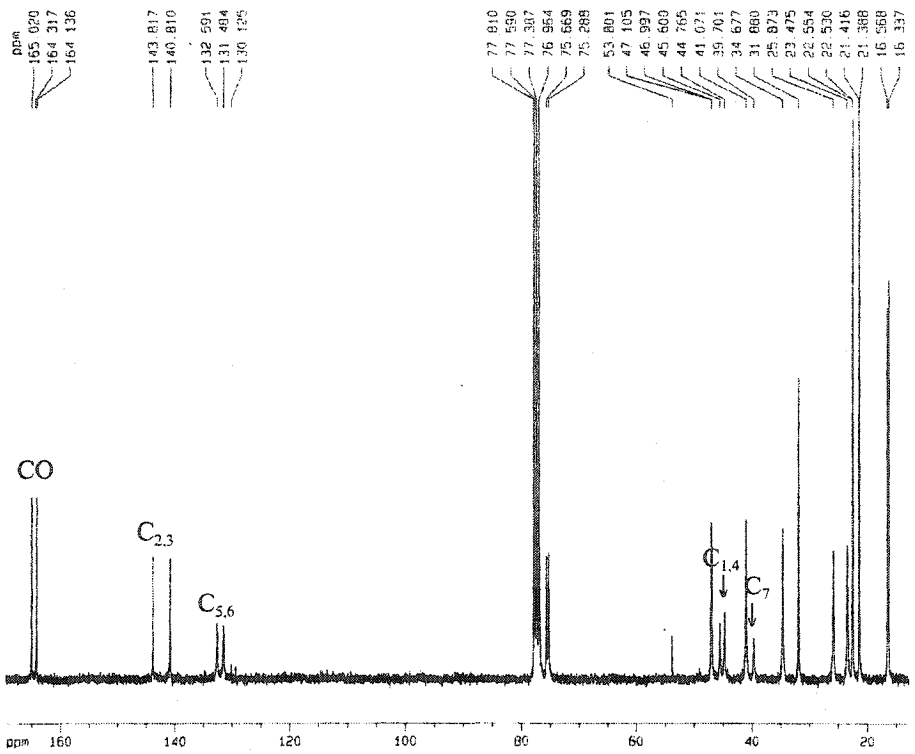
CO
C2,3
C5,6
C1,4
C7
ppm 160
140
120
100
80
60
40
20

d)

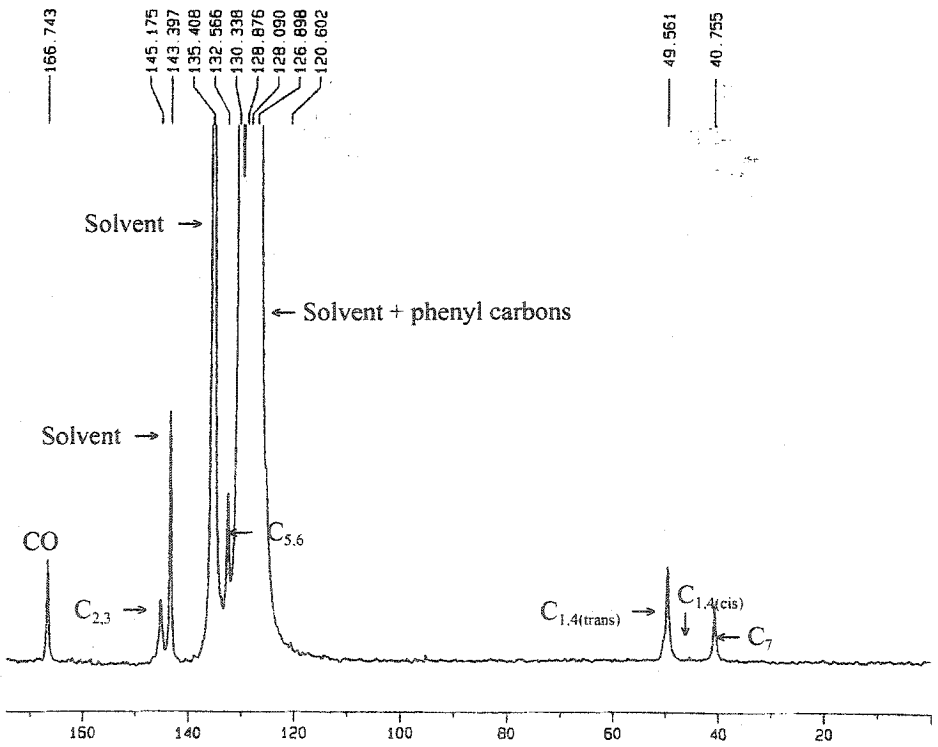
166.743
145.175
143.397
135.408
132.566
130.338
128.876
128.090
126.898
120.602
49.561
40.755
Solvent →
← Solvent + phenyl carbons
Solvent →
CO
C2,3 →
C5,6
C1,4(trans) →
C1,4(cis)
← C7
150
140
120
100
80
60
40
20

Appendix L. Thermal Analysis of Polymers of 53-56.

Figure L.1. Representative DSC Thermograms of Polymers of a) 535, b) 54, c) 55 and d) 56.

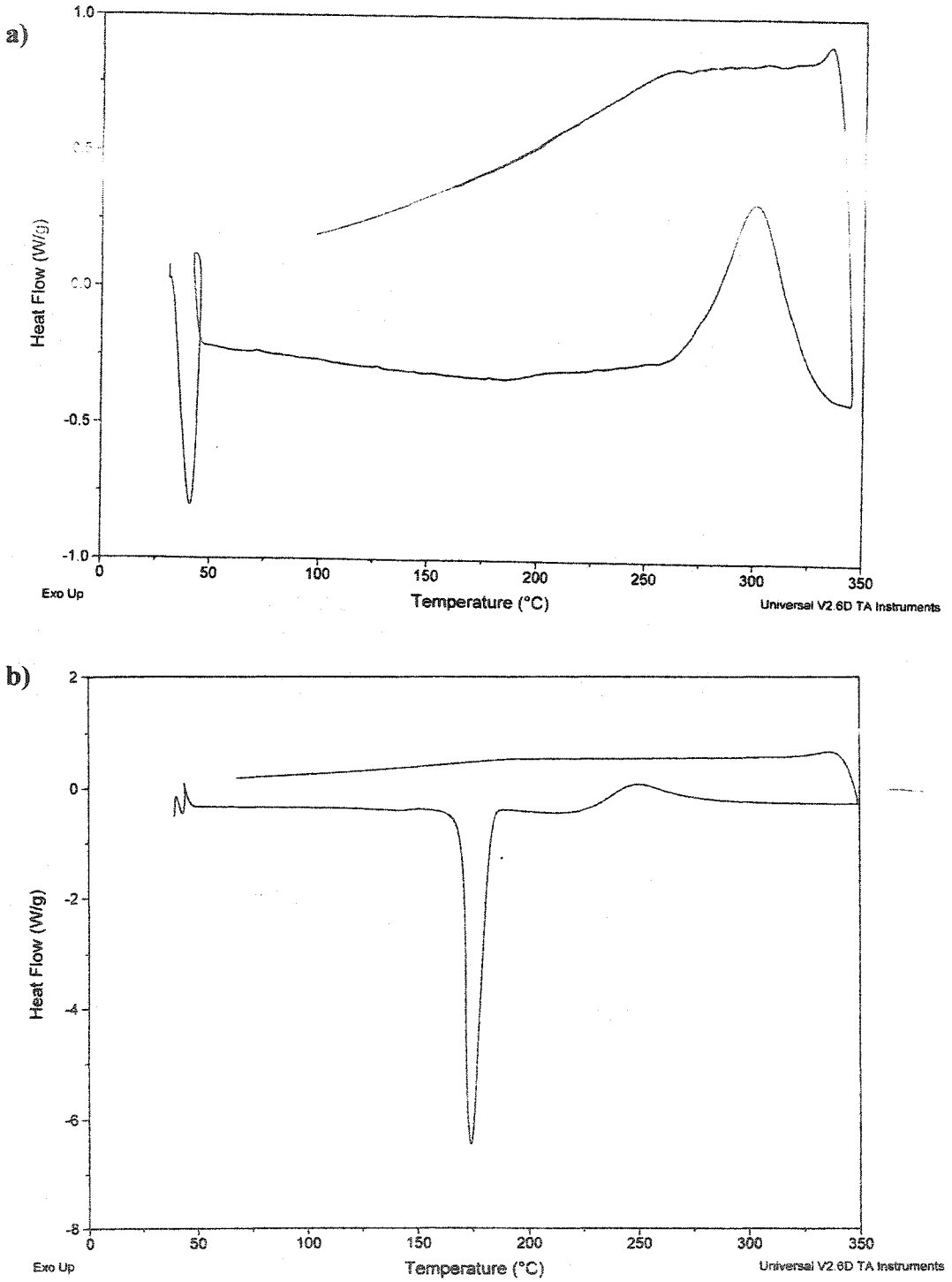

c)

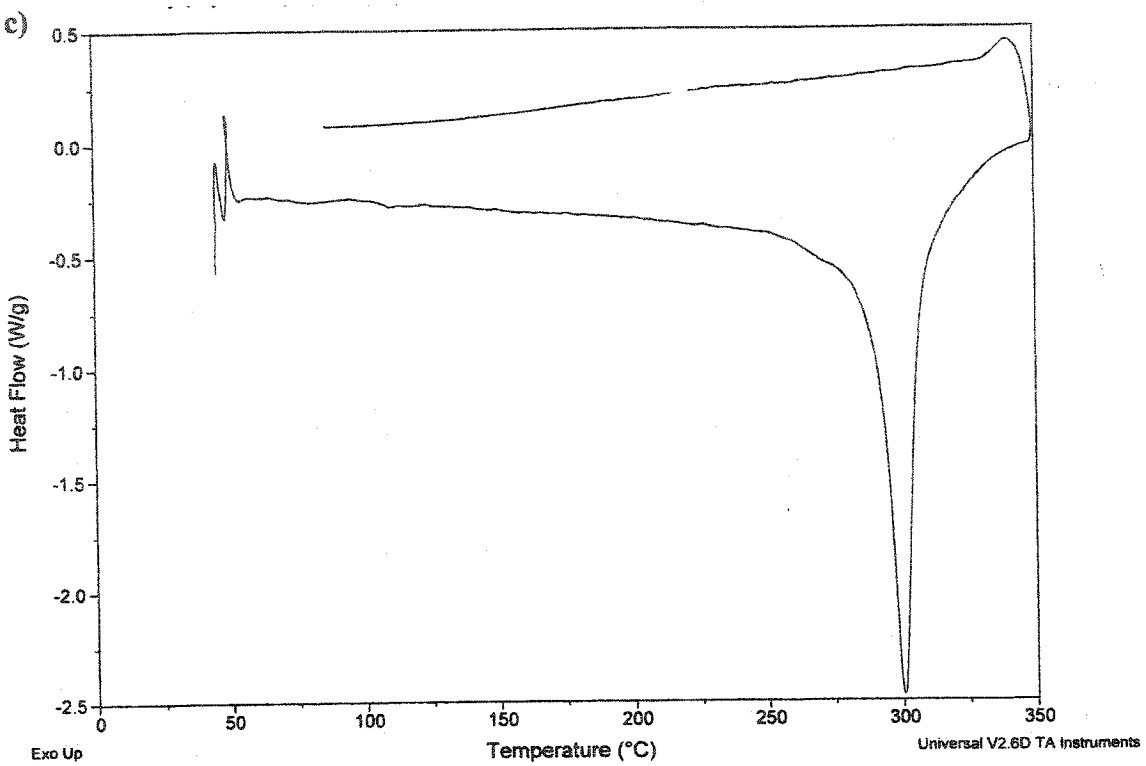
0.5
0.0
-0.5
-1.0
-1.5
-2.0
-2.5
Heat Flow (W/g)
0
50
100
150
200
250
300
350
Temperature (°C)
Exo Up
Universal V2.6D TA Instruments

d)

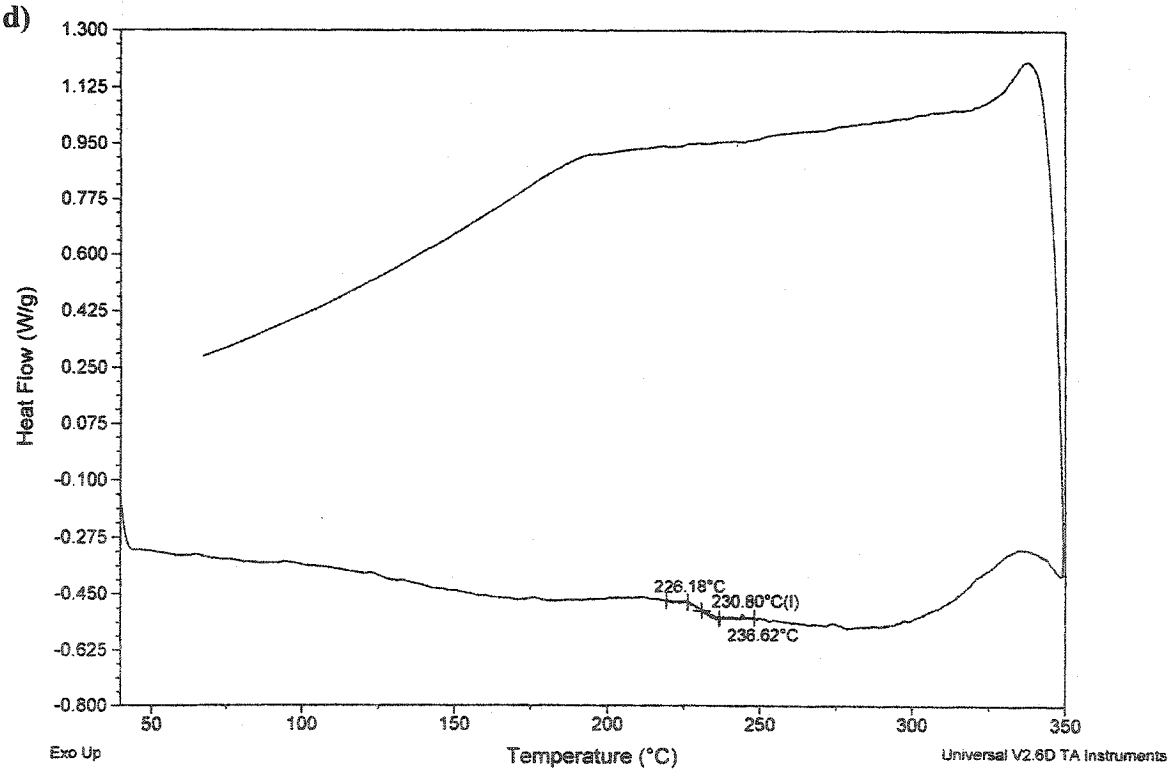
1.300
1.125
0.950
0.775
0.600
0.425
0.250
0.075
-0.100
-0.275
-0.450
-0.625
-0.800
Heat Flow (W/g)
226.18°C
230.80°C(I)
236.62°C
50
100
150
200
250
300
350
Temperature (°C)
Exo Up
Universal V2.6D TA Instruments

Figure L.2. Relative Mass Loss (TGA) for Polymers of a) 53 b) 54 c) 55 and d) 56.

a)

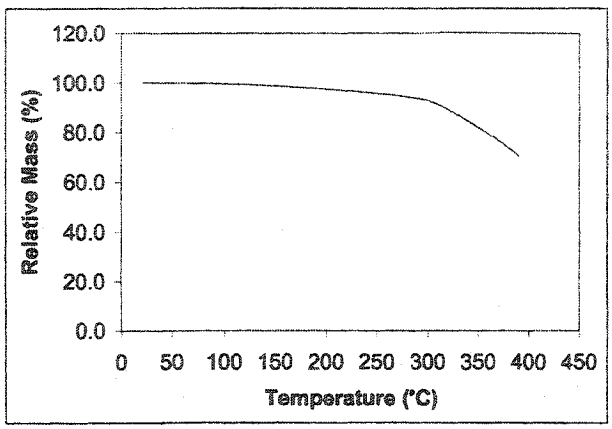

b)

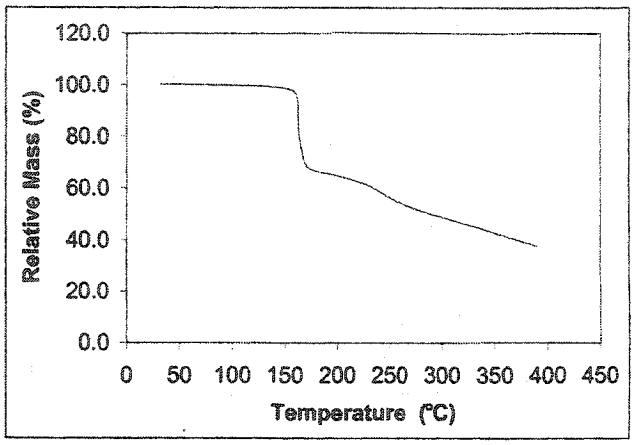

c)

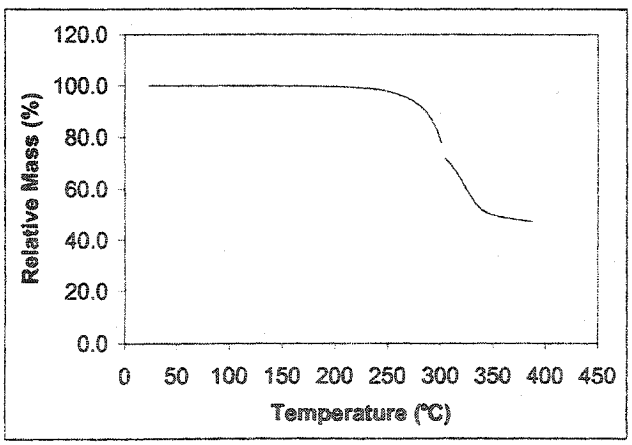

d)

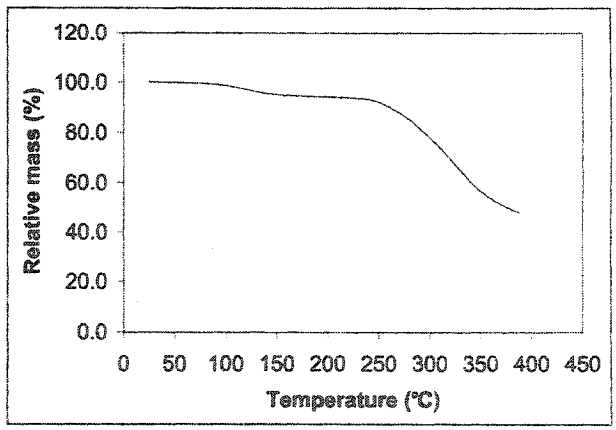

Figure L.3. Relative IR Peak Absorption vs. Time for Polymers of a) 53 b) 54 c) 55 and d) 56.

a)

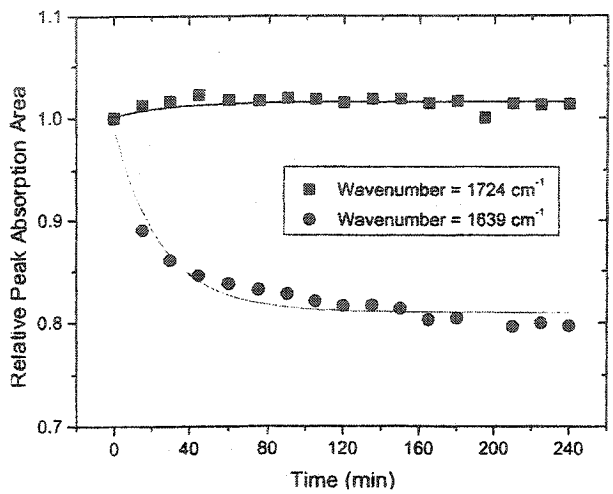

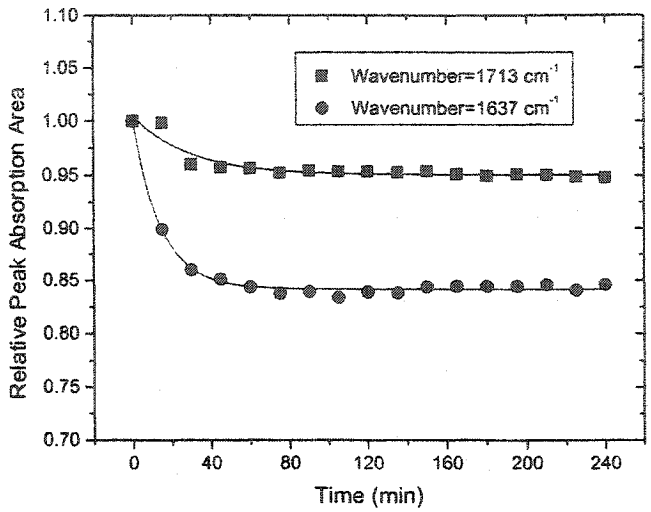

c)

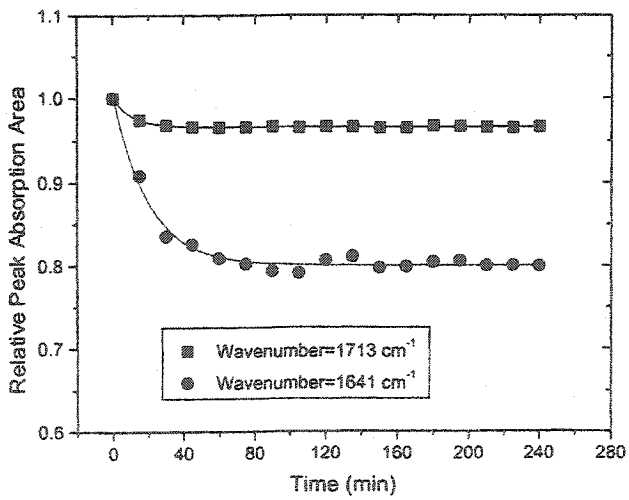

d)